UNIVERSITY OF CALIFORNIA
RIVERSIDE

Performance of Time Delay Estimation and Range-Based Localization in Wireless Channels

A Dissertation submitted in partial satisfaction
of the requirements for the degree of

Doctor of Philosophy

in

Electrical Engineering

by

Ning Liu

December 2010

Dissertation Committee:

Professor Zhengyuan Xu, Chairperson
Professor Jay A. Farrell
Professor Yingbo Hua

The Dissertation of Ning Liu is approved:

Committee Chairperson

University of California, Riverside

Acknowledgments

I would like to sincerely thank my research advisor, Dr. Zhengyuan Xu, for his guidance, patient advising, understanding and continuous support. He guided me through my Ph.D. research by sharing his enthusiasm, knowledge and experience with me. I am deeply grateful to him for the long discussions that helped me sort out the technical details of my work. I would also like to thank the Department of Electrical Engineering at UC Riverside, especially the members of my doctoral committee, Professor Jay Farrell and Professor Yingbo Hua, for their valuable input, discussions and feedback on my research. Their comments and suggestions to my dissertation were very helpful.

My research was benefited from insightful discussions with Dr. Brian M. Sadler in the Army Research Lab (ARL). This successful collaboration provides invaluable advice to my dissertation and I am grateful to the generous financial support from ARL [1].

My Ph.D. study and life at UCR have been enriched by all of the members of Dr. Xu's lab. I have learned a lot from discussions with them, and appreciate all their help and encouragements. These friends and colleagues also provided for some much needed humor and entertainment in what could have otherwise been a somewhat stressful laboratory environment. I am grateful to the friendship of all of the members of the research group. I especially thank my friend, Qunfeng He, for his great help on handling tedious administrative issues when I was working off-campus for internship. I cannot imagine to fulfill all the graduation requirements so smoothly without his help.

Finally, and most importantly, none of this would have been possible without the

[1] Prepared through collaborative participation in the Communications and Networks Consortium sponsored by the U. S. Army Research Laboratory under the Collaborative Technology Alliance program, cooperative agreement DAAD19-01-2-0011. The U. S. Government is authorized to reproduce and distribute reprints for Government purposes notwithstanding any copyright notation thereon. The views and conclusions contained in this document are those of the authors and should not be interpreted as representing the official policies, either expressed or implied, of the Army Research Laboratory or the U. S. Government.

love of my family. I would like to express my heart-felt gratitude to my wife Yujing. Her support, encouragement, patience and unwavering love were undeniably the bedrock upon which the past eight years of my life have been built. Her tolerance of my occasional depressed moods is a testament in itself of her unyielding devotion and love. I thank my parents, Hongyang Liu and Hong Zhou, for their faith in me and allowing me to be as ambitious as I wanted. It was under their watchful eye that I gained so much drive and an ability to tackle challenges head on. Also, I thank Yujing's parents, Jinyuan Zhang and Liping Nie. They provided me with unending encouragement and support. Without my family's endless love, this quality research work would not be possible. My dissertation is dedicated to them.

To my family.

ABSTRACT OF THE DISSERTATION

Performance of Time Delay Estimation and Range-Based Localization in Wireless Channels

by

Ning Liu

Doctor of Philosophy, Graduate Program in Electrical Engineering
University of California, Riverside, December 2010
Professor Zhengyuan Xu, Chairperson

This thesis studies the performance of time delay estimation and the range-based localization schemes in wireless multipath channels. The research focuses on the localization schemes based on time-of-arrival and time-difference-of-arrival measurements. In multipath environments, time delay measurements suffer from the errors due to weak line-of-sight and rich non-line-of-sight (NLOS) signal paths. Instead of proposing range measurement algorithms, the thesis is devoted to develop theoretical performance lower bounds used as benchmarks to guide algorithm design and provide insight into the behavior of time delay estimation (TDE).

The author develops Ziv-Zakai bounds (ZZBs) on Bayesian estimation of time delay, for known pulsed signal and frequency hopping waveforms that propagate through unknown random multipath channels following Rayleigh/Rician distribution, with a uniform prior on the delay. The bounds do not assume channel knowledge at receivers, providing more realistic and tighter performance limits than the average bound that assumes channel knowledge. The ZZBs also present good performance prediction for maximum a posteriori estimator, tracking a wide range of signal-to-noise ratios. The ZZB for wideband frequency hopping waveforms reveals the performance benefit for

TDE from frequency diversity over frequency-selective fading channels. To evaluate the ZZB, the author proposes a moment generating function approach. The closed-form expressions for independent flat-fading channels enable easy study of the effects of SNR, frequency diversity, and channel statistics on TDE.

The TDE errors lead to time-based ranging errors that in turn cause positioning errors and deteriorated localization performance. The thesis models the NLOS range measurement error as a deterministic or random positive bias, following widely adopted distributions for time delay over multipath channels. The error analysis for typical estimators shows that the MSE and bias performance is determined by the statistics of measurement bias and noise, the beacon array geometry and the estimator type.

Contents

List of Figures

List of Tables

Chapter 1

Introduction

1.1 Background

In the past decades significant attention and efforts have been placed on wireless networks. In addition to the communication capability, from the network service perspective, transceiver location information itself can be one of the services provided by a network. A well-known example is the E-911 service of cellular networks [1], which can provide the location information of the subscribers in emergency. Another example is the location-based services (LBS) in wireless networks, which support applications by commercial content providers in various contexts such as health, work and personal life. In such networks, mobile devices' location information is integrated with other information in order to provide added value to users. In other specialized areas such as military, scientific research, traffic control, agricultures and warehouse inventory management, low-cost unmanned localization capabilities for wireless sensor networks are desired for surveillance, data collection and remote control [2]. In fact, for these kinds of applications, when sensor data is reported, it should be accompanied with data's origination. The raw sensor data could be of very limited value if it is not combined

Localization Schemes	Area of Deployment	PHY Signal	Ranging Method	Location Entity	Security
GPS [3]	WAL	RF	ToA	Client	Open
TeleSentinel [5]	WAL	RF(TDMA)	AoA	Network	Open
Cursor [6]	WAL	RF(GSM)	TDoA	Network	Open
SnapTrack [7]	WAL	RF	ToA	Client	Open
Cricket [8]	LAL	Ultra Sound	ToA	Client	Open
LEASE [9]	LAL	RF(802.11)	RSS	Network	Open
HORUS [10]	LAL	RF(802.11)	RSS	Client	Open
DV-Hop [11]	AHL	RF	Conn	Client	Open
SeRLoc [12]	AHL	Any	AoA	Client	Secure
SPA [13]	AHL	RF	ToA	Client	Open
AHLoS [14]	AHL	Ultra Sound	ToA	Client	Open

Table 1.1: List of some localization schemes for wireless sensor networks.

with spatial information. With location information the sensor data can be treated as interconnected spatial samples to compute statistics rather than separate sensor readings. Furthermore, from the perspective of network administration, location information can also be used by commercial network operators to implement location based billing, network configuration and performance optimization.

Generally the location information of a mobile device is obtained by the sky-infrastructure-based GPS [3] receivers and assisted by cellular positioning methods, while the GPS signal is unavailable for indoor environments and thus standalone solutions utilizing terrestrial signals such as wireless LAN or Bluetooth become more appropriate for obtaining positions. In addition, for some cost and power constraint applications, for example wireless sensor networks, low complexity is a requirement of high priority and integrating a GPS receiver for each sensor is not an affordable solution. Thus terrestrial signal based localization schemes are more preferable in these scenarios. A shortened list of existing localization schemes from [4] is provided in Table 1.1.

Solutions to the localization problem in wireless systems can be categorized in various ways, as shown in Fig. 1.1, depending on different classification criteria. Among

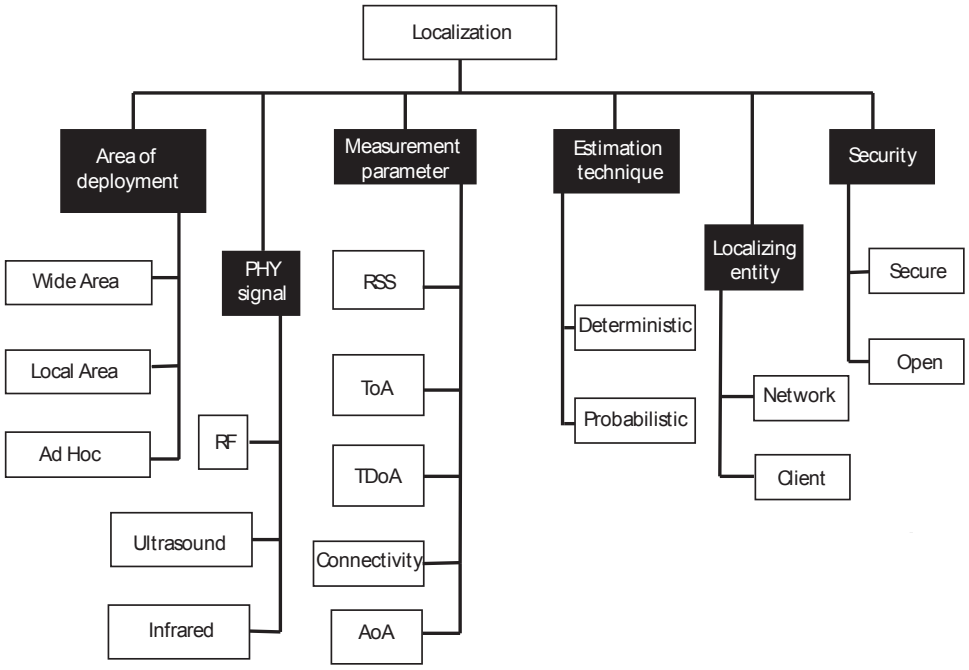

Figure 1.1: Classification of wireless localization schemes.

all kinds of classifications, one important is based on what measurement parameters are used. For instance they can be divided into *range-free* and *range-based* techniques [4], depending on available measurements. Range-free techniques can rely on angle-of-arrival (AoA) measurements or transceiver connectivity (Conn) [12, 15], as these measured parameters for location estimation do not utilize the knowledge of exact point-to-point distance. The standalone application of an AoA technique is limited [16, pp.19] because it often requires multiple antenna elements, which can contribute to transceiver cost and size. Range-based techniques are based on multiple range estimates from reference transceivers, or beacons, with known locations, typically based on measured time of arrival (ToA) [13, 14], time difference of arrival (TDoA) or received signal strength (RSS) [17] to estimate the distances from a transmitter to receivers. These techniques, also known as *source localization* schemes, have been widely explored as a research topic of long history for aerospace electronic navigation systems [18, 19, 20, 21]. Moreover, dif-

ferent measurement modalities can be combined to improve the accuracy and robustness of location estimation [22].

In the applications of wireless sensor networks, traditional localization techniques are not well suited for two particular features of sensor networks [23]. One is the energy and cost constraint on sensors due to battery power and poor communication capability. Thus the traditional way of including a GPS receiver on each device is obviously cost and energy prohibitive. The low-power consumption, low computation and communication cost schemes are preferred. The other feature is that wireless sensor networks are usually infrastructure-less, which means that the reference nodes or base stations that know their own coordinates are sparse in the network, and most of sensors may not have a direct radio link to those reference nodes. This challenge leads to investigation of the *cooperative* or *network localization* techniques [17]. In addition to the measurements between unknown-location sensors and known-location references, the measurements between pairs of unknown-location sensors are obtainable and these measurements can be propagated through the network depending on specific algorithms. The additional information from the measurements between unknown-location sensors enhances the accuracy and robustness of the localization systems.

1.2 Motivation and Related Works

Wireless localization depends on the range, angle or other measurements between transmitters and receivers. The accuracy of these measurements is affected by additive noise, interference, and environment-dependent errors [2]. Noise and interference can be reduced by averaging multiple measurements over time or filtering. Environment dependent errors are the result of the physical arrangement of obstructions, reflectors

and scatters in a particular transceiver setting. As range-based localization absolutely depends on the line-of-sight (LOS) signal path, range measurement is challenging and erroneous due to the random nature of the LOS path. In some cases, the LOS path is weak, ambiguous and difficult to be identified; in other cases, the LOS path is even totally blocked and non-existing, which leads to the non-line-of-sight (NLOS) channels. These multipath channels follow specific power delay profiles (PDP) and probability distributions [24]. In both scenarios, the range measurement errors due to weak LOS or NLOS propagation are inevitable.

To combat with the ranging errors in multipath environments, efficient algorithms and schemes for range measurement, obtained from time delay estimation (TDE) in ToA localization, are desired. The existing works in this category include the studies on LOS path detection under a multipath channel, the NLOS path identification and NLOS error mitigation. For LOS detection, [25] proposes a template-matching method based on the comparison between the PDP of the received signal and a template. This method is verified in [16]. [26] shows a maximum likelihood search algorithm for direct path detection in a dense multipath environment using ultra-wideband (UWB) signals.

In the multipath channels with blocked LOS, NLOS path identification and mitigation is a difficult yet problem. Although some methods have been proposed in the cellular network community, they usually depend on a priori information or redundant measurements. For the NLOS identification problem, [27] shows a decision theoretic framework using hypothesis tests under various a priori knowledge assumptions. [28] and [29] propose the NLOS mitigation techniques based on time and space redundancy of range measurements, respectively. In [30], the scattering-model-based methods for NLOS mitigation are presented. More signal processing techniques for NLOS error mitigation can be found in [31, 32, 33, 34].

Overall there is no universally applicable range estimation method, and all the proposed algorithms have to trade off the location estimation performance with the availability of a priori or redundant information in practice. To evaluate the performance of different range measurement algorithms in multipath channels, efficient and tight theoretical performance bounds are desired to which the optimum estimation algorithms are expected to achieve in the high signal-to-noise ratio (SNR) region and stay close in the low SNR region. Such lower bounds provide useful tools for algorithm designers and researchers. Without testing particular estimation algorithms, the best achievable performance based on particular measurements can be readily evaluated. As the ToA localization based on TDE is the mostly adopted scheme, this thesis will focus on TDE, or ToA estimation, in the part of developing the performance limits for range measurements. Theoretical performance bounds on TDE serve as benchmarks for the ToA estimation algorithms and help to provide insight into the behavior of TDE.

Various TDE bounds have been developed in the past [35]. The Cramér-Rao bound (CRB) has been extensively applied for bounding TDE performance in the case of a deterministic channel [36, 37]. However, the CRB is only tight at high SNRs and not applicable for unknown random channel. Ziv-Zakai lower bound (ZZB) [38, 39] is another attractive approach among the Bayesian mean-square-error (MSE) bounds for predicting optimal estimation performance over a wide range of SNRs [40]. ZZBs on TDE have been developed for narrowband frequency-hopping channels [41], parallel narrowband flat-fading channels [42, 43], and for ultra-wideband signals in additive white Gaussian noise (AWGN) channels [44]. Bayesian bounds for TDE have also been developed by Weinstein and Weiss [40, 45]. In wideband random multipath channels, the average ZZB for TDE, assuming receivers know perfect channel realizations, is derived for a given channel realization and then averaged over the channel distributions [46] .

By the above literature review, the performance bounds for TDE have not been developed before for unknown random multipath channel, assuming that the receiver only knows the channel statistic, but does not know the channel realization. For the scenarios in which channel estimations are unavailable, these performance bounds are the important indications to the performance of TDE algorithms and thus motivate the author's research on this topic. Furthermore, the errors in ranging will essentially propagate to the position estimation error by different range-based localization schemes, in which NLOS errors in range estimates are expressed in terms of positively biased and additive noise contaminated variables. [47] proposed an iterative localization algorithm, in which the bias of range measurements is assumed deterministic and identical for all sensors, and treated as a variable to be estimated. In [48], a localization bound with biased measurements was developed in UWB environments, where the bias follows uniform distributions. As these existing results assume specific types of ranging bias, the localization performance with general bias in range measurements is not clear. This inspires the localization performance study in this thesis, which models the general ranging bias as either deterministic or random following several common distributions, and analyzes the localization errors of typical estimators.

1.3 Contributions and Outline of Thesis

The thesis consists of five chapters and three appendices and is organized as follows:

Chapter 2 introduces the range measurements and models for range-based localization schemes, mainly focusing on ToA trilateration and TDoA multilateration. The localization model, and the linearization and iterative estimator for ToA are briefly reviewed. Regarding TDoA localization, the author derives a geometric view on the

TDoA-based linear localization algorithm for a linear array. The error analysis and simulation results show the performance of the linear algorithm in comparison with the CRB for TDoA localization. In addition, the thesis analyzes the challenges for range-based localization in multipath environments, and surveys on the techniques of LOS path identification and NLOS error detection and mitigation.

In *Chapter 3* the author develops the TDE performance bounds in unknown random multipath channels. Specifically, the Bayesian mean-square-error bounds by the Ziv-Zakai approach are developed for both pulsed signal and wideband frequency hopping waveforms. The development assumes that the receiver knows the channel distribution, but does not know the channel realization. The transmitted signal is assumed known to the receiver, and the time delay has a uniform prior distribution. The ZZBs represents more realistic and tighter performance limits, and provide good performance prediction for maximum a posteriori (MAP) time delay estimation, tracking the low, medium, and high SNR regimes. The ZZB for frequency hopping waveforms also reveals achievable TDE performance with frequency diversity in wideband frequency-selective fading channels. In addition, to evaluate the ZZBs numerically, the author proposes a moment generating function (MGF) approach to compute the probability density function (pdf) of the log-likelihood ratio (LLR), and the compact form of this MGF approach greatly lowers the computation complexity. Several implementation issues for numerical evaluations are also discussed.

Chapter 4 explores the ToA localization performance in the wireless multipath environments, in which the erroneous ToA range measurements are modeled as the true time delay contaminated by both additive Guassian noise and unknown bias due to NLOS errors. Except for the case of deterministic bias, the convolved pdf for the sum noise and ranging bias is developed based on several possible distributions for random

ranging bias. With these range measurement models for multipath channel, the author derives the bias and MSE of the widely adopted weighted least-square (WLS) and maximum-likelihood (ML) location estimators. The error expressions are developed via perturbation analysis, providing a means to study achievable localization performance, as a function of the measurement bias and variance, the reference array geometry and number of reference transceivers, as well as the estimator type. The numerical examples compare the performance of WLS and ML estimators with the CRB, showing that in general the estimator produces biased estimates.

Chapter 5 highlights the contents of the thesis and the major results.

Appendix A shows the CRB for TDoA localization scheme in AWGN channels. *Appendix B* develops the MGF for the quadratic functions of a Gaussian random vector, used for evaluating the ZZBs in Chapter 3. The two sections correspond to the real and complex Gaussian random vectors, respectively. *Appendix C* presents the expressions of the pulse signals that are used in the numerical ZZB examples. Their autocorrelation functions and mean-square bandwidth expressions are also derived.

Chapter 2

Range-Based Localization

Among all the localization schemes introduced in Chapter 1, the localization methods based on pair-wise range measurements between wireless transceivers are widely used in practice because of its relatively high accuracy and the wide availability of range measurements in real systems. In these schemes the geometric ranges between transceivers are computed from measurements of ToA, RSS or TDoA, and these measurements allow the formation of statistical models for trilateration and multilateration localization, based on which the transceiver locations are estimated with signal processing algorithms of moderate complexity. In this chapter, Sections 2.1 and 2.2 review the trilateration and multilateration localization schemes, respectively, including the localization models, range or range-difference measurements, as well as the location estimation algorithms. The linear algorithm for TDoA localization has low complexity and thus is attractive in practical applications. In Section 2.2, the author provides a geometric view and detail error analysis with numerical simulations on the linear estimation algorithm.

Because wireless signals are propagated through the environments full of obstructions, reflectors and scatters, the range measurement for accurate localization is challeng-

ing in the real world. Generally, range measurements used for localization are affected by noise, interference and environment-dependent errors. The additive noise and interference from other transceivers can be mitigated by averaging over multiple measurements and filtering techniques. However, the environment-dependent errors are mainly due to the predominantly stationary objects in particular environments, and thus these errors only have slight variation over time and difficult to avoid in range measurements. The commonly used multipath channel in wireless communications is well-suited for modeling these environment-dependent errors, and Section 2.3 will discuss challenging range measurement in multipath channels.

2.1 Trilateration with ToA or RSS Measurement

Trilateration methods determine transceiver locations by range measurement using the geometry of circles on 2-D plane or spheres in 3-D space. On a 2-D plane, when the range measurements from the unknown-location transceiver to more than three known-location transceivers (reference points) can be obtained, the position estimate of the unknown-location transceiver is determined by the intersection of the three circles, shown in Fig. 2.1. Similarly, in the 3-D space, the unknown-location transceiver can be located by the intersection of spheres, formed by the range measurements from at least four reference points. More than three reference points on 2-D planes or four in the 3-D space will lead to overdetermined localization model. Affected by noise and interference, the final estimated location is a point in the intersection region in the maximum likelihood sense.

The circles or spheres of range measurements can be acquired by different kinds of measurements. The most common measurements for ranging include RSS, ToA,

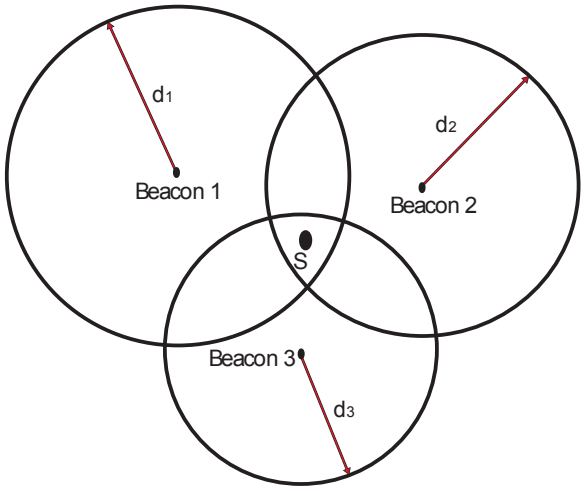

Figure 2.1: Geometry of ToA based location system.

and connectivity (Conn). The connectivity between two transceivers can be seen as the quantized version or approximation of the real range measurements, and then it is only appropriate for localization with low accuracy requirements in some network localization systems [11]. The next two subsections review the measurement models of RSS and ToA, which serve as the base for the trilateration localization model discussed in the last subsection.

2.1.1 Received Signal Strength Measurement

In most implementations RSS is reported as measured power, i.e., the squared magnitude of the signal strength. It can be measured in the receiver during normal data recovery without additional bandwidth or energy requirements. Because RSS measurements are simple to implement, they are preferred for low-cost localization system. The disadvantages are that it is unpredictable, and the dynamics of outdoor environment is usually along with low received RSS values. In practical environments, RSS varies

inversely with the distance d between the transmitter and the receiver as ([49])

$$\text{RSS} \propto \frac{1}{d^n} \tag{2.1}$$

where n is the path loss exponent (2 for free space). The ensemble mean power at distance d is typically modeled as ([2])

$$\bar{P}(d) = P_0 - 10n\log\frac{d}{d_0} \tag{2.2}$$

where P_0 is the received power (dBm) at a short reference distance d_0.

Due to the effect of shadowing, the standard deviation σ of RSS is modeled as log-normal [50, 51, 49]. Therefore the received power $P_{i,j}$ (dBm) at transceiver i transmitted by j, has the distribution as [2]

$$f(P_{i,j} = p|\boldsymbol{\theta}) = \mathcal{N}(p; \bar{P}(\|\mathbf{z}_i - \mathbf{z}_j\|), \sigma_{dB}^2), \tag{2.3}$$

where $\mathcal{N}(x; y, z)$ is the Gaussian p.d.f. for x with mean y and variance z, $\boldsymbol{\theta}$ is the coordinate parameter vector, and $\|\mathbf{z}_i - \mathbf{z}_j\|$ is the actual distance between transmitter and receiver.

With this distribution the maximum likelihood estimate can be derived as

$$d_{i,j}^{MLE} = d_0 10^{\frac{P_0 - P_{i,j}}{10n}} \tag{2.4}$$

and the expect value of $d_{i,j}^{MLE}$ is

$$\mathbb{E}\{d_{i,j}^{MLE}\} = C\|\mathbf{z}_i - \mathbf{z}_j\| \tag{2.5}$$

where $C = \exp(\gamma/2)$ and $\gamma = (\frac{10n}{\sigma_{dB}\log 10})^2$. The parameter C is a multiplicative bias factor. For typical channels, $C \approx 1.2$, adding 20% bias. Due to the log-normal model RSS-based range estimate has variance proportional to the actual range. This is why RSS errors are referred to as multiplicative.

2.1.2 Time of Arrival Measurement

Time of arrival, or time of flight, or time delay, is the time duration in which a signal travels from a transmitter to a receiver. When the receiver knows the transmitted time, ToA is equivalent to the propagation-induced time delay. The ToA between transceiver i and j is given by

$$T_{i,j} = \frac{\|\mathbf{z}_i - \mathbf{z}_j\|}{v_c}, \tag{2.6}$$

where v_c is the propagation velocity, and $\|\mathbf{z}_i - \mathbf{z}_j\|$ is defined in Eq. (2.3).

Generally range measurement by ToA is more accurate than RSS measurement because ToA is unaffected by the transmitting power and the path loss and fading effect of wireless channels. But all the time-based techniques depend on the accurate estimates of the arrival time of the LOS signal compoenent, which may be unavailable in some multipath channel environments. This issue will be discussed in more details in Section 2.3.

Measurements have shown that for short-range measurements in LOS channels, measured time delay can be roughly modeled with Gaussian distribution as [52, 53],

$$f(T_{i,j} = t|\boldsymbol{\theta}) = \mathcal{N}(t; (\|\mathbf{z}_i - \mathbf{z}_j\|)/v_c + \mu_T, \sigma_T^2), \tag{2.7}$$

where μ_T and σ_T^2 are the mean and variance of the time delay error, $\boldsymbol{\theta}$ is the same as in Eq. (2.3). Wideband DSSS measurements reported in [54] supported the Gaussian error model and showed $\mu_T = 10.9$ ns and $\sigma_T = 6.1$ ns. UWB measurements on a mostly-empty factory floor [16] showed $\mu_T = 0.3$ ns and $\sigma_T = 1.9$ ns. This mean error μ_T can be estimated (as a nuisance parameter) by the localization algorithm so that it can be subtracted out [55].

Other than the lack of LOS component in multipath channels, other issues exist in ToA measurement. The most significant is the relative clock bias between transmitters

and receivers. As ToA measurement acquires the absolute signal propagation time, small clock bias can generate huge ranging error by the high signal traveling speed. Thus clock tracking and bias correction is necessary, leading to increased implementation cost.

2.1.3 Trilateration Model and Algorithms

With pair-wise range measurements by ToA or RSS between the unknown-location transceiver and each reference point, one can build the trilateration model and estimate the unknown location. Assume the unknown-location transceiver in 3-D space is located at $\mathbf{p}_s = (x_s, y_s, z_s)$, and there are K reference transceivers for range measurement located at $\mathbf{p}_k = (x_k, y_k, z_k), k = 1, \cdots, K$. Then the trilateration positioning problem involves three unknown location quantities (x_s, y_s, z_s). For ToA based trilateration system, for example GPS [3], the receiver clock bias is treated as the fourth unknown quantity. Thus a system of equations representing the range measurements can be used to determine the unknowns, expressed as [3]

$$\begin{aligned} r_1 &= \sqrt{(x_1 - x_s)^2 + (y_1 - y_s)^2 + (z_1 - z_s)^2} + v_c \Delta t_r + \epsilon_1, \\ r_2 &= \sqrt{(x_2 - x_s)^2 + (y_2 - y_s)^2 + (z_2 - z_s)^2} + v_c \Delta t_r + \epsilon_2, \\ &\vdots \\ r_K &= \sqrt{(x_K - x_s)^2 + (y_K - y_s)^2 + (z_K - z_s)^2} + v_c \Delta t_r + \epsilon_K, \end{aligned} \tag{2.8}$$

in which $r_k, k = 1, \cdots, K$ are the range measurements between the unknown-location source and reference points, Δt_r is the receiver clock bias, v_c is the signal propagation speed, and $\epsilon_k, k = 1, \cdots, K$ are the composite measurement errors, including atmosphere delay, reference location errors, multipath error and receiver noise, etc. For trilateration with ToA measurements, if the receiver clock bias is treated as measurement error instead of an unknown quantity, $K \geq 3$ references or measurements are

required; otherwise, if the clock bias needs to be estimated, then $K \geq 4$ measurements are needed.

The system of equations in (2.8) is non-linear and the closed-form solutions exist [56, 57, 58]. However, the linearization technique by Taylor expansion is typically adopted in practical implementations as it is straightforward, converges quickly, and easy to be examined by linear error analysis. In addition, the linearization and solution procedure can be repeated iteratively for higher accuracy, with location estimations updated from the previous iteration. By linearization eq.(2.8) is expressed as

$$\mathbf{r} = \bar{\mathbf{r}} + \mathbf{H}\delta\mathbf{p} + \boldsymbol{\epsilon} + O(\delta\mathbf{p}), \tag{2.9}$$

or

$$\delta\mathbf{r} = \mathbf{r} - \bar{\mathbf{r}} = \mathbf{H}\delta\mathbf{p} + \boldsymbol{\epsilon} + O(\delta\mathbf{p}), \tag{2.10}$$

where $\mathbf{r} = [r_1, r_2, \cdots, r_K]^T$ is the range measurement vector, and $\bar{\mathbf{r}}$ is the range vector at the nominal point for linearization $\bar{\mathbf{p}} = (\bar{x}, \bar{y}, \bar{z})$, computed by substituting $\bar{\mathbf{p}}$ for $\mathbf{p}_s$ as $\bar{r_k} = \sqrt{(x_k - \bar{x})^2 + (y_k - \bar{y})^2 + (z_k - \bar{z})^2}, k = 1, \cdots, K$, and $\delta\mathbf{p} = [x_s - \bar{x}, y_s - \bar{y}, z_s - \bar{z}, v_c\Delta t_r]^T$. $\boldsymbol{\epsilon} = [\epsilon_1, \epsilon_2, \cdots, \epsilon_K]^t$ is the error vector, $O(\delta\mathbf{p})$ represents the higher-order terms in the linearization. Denote the true range for the kth reference point as $d_k = \sqrt{(x_k - x_s)^2 + (y_k - y_s)^2 + (z_k - z_s)^2}$, the geometric matrix $\mathbf{H}$ is dependent on the reference point locations, expressed as

$$\mathbf{H} = \begin{bmatrix} \frac{\partial d_1}{\partial x_s} & \frac{\partial d_1}{\partial y_s} & \frac{\partial d_1}{\partial z_s} & 1 \\ \frac{\partial d_2}{\partial x_s} & \frac{\partial d_2}{\partial y_s} & \frac{\partial d_2}{\partial z_s} & 1 \\ \vdots & \vdots & \vdots & \vdots \\ \frac{\partial d_K}{\partial x_s} & \frac{\partial d_K}{\partial y_s} & \frac{\partial d_K}{\partial z_s} & 1 \end{bmatrix}. \tag{2.11}$$

By ignoring the higher-order quantity $O(\delta\mathbf{p})$, the least-square solution to eq.(2.10) gives the estimation of $\delta\mathbf{p}$

$$\widehat{\delta\mathbf{p}} = (\mathbf{H}^T\mathbf{H})^{-1}\mathbf{H}^T\delta\mathbf{r}, \tag{2.12}$$

and the estimation of actual position is

$$\widehat{\mathbf{p}}_s = \bar{\mathbf{p}} + \widehat{\delta\mathbf{p}}. \tag{2.13}$$

Note that when iterative process is adopted, $\bar{\mathbf{p}}$ can be the location estimation in the previous iteration, and eq.(2.13) updates the estimation with the range measurement in the current iteration.

2.2 Multilateration with TDoA Measurements

Localization with TDoA measurements, also known as multilateration, was of much interest in the past [18]. Compared to ToA measurement and trilateration, TDoA measurement can be simply obtained by cross-correlation between two signals from two reference transceivers at different locations. Therefore, TDoA multilateration does not require accurate clock synchronization and bias correction between transmitters and receivers if only reference transceivers are synchronized with each other. In some practical applications, for instance sensor networks, low complexity is a requirement of high priority, and the absolute clock information from signal sources is mostly unavailable. Thus TDoA instead of ToA approaches are preferred.

2.2.1 Hyperbola Model

Consider a hyperbola shown in Fig. 2.2, where F_1 and F_2 are two foci, whose distance is $2c$. The difference of the distance from any point on the hyperbola to the

two foci is $2a$. If adopting a Cartesian coordinate system, the definition of hyperbola [59] is

$$\sqrt{(x+c)^2+y^2} - \sqrt{(x-c)^2+y^2} = 2a. \tag{2.14}$$

Moving the second term to the right, squaring both sides and after some manipulations, it becomes

$$\frac{x^2}{a^2} - \frac{y^2}{b^2} = 1,$$

where $b = \sqrt{c^2 - a^2}$. It is the standard equation of the hyperbola. For the general case that the center of hyperbola is not at the origin, the standard equation is

$$\frac{(x-x_c)^2}{a^2} - \frac{(y-y_c)^2}{b^2} = 1, \tag{2.15}$$

where (x_c, y_c) is the location of the center.

Consider a case of two receivers observing the signal from the source. The difference of the arrival time denoted by τ, depends on the path difference, denoted by d. As the signal propagates at speed v_c, then $d = v_c\tau$. Then what is known from the two receivers is the path difference from the source point to the receivers. Since hyperbola is the set of points that have the same difference in distance to two fix points, the source is on a hyperbola whose parameters are determined by the difference of arrival time and the distance of the two receivers, as shown in Fig.2.2. This is the basic idea of TDoA multilateration.

A hyperbola can also be defined as the locus of points whose distance from the focus is proportional to the horizontal distance from a vertical line known as the conic section directrix, where the ratio is the eccentricity $e = \frac{c}{a}$. As shown in Fig. 2.3, the equation of the right directrix is $x = x_R = \frac{a^2}{c}$. So for any point $P(x_P, y_P)$ on the hyperbola, the distance $D(P, F_2)$ to the right focus $F_2(c, 0)$ can be expressed as

$$D(P, F_2) = e|x_P - x_R|. \tag{2.16}$$

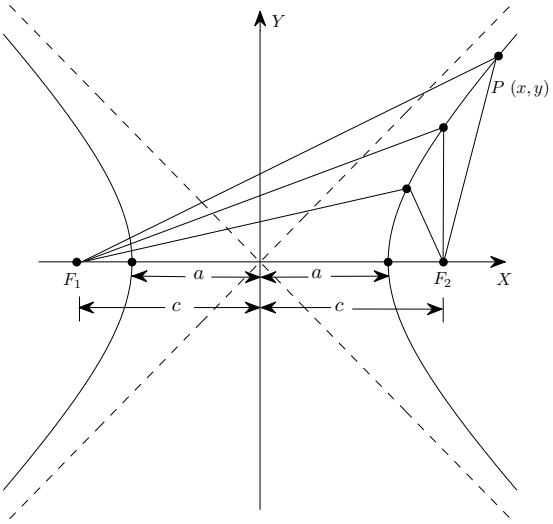

Figure 2.2: Definition of hyperbola.

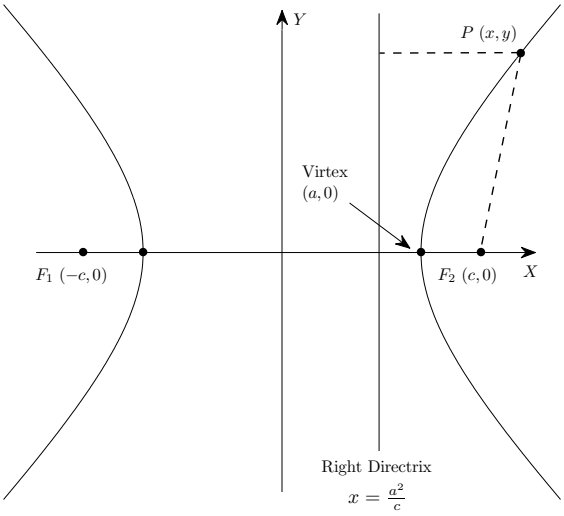

Figure 2.3: Directrix of a hyperbola.

Following the same line and using the left directrix $x = x_L = -\frac{a^2}{c}$, the distance $D(P, F_1)$ of any point $P(x_P, y_P)$ on the hyperbola to the left focus $F_1(-c, 0)$ is

$$D(P, F_1) = e|x_P - x_L|. \tag{2.17}$$

These two equations are fundamental to the development of the linear solver next.

2.2.2 Linear Algorithm for Multilateration with Linear Array

A traditional solver for TDoA localization involves linearization and iterative processing [18, 19], similar to the ToA localization algorithm described in Section 2.1.3. An iterative method typically incurs high computational complexity and its convergence requires initial estimate of the position at a tolerable accuracy. Closed-form algorithms for TDoA localization have been proposed in the past [60, 61, 62] with suboptimal estimators. [63] developed an explicit solution to TDoA multilateration exploiting a two-stage weighted least-square estimation process, which is an approximate realization of the maximum-likelihood estimator and is shown to achieve the Cramér-Rao bound in the high SNR region.

For applications requiring low-complexity implementation, localization with a linear array of reference transceivers is desired as the positioning process can be simplified. Some optimum processing techniques with different complexity and restrictions regarding linear array have been shown in [20, 64, 65]. This section will review the linear solver proposed in [60] from a geometric viewpoint when it is applied to linear sensor array [66]. Directrices of hyperbolas determined by TDoA measurements are used to obtain linear relations between the x-coordinate of the source and TDoAs of each reference pair in a linear array on the x-axis. Only moderate number of scalar multiplications and additions are involved, and no matrix inversion is required. Meanwhile, it is applicable

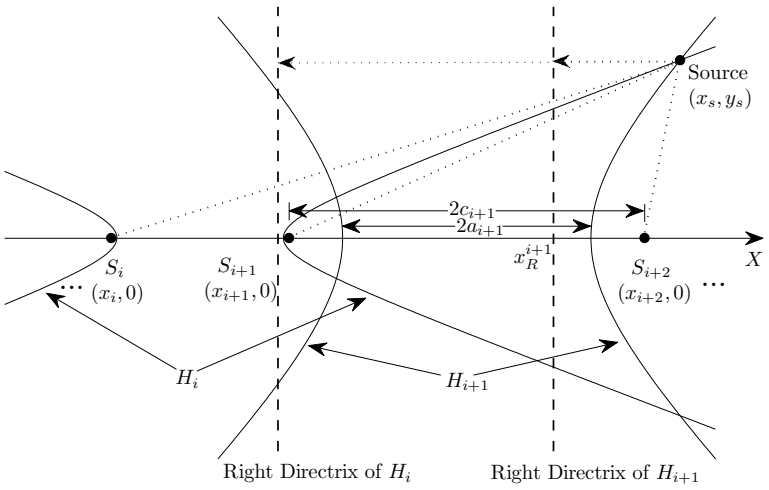

Figure 2.4: A linear sensor array with M sensors on X-axis. The signal source is at (x_s, y_s).

to both far-field and near-field setups. Localization performance is studied as well in the next subsection. Applying a perturbation technique, localization error and bias is derived analytically to be dependent on TDoA measurement errors.

Assume, in a sensor network application, a size M linear sensor array, from S_1 to S_M, is placed on the x-axis as shown in Fig. 2.4. The coordinates of S_i are $\mathbf{p}_i = [x_i, y_i]^T$, where $y_i = 0$. The signal source with unknown location is at $\mathbf{p}_s = [x_s, y_s]^T$. The hyperbola H_i centered in the middle of two sensors S_i and S_{i+1} is determined by the TDOA τ_i between them. Thus, the range difference $d_{i,i+1}$ from the TDOA τ_i is

$$d_{i,i+1} = v_c \tau_i = r_i - r_{i+1},\ i = 1, 2, \cdots, M-1, \tag{2.18}$$

where $r_i \triangleq \|\mathbf{p}_i - \mathbf{p}_s\|$ is the distance from the signal source to the ith sensor. In the following $d_{i,i+1}$ is replace by d_i to simplify the notation.

A closed-form solution for x_s can be derived directly from the alternative definition of a hyperbola: the locus of points whose distance from the focus is proportional to the horizontal distance from a vertical line known as the conic section directrix, where the ratio is the eccentricity. The signal source lies on a series of hyperbolas whose parameters

are determined by d_i as well as the distance between the two respective receiving sensors, as shown in Fig. 2.4. The parameters of hyperbola H_i can be obtained as

$$a_i = \frac{|d_i|}{2}, \quad c_i = \frac{x_{i+1} - x_i}{2}, \quad e_i = \frac{c_i}{a_i} = \frac{x_{i+1} - x_i}{|d_i|},$$

$$x_L^i = \frac{x_i + x_{i+1}}{2} - \frac{a_i^2}{c_i} = \frac{x_i + x_{i+1}}{2} - \frac{d_i^2}{2(x_{i+1} - x_i)}, \tag{2.19}$$

$$x_R^i = \frac{x_i + x_{i+1}}{2} + \frac{a_i^2}{c_i} = \frac{x_i + x_{i+1}}{2} + \frac{d_i^2}{2(x_{i+1} - x_i)}, \tag{2.20}$$

where e_i is the eccentricity of H_i, x_L^i and x_R^i are the x-coordinates of intersections of the left and right directrices of H_i with the horizontal axis respectively.

Since sensor $S_{i+1}(i = 1, 2, \cdots, M-2)$ is both the right focus of hyperbola H_i and the left focus of hyperbola H_{i+1}, the distance from the source to the sensor S_{i+1} can be equally expressed in terms of the directrices and eccentricities of both H_i and H_{i+1} as

$$e_i|x_s - x_R^i| = e_{i+1}|x_s - x_L^{i+1}|. \tag{2.21}$$

Note that $x_R^i < x_L^{i+1}$ always holds. Let ν_i be an indicator of relative location of source and sensor, equal to -1 when $x_R^i < x_s < x_L^{i+1}$, and 1 otherwise. The above equation can be written as

$$e_i(x_s - x_R^i) = \nu_i(e_{i+1}x_s - e_{i+1}x_L^{i+1}). \tag{2.22}$$

Substituting (2.19), (2.19) and (2.20), then (2.22) becomes

$$\left[\frac{x_{i+1} - x_i}{|d_i|} - \frac{\nu_i(x_{i+2} - x_{i+1})}{|d_{i+1}|}\right] x_s = \frac{x_{i+1}^2 - x_i^2}{2|d_i|} - \frac{\nu_i(x_{i+2}^2 - x_{i+1}^2)}{2|d_{i+1}|} + \frac{\nu_i|d_{i+1}| + |d_i|}{2}. \tag{2.23}$$

Collecting coefficients of x_s corresponding to $i = 1, \cdots, M-2$ in a column vector $\mathbf{e}$, and the right hand side in a column vector $\mathbf{g}$, the localization model can be written as

$$\mathbf{e}x_s = \mathbf{g}, \tag{2.24}$$

where

$$\mathbf{e} = \begin{bmatrix} \frac{x_2-x_1}{|d_1|} - \frac{\nu_1(x_3-x_2)}{|d_2|} \\ \vdots \\ \frac{x_{M-1}-x_{M-2}}{|d_{M-2}|} - \frac{\nu_{M-2}(x_M-x_{M-1})}{|d_{M-1}|} \end{bmatrix},$$

$$\mathbf{g} = \begin{bmatrix} \frac{x_2^2-x_1^2}{2|d_1|} - \frac{\nu_1(x_3^2-x_2^2)}{2|d_2|} + \frac{\nu_1|d_2|+|d_1|}{2} \\ \vdots \\ \frac{x_{M-1}^2-x_{M-2}^2}{2|d_{M-2}|} - \frac{\nu_{M-2}(x_M^2-x_{M-1}^2)}{2|d_{M-1}|} + \frac{\nu_{M-2}|d_{M-1}|+|d_{M-2}|}{2} \end{bmatrix}.$$

Eq. (2.24) is over-determined. By minimizing the following error

$$\widehat{x}_s = \underset{x_s}{\operatorname{argmin}} \|\mathbf{g} - x_s\mathbf{e}\|^2, \tag{2.25}$$

the least-square solution is

$$\widehat{x}_s = (\mathbf{e}^T\mathbf{e})^{-1}\mathbf{e}^T\mathbf{g}. \tag{2.26}$$

Notice that $\mathbf{e}^T\mathbf{e}$ is a scalar. No matrix inversion is required, but vector multiplications. The length of each vector is $M-2$.

From x_s, the location model for y_s can be obtained from $M-1$ hyperbola equations following a form of (2.15) as

$$\mathbf{f}y_s^2 = \mathbf{h}, \tag{2.27}$$

in which

$$\mathbf{f} = \begin{bmatrix} \frac{4}{(x_2-x_1)^2-d_1^2} \\ \vdots \\ \frac{4}{(x_M-x_{M-1})^2-d_{M-1}^2} \end{bmatrix}, \qquad \mathbf{h} = \begin{bmatrix} (\frac{2x_s-x_1-x_2}{d_1})^2 \\ \vdots \\ (\frac{2x_s-x_{M-1}-x_M}{d_{M-1}})^2 \end{bmatrix} - 1, \tag{2.28}$$

that suggests

$$y_s = \pm\sqrt{(\mathbf{f}^T\mathbf{f})^{-1}\mathbf{f}^T\mathbf{h}}. \tag{2.29}$$

By replacing x_s by its estimate $\widehat{x}_s$ in $\mathbf{h}$, an estimate of y_s is found from (2.29). Thus eq.(2.26) and (2.29) are the linear least-square (LS) solver for the source location.

The polarity of y_s and the value of ν_i depend on the source location relative to sensors. In a practical system, some prior information can be acquired through network or other measurements. For example, to determine ν_i, compare r_i, r_{i+1} and r_{i+2}. If $r_{i+1} < r_i$ and $r_{i+1} < r_{i+2}$, equivalently $d_i > 0$ and $d_{i+1} < 0$, then $\nu_i = -1$. Otherwise $\nu_i = 1$. In the following development, the attention is restricted to the case where the source sensor is located to the right of the sensor array, leading to $\nu_i = 1$ for all $i = 1, \cdots, M-2$ and $d_i > 0$ for all $i = 1, \cdots, M-1$. However, subsequent discussions are directly applicable to other scenarios. Also $y_s > 0$ is assumed to further resolve the ambiguity in estimating the source y-coordinate later on.

For comparison purposes, the maximum-likelihood estimator (MLE) can be derived assuming all noise samples from measuring d_i are jointly Gaussian. Denote noise covariance matrix by $\mathbf{C}_d$. Then the MLE can be described by

$$(x_s^{\mathrm{ML}}, y_s^{\mathrm{ML}}) = \underset{(x_s, y_s)}{\operatorname{argmin}} \ \mathbf{m}^T \mathbf{C}_d^{-1} \mathbf{m}, \tag{2.30}$$

where the i-th term of $\mathbf{m}$ is $\sqrt{(x_s - x_i)^2 + y_s^2} - \sqrt{(x_s - x_{i+1})^2 + y_s^2} - d_i$.

The advantage of the least-square estimator is that it is a linear solver in a closed-form and thus has a much lower computation complexity compared to the MLE or other iterative algorithms. If the MLE is implemented using a gradient method, the number of multiplications is at the order of MN, where N is the number of iterations. The linear estimator is at the order of M. When the required precision is high, N for MLE could be a very large number. Moreover the closed-form linear estimator does not have the slow convergence problem since it does not need an iterating process.

2.2.2.1 Connection with the Linear Algorithm for Arbitrary Array

The above development of the linear estimator for linear array presents a geometric perspective, which can be linked to the general solution proposed for arbitrary array in [60]. To show this, let us briefly review that approach. Consider an arbitrary sensor array which is not necessarily linear nor on the x-axis. Denote the sensor coordinates as $\mathbf{p}_i = [x_i, y_i]^T$, where $y_i = 0$ does not always hold. The distance from the origin to S_i is $R_i \stackrel{\Delta}{=} \|\mathbf{p}_i\|$. To be consistent with notation in [60], this section uses $d_{i,j}$ for range-difference, and $\tau_{i,j}$ for TDOA.

In [60], a nuisance parameter r_j is introduced, that is the distance from the source to an arbitrary reference sensor S_j in the array. The algorithm derivation starts from the definitions of r_i, and range difference $d_{i,j}$. After some algebraic manipulation, the following is obtained (eqn. (6) in [60])

$$(\mathbf{p}_i - \mathbf{p}_j)^T \mathbf{p}_0 = (R_i^2 - R_j^2 - d_{i,j}^2)/2 - r_j d_{i,j}, \quad i = 1 \cdots M, \ i \neq j. \tag{2.31}$$

Collecting all $M-1$ equations into a matrix form yields

$$\mathbf{S}_j \mathbf{p}_0 = \boldsymbol{\mu}_j - r_j \boldsymbol{\rho}_j, \tag{2.32}$$

where the ith rows of $\mathbf{S}_j$, $\boldsymbol{\mu}_j$ and $\boldsymbol{\rho}_j$ are $(\mathbf{p}_i - \mathbf{p}_j)^T$, $(R_i^2 - R_j^2 - d_{i,j}^2)/2$ and $d_{i,j}$, respectively. The nuisance parameter r_j, which depends on unknown $\mathbf{p}_0$, can be nicely eliminated after pre-multiplication by a null-space matrix of $\boldsymbol{\rho}_j$, denoted $\mathbf{M}_j$ (so that $\mathbf{M}_j \boldsymbol{\rho}_j = 0$),

$$\mathbf{M}_j \mathbf{S}_j \mathbf{p}_0 = \mathbf{M}_j \boldsymbol{\mu}_j. \tag{2.33}$$

A closed-form solution is then obtained as

$$\mathbf{p}_0 = (\mathbf{S}_j^T \mathbf{M}_j^T \mathbf{M}_j \mathbf{S}_j)^{-1} \boldsymbol{\mu}_j^T \mathbf{M}_j^T \mathbf{M}_j \boldsymbol{\mu}_j, \tag{2.34}$$

as long as matrix $\mathbf{M}_j\mathbf{S}_j$ has full column rank, which is highly probable for an arbitrary array of sufficient size. Note, however, that this algorithm excludes a linear array geometry because in this case $\mathbf{M}_j\mathbf{S}_j$ is singular.

In particular, for a linear array on the x-axis as in Fig. 2.4, the location of S_i becomes $\mathbf{p}_i = [x_i, 0]^T$. Thus, matrix $\mathbf{S}_j$ has an all-zero column and loses column rank. Now, from (2.33), only x_s can be determined, and y_s must be estimated by another method, such as via (2.29). For simplicity, suppose the sensor S_1 is chosen as the reference sensor. The hyperbola H_i with two foci S_1 and S_i is determined by the range difference $d_{i,1}$. Substituting expression for $\mathbf{M}_j$, $\mathbf{S}_j$ and $\boldsymbol{\mu}_j$ into (2.33) yields $M-1$ equations, but only $M-2$ are independent equations since any equation can be obtained as a linear combination of the other $M-2$ equations. Excluding the last equation, the remaining $M-2$ equations can be arranged as

$$\bar{\mathbf{e}} x_s = \bar{\mathbf{g}}, \tag{2.35}$$

where the i-th element of $\bar{\mathbf{e}}$ is $\frac{x_{i+1}-x_1}{d_{1,i+1}} - \frac{x_{i+2}-x_1}{d_{1,i+2}}$, and the i-th element of $\bar{\mathbf{g}}$ is $\frac{x_{i+1}^2-x_1^2}{2d_{1,i+1}} - \frac{x_{i+2}^2-x_1^2}{2d_{1,i+2}} + \frac{d_{1,i+2}-d_{1,i+1}}{2}$, for $i = 1, \cdots, M-2$.

Referring back to Section 2.2.2, with S_1 as the reference sensor, the range difference becomes $d_{1,i}, (i \neq 1)$ for sensors S_1 and S_i. The hyperbola H_i has the following parameters

$$\bar{a}_i = \frac{|d_{1,i}|}{2}, \tag{2.36}$$

$$\bar{c}_i = \frac{x_i - x_1}{2}, \tag{2.37}$$

$$\bar{e}_i = \frac{\bar{c}_i}{\bar{a}_i} = \frac{x_i - x_1}{|d_{1,i}|}, \tag{2.38}$$

$$\bar{x}_L^i = \frac{x_1 + x_i}{2} - \frac{\bar{a}_i^2}{\bar{c}_i} = \frac{x_1 + x_i}{2} - \frac{d_{1,i}^2}{2(x_i - x_1)}. \tag{2.39}$$

Now the distance r_1 from the source to sensor S_1 can be written in $M-1$ equations as

$$\begin{aligned} r_1 &= (x_s - \bar{x}_L^i)\bar{e}_i \\ &= \Big[x_s - \frac{x_1 + x_i}{2} + \frac{d_{1,i}^2}{2(x_i - x_1)}\Big]\frac{x_i - x_1}{d_{1,i}} \\ &= \frac{x_i - x_1}{d_{1,i}}x_s - \frac{x_i^2 - x_1^2}{2d_{1,i}} + \frac{d_{1,i}}{2}. \end{aligned} \tag{2.40}$$

Subtracting two consecutive equations for $i = 2, \cdots, M$ produces $M-2$ equations, which can be written in a matrix form identical to (2.35). Therefore, the WLS solution for x_s is mathematically equivalent to a modified version of the algorithm in [60] when the sensor array is linear and the reference sensor is fixed.

The derivation of the linear estimator for linear array provides an intuitive view and a geometric interpretation. The next subsection continues on to develop bias and mean-square error expressions for the linear algorithm with linear array.

2.2.3 Error Analysis on the Linear Algorithm

The location estimation error may be from the errors of TDoA measurements or inaccurate coordinates of sensors. Here only the TDoA measurement errors are considered, denoted by $\delta\mathbf{d} = [\delta d_1, \cdots, \delta d_{M-1}]^T$. For simplicity, assume these errors have zero means. However, the following analysis can easily incorporate non-zero means. If they are independent, then $\mathbf{C}_d$ becomes diagonal

$$\mathbf{C}_d = E\{(\delta\mathbf{d})(\delta\mathbf{d})^T\} = \text{diag}\{\sigma_1^2, \cdots, \sigma_{M-1}^2\}. \tag{2.41}$$

These errors will introduce errors to $\mathbf{e}$ and $\mathbf{g}$ in (2.26). Denoting the square error vector as $\boldsymbol{\epsilon} = [(\delta d_1)^2, \cdots, (\delta d_{M-1})^2]^T$, second-order perturbation analysis yields their errors as

$$\delta\mathbf{e} \approx \mathbf{P}\delta\mathbf{d} + \mathbf{R}\boldsymbol{\epsilon}, \tag{2.42}$$

$$\delta\mathbf{g} \approx \mathbf{Q}\delta\mathbf{d} + \mathbf{S}\boldsymbol{\epsilon}, \tag{2.43}$$

where

$$\mathbf{P} = \begin{bmatrix} p_1 & -p_2 & 0 & \dots & 0 \\ 0 & p_2 & -p_3 & \ddots & \vdots \\ \vdots & \ddots & \ddots & \ddots & 0 \\ 0 & \dots & 0 & p_{M-2} & -p_{M-1} \end{bmatrix},$$

$$\mathbf{Q} = \begin{bmatrix} \frac{q_1+1}{2} & \frac{-q_2+1}{2} & 0 & \dots & 0 \\ 0 & \frac{q_2+1}{2} & \frac{-q_3+1}{2} & \ddots & \vdots \\ \vdots & \ddots & \ddots & \ddots & 0 \\ 0 & \dots & 0 & \frac{q_{M-2}+1}{2} & \frac{-q_{M-1}+1}{2} \end{bmatrix},$$

$$\mathbf{R} = \begin{bmatrix} r_1 & -r_2 & 0 & \dots & 0 \\ 0 & r_2 & -r_3 & \ddots & \vdots \\ \vdots & \ddots & \ddots & \ddots & 0 \\ 0 & \dots & 0 & r_{M-2} & -r_{M-1} \end{bmatrix},$$

$$\mathbf{S} = \begin{bmatrix} s_1 & -s_2 & 0 & \dots & 0 \\ 0 & s_2 & -s_3 & \ddots & \vdots \\ \vdots & \ddots & \ddots & \ddots & 0 \\ 0 & \dots & 0 & s_{M-2} & -s_{M-1} \end{bmatrix}, \tag{2.44}$$

whose entries are related to p_i, q_i, r_i and s_i, $i = 1, \cdots, M-1$, defined as

$$p_i = \frac{x_i - x_{i+1}}{d_i^2}, \quad q_i = \frac{x_i^2 - x_{i+1}^2}{d_i^2}, \quad r_i = \frac{x_{i+1} - x_i}{d_i^3}, \quad s_i = \frac{x_{i+1}^2 - x_i^2}{2d_i^3}. \tag{2.45}$$

These errors lead to an error δx_s in estimating x_s. It can be derived from (2.26). Replace $\mathbf{e}$ by $\mathbf{e} + \delta\mathbf{e}$ and $\mathbf{g}$ by $\mathbf{g} + \delta\mathbf{g}$ respectively, and substitute (2.42) and (2.43). The estimation error up to the second order of $\delta\mathbf{d}$ can be easily found to be

$$\delta x_s \approx \mathbf{u}^T \delta\mathbf{d} + \delta\mathbf{d}^T \mathbf{V} \delta\mathbf{d} + \mathbf{w}^T \boldsymbol{\epsilon}, \tag{2.46}$$

where

$$\mathbf{u} = \frac{(\mathbf{e}^T\mathbf{e})\mathbf{P}^T\mathbf{g} - 2(\mathbf{e}^T\mathbf{g})\mathbf{P}^T\mathbf{e} + (\mathbf{e}^T\mathbf{e})\mathbf{Q}^T\mathbf{e}}{(\mathbf{e}^T\mathbf{e})^2}, \quad \mathbf{w} = \frac{(\mathbf{e}^T\mathbf{e})\mathbf{R}^T\mathbf{g} - 2(\mathbf{e}^T\mathbf{g})\mathbf{R}^T\mathbf{e} + (\mathbf{e}^T\mathbf{e})\mathbf{S}^T\mathbf{e}}{(\mathbf{e}^T\mathbf{e})^2},$$

$$\mathbf{V} = \frac{\mathbf{P}^T\mathbf{Q}}{\mathbf{e}^T\mathbf{e}} + \frac{4(\mathbf{e}^T\mathbf{g})\mathbf{P}^T\mathbf{e}\mathbf{e}^T\mathbf{P}}{(\mathbf{e}^T\mathbf{e})^3} - \frac{2\mathbf{P}^T\mathbf{e}\mathbf{g}^T\mathbf{P} + 2\mathbf{P}^T\mathbf{e}\mathbf{e}^T\mathbf{Q} + (\mathbf{e}^T\mathbf{g})\mathbf{P}^T\mathbf{P}}{(\mathbf{e}^T\mathbf{e})^2}.$$

The second order terms in (2.46) helps to obtain the mean error $E\{\delta x_s\}$ of the estimate. Expressing $\boldsymbol{\epsilon}$ as $\text{diag}\{(\delta d_1)^2, \cdots, (\delta d_{M-1})^2\}\mathbf{1}$ where $\mathbf{1} = [1, \cdots, 1]^T$, the mean error is

$$\beta_x \triangleq E\{\delta x_s\} = tr\{\mathbf{V}\mathbf{C}_d\} + \mathbf{w}^T(\mathbf{C}_d \odot \mathbf{I})\mathbf{1}, \tag{2.47}$$

where $\odot$ represents Hadamard product, $\mathbf{I}$ is an identity matrix of dimension $M-1$.

Keeping the first order term in (2.46), the mean-square error in estimating x_s is obtained as

$$\gamma_x^2 \triangleq E[(\widehat{x}_s - x_s)^2] = E\{(\delta x_s)^2\} \approx \mathbf{u}^T\mathbf{C}_d\mathbf{u}. \tag{2.48}$$

Eq. (2.48) shows that the MSE is approximately proportional to the variance of d_i. This trend will also be observed from the simulation results in the next section.

To obtain the estimation error for y_s, consider y_s^2 first for convenience. Notice that the square of (2.29) has a similar form as (2.26). The errors in measuring all d_i bring errors to $\mathbf{f}$ and $\mathbf{h}$ up to the second order of $\delta\mathbf{d}$ as

$$\delta\mathbf{f} \approx \mathbf{A}\delta\mathbf{d} + \mathbf{J}\boldsymbol{\epsilon}, \tag{2.49}$$

$$\delta\mathbf{h} \approx \mathbf{B}\delta\mathbf{d} + \mathbf{l}\delta\mathbf{d}^T\mathbf{V}\delta\mathbf{d} + \mathbf{K}\delta\mathbf{d}\delta\mathbf{d}^T\mathbf{u} + \mathbf{l}\mathbf{w}^T\boldsymbol{\epsilon}, \tag{2.50}$$

where

$$\mathbf{A} = \text{diag}\{a_1, \cdots, a_{M-1}\}, \quad \mathbf{J} = \text{diag}\{j_1, \cdots, j_{M-1}\}, \quad \mathbf{l} = [l_1, \cdots, l_{M-1}]^T,$$

$$\mathbf{B} = \text{diag}\{b_1, \cdots, b_{M-1}\} + \mathbf{l}\mathbf{u}^T, \quad \mathbf{K} = \text{diag}\{k_1, \cdots, k_{M-1}\} + [\frac{4}{d_1^2}, \cdots, \frac{4}{d_{M-1}^2}]^T\mathbf{u}^T, \tag{2.51}$$

whose entries are related to a_i, b_i, j_i, k_i and l_i defined as

$$a_i = \frac{8d_i}{[(x_{i+1}-x_i)^2 - d_i^2]^2}, \quad b_i = \frac{-2(2x_s - x_{i+1} - x_i)^2}{d_i^3},$$

$$j_i = \frac{4(x_{i+1}-x_i)^2 + 12d_i^2}{[(x_{i+1}-x_i)^2 - d_i^2]^3}, \quad k_i = \frac{8(x_{i+1}-x_i-2x_s)}{d_i^3}, \quad l_i = \frac{4(2x_s - x_{i+1} - x_i)}{d_i^2},$$

for $i = 1, \cdots, M-1$.

Applying the similar perturbation analysis technique as before, the error in estimating y_s^2 up to the second order of $\delta\mathbf{d}$ can be derived from as

$$\delta(y_s^2) \approx \boldsymbol{\eta}^T \delta\mathbf{d} + \delta\mathbf{d}^T \mathbf{T} \delta\mathbf{d} + \boldsymbol{\lambda}^T \boldsymbol{\epsilon}, \tag{2.52}$$

where

$$\begin{aligned}
\boldsymbol{\eta} &= \frac{(\mathbf{f}^T\mathbf{f})\mathbf{A}^T\mathbf{h} - 2(\mathbf{f}^T\mathbf{h})\mathbf{A}^T\mathbf{f} + (\mathbf{f}^T\mathbf{f})\mathbf{B}^T\mathbf{f}}{(\mathbf{f}^T\mathbf{f})^2}, \\
\mathbf{T} &= \frac{\mathbf{A}^T\mathbf{B} + \mathbf{f}^T\mathbf{l}\mathbf{V} + \mathbf{u}\mathbf{f}^T\mathbf{K}}{\mathbf{f}^T\mathbf{f}} + \frac{4(\mathbf{f}^T\mathbf{h})\mathbf{A}^T\mathbf{f}\mathbf{f}^T\mathbf{A}}{(\mathbf{f}^T\mathbf{f})^3} - \frac{2\mathbf{A}^T\mathbf{f}\mathbf{h}^T\mathbf{A} + 2\mathbf{A}^T\mathbf{f}\mathbf{f}^T\mathbf{B} + (\mathbf{f}^T\mathbf{h})\mathbf{A}^T\mathbf{A}}{(\mathbf{f}^T\mathbf{f})^2}, \\
\boldsymbol{\lambda} &= \frac{(\mathbf{f}^T\mathbf{f})\mathbf{J}^T\mathbf{h} - 2(\mathbf{f}^T\mathbf{h})\mathbf{J}^T\mathbf{f} + (\mathbf{f}^T\mathbf{f})\mathbf{w}\mathbf{l}^T\mathbf{f}}{(\mathbf{f}^T\mathbf{f})^2}.
\end{aligned} \tag{2.53}$$

Since $\delta(y_s^2) = 2y_s\delta y_s$, using (2.52), the mean error β_y and MSE γ_y^2 in estimating y_s can be found in terms of $\delta(y_s^2)$ as follows

$$\beta_y \triangleq E\{\delta y_s\} \approx \frac{E\{\delta(y_s^2)\}}{2y_s} = \frac{tr\{\mathbf{T}\mathbf{C}_d\} + \boldsymbol{\lambda}^T(\mathbf{C}_d \odot \mathbf{I})\mathbf{1}}{2y_s}, \tag{2.54}$$

$$\gamma_y^2 \triangleq E\{(\delta y_s)^2\} \approx \frac{E\{[\delta(y_s^2)]^2\}}{4y_s^2} = \frac{\boldsymbol{\eta}^T\mathbf{C}_d\boldsymbol{\eta}}{4y_s^2}. \tag{2.55}$$

These analytical results will be verified by simulations.

2.2.4 Optimum Weighted Least-Square Linear Solution

In the above closed-form linear algorithm, linear localization equations (2.24) and (2.27) are solved by the standard least squares technique. To improve the localization performance, it is possible to use the weighted least-square procedure instead. Then the

covariance matrices of the error vectors on both x- and y-coordinates need to be found firstly. In practice, the covariance matrices can be obtained by using previous estimated location via an iterative process. The following derivation is based on the theoretical error analysis in the previous section. The error vector in estimating x_s is

$$\boldsymbol{\phi}_x = \delta\mathbf{g} - x_s\delta\mathbf{e} \approx (\mathbf{Q} - x_s\mathbf{P})\delta\mathbf{d} + (\mathbf{S} - x_s\mathbf{R})\boldsymbol{\epsilon}, \tag{2.56}$$

and the mean vector of $\boldsymbol{\phi}_x$ is

$$E\{\boldsymbol{\phi}_x\} = E\{\delta\mathbf{g}\} - x_s E\{\delta\mathbf{e}\} \approx (\mathbf{S} - x_s\mathbf{R})(\mathbf{C}_d \odot \mathbf{I})\mathbf{1}, \tag{2.57}$$

because $E\{\delta\mathbf{d}\} = 0$. In practice the second-order item is small. When ignoring the second-order item in (2.56), $\boldsymbol{\phi}_x$ becomes a Gaussian vector, and the the covariance is

$$\boldsymbol{\Phi}_x = E\{\boldsymbol{\phi}_x\boldsymbol{\phi}_x^T\} \approx (\mathbf{Q} - x_s\mathbf{P})\mathbf{C}_d(\mathbf{Q} - x_s\mathbf{P})^T \tag{2.58}$$

Similarly, the error vector in estimating y-coordinate is

$$\boldsymbol{\phi}_y = \delta\mathbf{h} - y_s^2\delta\mathbf{f} \approx (\mathbf{B} - y_s^2\mathbf{A})\delta\mathbf{d} + (\mathbf{l}\mathbf{w}^T - y_s^2\mathbf{J})\boldsymbol{\epsilon} + \mathbf{l}\delta\mathbf{d}^T\mathbf{V}\delta\mathbf{d} + \delta\mathbf{d}^T\mathbf{u}\mathbf{K}\delta\mathbf{d}. \tag{2.59}$$

The mean vector of $\boldsymbol{\phi}_y$ is

$$E\{\boldsymbol{\phi}_y\} = E\{\delta\mathbf{h}\} - y_s^2 E\{\delta\mathbf{f}\} \approx (\mathbf{l}\mathbf{w}^T - y_s^2\mathbf{J})(\mathbf{C}_d \odot \mathbf{I})\mathbf{1} + \mathbf{l}tr\{\mathbf{V}\mathbf{C}_d\} + \mathbf{K}\mathbf{C}_d\mathbf{u}, \tag{2.60}$$

and the covariance matrix when ignoring the second-order items is

$$\boldsymbol{\Phi}_y = E\{\boldsymbol{\phi}_y\boldsymbol{\phi}_y^T\} \approx (\mathbf{B} - y_s^2\mathbf{A})\mathbf{C}_d(\mathbf{B} - y_s^2\mathbf{A})^T \tag{2.61}$$

With the covariance matrix, the x-coordinate estimation in (2.25) and (2.26) is optimized as

$$\begin{aligned} \widehat{x}_s &= \underset{x_s}{\operatorname{argmin}}\{(\mathbf{g} - x_s\mathbf{e})^T\mathbf{W}_x(\mathbf{g} - x_s\mathbf{e})\} \\ &= (\mathbf{e}^T\mathbf{W}_x\mathbf{e})^{-1}\mathbf{e}^T\mathbf{W}_x\mathbf{g}, \end{aligned} \tag{2.62}$$

in which $\mathbf{W}_x = \mathbf{\Phi}_x^{-1}$ is the weighting matrix. Eq.(2.62) is recognized as the WLS solution of (2.24). Also the y-coordinate WLS estimation can be found as

$$\begin{aligned}\widehat{y}_s &= \underset{y_s}{\operatorname{argmin}}\{(\mathbf{h} - y_s^2\mathbf{f})^T\mathbf{W}_y(\mathbf{h} - y_s^2\mathbf{f})\} \\ &= \pm\sqrt{(\mathbf{f}^T\mathbf{W}_y\mathbf{f})^{-1}\mathbf{f}^T\mathbf{W}_y\mathbf{h}},\end{aligned} \tag{2.63}$$

with $\mathbf{W}_y = \mathbf{\Phi}_y^{-1}$. For best performance, the weighting matrices $\mathbf{W}_x$ and $\mathbf{W}_y$ depend on the true source location, and can be found either by an iterative process based on the previous estimated location [60], or from the signal and noise power spectra [63]. The simulation results in the later section will use the theoretical error analysis results detailed in Section 2.2.3 to build the optimal weighting matrices.

The error analysis for WLS algorithm follows the similar procedure for the LS algorithm in Section 2.2.3, and the estimation bias and MSE have the same expressions as in eq.(2.47), (2.48), (2.54) and (2.55), except with the appropriate insertion of $\mathbf{W}_x$ and $\mathbf{W}_y$ in to the variables $\mathbf{u}$, $\mathbf{V}$ and $\mathbf{w}$, $\boldsymbol{\eta}$, $\mathbf{T}$ and $\boldsymbol{\lambda}$

$$\mathbf{u} = \frac{(\mathbf{e}^T\mathbf{\Phi}_x^{-1}\mathbf{e})\mathbf{P}^T\mathbf{\Phi}_x^{-1}\mathbf{g} - 2(\mathbf{e}^T\mathbf{\Phi}_x^{-1}\mathbf{g})\mathbf{P}^T\mathbf{\Phi}_x^{-1}\mathbf{e}}{(\mathbf{e}^T\mathbf{\Phi}_x^{-1}\mathbf{e})^2} + \frac{(\mathbf{e}^T\mathbf{\Phi}_x^{-1}\mathbf{e})\mathbf{Q}^T\mathbf{\Phi}_x^{-1}\mathbf{e}}{(\mathbf{e}^T\mathbf{\Phi}_x^{-1}\mathbf{e})^2}, \tag{2.64}$$

$$\begin{aligned}\mathbf{V} = &\frac{\mathbf{P}^T\mathbf{\Phi}_x^{-1}\mathbf{Q}}{\mathbf{e}^T\mathbf{\Phi}_x^{-1}\mathbf{e}} + \frac{4(\mathbf{e}^T\mathbf{\Phi}_x^{-1}\mathbf{g})\mathbf{P}^T\mathbf{\Phi}_x^{-1}\mathbf{e}\mathbf{e}^T\mathbf{\Phi}_x^{-1}\mathbf{P}}{(\mathbf{e}^T\mathbf{\Phi}_x^{-1}\mathbf{e})^3} \\ &- \frac{2\mathbf{P}^T\mathbf{\Phi}_x^{-1}\mathbf{e}(\mathbf{g}^T\mathbf{\Phi}_x^{-1}\mathbf{P} + \mathbf{e}^T\mathbf{\Phi}_x^{-1}\mathbf{Q})}{(\mathbf{e}^T\mathbf{\Phi}_x^{-1}\mathbf{e})^2} + \frac{(\mathbf{e}^T\mathbf{\Phi}_x^{-1}\mathbf{g})\mathbf{P}^T\mathbf{\Phi}_x^{-1}\mathbf{P}}{(\mathbf{e}^T\mathbf{\Phi}_x^{-1}\mathbf{e})^2},\end{aligned} \tag{2.65}$$

$$\mathbf{w} = \frac{(\mathbf{e}^T\mathbf{\Phi}_x^{-1}\mathbf{e})\mathbf{R}^T\mathbf{\Phi}_x^{-1}\mathbf{g} - 2(\mathbf{e}^T\mathbf{\Phi}_x^{-1}\mathbf{g})\mathbf{R}^T\mathbf{\Phi}_x^{-1}\mathbf{e}}{(\mathbf{e}^T\mathbf{\Phi}_x^{-1}\mathbf{e})^2} + \frac{(\mathbf{e}^T\mathbf{\Phi}_x^{-1}\mathbf{e})\mathbf{W}^T\mathbf{\Phi}_x^{-1}\mathbf{e}}{(\mathbf{e}^T\mathbf{\Phi}_x^{-1}\mathbf{e})^2}, \tag{2.66}$$

$$\boldsymbol{\eta} = \frac{(\mathbf{f}^T\mathbf{\Phi}_{y^2}^{-1}\mathbf{f})\mathbf{U}^T\mathbf{\Phi}_{y^2}^{-1}\mathbf{h} - 2(\mathbf{f}^T\mathbf{\Phi}_{y^2}^{-1}\mathbf{h})\mathbf{U}^T\mathbf{\Phi}_{y^2}^{-1}\mathbf{f}}{(\mathbf{f}^T\mathbf{\Phi}_{y^2}^{-1}\mathbf{f})^2} + \frac{(\mathbf{f}^T\mathbf{\Phi}_{y^2}^{-1}\mathbf{f})\mathbf{B}^T\mathbf{\Phi}_{y^2}^{-1}\mathbf{f}}{(\mathbf{f}^T\mathbf{\Phi}_{y^2}^{-1}\mathbf{f})^2}, \tag{2.67}$$

$$\begin{aligned}\mathbf{T} = &\frac{\mathbf{U}^T\mathbf{\Phi}_{y^2}^{-1}\mathbf{B} + \mathbf{f}^T\mathbf{\Phi}_{y^2}^{-1}\mathbf{l}\mathbf{v} + \mathbf{u}\mathbf{f}^T\mathbf{\Phi}_{y^2}^{-1}\mathbf{K}}{\mathbf{f}^T\mathbf{\Phi}_{y^2}^{-1}\mathbf{f}} + \frac{4(\mathbf{f}^T\mathbf{\Phi}_{y^2}^{-1}\mathbf{h})\mathbf{U}^T\mathbf{\Phi}_{y^2}^{-1}\mathbf{f}\mathbf{f}^T\mathbf{\Phi}_{y^2}^{-1}\mathbf{U}}{(\mathbf{f}^T\mathbf{\Phi}_{y^2}^{-1}\mathbf{f})^3} \\ &- \frac{2\mathbf{U}^T\mathbf{\Phi}_{y^2}^{-1}\mathbf{f}\mathbf{h}^T\mathbf{\Phi}_{y^2}^{-1}\mathbf{U} + 2\mathbf{U}^T\mathbf{\Phi}_{y^2}^{-1}\mathbf{f}\mathbf{f}^T\mathbf{\Phi}_{y^2}^{-1}\mathbf{B}}{(\mathbf{f}^T\mathbf{\Phi}_{y^2}^{-1}\mathbf{f})^2} + \frac{(\mathbf{f}^T\mathbf{\Phi}_{y^2}^{-1}\mathbf{h})\mathbf{U}^T\mathbf{\Phi}_{y^2}^{-1}\mathbf{U}}{(\mathbf{f}^T\mathbf{\Phi}_{y^2}^{-1}\mathbf{f})^2},\end{aligned} \tag{2.68}$$

$$\boldsymbol{\lambda} = \frac{(\mathbf{f}^T\mathbf{\Phi}_{y^2}^{-1}\mathbf{f})\mathbf{J}^T\mathbf{\Phi}_{y^2}^{-1}\mathbf{h} - 2(\mathbf{f}^T\mathbf{\Phi}_{y^2}^{-1}\mathbf{h})\mathbf{J}^T\mathbf{\Phi}_{y^2}^{-1}\mathbf{f}}{(\mathbf{f}^T\mathbf{\Phi}_{y^2}^{-1}\mathbf{f})^2} + \frac{(\mathbf{f}^T\mathbf{\Phi}_{y^2}^{-1}\mathbf{f})\mathbf{w}\mathbf{l}^T\mathbf{\Phi}_{y^2}^{-1}\mathbf{f}}{(\mathbf{f}^T\mathbf{\Phi}_{y^2}^{-1}\mathbf{f})^2}, \tag{2.69}$$

in which $\mathbf{u}$, $\mathbf{V}$ and $\mathbf{w}$, $\boldsymbol{\eta}$, $\mathbf{T}$ and $\boldsymbol{\lambda}$ are functions of error-free measurements, sensor locations and weighting matrix $\mathbf{W}_x$ and $\mathbf{W}_y$.

Given the estimation bias and MSE in both X and Y coordinates expressed in (2.47), (2.48), (2.54), and (2.55), the normalized MSE and bias of the total localization error can be obtained as

$$\gamma^2 = \frac{\gamma_x^2 + \gamma_y^2}{r_s^2}, \quad \beta = \frac{\sqrt{\beta_x^2 + \beta_y^2}}{r_s}, \tag{2.70}$$

where $r_s = \sqrt{x_s^2 + y_s^2}$, $x_s \neq 0$ and $y_s \neq 0$. The total variance is given by $\gamma^2 - \beta^2$.

2.2.5 Simulations

In this section the theoretical derivation and error analysis is verified by simulation and the performance of closed-form linear localization algorithms is compared with the MLE and CRLB. Consider a 10-element array with sensors located at $(x_i, y_i) = (i-1, 0)$, $i = 1, \cdots, 10$. The source is arbitrarily located at $(x_s, y_s) = (17, 22)$. The additive noise in the distance difference measurements is assumed zero mean, independent Gaussian distributed, and the noise variance for all sensor pairs is σ^2. Those measurements are generated by adding random noises (with zero mean and diagonal covariance matrix $\mathbf{C}_d$) to the true distance differences. The normalized MSEs of $E\{(\widehat{x}_s - x_s)^2\}/x_s^2$ and $E\{(\widehat{y}_s - y_s)^2\}/y_s^2$ are obtained from the average of 50,000 independent realizations.

Fig. 2.5 and Fig. 2.6 compare the average normalized MSE and bias between the LS (identity weighting matrix) and WLS algorithms versus $10\log_{10}(1/\sigma^2)$ from 500,000 independent realizations, and also shows the MLE performance and CRB [63]. In the low noise region each MSE curve of the linear algorithms decrease linearly with the increase of SNR, and the performance of the least-square algorithm approaches the WLS solution. The WLS performance coincides with the MLE at about 40dB, with

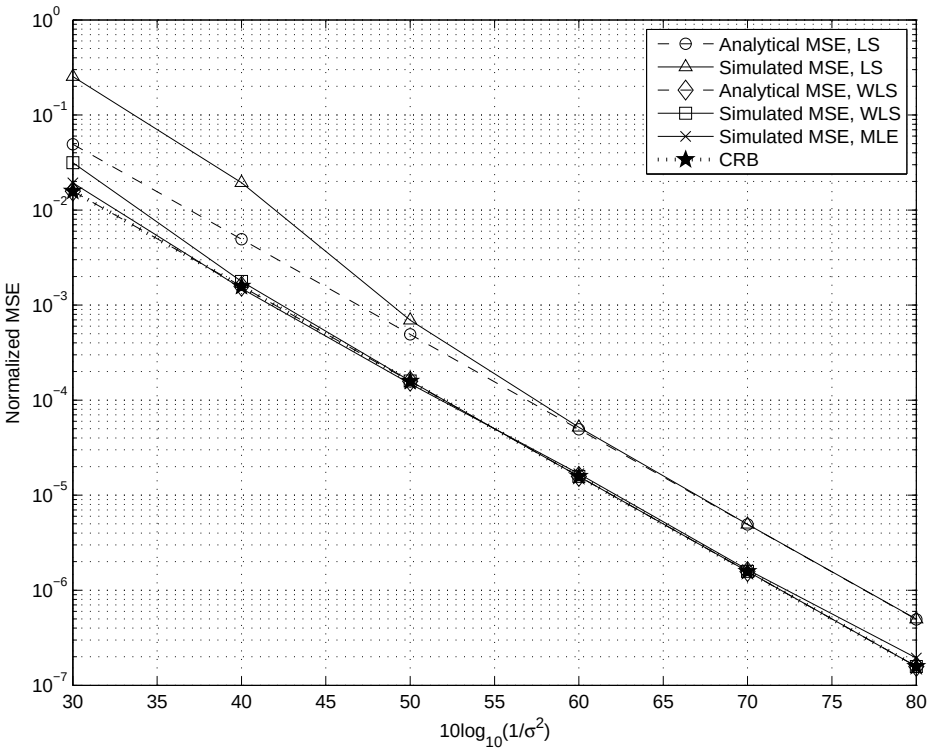

Figure 2.5: Performance comparison on normalized MSE between for LS, WLS, MLE and CRB.

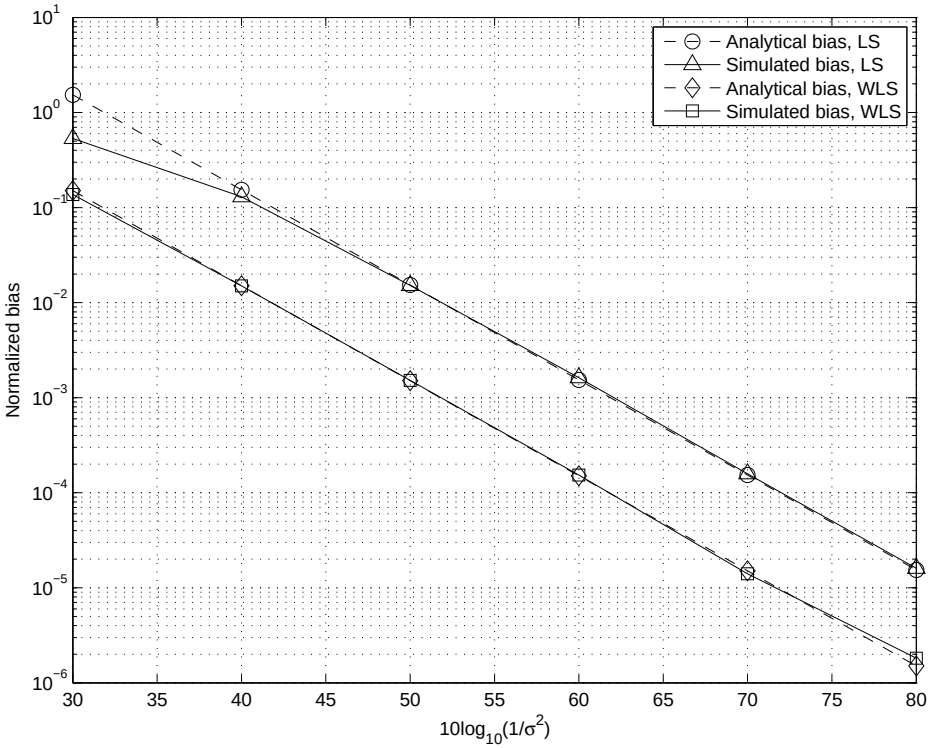

Figure 2.6: Performance comparison on normalized estimation bias between for LS, WLS, MLE and CRB.

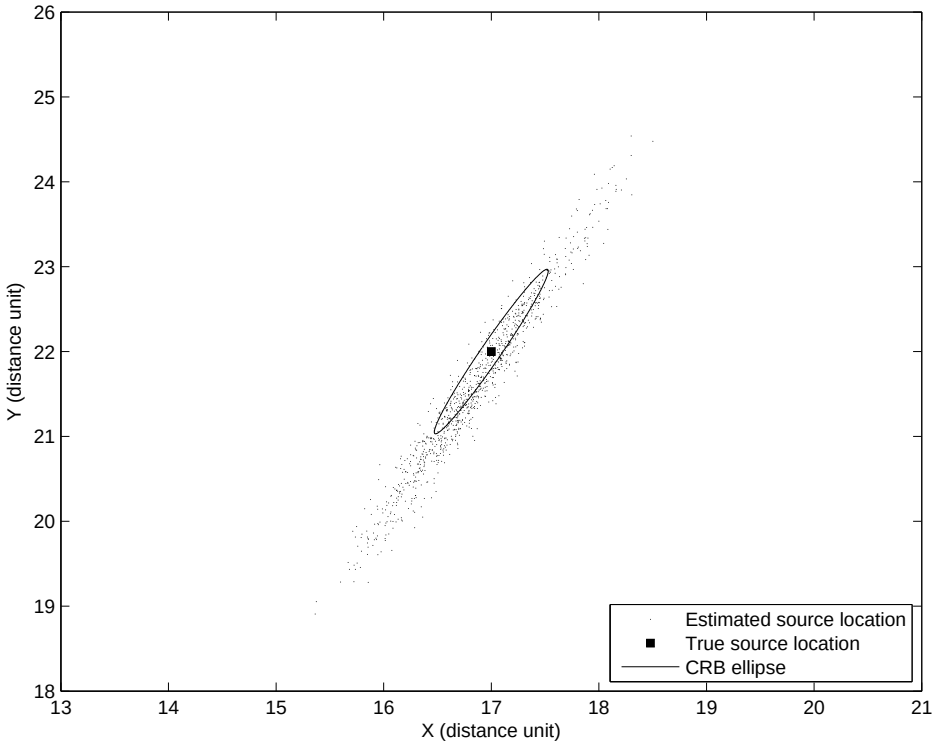

Figure 2.7: WLS estimated source locations over 1000 noise realizations with SNR=40dB.

much lower complexity. WLS shows a 5dB gain compared to LS for a large range of σ^2. The squared bias of the WLS algorithm is insignificant compared with the respective MSE from 40dB, such that the MSEs of the WLS and MLE coincide with the CRB at low measurement variance.

Fig. 2.7 presents the CRB ellipse and a scatter plot of the WLS location estimates from 1000 independent realizations at $10\log_{10}(1/\sigma^2) = 40$dB. It is visually evident that the WLS is asymptotically unbiased. Note that the error in angle is much smaller than that in range, which results from the source/array geometry. On the contrary, the least-square estimator is a biased estimator instead and have to be accompanied by a bias estimator for bias compensation.

Fig. 2.8 presents the performance of the WLS algorithm versus the ratio of the source distance to the half size of the sensor array ($\frac{r_0}{L/2}$). The array length is 9 distance

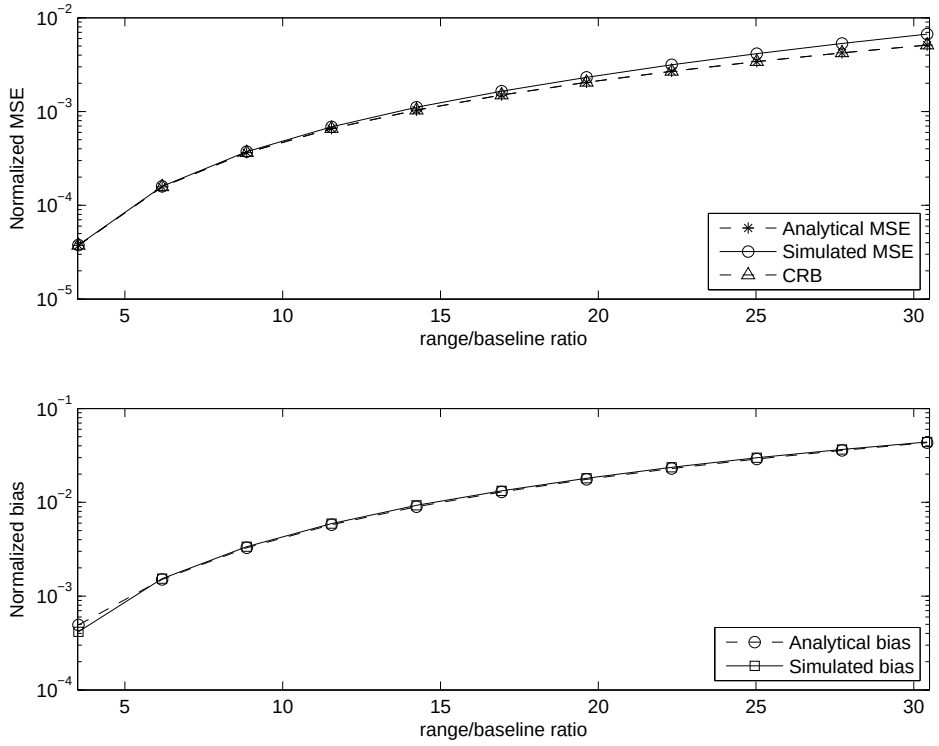

Figure 2.8: Performance of the WLS algorithm for varying range/baseline ratios.

units and $10\log_{10}(1/\sigma^2) = 50dB$. The MSE achieves 8×10^{-5} and 5×10^{-3} with a range/baseline ratio of 5 and 30 respectively. As the source moves to the far field, the range estimate becomes less and less accurate, while the angle error remains small.

2.3 Range Measurement in Multipath Channels

The ToA or TDoA localization schemes described in previous sections can provide accurate position estimation with wideband or UWB signals. However, these range-based localization methods highly rely on the LOS signal propagation, or direct path, which is a straight line path that connects the transmitter and the receiver. In modern wideband wireless networks, including cellular networks, wireless LAN or sensor networks employing UWB signals, wideband signals typically suffer from the dense reflec-

tions, scattering and diffractions, which leads to the multipath propagation environment. Multipath channel is usually modeled as a tap delay line response profile, which is a sum of several attenuated, phase-shifted, and time-delayed path impulses. The most important path among them for localization is the LOS path. If the LOS path is blocked, the transmitted signal could only reach the receiver through reflected, diffracted, or scattered paths, which may generate erroneous range measurements. This kind of error, also known as NLOS error, is defined as the excessive travelling distance with respect to the LOS path, and to be one major source of ranging error. The NLOS problem has been reported as the killer issue in ToA or TDoA measurements and range-based localizations as per the measurements in real wireless environments [67, 68].

According to whether LOS path exists in multipath channels, three different channel environments regarding localization are categorized as following [69]:

- Dominant Direct Path (DDP). In this case a LOS path exists and the strongest path of the channel estimate corresponds to LOS.

- Non-Dominant or Weak Direct Path (NDDP). In these channel response profiles, a LOS path exists but it is not the strongest. The direct path is still detectable with an appropriate receiver.

- Undetected Direct Path (UDP). If the direct path is not detectable or does not exist, only NLOS paths can be used for range estimation. In some rare cases, the LOS path is not the first or earliest-arriving path. This can also be treated as a NLOS situation. For example, the LOS path is blocked by a material with a very high dielectric constant such as a water container, then there may exist multipath components that arrive earlier than the LOS path signal since the LOS path signal suffers a considerable propagation delay.

To obtain robust localization in NLOS channels, reliable methods for range measurements are very desirable, and many research work has been done. For example, in deterministic channels, if the number of available range measurements is greater than required, the redundancy can be used to identify NLOS errors [29, 70]. In a time-varying channel, the ToA measurements including excess delays can be identified and ignored [27]. The following two subsections will discuss more details about LOS path detection, NLOS errors identification and mitigation in range measurements, and summarize the existing ranging methods. In addition, as a fundamental theoretical problem, an efficient and tight benchmark for evaluating all kinds of proposed range measurement algorithms is also highly needed. In chapter 3 the author will discuss theoretical performance limits of ToA estimation, or time delay estimation, in multipath environments. The proposed Ziv-Zakai lower bounds for TDE in unknown random multipath channel is shown to be a tight benchmark for both pulsed signal and frequency hopping waveform.

From the perspective of statistical models, the NLOS errors in multipath channel can invalidate the Gaussian model of ToA measurement in eq.(2.7). The NLOS errors are usually treated as positive bias in range measurements and thus can also be modeled with exponential, uniform or Maxwell distributions [71, pp.340-341]. In Chapter 4 the author will propose detailed analysis and simulation on the localization performance of weighted least-square and maximum-likelihood estimators with these ranging bias models.

2.3.1 LOS Path Detection

The LOS path can be simply detected by measuring the time that the cross-correlation first crosses a threshold. However, the threshold depends on the propagation environments, which leads to an inaccurate detection. Alternatively, the template-

matching method [25] provides a robust ToA estimation algorithm for greatly attenuated LOS path detection. In template-matching, samples of the leading edge of the PDP are compared to a normalized and oversampled template. The ToA estimate is the delay which minimizes the square-error between the samples of the PDP and the template.

While early-arriving multipath components cause smaller errors than late-arriving multipath, they may arrive very soon after the LOS path and are difficult to combat. Wider signal bandwidths, such as direct-sequence spread-spectrum or UWB are necessary for greater temporal resolution. [26] proposed a search algorithm for the LOS path detection of UWB signals in a dense multipath environment. This search is based on generalized maximum-likelihood (GML) estimation and can also been treated as one of the template-matching methods. It is shown briefly in the following.

The received multipath signal can be composited with LOS path signal, reflected signals, additive noise and interference. If interference from other nodes can be neglected and assume to be zero, then the received signal can be represented by

$$r_m(t) = a_d s(t - \tau_d) + \sum_{n=1}^{L} a_n s(t - \tau_n) + n_m(t), \tag{2.71}$$

where $\tau_d < \tau_1 < \ldots < \tau_L$. a_d is the path gain of the LOS path and τ_d is its time delay. The signal $s(t)$ is a correlator template with a width of T_p. The number of multipath signals L is unknown *a priori*.

If all the paths are normalized and shifted with respect to the strongest path and the paths later than the strongest are truncated, the received signal is represented by

$$r(t) = \rho_d s(t + \delta) + \sum_{k=1}^{M} \alpha_k s(t + \beta_k) + n(t), \quad t \leq \frac{T_p}{2} \tag{2.72}$$

where

$$\delta = \tau_{peak} - \tau_d, \delta \geq 0,$$

$$\rho_d = a_d/|a_{peak}|, -1 \leq \rho_d \leq 1,$$

$$\beta_k = \tau_{peak} - \tau_k, \delta > \beta_1 > \ldots > \beta_L,$$

$$\alpha_k = a_k/|a_{peak}|, -1 \leq \alpha_k \leq 1, \tag{2.73}$$

and M is the number of signal components that arrived earlier than the peak component. Then the correlation function of the noise $n(t)$ is represented by $R_N(\tau) = \sigma_A^2 \delta_D(\tau)$. Assuming $r(t)$ is sampled, it can be represented as a vector of samples

$$\underline{r} = \rho_d \underline{s}_\delta + \sum_{k=1}^{M} \alpha_k \underline{s}_{\beta_k} + \underline{n} \tag{2.74}$$

where $\underline{s}_{\beta_k}$ is the sample vector of $s(t+\beta)$ with the same length as $\underline{r}$. The correlation matrix of the noise sample vector $\underline{n}$ is $R_N = \sigma_N^2 I$. Then the GML estimation of δ to be

$$\begin{aligned} \widehat{\delta} &= \underset{\delta}{\text{argmax}} \left[\max_{\rho_d, M, \underline{\alpha}, \underline{\beta}} f(\underline{r}|\delta, \rho_d, M, \underline{\alpha}^M, \underline{\beta}^M) \right] \\ &= \underset{\delta}{\text{argmin}} \left[\min_{\rho_d, M, \underline{\alpha}, \underline{\beta}} \|r - \rho_d \underline{s}_\delta - \sum_{k=1}^{M} \alpha_k \underline{s}_{\beta_k}\|^2 \right]. \end{aligned} \tag{2.75}$$

The above solution is computation intensive because $2(M+1)$ parameters need to be calculated. An iterative nonlinear programming technique can be employed to estimate the parameters in a sequential manner [72].

2.3.2 NLOS Identification and Mitigation

The NLOS error mostly appears as a bias in the position error [28] and it is the major source of error in ToA range estimation. To deal with NLOS problem two consecutive processing steps need to be utilized. The first step is to identify whether the measurement is from LOS or NLOS path, denoted as NLOS detection; the second step is

to correct the error from NLOS measurements, called NLOS mitigation. The main idea is to exploit the information from one or more ToA measurements or channel responses and try to get an appropriate position estimate.

There are many exisiting NLOS detection and mitigation methods from the cellular networks community. Generally they can be categorized as following [73]:

1. ***Based on range estimates.***

   The time series or time history of range measurements can be utilized to obtain redundancy in a hypothesis testing of ranging error distributions [28, 27]. In [27] a binary hypothesis test is used as the general framework for NLOS identification:

$$H_0: \quad \mathbf{X} \sim f_{\mathbf{X}_{LOS}} \text{ with probability } P(H_0) \quad \text{(LOS condition)}$$
$$H_1: \quad \mathbf{X} \sim f_{\mathbf{X}_{NLOS}} \text{ with probability } P(H_1) \quad \text{(NLOS condition)}$$

   where X is a vector of independent range measurements that are distributed with probability density function (pdf) $f_{\mathbf{X}_{LOS}}$ under hypothesis H_0 and distributed with pdf $f_{\mathbf{X}_{NLOS}}$ under hypothesis H_1. Five types of tests are proposed in [27]. Different tests correspond to different *a priori* information available about the ditribution of NLOS error. All the tests assume zero-mean Gaussian distribution with known variance for LOS case, and compare likelihood ratio to some threshold:

   (a) Gaussian NLOS probability model with known a priori probabilities and unknown deterministic mean and variance parameters ⇒ Generalized Likelihood Ratio Test (GLRT).

   (b) Gaussian NLOS probability model with known a priori probabilities and unknown random mean and variance parameters ⇒ Use Jeffreys' Priors for parameter distribution.

(c) Gaussian NLOS probability model with unknown a priori probabilities and unknown deterministic mean and variance parameters ⇒ Uniformly Most Powerful (UMP) test (Neyman-Pearson criteria).

(d) Gaussian NLOS probability model with unknown a priori probabilities and unknown random mean and variance parameters ⇒ Use Jeffreys' Priors for parameter distribution and use Neyman-Pearson criteria.

(e) Unknown NLOS probability model ⇒ Simple comparison of unbiased sample variance with LOS variance using some predetermined threshold. This test is also called *running variance* and the corresponding test is given by:

$$H_0: \quad \sigma^2 = \sigma^2_{LOS} \text{ with probability } P(H_0) \text{ (LOS condition)}$$
$$H_1: \quad \sigma^2 > \sigma^2_{LOS} \text{ with probability } P(H_1) \text{ (NLOS condition)}$$

These hypothesis tests are all based on time history of range measurements, which incur the unavoidable latency. In addition, the valid error distributions must be available. Both requirements are very difficult to satisfy in reality.

2. ***Based on channel impulse response.***

The approaches in this category try to exploit more information out of the channel impulse response than the ToA estimate. One of them is to use the shape of channel impulse response to identify NLOS. This method is a little similar with the template matching algorithm for LOS detection. It uses the joint power and ToA estimates of the detected path [74]. In [75] the *confidence metric* algorithm uses the joint power and ToA estimates of both the maximum and detected path. Similar with LOS path, simple statistical metrics, e.g. threshold crossing rate or delay spread [74], can also be used to identify NLOS. More complicated statistical

metrics requires to compare the channel impulse response with different channel models [74, 76, 30]. In [73] a NLOS detection method based on SNR variations is used to indicate the environment transition.

3. ***Based on position estimate.***

These methods exploit the several range estimates after the measurement fusion to detect NLOS. Some methods try to derive environment data and to detect NLOS based on given floor maps [77, 78, 79]. Others uses the redundancy of the range estimates, e.g. Minimax or Least Square approaches [80, 81]. The Residule weighting NLOS mitigation algorithm in [29] utilize the range measurement combinations to obtain the space redundancy. Each combination consists of a subset of all the measurements from the base stations around the mobile station, and can generate a location estimate. Then the normalized error residule from each combination can be evaluated as

$$\widetilde{R}_{es}(\mathbf{x}; S) = \frac{\sum_{i \in S}[r_i - (\widehat{\mathbf{x}} - \mathbf{X}_i)]^2}{Size\ of\ S}, \tag{2.76}$$

where S is the subset of the measurements combination, r_i is the range measurement from base station i with the location of $\mathbf{X}_i$, and $\widehat{\mathbf{x}}$ is the estimated location by the combination S. For ToA location the size of S must be equal or greater than 3, therefore the total combinations for M base stations is $N = \sum_{i=3}^{M} \binom{M}{i}$. By weighting the location estimates from all the groups with the residues, the final location estimate of mobile station is given by

$$\widehat{\mathbf{x}} = \frac{\sum_{k=1}^{N} \widehat{\mathbf{x}}_k (\widetilde{R}_{es}(\widehat{\mathbf{x}}_k, S_k))^{-1}}{\sum_{k=1}^{N} (\widetilde{R}_{es}(\widehat{\mathbf{x}}_k, S_k))^{-1}}. \tag{2.77}$$

This mitigation algorithm does not have the latency problem and error distribution requirement. However, it assumes the availability of enough base stations and

some of them has LOS path with the mobile station. For some outdoor application of sensor networks, the sparse nodes deployments cannot satisfy the minimum requirement of the number of measurements. For indoor location, all the measurements may be from NLOS paths with a high probability. Thus the prerequisites of the algorithm may not be satisfied in many sensor network applications.

2.4 Summary

Ranged-based localization schemes are commonly used in practical applications. The measurement and localization models, and estimators are reviewed in this chapter. Although linearization technique combined with iterative process serves as straightforward and robust ToA or TDoA estimator with wide applicability, it has relatively high complexity and requires appropriate initialization point for iterative update in order to converge to global minimum. On the other side, closed-form linear estimators are attractive to cost and power sensitive applications due to its low computational complexity. The geometric explanation on the WLS TDoA estimation with linear reference array provides an intuitive perspective on the linear algorithm.

The performance of range-based localization is degraded in multipath propagation environments due to lack of or weak LOS received signal component. Solutions to this problem by identifying LOS signal path and mitigating NLOS errors have been discussed in the literature. The next chapter will develop the fundamental theoretical limits on the ToA estimation in multipath channel. The tight bounds based on the Ziv-Zakai approach are proposed by the author, which are for both pulsed signal and frequency hopping waveforms and do not suppose channel estimation available at receivers.

Chapter 3

Performance Bounds for Time Delay Estimation in Multipath Channels

3.1 Introduction

Time delay estimation, or ToA estimation, is the fundamental range measurement for ToA localization. However, as described in Chapter 2, the encountered channel for TDE in modern wireless networks is often wideband, random, and unknown with multipath fading, or frequency-selective fading [82]. In this wireless multipath environment, the TDE faces great challenge on the identification of LOS signal component and suffers NLOS errors that may introduce large bias to range measurements and lead to unreliable location estimation.

To evaluate the performance of TDE with different algorithms in the multipath channel, efficient and tight theoretical performance bounds are desired to which the

optimum estimation algorithms are expected to achieve in the high SNR region and stay close in the low SNR region. Such lower bounds provide useful tools for algorithm designers and researchers. Without testing particular estimation algorithms, the best achievable performance based on particular measurements can be quickly obtained. Theoretical performance bounds on TDE serve as benchmarks for the estimation algorithms and help to provide insight into the behavior of TDE.

Various TDE bounds have been developed in the past [35]. In the literature the performance of TDE is often analyzed in AWGN channels or narrowband fading channels [35]. The CRB has been extensively applied for bounding TDE performance in the case of a deterministic channel model, e.g., Yau and Bresler developed CRBs for superimposed and delayed parameterized signals [36], and that approach is readily adapted to the case of TDE in a known deterministic multipath channel [37]. Nonetheless, the CRB is only tight at high SNRs and not applicable for unknown random channel.

Ziv-Zakai lower bound [38, 39] is another attractive approach in all the various TDE bounds, and it is among the best Bayesian mean-square-error bounds for predicting optimal estimation performance over a wide range of SNRs, e.g., see Van Trees and Bell and references therein [40]. ZZBs on TDE have been developed for narrowband frequency-hopping channels [41], parallel narrowband flat-fading channels [42, 43], and for ultra-wideband signals in AWGN channels [44]. Bayesian bounds have also been developed by Weinstein and Weiss and applied to TDE [45, 40].

Regarding the case of wideband random multipath channels, in [46] the ZZB for TDE is derived for a given channel realization and then averaged over the channel distribution. This average ZZB assumes the receiver knows the perfect channel realization, and then it belongs to the category of perfect measurement based lower bounds [83]. The beginning section of this chapter reviews this average ZZB.

In Section 3.3, the author develops the ZZB for TDE with pulsed signal in unknown random multipath Gaussian channel, assuming that the receiver knows the channel distribution, but does not know the channel realization. Here, both the multipath channel taps and noise are treated as Gaussian random variables, which is a widely adopted model, for example, for narrow band and wideband wireless communication fading channels [82, 84, 85]. The signal is assumed known to the receiver, and the time delay has a uniform prior distribution. This ZZB represents a more realistic and tighter bound, and comparison of our new results with [46] reveals the TDE accuracy penalty associated with the unknown channel. The ZZB derivation differs considerably from that in [46]. The LLR for the associated hypothesis test in the ZZB derivation is shown to follow a general quadratic form of a Gaussian random vector. Then the pdf of the LLR via a MGF approach is found, that in turn leads to the minimum detection error probability expression needed to complete the ZZB derivation.

The ZZB for TDE is compared with a CRB, as well as the performance of a MAP time delay estimator. With a uniform prior on the time delay parameter, the Bayesian CRB is inapplicable due to the violation of regularity conditions, so the development turns to the expected value of a conditional CRB [40], conditioned on the random Gaussian channel. It is shown that the ZZB provides much better prediction of the MAP estimator performance for high, medium, and low SNR regimes, than does the CRB. It is also compared to a GML time delay estimator, which is equivalent to minimum mean-square error (MMSE) estimator by assuming deterministic channel realizations. The MAP estimator exploits knowledge of the channel distribution, and so performs considerably better than the GML estimator.

Furthermore, in Section 3.4 the ZZB is extended for frequency-hopping waveforms in the unknown random frequency-selective fading channels and generalizes previous

results [43, 42, 46, 86]. The same random Gaussian channel model as for pulsed signal is still adopted that captures possible correlation across time and frequency. The derivation follows the same approach used in [86], except with the frequency-hopping signal model as well as generalizing from a real to a complex Gaussian channel model. Then the log-likelihood ratio for the associated hypothesis test follows a general quadratic form of a complex Gaussian random vector. The resulting tight bound reveals achievable TDE performance for frequency-hopping waveforms that provide frequency diversity in wideband fading channels, in which the receiver does not have perfect channel state information. In particular, the closed-form expression of ZZB in the independent Rician and Rayleigh flat fading channels allows study of the choice of frequency-hopping waveform parameters, as well as the effects of channel statistics.

3.2 Average Ziv-Zakai Bounds for Pulsed Signal

In [46], the average ZZB for TDE in multipath channel is developed with the assumption of perfect channel estimation. Moreover, a known transmitted signal, a tapped delay line random channel model, and a uniform prior on the delay are assumed.

3.2.1 Channel and Pulsed Signal Models

The transmitted signal is assumed known to the receiver and given by $p(t) = \sqrt{E_{\text{tx}}}s(t)$, where $s(t)$ is normalized to have unit energy, so that E_{tx} is the transmitted signal energy. The signal propagates through a convolutive random channel, or tapped delay line, with fixed spacing T_t, given by

$$g(t) = \sqrt{G_0}\sum_{l=0}^{L-1}\alpha_l\delta(t - lT_t). \tag{3.1}$$

Here G_0 is the total gain factor, L is the total number of taps, α_l is the gain for the $(l+1)$-th tap, and let $\boldsymbol{\alpha} = [\alpha_1, \cdots, \alpha_L]^T$. The model $\boldsymbol{\alpha}$ is modeled as a Gaussian random vector with distribution denoted $\mathcal{N}(\boldsymbol{\mu}_\alpha, \mathbf{V})$, where $\boldsymbol{\mu}_\alpha$ is the mean vector and $\mathbf{V}$ is the covariance matrix. The channel is assumed to have unit power such that $tr(\boldsymbol{\mu}_\alpha \boldsymbol{\mu}_\alpha^T + \mathbf{V}) = 1$, where tr is the trace operator. Define $E_{\text{rx}} \triangleq G_0 E_{\text{tx}}$ and denote the propagation delay as $t_0 \in \mathbb{R}^+$. The received signal is given by

$$y(t) = \sqrt{E_{\text{rx}}} \sum_{l=0}^{L-1} \alpha_l s(t - lT_t - t_0) + n(t) = \sqrt{E_{\text{rx}}} \boldsymbol{\alpha}^T \mathbf{s}(t - t_0) + n(t), \tag{3.2}$$

where

$$\mathbf{s}(t - t_0) = [s(t - t_0), s(t - T_t - t_0), \cdots, s(t - (L-1)T_t - t_0)]^T, \tag{3.3}$$

and $n(t)$ is AWGN with double sided spectral density $\sigma_n^2 = N_0/2$, from which the signal to noise ratio is defined as $\xi_b = \frac{E_{\text{rx}}}{\sigma_n^2}$. A uniform prior distribution is assumed for t_0 in $[0, T]$. The TDE problem is to estimate t_0, and the ZZB is developed for TDE.

3.2.2 The Ziv-Zakai Bound

The development of the ZZB links estimation of time delay t_0 to a hypothesis testing problem that discriminates a signal at two possible delays [39]. Let $\widehat{t_0}$ be a time delay estimate. For a received signal $y(t)$ at one of the two possible delays $y(t-a)$ or $y(t-a-\Delta)$, where $\Delta > 0$ and $a, a+\Delta \in [0, T]$, the hypothesis test is given by

$$\begin{aligned} &\text{Decide } H_0: \quad t_0 = a \qquad \text{if } |\widehat{t_0} - a| < |\widehat{t_0} - a - \Delta|, \\ &\text{Decide } H_1: \quad t_0 = a + \Delta \quad \text{if } |\widehat{t_0} - a| > |\widehat{t_0} - a - \Delta|. \end{aligned} \tag{3.4}$$

Denote the estimation error by $\epsilon = \widehat{t_0} - t_0$, and let $P_e(a, a+\Delta)$ be the minimal probability of error achieved by the optimum detection scheme in making the above decision. If the two hypothesized delays are equally likely to occur, then the estimation MSE is lower

bounded by [39]

$$\overline{\epsilon^2} \geq \frac{1}{T}\int_0^T \Delta \int_0^{T-\Delta} P_e(a, a+\Delta)da\ d\Delta. \tag{3.5}$$

In general, with equally likely hypotheses, $P_e(a, a+\Delta)$ is only a function of the offset Δ and not a. Thus, write $P_e(\Delta) = P_e(a, a+\Delta)$, and it follows that

$$\overline{\epsilon^2} \geq \frac{1}{T}\int_0^T \Delta(T-\Delta)P_e(\Delta)d\Delta. \tag{3.6}$$

3.2.3 Development of Average ZZB

Evaluation of the bound (3.6) relies on finding the minimal probability of error $P_e(\Delta)$. For our case, consider the received signal

$$y(t) = \sqrt{E_{\text{rx}}}\boldsymbol{\alpha}^T\mathbf{s}(t - m\Delta) + n(t), \tag{3.7}$$

where m takes values of 0 or 1 corresponding to the two hypotheses, and Δ is the relative delay in the hypothesis test. Here, $P_e(\Delta)$ is equivalent to the error probability of a maximum likelihood detector for a binary pulse position modulation (PPM) communications scheme, as a function of the relative delay Δ. Thus, the development can appeal to binary PPM error results, but with the added complication of the random channel. Resorting to the optimal binary PPM detector, $P_e(\Delta)$ conditioned on a channel realization is found as [46]

$$P_e(\Delta) = Q(\sqrt{D}) = Q(\sqrt{\xi_b(R_0 - R_\Delta)}), \tag{3.8}$$

where $R_{\tau_1-\tau_2}$ is the correlation of $\boldsymbol{\alpha}^T\mathbf{s}(t-\tau_1)$ and $\boldsymbol{\alpha}^T\mathbf{s}(t-\tau_2)$, and

$$D = \xi_b(R_0 - R_\Delta) \quad \text{and} \quad \text{SNR} = \xi_b \triangleq E_{\text{rx}}/\sigma_n^2. \tag{3.9}$$

$P_e(\Delta)$ is then averaged over channel realizations to find the average error probability $\overline{P_e}(\Delta)$. Define the random channel gain vector $\boldsymbol{\alpha} = [\alpha_0, \cdots, \alpha_{L-1}]^T$. The average

probability of error is given by

$$\overline{P}_e(\Delta) = E\{P_e(\Delta)\} = E\{Q(\sqrt{D})\}, \tag{3.10}$$

where the expectation is over random gain $\boldsymbol{\alpha} \in \mathcal{R}^L$. The Q-function is difficult to work with. The evaluation of the expectation value is done by using the MGF of the quadratic forms of Gaussian variables. The final form of the averaged ZZB on TDE is expressed as ([46])

$$\overline{P}_e(\Delta) = \frac{2^{\frac{L}{2}}}{\pi} \int_0^{\frac{\pi}{2}} \exp[-\frac{\xi_b}{2} \boldsymbol{\mu}_\alpha^T \boldsymbol{\Phi} \mathbf{B}^{-1} \boldsymbol{\mu}_\alpha] \ |\mathbf{B}|^{-\frac{1}{2}} (\sin\phi)^L d\phi, \tag{3.11}$$

where

$$\begin{aligned} \mathbf{B} &= 2\sin^2\phi \mathbf{I} + \xi_b \mathbf{V} \boldsymbol{\Phi}, \\ \boldsymbol{\Phi} &= \sum_{k=-(L-1)}^{L-1} (2\beta_{kT_t} - \beta_{\Delta+kT_t} - \beta_{\Delta-kT_t}) \mathbf{J}^k, \\ \beta_\tau &= \int_{-\infty}^{\infty} s(t) s(t-\tau) dt \end{aligned} \tag{3.12}$$

and $\mathbf{J}$ is a $L \times L$ down-shifting matrix, whose first sub-diagonal elements below the main diagonal are ones while all others are zeros.

After finding the averaged error probability, the averaged ZZB is found by using $\overline{P_e}(\Delta)$ in (3.6), which is one of the so-called perfect-measurement-based lower bounds [83].

3.3 Ziv-Zakai Bounds for Pulsed Signal in Unknown Multipath Channel

This section presents the author's work on the Ziv-Zakai bounds for TDE with pulsed signal for unknown multipath channel. The same signal and channel models are assumed as described for the average ZZB in the last section. The difference between

this work and the average ZZB in [46] is that receivers only know the statistics of the channel vector $\boldsymbol{\alpha}$ but do not know its realizations. The development is organized as follows. The received signal distribution is established in Section 3.3.1, along with the ZZB derivation. In Section 3.3.2, development of the ZZB is facilitated via a MGF approach using quadratic forms of Gaussian random vectors. The ZZB is analyzed asymptotically for both low and high SNRs in Section 3.3.3, and an approach to find the SNR thresholds is described. Some important special cases of the ZZB are then considered in Section 3.3.4, including the cases of memoryless random channels (flat fading) and known channels. A detailed road map for computation of the ZZB, as well as low and high SNR limiting cases, is provided in Section 3.3.5. In Section 3.3.6 the ZZB is compared against the performance of time delay estimators and the CRB that is averaged over the random unknown channel. Numerical examples of the estimations and the bounds are shown in Section 3.3.7.

3.3.1 Development

Based on the signal and channel models in Section 3.2.1, the development of ZZB generally follows the procedure in Section 3.2.2. The ZZB in (3.6) depends on the minimal probability of error $P_e(\Delta)$ in making the hypothesis test, which will be found by evaluating the LLR test, as follows. The conditional distribution of the received signal is obtained conditioned on the channel realization. This is then averaged over the channel distribution, yielding the distribution of the received signal, reflecting the lack of knowledge of the channel at the receiver. Note this averaging of the signal distribution is over the unknown random channel with the information of channel statistics, which is different with the averaging $P_e(\Delta)$ over channel realizations in the development of average ZZB. The LLR is shown to depend quadratically on the received signal, and in

Section 3.3.2 a moment generating function approach is used to find an expression for the LLR distribution. Finally, $P_e(\Delta)$ is found using the LLR distribution.

3.3.1.1 Received Signal Distribution

From equation (3.106), the received signal can be written as

$$y(t) = \sqrt{E_{\rm rx}}\boldsymbol{\alpha}^T \mathbf{s}_m + n(t), \tag{3.13}$$

where m takes the value 0 or 1 corresponding to hypotheses H_0 or H_1 respectively, and

$$\mathbf{s}_m = \mathbf{s}(t - m\Delta) = [s(t - m\Delta), s(t - T_t - m\Delta), \cdots, s(t - (L-1)T_t) - m\Delta]^T.$$

Note that, in the context of developing the bound, the delay parameter t_0 in eq. (3.3) has been replaced by $m\Delta$. The duration of the observation window at the receiver is denoted as T_0, is much larger than the sum of T and the duration of the channel output waveform, where the output waveform duration is $(L-1)T_t$ plus the duration of transmitted signal $p(t)$. From (3.108), the distribution of $y(t)$ conditioned on channel gain $\boldsymbol{\alpha}$ and time delay $m\Delta$ is [84]

$$\begin{aligned} p(y(t)|\boldsymbol{\alpha}, m\Delta) &= \mathcal{K} \exp\left[-\frac{1}{2\sigma_n^2}\int_{T_0}\left(y(t) - \sqrt{E_{\rm rx}}\boldsymbol{\alpha}^T\mathbf{s}_m\right)^2 dt\right] \\ &= \mathcal{K} \exp\left[-\frac{1}{2\sigma_n^2}\left(E_{\rm rx}\boldsymbol{\alpha}^T\mathbf{S}_{00}\boldsymbol{\alpha} - 2\sqrt{E_{\rm rx}}\mathbf{r}_m^T\boldsymbol{\alpha} + I_y\right)\right]. \end{aligned} \tag{3.14}$$

where $\mathcal{K}$ absorbs all of the integration constants independent of $\boldsymbol{\alpha}$ and $m\Delta$, and

$$\mathbf{S}_{m_1 m_2} \triangleq \int_{T_0} \mathbf{s}_{m_1}\mathbf{s}_{m_2}^T dt, \quad \mathbf{r}_m \triangleq \int_{T_0} \mathbf{s}_m y(t) dt, \quad I_y \triangleq \int_{T_0} y^2(t) dt, \tag{3.15}$$

with $m, m_1, m_2 = \{0, 1\}$. $\mathbf{S}_{mm} = \mathbf{S}_{00} = \mathbf{S}_{11}$ is a symmetric Toeplitz matrix independent of m. Also the non-symmetric Toeplitz matrices $\mathbf{S}_{01}$ and $\mathbf{S}_{10}$ are to be used in the ZZB development in Section 3.3.1. Denoting the transmitted waveform autocorrelation by

$$\beta_\tau = \int_{T_o} s(t)s(t-\tau)dt$$

and defining the $L \times L$ down-shifting matrix $\mathbf{J}$ whose first subdiagonal elements below the main diagonal are ones while all others are zeros, the matrices are compacted as [46]

$$\mathbf{S}_{00} = \mathbf{S}_{11} = \sum_{k=-(L-1)}^{L-1} \beta_{-kT_t} \mathbf{J}^k, \quad \mathbf{S}_{01} = \mathbf{S}_{10}^T = \sum_{k=-(L-1)}^{L-1} \beta_{\Delta - kT_t} \mathbf{J}^k, \tag{3.16}$$

where $\mathbf{J}^{-1} \triangleq \mathbf{J}^T$, $\mathbf{J}^0 \triangleq \mathbf{I}$. Next, (3.14) is averaged over the probability distribution of the channel vector $\boldsymbol{\alpha}$, given by

$$\begin{aligned} p(y(t)|m\Delta) &= E_\alpha \left\{ p(y(t)|\boldsymbol{\alpha}, m\Delta) \right\} \\ &= \mathcal{K} E_\alpha \left\{ \exp\left[-\frac{1}{2\sigma_n^2} \left(E_{\text{rx}} \boldsymbol{\alpha}^T \mathbf{S}_{00} \boldsymbol{\alpha} - 2\sqrt{E_{\text{rx}}} \mathbf{r}_m^T \boldsymbol{\alpha} + I_y \right) \right] \right\}. \end{aligned} \tag{3.17}$$

The expected value of the exponential of a quadratic form of the normal random vector $\boldsymbol{\alpha}$ can be obtained from its moment generating function [87]. Let Q be the exponent in (3.17), given by

$$Q = -\frac{1}{2\sigma_n^2} \left(E_{\text{rx}} \boldsymbol{\alpha}^T \mathbf{S}_{00} \boldsymbol{\alpha} - 2\sqrt{E_{\text{rx}}} \mathbf{r}_m^T \boldsymbol{\alpha} + I_y \right).$$

Using equation (B.3) in Appendix B, with $s = 1$, then

$$p(y(t)|m\Delta) = \mathcal{K} |\mathbf{X}|^{-\frac{1}{2}} \exp\left\{ \frac{1}{2} \mathbf{v}_m^T \mathbf{X}^{-1} \mathbf{v}_m + c_m \right\} \tag{3.18}$$

where

$$\mathbf{X} = \mathbf{I} + \frac{E_{\text{rx}}}{\sigma_n^2} \mathbf{V}^{\frac{1}{2}} \mathbf{S}_{00} \mathbf{V}^{\frac{1}{2}} = \mathbf{I} + \xi_b \mathbf{V}^{\frac{1}{2}} \mathbf{S}_{00} \mathbf{V}^{\frac{1}{2}}, \tag{3.19}$$

and ξ_b is the SNR as defined in Section 3.2.1. The received signal is embedded in $\mathbf{v}_m$ and c_m, given by

$$\mathbf{v}_m = \frac{\sqrt{E_{\text{rx}}}}{\sigma_n^2} \mathbf{V}^{\frac{1}{2}} \mathbf{r}_m - \frac{E_{\text{rx}}}{\sigma_n^2} \mathbf{V}^{\frac{1}{2}} \mathbf{S}_{00} \boldsymbol{\mu}_\alpha, \quad c_m = \frac{\sqrt{E_{\text{rx}}}}{\sigma_n^2} \boldsymbol{\mu}_\alpha^T \mathbf{r}_m - \frac{E_{\text{rx}}}{2\sigma_n^2} \boldsymbol{\mu}_\alpha^T \mathbf{S}_{00} \boldsymbol{\mu}_\alpha - \frac{I_y}{2\sigma_n^2}.$$

Using $\mathbf{v}_m$ and c_m, eq. (3.18) can be expressed as a function of $\mathbf{r}_m$, given by

$$p(y(t)|m\Delta) = \mathcal{K} |\mathbf{X}|^{-\frac{1}{2}} \exp\left\{ \mathbf{r}_m^T \mathbf{W} \mathbf{r}_m + \mathbf{h}^T \mathbf{r}_m + \widetilde{c} \right\}, \tag{3.20}$$

where

$$\widetilde{c} = \frac{E_{\rm rx}^2}{2\sigma_n^4}\boldsymbol{\mu}_\alpha^T \mathbf{S}_{00}\mathbf{V}^{\frac{1}{2}}\mathbf{X}^{-1}\mathbf{V}^{\frac{1}{2}}\mathbf{S}_{00}\boldsymbol{\mu}_\alpha - \frac{E_{\rm rx}}{2\sigma_n^2}\boldsymbol{\mu}_\alpha^T\mathbf{S}_{00}\boldsymbol{\mu}_\alpha - \frac{I_y}{2\sigma_n^2},$$

$$\mathbf{W} = \frac{E_{\rm rx}}{2\sigma_n^4}\mathbf{V}^{\frac{1}{2}}\mathbf{X}^{-1}\mathbf{V}^{\frac{1}{2}} = \frac{\xi_b^2}{2E_{\rm rx}}\mathbf{V}^{\frac{1}{2}}\mathbf{X}^{-1}\mathbf{V}^{\frac{1}{2}}, \tag{3.21}$$

$$\mathbf{h} = \frac{\sqrt{E_{\rm rx}}}{\sigma_n^2}\boldsymbol{\mu}_\alpha - \frac{\sqrt{E_{\rm rx}}E_{\rm rx}}{\sigma_n^4}\mathbf{V}^{\frac{1}{2}}\mathbf{X}^{-1}\mathbf{V}^{\frac{1}{2}}\mathbf{S}_{00}\boldsymbol{\mu}_\alpha = \frac{\xi_b}{\sqrt{E_{\rm rx}}}\left(\mathbf{I} - \xi_b\mathbf{V}^{\frac{1}{2}}\mathbf{X}^{-1}\mathbf{V}^{\frac{1}{2}}\mathbf{S}_{00}\right)\boldsymbol{\mu}_\alpha = \mathbf{H}\boldsymbol{\mu}_\alpha. \tag{3.22}$$

Note that $\widetilde{c}$ does not depend on m, i.e., it does not depend on the hypothesis choice. Note also that $\mathbf{h} = \mathbf{0}$ in the zero-mean channel case, i.e., when $\boldsymbol{\mu}_\alpha = \mathbf{0}$.

3.3.1.2 Log-likelihood Ratio Test

By the received signal distribution in (3.20) the likelihood ratio (LR) for the hypothesis test can be evaluated. The LR to decide on hypothesis H_m, $m = 0, 1$, is

$$\Lambda \triangleq \frac{p(y(t)|0)}{p(y(t)|\Delta)} \underset{H_1}{\overset{H_0}{\gtrless}} 1. \tag{3.23}$$

Because $\widetilde{c}$ in (3.20) does not depend on the hypothesis choice, then it will not affect the error probability of the hypothesis test and can be dropped. Consequently, employing (3.20), the LLR becomes

$$\begin{aligned}
\mathcal{L} \triangleq \ln\Lambda &= \ln p(y(t)|0) - \ln p(y(t)|\Delta) = \mathbf{r}_0^T\mathbf{W}\mathbf{r}_0 - \mathbf{r}_1^T\mathbf{W}\mathbf{r}_1 + \mathbf{h}^T\mathbf{r}_0 - \mathbf{h}^T\mathbf{r}_1 \\
&= \mathbf{r}^T\boldsymbol{\Psi}\mathbf{r} + \mathbf{g}^T\mathbf{r} \\
&\underset{H_1}{\overset{H_0}{\lessgtr}} 0,
\end{aligned} \tag{3.24}$$

where

$$\mathbf{r} = \begin{bmatrix} \mathbf{r}_0 \\ \mathbf{r}_1 \end{bmatrix}, \quad \boldsymbol{\Psi} = \begin{bmatrix} \mathbf{W} & \mathbf{0} \\ \mathbf{0} & -\mathbf{W} \end{bmatrix}, \quad \mathbf{g} = \begin{bmatrix} \mathbf{h} \\ -\mathbf{h} \end{bmatrix} = \begin{bmatrix} \mathbf{H}\boldsymbol{\mu}_\alpha \\ -\mathbf{H}\boldsymbol{\mu}_\alpha \end{bmatrix} = \mathbf{G}\boldsymbol{\mu}_\alpha. \tag{3.25}$$

An error occurs if $\mathcal{L} < 0 | m = 0$, or if $\mathcal{L} > 0 | m = 1$. Thus, the hypothesis test minimum error probability can be written as

$$\begin{aligned} P_e(\Delta) &= Pr\{\mathcal{L} < 0 | H_0\} Pr\{H_0\} + Pr\{\mathcal{L} > 0 | H_1\} Pr\{H_1\} \\ &= \frac{1}{2} Pr\{\mathcal{L} < 0 | H_0\} + \frac{1}{2} Pr\{\mathcal{L} > 0 | H_1\}, \end{aligned} \tag{3.26}$$

where the second equality assumes equally likely hypotheses. Let $\mathcal{L}_m \stackrel{\Delta}{=} \mathcal{L} | H_m$, and $\widetilde{\mathbf{r}}_m \stackrel{\Delta}{=} \mathbf{r} | H_m$. Then eqs. (3.112) and (3.26) become

$$\mathcal{L}_m = \widetilde{\mathbf{r}}_m^T \mathbf{\Psi} \widetilde{\mathbf{r}}_m + \mathbf{g}^T \widetilde{\mathbf{r}}_m, \tag{3.27}$$

$$P_e(\Delta) = \frac{1}{2} Pr\{\mathcal{L}_0 < 0\} + \frac{1}{2} Pr\{\mathcal{L}_1 > 0\}. \tag{3.28}$$

The goal now is to evaluate the probabilities in (3.115), in order to use $P_e(\Delta)$ in the ZZB expression (3.6). The next subsection will find the distribution of $\widetilde{\mathbf{r}}_m$. Then, in the next section, the distribution of $\mathcal{L}_m$ is derived, from which the probabilities are obtained.

3.3.1.3 The Distribution of $\widetilde{\mathbf{r}}_m$

Using (3.110) and (3.108) conditioned on H_0, then $\mathbf{r}_0$ and $\mathbf{r}_1$ can be expressed as

$$\begin{aligned} \mathbf{r}_0 | H_0 &= \int_{T_0} \mathbf{s}_0 \left[\sqrt{E_{\text{rx}}} \boldsymbol{\alpha}^T \mathbf{s}_0 + n(t) \right] dt = \sqrt{E_{\text{rx}}} \left(\int_{T_0} \mathbf{s}_0 \mathbf{s}_0^T dt \right) \boldsymbol{\alpha} + \int_{T_0} \mathbf{s}_0 n(t) dt \\ &= \sqrt{E_{\text{rx}}} \mathbf{S}_{00} \boldsymbol{\alpha} + \mathbf{z}_0, \end{aligned} \tag{3.29}$$

$$\begin{aligned} \mathbf{r}_1 | H_0 &= \int_{T_0} \mathbf{s}_1 \left[\sqrt{E_{\text{rx}}} \boldsymbol{\alpha}^T \mathbf{s}_0 + n(t) \right] dt = \sqrt{E_{\text{rx}}} \left(\int_{T_0} \mathbf{s}_1 \mathbf{s}_0^T dt \right) \boldsymbol{\alpha} + \int_{T_0} \mathbf{s}_1 n(t) dt \\ &= \sqrt{E_{\text{rx}}} \mathbf{S}_{10} \boldsymbol{\alpha} + \mathbf{z}_1, \end{aligned} \tag{3.30}$$

where

$$\mathbf{z}_0 \stackrel{\Delta}{=} \int_{T_0} \mathbf{s}_0 n(t) dt, \quad \mathbf{z}_1 \stackrel{\Delta}{=} \int_{T_0} \mathbf{s}_1 n(t) dt.$$

Stack $\mathbf{r}_0|H_0$ and $\mathbf{r}_1|H_0$ as in (3.25) and obtain

$$\widetilde{\mathbf{r}}_0 = \mathbf{r}|H_0 = \sqrt{E_{\rm rx}}\mathbf{R}_0\boldsymbol{\alpha} + \mathbf{z}, \quad \mathbf{R}_0 = \begin{bmatrix} \mathbf{S}_{00} \\ \\ \mathbf{S}_{10} \end{bmatrix}, \quad \mathbf{z} = \begin{bmatrix} \mathbf{z}_0 \\ \\ \mathbf{z}_1 \end{bmatrix}. \tag{3.31}$$

Similarly, conditioned on H_1, it follows

$$\widetilde{\mathbf{r}}_1 = \mathbf{r}|H_1 = \sqrt{E_{\rm rx}}\mathbf{R}_1\boldsymbol{\alpha} + \mathbf{z}, \quad \mathbf{R}_1 = \begin{bmatrix} \mathbf{S}_{01} \\ \\ \mathbf{S}_{00} \end{bmatrix}. \tag{3.32}$$

Therefore, under either hypothesis the data vector $\widetilde{\mathbf{r}}_0$ or $\widetilde{\mathbf{r}}_1$ is a linear combination of Gaussian vectors $\boldsymbol{\alpha}$ and $\mathbf{z}$, so that $\widetilde{\mathbf{r}}_m$ follows a normal distribution as $\widetilde{\mathbf{r}}_m \sim \mathcal{N}(\boldsymbol{\mu}_m, \boldsymbol{\Sigma}_m)$. Using (3.117) and (3.118), the mean and variance of $\widetilde{\mathbf{r}}_m$ can be compactly expressed as

$$\boldsymbol{\mu}_m = \sqrt{E_{\rm rx}}\mathbf{m}_m, \quad \mathbf{m}_m = \mathbf{R}_m\boldsymbol{\mu}_\alpha, \quad \boldsymbol{\Sigma}_m = E_{\rm rx}\left(\mathbf{R}_m\mathbf{V}\mathbf{R}_m^T + \xi_b^{-1}\boldsymbol{\Gamma}\right), \tag{3.33}$$

where

$$\boldsymbol{\Gamma} = E\{\mathbf{z}\mathbf{z}^T\}/\sigma_n^2 = \begin{bmatrix} \mathbf{S}_{00} & \mathbf{S}_{01} \\ \\ \mathbf{S}_{10} & \mathbf{S}_{00} \end{bmatrix} = \begin{bmatrix} \mathbf{R}_0 & \mathbf{R}_1 \end{bmatrix}. \tag{3.34}$$

Thus, the pdf of the $2L$-dimensional Gaussian vector $\widetilde{\mathbf{r}}_m$ can be written as

$$f_m(\mathbf{x}) = \frac{1}{(\sqrt{2\pi})^{2L}|\boldsymbol{\Sigma}_m|}\exp\left\{-\frac{1}{2}(\mathbf{x}-\boldsymbol{\mu}_m)^T\boldsymbol{\Sigma}_m^{-1}(\mathbf{x}-\boldsymbol{\mu}_m)\right\},$$

which will be useful in the next section.

Note that with the distribution of $\widetilde{\mathbf{r}}_m$, it is easy to express the probabilities in (3.115) as

$$Pr\{\mathcal{L}_0 < 0\} = Pr\Big\{\mathbf{x} \in \big\{\mathbf{x}:\ \mathbf{x}^T\boldsymbol{\Psi}\mathbf{x}+\mathbf{g}^T\mathbf{x} < 0\big\}\Big\} = \underbrace{\int\cdots\int}_{\text{2L fold}}{}_{\mathbf{x}\in\left\{\mathbf{x}:\ \mathbf{x}^T\boldsymbol{\Psi}\mathbf{x}+\mathbf{g}^T\mathbf{x}<0\right\}} f_0(\mathbf{x})d\mathbf{x}, \tag{3.35}$$

$$Pr\{\mathcal{L}_1 > 0\} = Pr\Big\{\mathbf{x} \in \big\{\mathbf{x}:\ \mathbf{x}^T\boldsymbol{\Psi}\mathbf{x}+\mathbf{g}^T\mathbf{x} > 0\big\}\Big\} = \underbrace{\int\cdots\int}_{\text{2L fold}}{}_{\mathbf{x}\in\left\{\mathbf{x}:\ \mathbf{x}^T\boldsymbol{\Psi}\mathbf{x}+\mathbf{g}^T\mathbf{x}>0\right\}} f_1(\mathbf{x})d\mathbf{x}. \tag{3.36}$$

However, these require finding the bounding set for $\mathbf{x}$ and evaluating the $2L$-dimensional integrals. In the next section an MGF approach is introduced that results in a 2-dimensional integration and is much more computationally attractive.

3.3.2 Evaluation of the ZZB using the moment generating function

Using the results from Section 3.3.1, the ZZB can be evaluated as follows. With the distribution of the log-likelihood ratio $\mathcal{L}_m$ in (3.114), it is straightforward to evaluate the probabilities in (3.115) via 1-dimensional integration, and then use the resulting $P_e(\Delta)$ to find the ZZB in (3.6). Note that $\mathcal{L}_m$ is a quadratic function of the Gaussian vector $\widetilde{\mathbf{r}}_m$, and so no closed form is available for the distribution of $\mathcal{L}_m$. Consequently, adopting an MGF approach can find it.

The MGF of $\mathcal{L}_m$ is given by

$$\Theta_m(s) \triangleq E_{\widetilde{r}_m}\{\exp(s\mathcal{L}_m)\} = E_{\widetilde{r}_m}\{\exp[s(\widetilde{\mathbf{r}}_m^T\boldsymbol{\Psi}\widetilde{\mathbf{r}}_m + \mathbf{g}^T\widetilde{\mathbf{r}}_m)]\}. \tag{3.37}$$

Consider two alternative forms for $\Theta_m(s)$ referred to as the direct form and the compact form. The compact form relies on eigendecomposition, but does not require explicit matrix inversion as does the direct form. So, in general the compact form is preferred for numerical evaluation. However, the direct form is convenient to carry out asymptotic analysis in Section 3.3.3. Further numerical details are deferred until Section 3.3.5.

3.3.2.1 MGF Direct Form

Applying (B.4) from Appendix B, and using the mean and variance of $\widetilde{r}_m$ from (3.119), evaluation of (3.37) obtain

$$\Theta_m(s) = |\widetilde{\mathbf{A}}_m(s)|^{-\frac{1}{2}} \exp\{sk_m + \frac{1}{2}s^2\widetilde{\mathbf{p}}_m^T\widetilde{\mathbf{A}}_m^{-1}(s)\boldsymbol{\Sigma}_m\widetilde{\mathbf{p}}_m\}, \tag{3.38}$$

where

$$\widetilde{\mathbf{A}}_m(s) = \mathbf{I} - 2s\boldsymbol{\Sigma}_m\boldsymbol{\Psi}, \quad k_m = \boldsymbol{\mu}_m^T\boldsymbol{\Psi}\boldsymbol{\mu}_m + \mathbf{g}^T\boldsymbol{\mu}_m, \quad \widetilde{\mathbf{p}}_m = \mathbf{g} + 2\boldsymbol{\Psi}\boldsymbol{\mu}_m. \tag{3.39}$$

Setting $s = j2\pi f$, the Fourier transform of $\Theta_m(j2\pi f)$ yields the pdf of $\mathcal{L}_m$, and the probabilities $Pr\{\mathcal{L}_0 < 0\}$ and $Pr\{\mathcal{L}_1 > 0\}$ are given by

$$Pr\{\mathcal{L}_0 < 0\} = \int_{-\infty}^{0}\int_{-\infty}^{\infty} \Theta_0(j2\pi f)e^{-j2\pi fu}dfdu, \tag{3.40}$$

$$Pr\{\mathcal{L}_1 > 0\} = \int_{0}^{\infty}\int_{-\infty}^{\infty} \Theta_1(j2\pi f)e^{-j2\pi fu}dfdu. \tag{3.41}$$

Substituting $Pr\{\mathcal{L}_0 < 0\}$ and $Pr\{\mathcal{L}_1 > 0\}$ into (3.115), the minimum error probability $P_e(\Delta)$ follows.

The fast Fourier transform (FFT) algorithm can be employed to approximate the continuous Fourier transform in the inner-most integration in (3.40) and (3.41). However, to do this, then for each $s = 2\pi f$ the matrix inverse and determinant of $\widetilde{\mathbf{A}}_m(s)$ must be computed, which has high computational complexity. In the next subsection the eigendecomposition approach is adopted to derive a compact form for the MGF, leading to lower complexity. Note that (3.38) will prove useful to carry out asymptotic analysis of the ZZB in Section 3.3.3.

3.3.2.2 MGF Compact Form

Next consider an alternative evaluation of the MGF relying on eigendecomposition. Let us begin with the LLR in (3.114). Using the definitions of $\boldsymbol{\Psi}$ and $\mathbf{g}$ in (3.25), it can be easily shown that $\mathbf{g}^T\boldsymbol{\Psi}^{-1}\mathbf{g} = 0$. Therefore, the LLR becomes

$$\mathcal{L}_m = \widetilde{\mathbf{x}}_m^T\boldsymbol{\Psi}\widetilde{\mathbf{x}}_m, \quad \widetilde{\mathbf{x}}_m = \widetilde{\mathbf{r}}_m + \frac{1}{2}\boldsymbol{\Psi}^{-1}\mathbf{g}. \tag{3.42}$$

Note that $\widetilde{\mathbf{x}}_m$ is a Gaussian random vector with variance $\boldsymbol{\Sigma}_m$, and whose mean is

$$\boldsymbol{\mu}_{xm} = \boldsymbol{\mu}_m + \frac{1}{2}\boldsymbol{\Psi}^{-1}\mathbf{g} = (\sqrt{E_{\text{rx}}}\mathbf{R}_m + \frac{1}{2}\boldsymbol{\Psi}^{-1}\mathbf{G})\boldsymbol{\mu}_\alpha.$$

Introduce the zero mean Gaussian random vector $\mathbf{u}_m$, obtained from $\widetilde{\mathbf{x}}_m$ by the transformation

$$\widetilde{\mathbf{x}}_m = \mathbf{\Sigma}_m^{\frac{1}{2}} \mathbf{P}_m \mathbf{u}_m + \boldsymbol{\mu}_{xm} = \mathbf{\Sigma}_m^{\frac{1}{2}} \mathbf{P}_m (\mathbf{u}_m + \mathbf{b}_m),$$

so that the variance of $\mathbf{u}_m$ is the identity matrix $\mathbf{I}$, and the vector $\mathbf{b}_m$ is a linear transformation of channel mean $\boldsymbol{\mu}_\alpha$ given by

$$\mathbf{b}_m = \mathbf{P}_m^T \mathbf{\Sigma}_m^{-\frac{1}{2}} \boldsymbol{\mu}_{xm} = \mathbf{P}_m^T \mathbf{\Sigma}_m^{-\frac{1}{2}} (\sqrt{E_{\text{rx}}} \mathbf{R}_m + \frac{1}{2} \mathbf{\Psi}^{-1} \mathbf{G}) \boldsymbol{\mu}_\alpha. \tag{3.43}$$

In this transformation, $\mathbf{P}_m$ is a unitary matrix in the eigendecomposition of the symmetric matrix given by

$$\mathbf{\Sigma}_m^{\frac{1}{2}} \mathbf{\Psi} \mathbf{\Sigma}_m^{\frac{1}{2}} = \mathbf{P}_m \text{diag}\{\lambda_1, \cdots, \lambda_J, -\lambda_{J+1}, \cdots, -\lambda_{2L}\} \mathbf{P}_m^T. \tag{3.44}$$

From the structure of $\mathbf{\Psi}$ and the fact that $\mathbf{W}$ is positive definite, it follows that $\lambda_k \geq 0$ for all k.

From this, the elements u_{mk} of $\mathbf{u}_m$ are independent Gaussian random variables, each with zero mean and unit variance. It follows that (3.119) can be written as

$$\begin{aligned} \mathcal{L}_m &= (\mathbf{u}_m + \mathbf{b}_m)^T \text{diag}\{\lambda_1, \cdots, \lambda_J, -\lambda_{J+1}, \cdots, -\lambda_{2L}\} (\mathbf{u}_m + \mathbf{b}_m) & (3.45) \\ &= \sum_{k=1}^{J} \lambda_k (u_{mk} + b_{mk})^2 - \sum_{k=J+1}^{2L} \lambda_k (u_{mk} + b_{mk})^2, & (3.46) \end{aligned}$$

where b_{mk} is the k-th element of $\mathbf{b}_m$.

The MGF is now obtained by using (3.121) in equation (B.5) from Appendix B,

$$\Theta_m(s) = \left\{ \prod_{k=1}^{J} (1 - 2s\lambda_k)^{-\frac{1}{2}} \exp\{\frac{s\lambda_k b_{mk}^2}{1 - 2s\lambda_k}\} \right\} \left\{ \prod_{k=J+1}^{2L} (1 + 2s\lambda_k)^{-\frac{1}{2}} \exp\{\frac{-s\lambda_k b_{mk}^2}{1 + 2s\lambda_k}\} \right\}. \tag{3.47}$$

In this case, each of the $2L$ product factors stems from the MGF of a scaled noncentral Chi-square random variable with one degree of freedom [87]. This observation is consistent with (3.46), consisting of two weighted sums of independent noncentral Chi-square

random variables, where each term in the summation results in a multiplicative factor in (3.122). As with the MGF direct form, substituting into (3.40) and (3.41), the decision error probabilities can be found, and the ZZB follows.

Note that compact form of the MGF in (3.122) does not require matrix inversion at each frequency, though it is necessary to re-compute $\mathbf{\Sigma}_m$, $\mathbf{R}_m$, and the eigendecomposition in (3.121) for each value of Δ. Overall, the compact form requires less computation than the direct form, and it will be used in our numerical examples in Section 3.3.7.

3.3.3 ZZB Asymptotic Analysis and Threshold Regions

In this section, the author derives asymptotic expressions for the ZZB at both low and high SNRs, and show how SNR thresholds can be found to isolate the low and high SNR regimes. The MGF direct form of (3.38) is expanded in a power series as a function of SNR ξ_b for low SNR, and ξ_b^{-1} for high SNR. The MGF in (3.38) is a function of $\widetilde{\mathbf{A}}_m(s)$, k_m, and $\widetilde{\mathbf{p}}_m$. These quantities depend on $\mathbf{\Psi}$, that in turn depends on $\mathbf{W}$ in (3.21), where $\mathbf{W}$ incorporates $\mathbf{X}^{-1}$, and finally $\mathbf{X}$ in (3.19) is a function of the desired expansion variable ξ_b. So, the derivation begins by expanding $\mathbf{X}$ in ξ_b, or $\mathbf{X}^{-1}$ in ξ_b^{-1}, and then substitute these until the desired expansion of the MGF is obtained[1].

3.3.3.1 Low SNR Regime

Using the results from Appendix B.1.1, a Taylor expansion of $\mathbf{X}^{-1}$ is given by

$$\mathbf{X}^{-1} = (\mathbf{I} + \xi_b \mathbf{V}^{\frac{1}{2}} \mathbf{S}_{00} \mathbf{V}^{\frac{1}{2}})^{-1} = \mathbf{I} - \xi_b \mathbf{V}^{\frac{1}{2}} \mathbf{S}_{00} \mathbf{V}^{\frac{1}{2}} + \mathbf{O}(\xi_b^2). \tag{3.48}$$

The expansion of $\mathbf{V}^{\frac{1}{2}} \mathbf{X}^{-1} \mathbf{V}^{\frac{1}{2}}$ follows, contained in $\mathbf{W}$, as

$$\mathbf{V}^{\frac{1}{2}} \mathbf{X}^{-1} \mathbf{V}^{\frac{1}{2}} = \mathbf{V} - \xi_b \mathbf{V} \mathbf{S}_{00} \mathbf{V} + \mathbf{O}(\xi_b^2). \tag{3.49}$$

[1] A similar approach can be applied beginning with the MGF compact form. Along with some common terms arising in the MGF direct form expansion, this also requires expansion of eigendecomposition components $\mathbf{P}_m$ and λ_k in (3.121) that can be obtained using a perturbation analysis technique.

Subsequently, $\mathbf{\Psi}$ and $\mathbf{g}$ become

$$\mathbf{\Psi} = \frac{\xi_b^2}{E_{\text{rx}}}\mathbf{\Psi}_2 + \mathbf{O}(\xi_b^3), \quad \mathbf{g} = \frac{\xi_b}{\sqrt{E_{\text{rx}}}}\mathbf{g}_1 + \mathbf{O}(\xi_b^2), \quad \mathbf{\Psi}_2 = \begin{bmatrix} \frac{\mathbf{V}}{2} & \mathbf{0} \\ \mathbf{0} & -\frac{\mathbf{V}}{2} \end{bmatrix}, \quad \mathbf{g}_1 = \begin{bmatrix} \boldsymbol{\mu}_\alpha \\ -\boldsymbol{\mu}_\alpha \end{bmatrix}. \tag{3.50}$$

Then, $\widetilde{\mathbf{A}}_m(s)$, $\widetilde{\mathbf{p}}_m$ and k_m become

$$\widetilde{\mathbf{A}}_m(s) = \mathbf{I} - 2s\mathbf{\Sigma}_m\mathbf{\Psi} = \mathbf{I} - 2sE_{\text{rx}}(\mathbf{R}_m\mathbf{V}\mathbf{R}_m^T + \xi_b^{-1}\mathbf{\Gamma})\mathbf{\Psi} = \mathbf{I} - 2s\mathbf{\Gamma}\mathbf{\Psi}_2\xi_b + \mathbf{O}(\xi_b^2), \tag{3.51}$$

$$\widetilde{\mathbf{p}}_m = \mathbf{g} + 2\mathbf{\Psi}\boldsymbol{\mu}_m = \frac{\xi_b}{\sqrt{E_{\text{rx}}}}\mathbf{g}_1 + \mathbf{O}(\xi_b^2), \quad k_m = \boldsymbol{\mu}_m^T\mathbf{\Psi}\boldsymbol{\mu}_m + \mathbf{g}^T\boldsymbol{\mu}_m = \mathbf{g}_1^T\mathbf{m}_m\xi_b + O(\xi_b^2). \tag{3.52}$$

Using the Taylor expansions in (B.11), (B.12) and (B.13) in Appendix B.1.1, the inverse and determinant of $\widetilde{\mathbf{A}}_m(s)$ can be expanded as

$$\begin{aligned} \widetilde{\mathbf{A}}_m^{-1}(s) &= \mathbf{I} + 2s\xi_b\mathbf{\Gamma}\mathbf{\Psi}_2 + \mathbf{O}(\xi_b^2), \\ |\widetilde{\mathbf{A}}_m(s)| &= 1 - 2s\xi_b tr(\mathbf{\Gamma}\mathbf{\Psi}_2) + O(\xi_b^2), \\ |\widetilde{\mathbf{A}}_m(s)|^{-\frac{1}{2}} &= 1 + s\xi_b tr(\mathbf{\Gamma}\mathbf{\Psi}_2) + O(\xi_b^2). \end{aligned} \tag{3.53}$$

From eqs. (3.52) and (3.53), the following is obtained as

$$\widetilde{\mathbf{p}}_m^T\widetilde{\mathbf{A}}_m^{-1}(s)\mathbf{\Sigma}_m\widetilde{\mathbf{p}}_m = \xi_b\mathbf{g}_1^T\mathbf{\Gamma}\mathbf{g}_1 + O(\xi_b^2). \tag{3.54}$$

Substituting (3.52) and (3.53) into (3.38), the MGF expansion is

$$\Theta_m(s) = \left\{1 + s\xi_b tr(\mathbf{\Gamma}\mathbf{\Psi}_2) + O(\xi_b^2)\right\} \times \exp\left\{s\xi_b\mathbf{g}_1^T\mathbf{m}_m + \frac{s^2}{2}\xi_b\mathbf{g}_1^T\mathbf{\Gamma}\mathbf{g}_1 + O(\xi_b^2)\right\}. \tag{3.55}$$

As $\xi_b \to 0$, the leading coefficient in (3.55) goes to unity, and the first order approximation of the MGF in the low SNR regime is

$$\Theta_m(s) \approx \exp\left\{s\xi_b\mathbf{g}_1^T\mathbf{m}_m + \frac{s^2}{2}\xi_b\mathbf{g}_1^T\mathbf{\Gamma}\mathbf{g}_1\right\}. \tag{3.56}$$

This is the MGF of a normally distributed random variable with mean $\xi_b\mathbf{g}_1^T\mathbf{m}_m$ and variance $\xi_b\mathbf{g}_1^T\mathbf{\Gamma}\mathbf{g}_1$. So at low SNR, $\mathcal{L}_m \sim \mathcal{N}(\xi_b\mathbf{g}_1^T\mathbf{m}_m, \xi_b\mathbf{g}_1^T\mathbf{\Gamma}\mathbf{g}_1)$, (3.40) and (3.41) are

$$Pr\{\mathcal{L}_0 < 0\} = Q\left(\frac{\xi_b\mathbf{g}_1^T\mathbf{m}_0}{\sqrt{\xi_b\mathbf{g}_1^T\mathbf{\Gamma}\mathbf{g}_1}}\right), \quad Pr\{\mathcal{L}_1 > 0\} = Q\left(-\frac{\xi_b\mathbf{g}_1^T\mathbf{m}_1}{\sqrt{\xi_b\mathbf{g}_1^T\mathbf{\Gamma}\mathbf{g}_1}}\right), \tag{3.57}$$

where $Q(x) = \frac{1}{\sqrt{2\pi}} \int_x^\infty \exp(-\frac{t^2}{2})dt$ is the Q-function. Substituting (3.57) into (3.26) and using the following expansion of the Q-function for small x [46]

$$Q(x) = \frac{1}{2} - \frac{1}{\sqrt{\pi}} \sum_{n=0}^{\infty} \frac{(-1)^n (\frac{x}{\sqrt{2}})^{2n+1}}{(2n+1)n!},$$

eq. (3.26) becomes

$$P_e(\Delta) \approx \frac{1}{2} - \frac{1}{2} \frac{\sqrt{\xi_b} \mathbf{g}_1^T (\mathbf{m}_0 - \mathbf{m}_1)}{\sqrt{\pi \mathbf{g}_1^T \mathbf{\Gamma} \mathbf{g}_1}}. \tag{3.58}$$

Substituting into (3.6), the low SNR ZZB is approximately

$$\overline{\epsilon^2} \geq \frac{1}{T} \int_0^T \Delta(T-\Delta) \Big[\frac{1}{2} - \frac{1}{2} \frac{\sqrt{\xi_b} \mathbf{g}_1^T (\mathbf{m}_0 - \mathbf{m}_1)}{\sqrt{\pi \mathbf{g}_1^T \mathbf{\Gamma} \mathbf{g}_1}} \Big] d\Delta. \tag{3.59}$$

Using the definitions of $\mathbf{g}_1$ in (3.50), $\mathbf{\Gamma}$ in (3.119), $\mathbf{R}_m$ in (3.117) and (3.118), and $\mathbf{m}_m$ in (3.119), it can be easily shown that

$$\mathbf{g}_1^T (\mathbf{m}_0 - \mathbf{m}_1) = \mathbf{g}_1^T \mathbf{\Gamma} \mathbf{g}_1 = 2 \boldsymbol{\mu}_\alpha^T (\mathbf{S}_{00} - \mathbf{S}_{01}) \boldsymbol{\mu}_\alpha = \sum_{k=-(L-1)}^{L-1} 2(\beta_{-kT_t} - \beta_{\Delta - kT_t}) \boldsymbol{\mu}_\alpha^T \mathbf{J}^k \boldsymbol{\mu}_\alpha.$$

Therefore, the desired low SNR ZZB is arrived, given by

$$\overline{\epsilon^2} \geq \frac{1}{T} \int_0^T \Delta(T-\Delta) \left[\frac{1}{2} - \sqrt{\frac{\xi_b}{2\pi}} \sqrt{\sum_{k=-(L-1)}^{L-1} (\beta_{-kT_t} - \beta_{\Delta - kT_t}) \boldsymbol{\mu}_\alpha^T \mathbf{J}^k \boldsymbol{\mu}_\alpha} \right] d\Delta. \tag{3.60}$$

The resulting bound is a function of the channel mean $\boldsymbol{\mu}_\alpha$ and signal correlation β_τ, while not depending on the channel correlation because the term associated with $\mathbf{\Psi}_2$ in (3.55) has been neglected.

3.3.3.2 High SNR Regime

Now consider large ξ_b. Rewrite (3.19) as

$$\mathbf{X} = (\mathbf{I} + \mathbf{V}^{-\frac{1}{2}} \mathbf{S}_{00}^{-1} \mathbf{V}^{-\frac{1}{2}} \xi_b^{-1})(\xi_b \mathbf{V}^{\frac{1}{2}} \mathbf{S}_{00} \mathbf{V}^{\frac{1}{2}}),$$

so that the Taylor expansion of $\mathbf{X}^{-1}$ can be expressed as

$$\mathbf{X}^{-1} = \mathbf{V}^{-\frac{1}{2}} \mathbf{S}_{00}^{-1} \mathbf{V}^{-\frac{1}{2}} \xi_b^{-1} - \mathbf{V}^{-\frac{1}{2}} \mathbf{S}_{00}^{-1} \mathbf{V}^{-1} \mathbf{S}_{00}^{-1} \mathbf{V}^{-\frac{1}{2}} \xi_b^{-2} + \mathbf{O}(\xi_b^{-3}). \tag{3.61}$$

It follows that

$$\mathbf{V}^{\frac{1}{2}}\mathbf{X}^{-1}\mathbf{V}^{\frac{1}{2}} = \mathbf{S}_{00}^{-1}\xi_b^{-1} - \mathbf{S}_{00}^{-1}\mathbf{V}^{-1}\mathbf{S}_{00}^{-1}\xi_b^{-2} + \mathbf{O}(\xi_b^{-3}). \tag{3.62}$$

Subsequently, $\mathbf{\Psi}$ and $\mathbf{g}$ become[2]

$$\mathbf{\Psi} = \frac{1}{E_{\rm rx}}\left[\xi_b\mathbf{\Psi}_1 + \xi_b^0\mathbf{\Psi}_0 + \mathbf{O}(\xi_b^{-1})\right], \quad \mathbf{g} = \frac{1}{\sqrt{E_{\rm rx}}}\left[\xi_b^0\mathbf{g}_0 + \mathbf{O}(\xi_b^{-1})\right],$$

in which

$$\mathbf{\Psi}_1 = \frac{1}{2}\begin{bmatrix} \mathbf{S}_{00}^{-1} & \mathbf{0} \\ \mathbf{0} & -\mathbf{S}_{00}^{-1} \end{bmatrix}, \quad \mathbf{\Psi}_0 = \frac{1}{2}\begin{bmatrix} -\mathbf{S}_{00}^{-1}\mathbf{V}^{-1}\mathbf{S}_{00}^{-1} & \mathbf{0} \\ \mathbf{0} & \mathbf{S}_{00}^{-1}\mathbf{V}^{-1}\mathbf{S}_{00}^{-1} \end{bmatrix},$$
$$\mathbf{g}_0 = \begin{bmatrix} \mathbf{S}_{00}^{-1}\mathbf{V}^{-1}\boldsymbol{\mu}_\alpha \\ -\mathbf{S}_{00}^{-1}\mathbf{V}^{-1}\boldsymbol{\mu}_\alpha \end{bmatrix}. \tag{3.63}$$

Now $\widetilde{\mathbf{A}}_m(s)$, $\widetilde{\mathbf{p}}_m$ and k_m have Taylor expansions

$$\begin{aligned}
\widetilde{\mathbf{A}}_m(s) &= \mathbf{I} - 2s\mathbf{\Sigma}_m\mathbf{\Psi} = \mathbf{I} - 2sE_{\rm rx}(\mathbf{R}_m\mathbf{V}\mathbf{R}_m^T + \xi_b^{-1}\mathbf{\Gamma})\cdot\frac{1}{E_{\rm rx}}\left[\xi_b\mathbf{\Psi}_1 + \xi_b^0\mathbf{\Psi}_0 + \mathbf{O}(\xi_b^{-1})\right] \\
&= \mathbf{I} + s\left[\underbrace{-2\mathbf{R}_m\mathbf{V}\mathbf{R}_m^T\mathbf{\Psi}_1}_{\mathbf{A}_1}\xi_b + \underbrace{(-2\mathbf{R}_m\mathbf{V}\mathbf{R}_m^T\mathbf{\Psi}_0 - 2s\mathbf{\Gamma}\mathbf{\Psi}_1)}_{\mathbf{A}_0}\xi_b^0\right] + \mathbf{O}(\xi_b^{-1}) \\
&= \mathbf{I} + s\left(\mathbf{A}_1\xi_b + \mathbf{A}_0\xi_b^0\right) + \mathbf{O}(\xi_b^{-1}),
\end{aligned} \tag{3.64}$$

$$\begin{aligned}
\widetilde{\mathbf{p}}_m = \mathbf{g} + 2\mathbf{\Psi}\boldsymbol{\mu}_m &= \frac{1}{\sqrt{E_{\rm rx}}}\left[\underbrace{2\mathbf{\Psi}_1\mathbf{m}_m}_{\mathbf{p}_1}\xi_b + \underbrace{(\mathbf{g}_0 + 2\mathbf{\Psi}_0\mathbf{m}_m)}_{\mathbf{p}_0}\xi_b^0 + \mathbf{O}(\xi_b^{-1})\right] \\
&= \frac{1}{\sqrt{E_{\rm rx}}}\left[\mathbf{p}_1\xi_b + \mathbf{p}_0\xi_b^0 + \mathbf{O}(\xi_b^{-1})\right],
\end{aligned} \tag{3.65}$$

$$k_m = \boldsymbol{\mu}_m^T\mathbf{\Psi}\boldsymbol{\mu}_m + \mathbf{g}^T\boldsymbol{\mu}_m = \mathbf{m}_m^T\mathbf{\Psi}_1\mathbf{m}_m\xi_b + (\mathbf{g}_0^T\mathbf{m}_m + \mathbf{m}_m^T\mathbf{\Psi}_0\mathbf{m}_m)\xi_b^0 + O(\xi_b^{-1}), \tag{3.66}$$

where $\mathbf{A}_1$ is singular and $\mathbf{A}_0$ is non-singular.

Here the development focuses on the case of large ξ_b, but note that $|s|$ will vary from small to large. In order to easily evaluate the inverse and determinant of $\widetilde{\mathbf{A}}_m(s)$

[2]For clarity in the expansion in terms of SNR ξ_b, the notation ξ_b^0 is preserved, although $\xi_b^0 = 1$.

for large ξ_b and small-to-large $|s|$, it is inappropriate to view $s\mathbf{A}_1$ as the dominant term in (3.64) due to the singularity of $\mathbf{A}_1$ and possibly small $|s|$. Thus, (3.64) should not be regarded as a power series in ξ_b alone. Instead, an analytically elegant approach would be to expand the appropriate quantities as a function of both s and ξ_b in order to cope with a large range of $|s|$ and large ξ_b. However, this leads to significant complexity, e.g., using piece-wise approximations for different variable range combinations to complete the integration in the probability evaluation. Fortunately, numerical study reveals that the MGF is very steep around its peak at high SNR (the pdf is much flatter than for the low SNR case). This observation permits us to focus on the small $|s|$ region only. Accordingly, the inverse and determinant of $\widetilde{\mathbf{A}}_m(s)$ is firstly expressed with respect to s using the Taylor expansions (B.11), (B.12) and (B.13) in Appendix B.1.1

$$\begin{aligned}
\widetilde{\mathbf{A}}_m^{-1}(s) &= \left[\mathbf{I} + s\left(\mathbf{A}_1\xi_b + \mathbf{A}_0\xi_b^0\right) + \mathbf{O}(\xi_b^{-1})\right]^{-1} \\
&= \mathbf{I} - s\left(\mathbf{A}_1\xi_b + \mathbf{A}_0\xi_b^0\right) + \mathbf{O}(|s|^2) + \mathbf{O}(\xi_b^{-1}) \\
&= \xi_b \underbrace{(-s\mathbf{A}_1)}_{\mathbf{B}_1} + \xi_b^0 \underbrace{(\mathbf{I} - s\mathbf{A}_0)}_{\mathbf{B}_0} + \mathbf{O}(|s|^2) + \mathbf{O}(\xi_b^{-1}) \\
&= \xi_b\mathbf{B}_1 + \mathbf{B}_0 + \mathbf{O}(|s|^2) + \mathbf{O}(\xi_b^{-1}), \qquad (3.67)
\end{aligned}$$

$$\begin{aligned}
|\widetilde{\mathbf{A}}_m(s)| &= \left|\mathbf{I} + s\left(\mathbf{A}_1\xi_b + \mathbf{A}_0\xi_b^0\right) + \mathbf{O}(\xi_b^{-1})\right| \\
&= 1 + s\cdot tr(\xi_b\mathbf{A}_1 + \mathbf{A}_0) + O(|s|^2) + O(\xi_b^{-1}), \qquad (3.68)
\end{aligned}$$

$$|\widetilde{\mathbf{A}}_m(s)|^{-\frac{1}{2}} = \xi_b\left[-\frac{s}{2}tr(\mathbf{A}_1)\right] + \left[1 - \frac{s}{2}tr(\mathbf{A}_0)\right] + O(|s|^2) + O(\xi_b^{-1}). \qquad (3.69)$$

By eqs. (3.65) and (3.67), it follows that

$$\begin{aligned}
\widetilde{\mathbf{p}}_m^T\widetilde{\mathbf{A}}_m^{-1}(s)\mathbf{\Sigma}_m\widetilde{\mathbf{p}}_m &= \left[\mathbf{p}_1\xi_b + \mathbf{p}_0\xi_b^0 + \mathbf{O}(\xi_b^{-1})\right]^T\left[\xi_b\mathbf{B}_1 + \mathbf{B}_0 + \mathbf{O}(|s|^2) + \mathbf{O}(\xi_b^{-1})\right] \\
&\quad \times(\mathbf{R}_m\mathbf{V}\mathbf{R}_m^T + \xi_b^{-1}\mathbf{\Gamma})\left[\mathbf{p}_1\xi_b + \mathbf{p}_0\xi_b^0 + \mathbf{O}(\xi_b^{-1})\right] \\
&= \xi_b^3q_3 + \xi_b^2q_2 + \xi_bq_1 + q_0 + O(|s|^2) + O(\xi_b^{-1}), \qquad (3.70)
\end{aligned}$$

where

$$q_3 = \mathbf{p}_1^T \mathbf{B}_1 \mathbf{R}_m \mathbf{V} \mathbf{R}_m^T \mathbf{p}_1,$$

$$q_2 = \mathbf{p}_1^T \mathbf{B}_1 (\mathbf{R}_m \mathbf{V} \mathbf{R}_m^T \mathbf{p}_0 + \mathbf{\Gamma} \mathbf{p}_1) + (\mathbf{p}_1^T \mathbf{B}_0 + \mathbf{p}_0^T \mathbf{B}_1) \mathbf{R}_m \mathbf{V} \mathbf{R}_m^T \mathbf{p}_1,$$

$$q_1 = \mathbf{p}_1^T \mathbf{B}_1 \mathbf{\Gamma} \mathbf{p}_0 + (\mathbf{p}_1^T \mathbf{B}_0 + \mathbf{p}_0^T \mathbf{B}_1)(\mathbf{R}_m \mathbf{V} \mathbf{R}_m^T \mathbf{p}_0 + \mathbf{\Gamma} \mathbf{p}_1) + \mathbf{p}_0^T \mathbf{B}_0 \mathbf{R}_m \mathbf{V} \mathbf{R}_m^T \mathbf{p}_1,$$

$$q_0 = (\mathbf{p}_1^T \mathbf{B}_0 + \mathbf{p}_0^T \mathbf{B}_1) \mathbf{\Gamma} \mathbf{p}_0 + \mathbf{p}_0^T \mathbf{B}_0 (\mathbf{R}_m \mathbf{V} \mathbf{R}_m^T \mathbf{p}_0 + \mathbf{\Gamma} \mathbf{p}_1). \tag{3.71}$$

Substituting eqs. (3.66), (3.69) and (3.70) into (3.38), the MGF becomes

$$\begin{aligned} \Theta_m(s) \;=\; & \left\{ \xi_b \left[-\frac{s}{2} tr(\mathbf{A}_1) \right] + \left[1 - \frac{s}{2} tr(\mathbf{A}_0) \right] + O(|s|^2) + O(\xi_b^{-1}) \right\} \\ & \times \exp\left\{ \xi_b^3 q_3 + \xi_b^2 q_2 + \xi_b [q_1 + s(\mathbf{m}_m^T \mathbf{\Psi}_1 \mathbf{m}_m)] + q_0 + O(|s|^2) + O(\xi_b^{-1}) \right\}. \end{aligned} \tag{3.72}$$

Finally, by ignoring the high order terms of both s and ξ_b the desired high SNR MGF approximation follows

$$\begin{aligned} \Theta_m(s) \approx & \left\{ \xi_b \left[-\frac{s}{2} tr(\mathbf{A}_1) \right] + \left[1 - \frac{s}{2} tr(\mathbf{A}_0) \right] \right\} \\ & \exp\left\{ \xi_b^3 q_3 + \xi_b^2 q_2 + \xi_b [q_1 + s(\mathbf{m}_m^T \mathbf{\Psi}_1 \mathbf{m}_m)] + q_0 \right\}. \end{aligned} \tag{3.73}$$

Setting $s = j2\pi f$ in (3.73) and substituting into (3.40) and (3.41), the probabilities can be found for $P_e(\Delta)$ in (3.115).

3.3.3.3 Thresholds and Performance Regions

Our asymptotic analysis results at low and high SNRs are valuable in determining disjoint segments of SNR ξ_b, separated by thresholds, that characterize different performance regions. The thresholds are defined as the SNR values where the ZZBs and the asymptotic ZZB approximations differ by 1/2 [46]. Let us apply this rule to the low SNR regime first based on (3.60). Taking the limit $\xi_b \to 0$, the convergence level is

$\frac{1}{12}T^2$. Therefore, one can find the threshold $\xi_b = \delta_1$ that yields half of the convergence level

$$\frac{1}{T}\int_0^T \Delta(T-\Delta)\left[\frac{1}{2} - \sqrt{\frac{\delta_1}{2\pi}}\sqrt{\sum_{k=-(L-1)}^{L-1}(\beta_{-kT_t} - \beta_{\Delta-kT_t})\boldsymbol{\mu}_\alpha^T \mathbf{J}^k \boldsymbol{\mu}_\alpha}\right] d\Delta = \frac{1}{24}T^2. \quad (3.74)$$

Solving this equation numerically, one can obtain δ_1.

The threshold $\xi_b = \delta_2$ at high SNR can be found similarly. Substituting (3.73) into (3.40) and (3.41), and subsequently into (3.115), $P_e(\Delta)$ follows. Using that result in (3.6) and setting it equal to half the general ZZB from (3.6), an equation in δ_2 results.

3.3.4 Important ZZB Special Cases

In this section, the ZZB for three cases of broad interest is considered. First is narrowband channels, corresponding to Rayleigh/Rician flat fading, and a result is recovered, derived differently by Kozick and Sadler [42, 43]. Then wideband channels with independent taps are considered, with the signal bandwidth matching the channel bandwidth. Finally, the deterministic case when the receiver knows the channel is discussed.

3.3.4.1 Single Tap Channel

With $L = 1$, the channel gain α follows $\mathcal{N} \sim (\mu_\alpha, \sigma_\alpha^2)$ corresponding to Rayleigh/Rician flat fading. The received signal is modeled by

$$y(t) = \sqrt{E_{\text{rx}}}\alpha s_m(t) + n(t), \quad (3.75)$$

and correlation and other terms are

$$I_y \triangleq \int_{T_0} y^2(t)dt, \;\; r_m \triangleq \int_{T_0} s_m y(t)dt, \;\; S_{mm} \triangleq \int_{T_0} s_m^2(t)dt, \;\; S_{01} = S_{10} \triangleq \int_{T_0} s_0(t)s_1(t)dt.$$

$$X = 1+\xi_b\sigma_\alpha^2 S_{00}, \;\; v_m = \frac{\sqrt{E_{\text{rx}}}}{\sigma_n^2}\sigma_\alpha r_m - \frac{E_{\text{rx}}}{\sigma_n^2}\sigma_\alpha S_{00}\mu_\alpha, \;\; c_m = \frac{\sqrt{E_{\text{rx}}}}{\sigma_n^2}\mu_\alpha r_m - \frac{E_{\text{rx}}}{2\sigma_n^2}\mu_\alpha^2 S_{00} - \frac{I_y}{2\sigma_n^2}.$$

The distribution of the received signal is proportional to

$$p(y(t)|m\Delta) \propto \exp\left\{Wr_m^2 + hr_m\right\}, \tag{3.76}$$

where

$$W = \frac{\xi_b^2\sigma_\alpha^2}{2(1+\xi_b\sigma_\alpha^2 S_{00})}, \quad h = \left[\xi_b - \frac{\xi_b^2\sigma_\alpha^2 S_{00}}{(1+\xi_b\sigma_\alpha^2 S_{00})}\right]\mu_\alpha.$$

The mean and variance for $\widetilde{\mathbf{r}}_m$ are given by

$$\boldsymbol{\mu}_0 = \sqrt{E_{\rm rx}}\begin{bmatrix} S_{00}\mu_\alpha \\ S_{10}\mu_\alpha \end{bmatrix}, \quad \boldsymbol{\Sigma}_0 = E_{\rm rx}\begin{bmatrix} S_{00}^2 + \xi_b^{-1}S_{00} & S_{00}S_{10} + \xi_b^{-1}S_{01} \\ S_{00}S_{10} + \xi_b^{-1}S_{10} & S_{10}^2 + \xi_b^{-1}S_{00} \end{bmatrix},$$

$$\boldsymbol{\mu}_1 = \sqrt{E_{\rm rx}}\begin{bmatrix} S_{01}\mu_\alpha \\ S_{00}\mu_\alpha \end{bmatrix}, \quad \boldsymbol{\Sigma}_1 = E_{\rm rx}\begin{bmatrix} S_{01}^2 + \xi_b^{-1}S_{00} & S_{00}S_{01} + \xi_b^{-1}S_{01} \\ S_{00}S_{01} + \xi_b^{-1}S_{10} & S_{00}^2 + \xi_b^{-1}S_{00} \end{bmatrix}.$$

In this case, the log-likelihood ratio becomes

$$\mathcal{L} = W(r_0^2 - r_1^2) + h(r_0 - r_1) = \mathbf{r}^T\boldsymbol{\Psi}\mathbf{r} + \mathbf{g}^T\mathbf{r}, \tag{3.77}$$

$$\boldsymbol{\Psi} = \begin{bmatrix} W & 0 \\ 0 & -W \end{bmatrix}, \quad \mathbf{g} = \begin{bmatrix} h \\ -h \end{bmatrix}.$$

In particular for the Rayleigh fading case $\mu_\alpha = 0$, then $h = 0$ and $\mathcal{L} = W(r_0^2 - r_1^2)$. Since $W > 0$, the LLR test reduces to comparison of r_0^2 with r_1^2, the signal power[3]. Thus, the error probability expression before simplification matches eq. (113) in [43] under $N = 1$ therein. Moreover, $\boldsymbol{\mu}_0 = [0, 0]^T$, and

$$\begin{aligned} \boldsymbol{\Sigma}_0 &= E_{\rm rx}\xi_b^{-1}\begin{bmatrix} S_{00} + \xi_b S_{00}^2 & (1+\xi_b S_{00})S_{01} \\ (1+\xi_b S_{00})S_{01} & S_{00} + \xi_b S_{10}^2 \end{bmatrix} \\ &= S_{00}\sigma_n^2(1+\xi_b S_{00})\begin{bmatrix} 1 & \frac{S_{01}}{S_{00}} \\ \frac{S_{01}}{S_{00}} & \frac{1+\xi_b(\frac{S_{01}^2}{S_{00}})}{1+\xi_b S_{00}} \end{bmatrix}. \end{aligned} \tag{3.78}$$

[3]As pointed out in [42, 43], the optimal detector corresponds to a non-coherent matched filter.

If defining the SNR as in eq. (75) in [43],

$$\overline{\mathrm{SNR}} \triangleq \xi_b, \quad \rho(0) \triangleq S_{00}, \quad \rho(\theta) \triangleq S_{01}, \quad \mathcal{N}_o \triangleq \sigma_n^2, \tag{3.79}$$

then our eq. (3.78) above becomes

$$\mathbf{\Sigma}_0 = \rho_0 \mathcal{N}_0 \left(1 + \overline{\mathrm{SNR}}\rho_0\right) \begin{bmatrix} 1 & \frac{\rho(\theta)}{\rho_0} \\ \frac{\rho(\theta)}{\rho_0} & \frac{1+\overline{\mathrm{SNR}}(\frac{\rho(\theta)^2}{\rho_0})}{1+\overline{\mathrm{SNR}}\rho_0} \end{bmatrix}, \tag{3.80}$$

which takes the same form as eq. (115) in [43]. With the above results, the same closed form expression for error probability P_e as in eq. (116) and (117) of [43] can be obtained

$$P_e = \frac{1}{2} - \frac{1}{2}\left[1 + \frac{4(1 + \overline{\mathrm{SNR}} \cdot \rho(0))}{\left(\rho(0) \cdot \overline{\mathrm{SNR}}\right)^2 \cdot [1 - |\rho(\theta)/\rho(0)|^2]}\right]^{-1/2}. \tag{3.81}$$

See [42, 43] for extension to multiple narrowband independent channels, and further results including CRBs and estimation.

3.3.4.2 Wideband Waveform with Independent Channel Taps

This case assumes that the waveform bandwidth matches the channel, with an ideal correlation function such that $\beta_\tau = 0$ for $\tau > T_t$ and $\beta_\tau \neq 0$ for $|\tau| \leq T_t$. Thus, the waveform autocorrelation matrix $\mathbf{S}_{00}$ in (3.16) becomes $\beta_0\mathbf{I}$, and $\mathbf{S}_{01}$ has at most two nonzero subdiagonals. Independent channel taps are also assumed, where each channel tap may have different mean and variance. This corresponds to many measured wireless fading channel models, e.g., with an exponential decay in the variance. Now, the channel mean vector is $\boldsymbol{\mu}_\alpha = [\mu_{\alpha_1}, \cdots, \mu_{\alpha_L}]^T$ and covariance matrix $\mathbf{V} = \mathrm{diag}[\sigma^2_{\alpha_1}, \cdots, \sigma^2_{\alpha_L}]$.

Let us examine the dependence of the two data vectors $\mathbf{r}_0$ and $\mathbf{r}_1$ in the LLR expression. As an example, assume hypothesis H_0. Using (3.116) and (3.30) finds

$$\mathrm{VAR}(\mathbf{r}_0|H_0) = E_{\mathrm{rx}}\beta_0^2\mathbf{V} + \sigma_n^2\mathbf{I}, \quad \mathrm{VAR}(\mathbf{r}_1|H_0) = E_{\mathrm{rx}}\mathbf{S}_{10}\mathbf{V}\mathbf{S}_{10}^T + \sigma_n^2\mathbf{I},$$

$$\mathrm{COV}(\mathbf{r}_0|H_0, \mathbf{r}_1|H_0) = E_{\mathrm{rx}}\beta_0\mathbf{V}\mathbf{S}_{10}^T + \sigma_n^2\mathbf{S}_{10}^T. \tag{3.82}$$

These simplified expressions can be used to replace their counterparts in our earlier ZZB development.

Remark: Further simplifications do not appear to be straightforward. For example, with multiple independent flat fading (single tap) channels, a simplified ZZB expression is obtained in Section 5.3 in [43], using results from Appendix B of [84] or Appendix 9A of [82]. However, in our case, note that $\mathbf{S}_{10}$ is a function of the continuous variable Δ. While the elements of $\mathbf{r}_0$ are independent, the entries of $\mathbf{r}_1$ are not necessarily independent except for some special values of Δ such that $\mathbf{S}_{10}$ has only one non-zero subdiagonal. Also, from the above covariance, $\mathbf{r}_0$ and $\mathbf{r}_1$ are generally correlated for most values of Δ. These conditions violate the assumptions used in [43].

3.3.4.3 Known Channel

Here comes the case when the channel $\boldsymbol{\alpha}$ is fixed and known to the receiver. Now, the LLR is governed by (3.14), rather than taking the expectation over channel realizations as in (3.17). The LLR can be easily shown to be $\mathbf{r}_0^T\boldsymbol{\alpha} - \mathbf{r}_1^T\boldsymbol{\alpha}$, with some constants suppressed[4]. It follows that

$$\mathcal{L}_0 = \sqrt{E_{\text{rx}}}\boldsymbol{\alpha}^T(\mathbf{S}_{00} - \mathbf{S}_{10})\boldsymbol{\alpha} + \boldsymbol{\alpha}^T(\mathbf{z}_0 - \mathbf{z}_1) \underset{H_1}{\overset{H_0}{\gtrless}} 0,$$

which is Gaussian distributed with mean $\sqrt{E_{\text{rx}}}\boldsymbol{\alpha}^T(\mathbf{S}_{00}-\mathbf{S}_{10})\boldsymbol{\alpha}$ and variance $\sigma_n^2[\boldsymbol{\alpha}^T(\mathbf{s}_0 - \mathbf{s}_1)]^2$. Then,

$$Pr\{\mathcal{L}_0 < 0\} = Q\left(\frac{\sqrt{E_{\text{rx}}}\boldsymbol{\alpha}^T(\mathbf{S}_{00} - \mathbf{S}_{10})\boldsymbol{\alpha}}{\sigma_n|\boldsymbol{\alpha}^T(\mathbf{s}_0 - \mathbf{s}_1)|}\right).$$

Similarly, it follows that $Pr\{\mathcal{L}_1 > 0\}$ takes the same expression as above. Therefore,

$$P_e(\Delta) = Pr\{\mathcal{L}_0 < 0\} = Q\left(\frac{\sqrt{\xi_b}\boldsymbol{\alpha}^T(\mathbf{S}_{00} - \mathbf{S}_{10})\boldsymbol{\alpha}}{|\boldsymbol{\alpha}^T(\mathbf{s}_0 - \mathbf{s}_1)|}\right). \tag{3.83}$$

[4]With the signal and channel known to the receiver, the corresponding optimal detector is a coherent matched filter.

Notice that $\mathbf{S}_{10}$ and $\mathbf{s}_1$ are functions of Δ. Substituting into (3.6), the ZZB can be evaluated. The low and high SNR asymptotic ZZB expressions can also be found by incorporating the power series expansion of the Q-function in, as in Section 3.3.3.

3.3.5 Summary of the ZZB Computation

This section summarizes the computation of the ZZB. The ZZB can be evaluated for the various cases as follows, with reference to Table 3.1. The computation flows downward in the table. Below the author describes the general ZZB computation, as well as the low and high SNR approximations from Section 3.3.3. See also Section 3.3.4 for other special cases.

Step 0 *(Initialization).* The input parameters to the bound are given as follows. The uniform prior on the time delay is specified by duration T, the signal is specified by its deterministic autocorrelation β_τ, and the random Gaussian channel parameters are mean $\boldsymbol{\mu}_\alpha$, covariance matrix $\mathbf{V}$, number of taps L, and the tap spacing in time T_t.

Step 1 *(Intermediate variables).* Using the initial specification from Step 0, simple linear algebraic operations yield the intermediate variables $\mathbf{S}_{00}$, $\mathbf{S}_{01}$, $\mathbf{S}_{10}$, $\mathbf{S}_{11}$, $\mathbf{R}_0$, $\mathbf{R}_1$, $\mathbf{X}$, $\mathbf{W}$, $\mathbf{h}$, $\boldsymbol{\Psi}$, $\mathbf{g}$, $\boldsymbol{\Gamma}$, and the distribution parameters $\boldsymbol{\mu}_m$, $\mathbf{m}_m$ and $\boldsymbol{\Sigma}_m$ of the data vector $\mathbf{r}_m$.

Step 2 *(Moment generating function).* Next the MGF is calculated. Generally, either the direct form or the compact form can be employed (see the discussion in Section 3.4.3). The table also shows the variables associated with the low and high SNR asymptotic cases.

1. *MGF direct form.* The variables $\widetilde{\mathbf{A}}_m(s)$, k_m and $\widetilde{\mathbf{p}}_m$ are calculated, and then the MGF is computed by (3.38).

2. *MGF compact form.* The variable $\mathbf{b}_m$ is found by (3.120), and the eigenvalues λ_k of $\mathbf{\Sigma}_m^{\frac{1}{2}}\mathbf{\Psi}\mathbf{\Sigma}_m^{\frac{1}{2}}$ using (3.121). The MGF is computed by substitution into (3.122).

3. *Low SNR approximation.* Compute $\mathbf{g}_1$ from (3.50), and then use (3.56).

4. *High SNR approximation.* Compute variables $\mathbf{A}_0$, $\mathbf{A}_1$, q_0, q_1, q_2, q_3, $\mathbf{\Psi}_0$, and $\mathbf{\Psi}_1$, and then use (3.73).

Step 3 *(Probability of error).* Next P_e, the probability of error of the hypothesis test associated with the ZZB, is found by substituting the MGF from Step 2 into (3.40) and (3.41), and then into (3.115). Note that for the low SNR approximation, P_e can alternatively be computed using (3.58).

Step 4. The ZZB is obtained by substituting P_e into (3.6).

Next let us discuss some numerical issues in the ZZB computation relating to the MGF. The MGF can be computed using the direct or the compact form. The direct form relies on computing the determinant and inverse of $\widetilde{\mathbf{A}}_m(s)$ for each $s = j2\pi f$, which is computationally expensive. The compact form allows us to exploit the symmetry of $\mathbf{\Sigma}_m^{\frac{1}{2}}\mathbf{\Psi}\mathbf{\Sigma}_m^{\frac{1}{2}}$ to compute the determinant and inverse efficiently from its eigenvalues and eigenvectors, which are independent of s, and then (3.122) follows easily. Thus, the compact form is generally preferred, and it is adopted in our numerical studies that follow.

Step 3 relies on the Fourier transform of the MGF in (3.40) and (3.41), which can be computed efficiently using the FFT, but requires truncation in the frequency variable f due to the infinite integration limits. Thus, the truncation value must be specified, as well as the size of the FFT used to sample the MGF up to its truncation point. As noted in Section 3.3.3, the MGF concentrates around its peak at high SNR, and in the cases studied, the truncation error diminishes rapidly. However, at lower SNR, larger

Table 3.1: Symbols and equations for evaluating the ZZB and its approximations

		Notation	Equations
(0) Initialization		T, β_τ, $\boldsymbol{\mu}_\alpha$, $\mathbf{V}$, L, T_t	
(1) Intermediate Variables		$\mathbf{S}_{00}$, $\mathbf{S}_{01}$, $\mathbf{S}_{10}$, $\mathbf{S}_{11}$	(3.16)
		$\mathbf{R}_0$	(3.117)
		$\mathbf{R}_1$	(3.118)
		$\mathbf{X}$	(3.19)
		$\mathbf{W}$	(3.21)
		$\mathbf{h}$	(3.22)
		$\boldsymbol{\Psi}$, $\mathbf{g}$	(3.25)
		$\boldsymbol{\Gamma}$	(3.119)
		$\boldsymbol{\mu}_m$, $\mathbf{m}_m$, $\boldsymbol{\Sigma}_m$	(3.119)
(2) MGF Associated Variables	Direct Form	$\widetilde{\mathbf{A}}_m(s)$, k_m, $\widetilde{\mathbf{p}}_m$	(3.39)
	Compact Form	$\mathbf{b}_m$	(3.120)
		λ_k	(3.121)
	Low SNR Approx.	$\mathbf{g}_1$	(3.50)
	High SNR Approx.	$\mathbf{A}_0$, $\mathbf{A}_1$	(3.64)
		q_0, q_1, q_2, q_3	(3.71)
		$\boldsymbol{\Psi}_0$, $\boldsymbol{\Psi}_1$	(3.63)
MGF	Direct Form	$\Theta_m(s)$	(3.38)
	Compact Form		(3.122)
	Low SNR Approx.		(3.56)
	High SNR Approx.		(3.73)
(3) Probability of Error		P_e	(3.115) (3.40) (3.41)
(4) ZZB		$\overline{\epsilon^2}$	(3.6)

truncation thresholds are generally required, and longer FFTs are needed to sample the truncated MGF.

A related issue, arising with the MGF transform computation, is the inherent rectangular window weighting; the pdf estimate is convolved with a sinc function. When P_e is large (i.e., low SNR), any numerically induced error is generally negligible. But when P_e is small (high SNR), then oscillations in the pdf estimate may lead to an error in P_e. Therefore generally at high SNR, the pdf estimate is smoothed by convolving with a positive valued smoothing function, ensuring that the pdf estimate is strictly greater than or equal to zero. The appropriate length of the averaging window depends on the sampling interval of the pdf. The oscillation can also be alleviated by increasing the MGF truncation window length as well as the FFT length within the window, with an increase in computational complexity.

3.3.6 Bayesian TDE Estimation, the Average Conditional CRB, and the ZZB

For comparison with our ZZB, the author first presents the MAP and Bayesian maximum-likelihood time delay estimators. Then an alternative bound is developed, deriving the expected value of the conditional CRB, averaging over the random channel. Finally, the comparison of the MAP estimator mean square error performance at low SNR to that predicted by the ZZB is given, showing how the approximations in the ZZB lead to a bound that does not precisely converge to the prior distribution at low SNR, whereas the MAP estimator does. Convergence of the MAP estimate to the ZZB at high SNR is shown in the examples in Section 3.3.7.

3.3.6.1 Bayesian Time Delay Estimation

The MAP and Bayesian ML estimators are commonly used for estimating random parameters. Generally they are equivalent as the SNR increases to infinity. However, if the *a priori* distribution of the parameter is uniformly distributed, these two estimators are the same in the whole range of SNR [88]. For our case the unconditional distribution of the received signal, averaged over the channel distribution, is given by equation (3.20). With the uniform prior on the time delay $f_{t_0}(t_0) = \frac{1}{T}$, then the MAP and Bayesian ML estimators are

$$\widehat{t}_{0,\mathrm{MAP}} = \arg\max_{t_0} \left\{ f_{t_0}(t_0) p(y(t)|t_0) \right\} = \arg\max_{t_0} \left\{ \frac{1}{T} \exp\left(\mathbf{r}_{t_0}^T \mathbf{W} \mathbf{r}_{t_0} + \mathbf{h}^T \mathbf{r}_{t_0} \right) \right\}, \quad (3.84)$$

$$\widehat{t}_{0,\mathrm{ML}} = \arg\max_{t_0} \left\{ p(y(t)|t_0) \right\} = \arg\max_{t_0} \left\{ \exp\left(\mathbf{r}_{t_0}^T \mathbf{W} \mathbf{r}_{t_0} + \mathbf{h}^T \mathbf{r}_{t_0} \right) \right\}, \quad (3.85)$$

and so they are identical in this case.

For later comparison, the generalized maximum-likelihood estimator is also stated. For our problem, this assumes deterministic channel and estimates the time delay by

$$\widehat{t}_{0,\mathrm{GML}} = \arg\max_{t_0} \left\{ p(y(t)|t_0, \boldsymbol{\alpha}) \right\} = \arg\max_{t_0} \left\{ \mathbf{r}_{t_0}^T \mathbf{S}_{00}^{-1} \mathbf{r}_{t_0} \right\}. \quad (3.86)$$

This GML estimator does not use knowledge of the channel distribution, and is then equivalent to a MMSE estimator [89]. Section 3.3.7 will show that lack of knowledge of the channel distribution significantly impairs the performance of the GML estimation with respect to MAP estimation.

3.3.6.2 Cramér-Rao Bound

Next consider the Cramér-Rao bound for the problem and the Bayesian CRB (BCRB) should be employed generally. However here, with a uniform prior, the regularity condition for computing the BCRB is not satisfied and consequently the BCRB

does not exist [83]. As an alternative, the author derives the expectation of the CRB conditioned on the random channel, which is referred to as the expected conditional CRB (ECRB) [40].

Generally, if the estimator is assumed asymptotically conditionally unbiased for every value of the random parameter, the MAP/ML estimators should provide performance converging to the ECRB at infinite SNR, as established in [40]. For the time delay estimation problem at hand, the ZZB and MLE are based on the distribution in (3.20), which has been averaged on the channel distribution, while the ECRB is to be derived from the distribution in (3.14) which is conditioned on the channel. Thus the ECRB may not converge to the prior distribution at low SNR, and at high SNR it may be a slightly weaker bound than the ZZB, as will be demonstrated in our numerical examples in Section 3.3.7.

From (3.14), the log-probability conditioned on the random time delay t_0 and the random channel vector $\boldsymbol{\alpha}$ is given by

$$\ln p(y|t_0,\boldsymbol{\alpha}) = -\frac{1}{2\sigma_n^2}\int_{T_0}\left[y(t)-\sqrt{E_{rx}}\boldsymbol{\alpha}^T\mathbf{s}(t-t_0)\right]^2 dt + \ln\mathcal{K}. \tag{3.87}$$

Differentiating leads to

$$\frac{d\ln p(y|t_0,\boldsymbol{\alpha})}{dt_0} = -\frac{1}{2\sigma_n^2}\int_{T_0} 2\left[y(t)-\sqrt{E_{rx}}\boldsymbol{\alpha}^T\mathbf{s}(t-t_0)\right]\left[-\sqrt{E_{rx}}\boldsymbol{\alpha}^T\frac{d\mathbf{s}(t-t_0)}{dt_0}\right] dt. \tag{3.88}$$

Note that the required regularity condition is satisfied

$$\begin{aligned} E_{y|t_0,\alpha}\left\{\frac{d\ln p(y|t_0,\boldsymbol{\alpha})}{dt_0}\right\} &= -\frac{1}{2\sigma_n^2}\int_{T_0} 2\left[E_{y|t_0,\alpha}\left\{y(t)|t_0,\boldsymbol{\alpha}\right\}-\sqrt{E_{rx}}\boldsymbol{\alpha}^T\mathbf{s}(t-t_0)\right] \\ &\quad\times\left[-\sqrt{E_{rx}}\boldsymbol{\alpha}^T\frac{d\mathbf{s}(t-t_0)}{dt_0}\right] dt \\ &= 0, \end{aligned} \tag{3.89}$$

where

$$E_{y|t_0,\alpha}\left\{y(t)|t_0,\boldsymbol{\alpha}\right\} = \sqrt{E_{\mathrm{rx}}}\boldsymbol{\alpha}^T\mathbf{s}(t-t_0). \tag{3.90}$$

The second derivative is

$$\begin{aligned}\frac{d^2\ln p(y|t_0,\boldsymbol{\alpha})}{dt_0^2} &= \frac{1}{\sigma_n^2}\int_{T_0}\Big\{\sqrt{E_{rx}}y(t)\boldsymbol{\alpha}^T\frac{d^2\mathbf{s}(t-t_0)}{dt_0^2} - E_{rx}\frac{d\mathbf{s}^T(t-t_0)}{dt_0}\boldsymbol{\alpha}\boldsymbol{\alpha}^T\frac{d\mathbf{s}(t-t_0)}{dt_0} \\ &\quad -E_{rx}\mathbf{s}^T(t-t_0)\boldsymbol{\alpha}\boldsymbol{\alpha}^T\frac{d^2\mathbf{s}(t-t_0)}{dt_0^2}\Big\}dt. \end{aligned}\tag{3.91}$$

The Fisher information is

$$\begin{aligned}J_F(t_0,\boldsymbol{\alpha}) &= E_{y|t_0,\alpha}\left\{-\frac{d^2\ln p(y|t_0,\boldsymbol{\alpha})}{dt_0^2}\right\} = \xi_b\int_{T_0}\frac{d\mathbf{s}^T(t-t_0)}{dt_0}\boldsymbol{\alpha}\boldsymbol{\alpha}^T\frac{d\mathbf{s}(t-t_0)}{dt_0}dt \\ &= \xi_b\boldsymbol{\alpha}^T\left[\int_{T_0}\frac{d\mathbf{s}(t-t_0)}{dt_0}\frac{d\mathbf{s}^T(t-t_0)}{dt_0}dt\right]\boldsymbol{\alpha} = \xi_b\boldsymbol{\alpha}^T\boldsymbol{\Phi}\boldsymbol{\alpha} = \xi_b\Upsilon(\boldsymbol{\alpha}), \end{aligned}\tag{3.92}$$

where $\boldsymbol{\Phi} = \int_{T_0}\frac{d\mathbf{s}(t-t_0)}{dt_0}\frac{d\mathbf{s}^T(t-t_0)}{dt_0}dt$ and $\Upsilon(\boldsymbol{\alpha}) = \boldsymbol{\alpha}^T\boldsymbol{\Phi}\boldsymbol{\alpha}$.

To compute the ECRB, the inverse of the above Fisher information is computed conditioned on both the prior on the time delay and the random channel, and then its expected value is evaluated with respect to both quantities

$$\mathrm{ECRB} \triangleq E_{t_0,\alpha}\left\{J_F^{-1}(t_0,\boldsymbol{\alpha})\right\} = \frac{1}{\xi_b}\int\frac{1}{\boldsymbol{\alpha}^T\boldsymbol{\Phi}\boldsymbol{\alpha}}\cdot p(\boldsymbol{\alpha})d\boldsymbol{\alpha} = \frac{1}{\xi_b}E_\alpha\left\{\Upsilon^{-1}(\boldsymbol{\alpha})\right\}, \tag{3.93}$$

where the distribution of $\boldsymbol{\alpha}$ is multivariate normal with mean $\boldsymbol{\mu}_{\boldsymbol{\alpha}}$ and variance $\mathbf{V}$

$$p(\boldsymbol{\alpha}) = \frac{1}{(2\pi)^{L/2}|\mathbf{V}|^{1/2}}\exp\left[-\frac{1}{2}(\boldsymbol{\alpha}-\boldsymbol{\mu}_{\boldsymbol{\alpha}})^T\mathbf{V}^{-1}(\boldsymbol{\alpha}-\boldsymbol{\mu}_{\boldsymbol{\alpha}})\right]. \tag{3.94}$$

Note that log(ECRB) is linearly decreasing with log(SNR), so the slope of its root mean square equals $-\frac{1}{2}$.

Next evaluate $E_\alpha\left\{\Upsilon^{-1}(\boldsymbol{\alpha})\right\}$ in (3.93). The result of eq. (4.5d.4) in [87] shows the negative power of a quadratic form can be expressed as an integral

$$[\Upsilon(\mathbf{x})]^{-h} = \frac{1}{\Gamma(h)}\int_0^\infty z^{h-1}e^{-z\Upsilon(\mathbf{x})}dz, \tag{3.95}$$

where $\Gamma(h)$ is the Gamma function. Applying this result generates

$$\begin{aligned} E_\alpha\left\{\Upsilon^{-1}(\boldsymbol{\alpha})\right\} &= E_\alpha\left\{\int_0^\infty e^{-z\Upsilon(\boldsymbol{\alpha})}dz\right\} = \int_0^\infty E_\alpha\left\{e^{-z\Upsilon(\boldsymbol{\alpha})}\right\}dz \\ &= -\int_{-\infty}^0 E_\alpha\left\{e^{s\Upsilon(\boldsymbol{\alpha})}\right\}ds, \end{aligned} \tag{3.96}$$

in which $E_\alpha\left\{e^{s\Upsilon(\boldsymbol{\alpha})}\right\}$ is the moment generating function of $\Upsilon(\boldsymbol{\alpha})$. By the result of eq. (B.3) in Appendix B it is expressed as

$$\begin{aligned} E_\alpha\left\{e^{s\Upsilon(\boldsymbol{\alpha})}\right\} =& |\mathbf{I} - 2s\mathbf{V}^{\frac{1}{2}}\boldsymbol{\Phi}\mathbf{V}^{\frac{1}{2}}|^{-\frac{1}{2}} \\ & \times \exp\left\{s\boldsymbol{\mu}_\alpha^T\boldsymbol{\Phi}\boldsymbol{\mu}_\alpha + 2s^2\boldsymbol{\mu}_\alpha^T\boldsymbol{\Phi}\mathbf{V}^{\frac{1}{2}}\left(\mathbf{I} - 2s\mathbf{V}^{\frac{1}{2}}\boldsymbol{\Phi}\mathbf{V}^{\frac{1}{2}}\right)^{-1}\mathbf{V}^{\frac{1}{2}}\boldsymbol{\Phi}\boldsymbol{\mu}_\alpha\right\}. \end{aligned} \tag{3.97}$$

This closed form MGF can be computed numerically, and note that a compact form similar to that in Section 3.3.2.2 can be used to accelerate the computation. The ECRB is then easily obtained from (3.97), (3.96), and (3.93) by numerical integration.

3.3.6.3 Comparing Bayesian TDE and the ZZB at Low SNR

In the low SNR regime, the Bayesian TDE is noise dominated, and the TDE mean-square error converges to the variance of the prior as the SNR goes to zero. With the uniform prior $f_{\widehat{t}_0}(\widehat{t}_0) = \frac{1}{T}$ over $[0, T]$, the MSE of our Bayesian estimate is $\epsilon^2 = \frac{T^2}{6}$. However, the low SNR convergence level of the ZZB was derived in Section 3.3.3.3 to be $\frac{T^2}{12} = \frac{1}{2}\epsilon^2$, so the ZZB does not converge to the prior at low SNR. (For example see Figure 3.2 in the next section.) This occurs because two key inequalities applied throughout the bound development by Ziv and Zakai [39] are not tight at low SNR. In the following, the author explains this gap by computing the bounding errors for our problem.

First, considering the last inequality in eq. (3) of [39], one can obtain

$$\begin{aligned}
\frac{1}{2}\int_0^{\Delta} \Pr\left\{\epsilon < -\frac{\Delta}{2}|a\right\} da &= \frac{1}{2}\int_0^{\Delta} \Pr\left\{(\widehat{t_0} - a) < -\frac{\Delta}{2}|a\right\} da \\
&= \frac{1}{2}\int_0^{\Delta} \Pr\left\{\widehat{t_0} < (a - \frac{\Delta}{2})|a\right\} da \\
&= \frac{1}{2}\int_{\frac{\Delta}{2}}^{\Delta} \frac{1}{T}(a - \frac{\Delta}{2}) da = \frac{1}{2}\cdot\frac{\Delta^2}{8T}, \qquad (3.98) \\
\frac{1}{2}\int_{T-\Delta}^{T} \Pr\left\{\epsilon > -\frac{\Delta}{2}|a\right\} da &= \frac{1}{2}\int_{T-\Delta}^{T} \Pr\left\{(\widehat{t_0} - a) > \frac{\Delta}{2}|a\right\} da \\
&= \frac{1}{2}\int_{T-\Delta}^{T} \Pr\left\{\widehat{t_0} > (a + \frac{\Delta}{2})|a\right\} da \\
&= \frac{1}{2}\int_{T-\Delta}^{T-\frac{\Delta}{2}} \frac{1}{T}\left[T - (a + \frac{\Delta}{2})\right] da = \frac{1}{2}\cdot\frac{\Delta^2}{8T}. \qquad (3.99)
\end{aligned}$$

Then the extra error $\overline{\epsilon^2_{\text{inc1}}}$ corresponding to $\frac{1}{T}\int_0^T \Delta \int_0^{T-\Delta} P_e(a, a+\Delta) da d\Delta$ in the same equation is

$$\begin{aligned}
\overline{\epsilon^2_{\text{inc1}}} &= \frac{1}{2}\int_0^T \Delta \left[\frac{1}{T}\int_0^{\Delta} \Pr\left\{\epsilon < -\frac{\Delta}{2}|a\right\} + \Pr\left\{\epsilon > -\frac{\Delta}{2}|a\right\} da\right] d\Delta \\
&= \frac{1}{2}\int_0^T \Delta \left(\frac{1}{T}\frac{\Delta^2}{8T} \times 2\right) d\Delta = \frac{T^2}{32}. \qquad (3.100)
\end{aligned}$$

The other inequality causing an extra bounding error is from $4\int_0^{\frac{T}{2}} xF(x)dx$ to $4\int_0^T xF(x)dx$ in the derivation above eq. (5) of [39], in which $F(x)$ has the following expression

$$\begin{aligned}
F(x) &= \frac{1}{T}\int_0^T \Pr\{|\epsilon| \geq x|a\} da = \frac{1}{T}\int_0^T \Pr\{|\widehat{t_0} - a| \geq x|a\} da \\
&= \frac{1}{T}\int_0^T \Pr\{\widehat{t_0} \geq a + x \text{ or } \widehat{t_0} \leq a - x|a\} da \\
&= \frac{1}{T}\int_0^{T-x} \Pr\{\widehat{t_0} \geq a + x|a\} da + \frac{1}{T}\int_x^T \Pr\{\widehat{t_0} \leq a - x|a\} da \\
&= \frac{1}{T}\int_0^{T-x} \left(\int_{a+x}^T \frac{1}{T} d\widehat{t_0}\right) da + \frac{1}{T}\int_x^T \left(\int_{a+x}^T \frac{1}{T} d\widehat{t_0}\right) da = \left(1 - \frac{x}{T}\right)^2 \qquad (3.101)
\end{aligned}$$

Then the additional error $\overline{\epsilon^2_{\text{inc2}}}$ corresponding to $\frac{1}{T}\int_0^T \Delta \int_0^{T-\Delta} P_e(a, a+\Delta) da d\Delta$ is

$$\overline{\epsilon^2_{\text{inc2}}} = 2\int_{\frac{T}{2}}^T xF(x)dx = 2\int_{\frac{T}{2}}^T x\left(1 - \frac{x}{T}\right)^2 dx = \left(\frac{1}{12} - \frac{1}{32}\right)T^2. \qquad (3.102)$$

Finally, during the development in [39] from $\frac{1}{T}\int_0^T \Delta \int_0^{T-\Delta} P_e(a, a+\Delta) da d\Delta$ to $\overline{\epsilon^2} =$

$-\int_0^{T+} x^2 dF(x)$, the total extra error is

$$\overline{\epsilon_{\text{inc}}^2} = \overline{\epsilon_{\text{inc1}}^2} + \overline{\epsilon_{\text{inc2}}^2} = \frac{T^2}{32} + \left(\frac{1}{12} - \frac{1}{32}\right) T^2 = \frac{T^2}{12}. \tag{3.103}$$

Noting that $\frac{T^2}{6} - \frac{T^2}{12} = \frac{T^2}{12}$, this verifies the bound gap between the prior and the ZZB.

3.3.7 Numerical Examples

In this section, examples of estimation performance and the corresponding bounds are presented. The ZZB evaluation uses the compact form, as described in Section 3.3.5. In addition to the ZZB and ECRB developed in this paper, the "average ZZB" derived in [46] is also plotted; this version of the ZZB assumes the channel is known to the receiver, and the bound is averaged over the channel statistics. It is interesting to compare the average ZZB to the ZZB developed here, which does not assume knowledge of the channel and so is more realistic for the random channel case.

The root MSE (RMSE) of the TDE as the performance metric is adopted. Unless otherwise specified, the signal is a square-root raised cosine (SRRC) pulse (see Appendix C) with roll-off factor $\beta = 0$ and parameter $T_p = 2$. The channel is Gaussian with $T_t = 1$, and $L = 5$ independent taps, and the prior has $T = 30$. Note all the time variables are normalized to the channel tap spacing. Based on measured wideband channels [85], an exponential power delay profile is employed with decay factor $\lambda = 6$, the mean of the first tap corresponding to a Rician-K factor for the first path of $K = 20$ dB, and all other taps with zero mean.

Figure 3.1 plots the ZZB and the average ZZB, illustrating the low, medium, and high SNR regions with thresholds. The ZZB and average ZZB are coincident at low SNR, converging to $T/\sqrt{12}$ plotted as a horizontal line. The low SNR approximation from (3.59) or (3.60) is valid up to 0 dB, and converges to $T/\sqrt{12}$ as the SNR decreases to

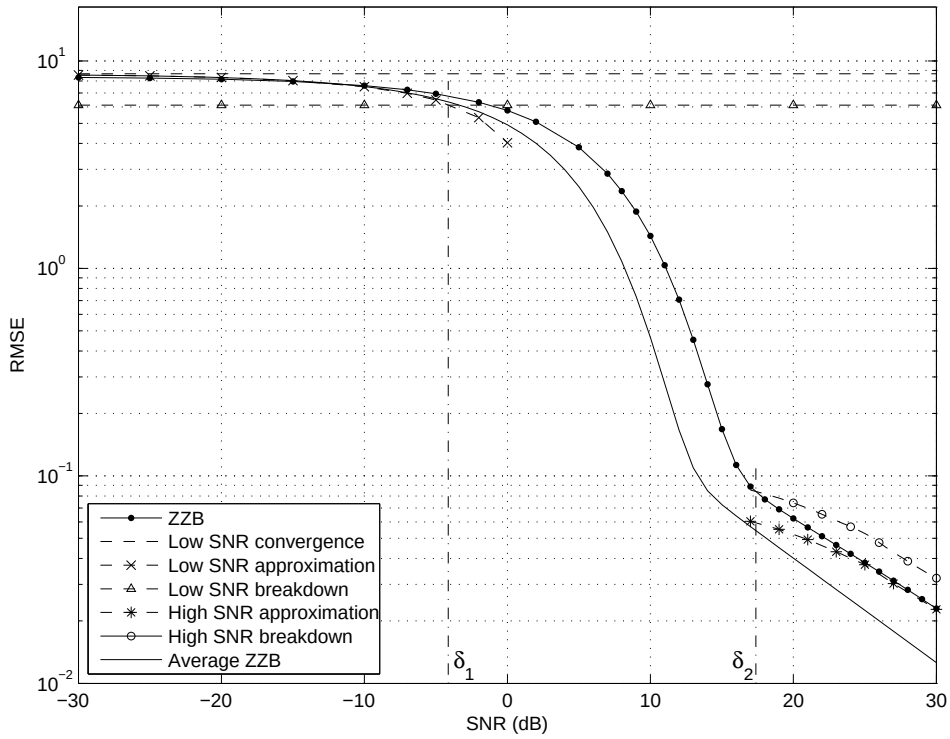

Figure 3.1: Typical ZZB behavior for time delay estimation, including low, medium, and high SNR regimes with thresholds δ_1 and δ_2. The channel is Gaussian with strong Rician K-factor in the first tap, and exponential power decay profile. The average ZZB is a weaker bound that assumes the channel is known to the receiver.

zero. Using (3.74) and shifting 3dB down from the convergence MSE level (i.e., 1.5dB in terms of RMSE), the low-SNR breakdown point to be $\delta_1 \approx -4.1$dB is obtained. Beyond δ_1, the ZZB and the average ZZB separate, with a roughly 3 dB loss in RMSE performance due to the lack of channel knowledge that is reflected in the tighter ZZB. The high SNR threshold occurs at $\delta_2 \approx 17.4$ dB. Beyond δ_2, the ZZB and average ZZB both linearly decrease with increasing SNR, with a slope of about -0.5, consistent with bandwidth limited pulse cases studied by Ziv and Zakai [39], [38].

Figure 3.2 compares estimators and bounds, averaging over 30,000 realizations. The MAP estimator (3.133) converges to the ZZB at high SNR, with a few dB gap between the ZZB and MAP estimator in the mid-SNR threshold region, as occurs in frequency estimation and other problems [40]. Also shown is the GML estimate from (3.86), which

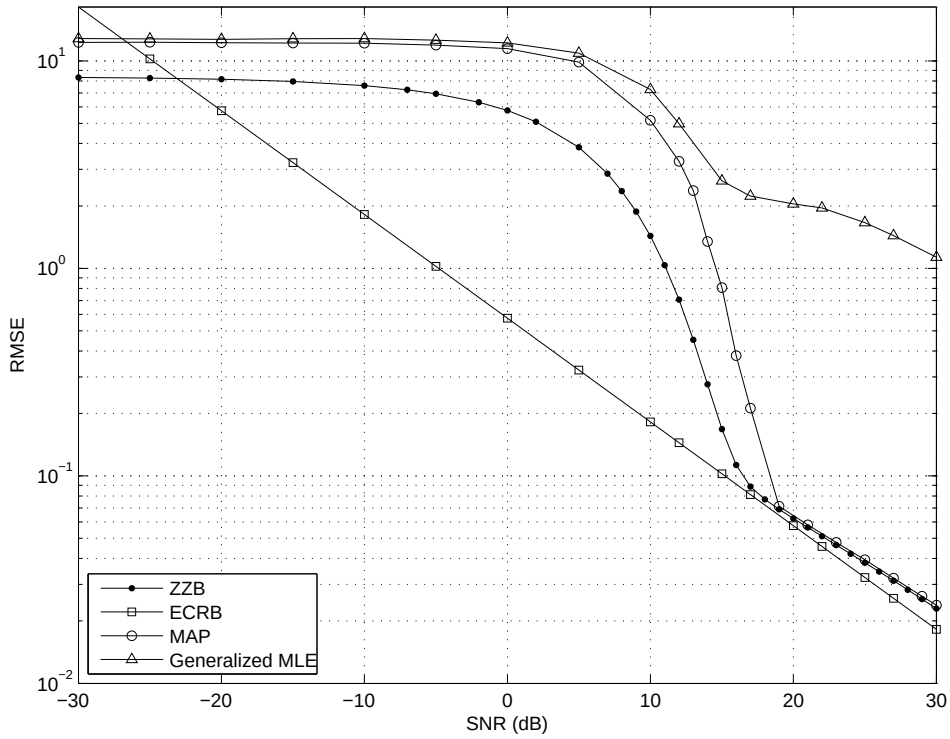

Figure 3.2: MAP time delay estimation performance, with ZZB and ECRB comparison. The ZZB tracks the estimator threshold behavior, while the ECRB is not tight below the SNR threshold. The GMLE minimizes the MSE without knowledge of the channel statistics and consequently has much worse performance.

tracks the MAP performance only at low SNR and generally has weak performance. At high SNR, the ECRB is slightly looser than the ZZB. As the CRB is a local bound it does not track the MAP threshold behavior and becomes loose for low to medium SNR.

Figure 3.3 plots the ZZB with curves parameterized by the uniform prior distribution duration $[0, T]$, varying T over $T = (5, 15, 20, 100)$. With the prior equal to the channel duration $T = LT_t = 5$, the threshold behavior is enhanced by several dB. At high SNR, the RMSE performance is independent of the prior.

Next Figure 3.4 shows the ZZB as a function of signal bandwidth, employing the mean-square bandwidth (MSB) defined by (C.1) in Appendix C. The root-raised cosine pulse was used, with root-MSBs of (0.15,0.3,0.5,1). See Appendix C for the relevant expressions. Increased bandwidth has significant impact above the high SNR thresh-

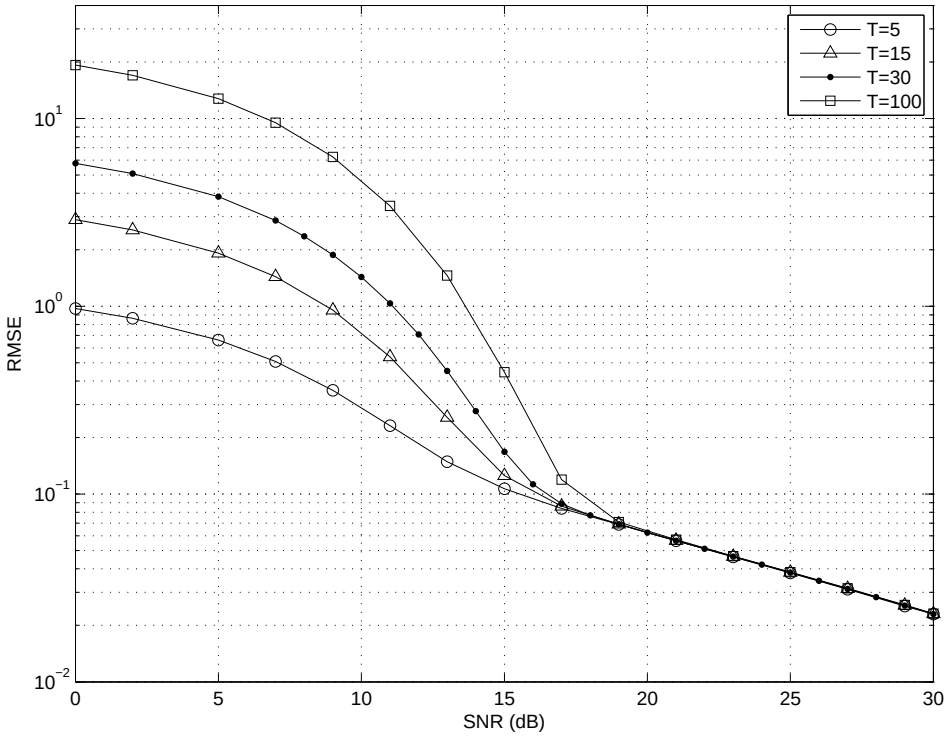

Figure 3.3: ZZB on time delay with curves parameterized by prior distribution $[0, T]$, $T = (5, 15, 30, 100)$. The threshold performance improves when T is close to the channel duration LT_t, while the performance is independent of the prior at high SNR.

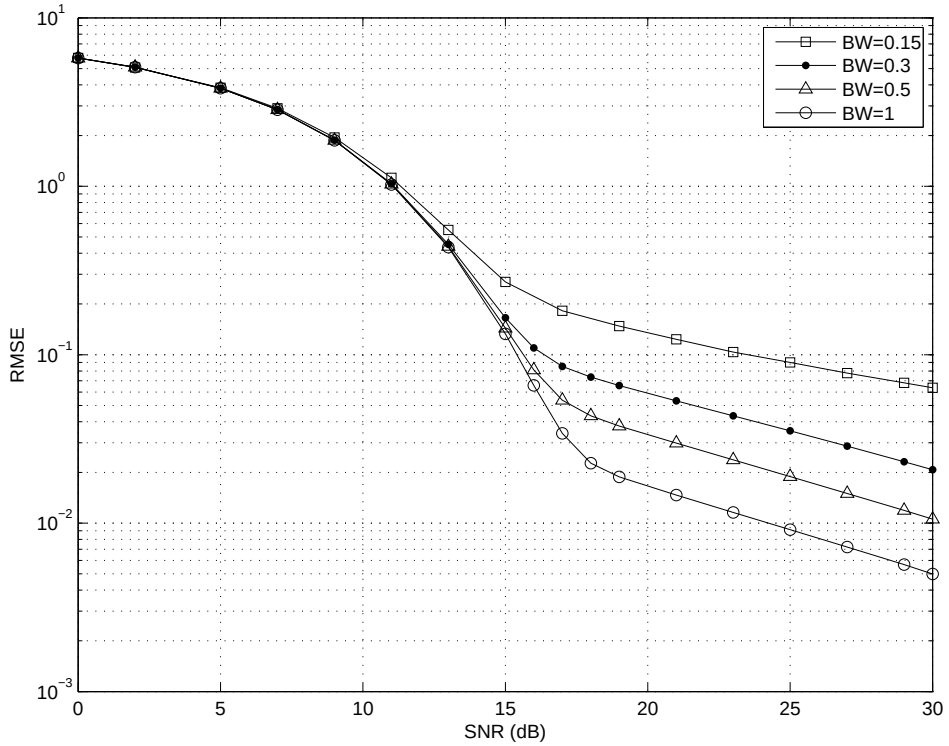

Figure 3.4: ZZB on TDE with varying signal bandwidth. A square-root raised cosine pulse with roll-off factor $\beta = 0$ is assumed. Curves are parameterized by the root-mean-squared bandwidth for $(0.15, 0.3, 0.5, 1)$. At high SNR, increasing the bandwidth by roughly an order of magnitude decreases the TDE RMSE by an order of magnitude.

old, where performance is dominated by the signal autocorrelation and the associated ambiguities [90]. Increasing the root-MSB from 0.15 to 1 yields roughly an order of magnitude reduction in the TDE RMSE in the high SNR regime.

To illustrate the effect of the signal choice, several different signals including SRRC, pseudo-random (PN) coded SRRC pulse train, Gaussian, and Gaussian doublet are considered in Figure 3.5. The root-MSBs were all set to $1/\sqrt{12}$ unit frequency (see Appendix C for the signal and bandwidth expressions). From (3.119) and (3.119), the pulse shaping only affects the distributions of the LLR and the ZZB through their autocorrelation matrices $\mathbf{S}_{00}$ and $\mathbf{S}_{01}$, accounting for the small variation in RMSE error slope in the high SNR regime. Given the same MSB, the threshold and low SNR behaviors are identical.

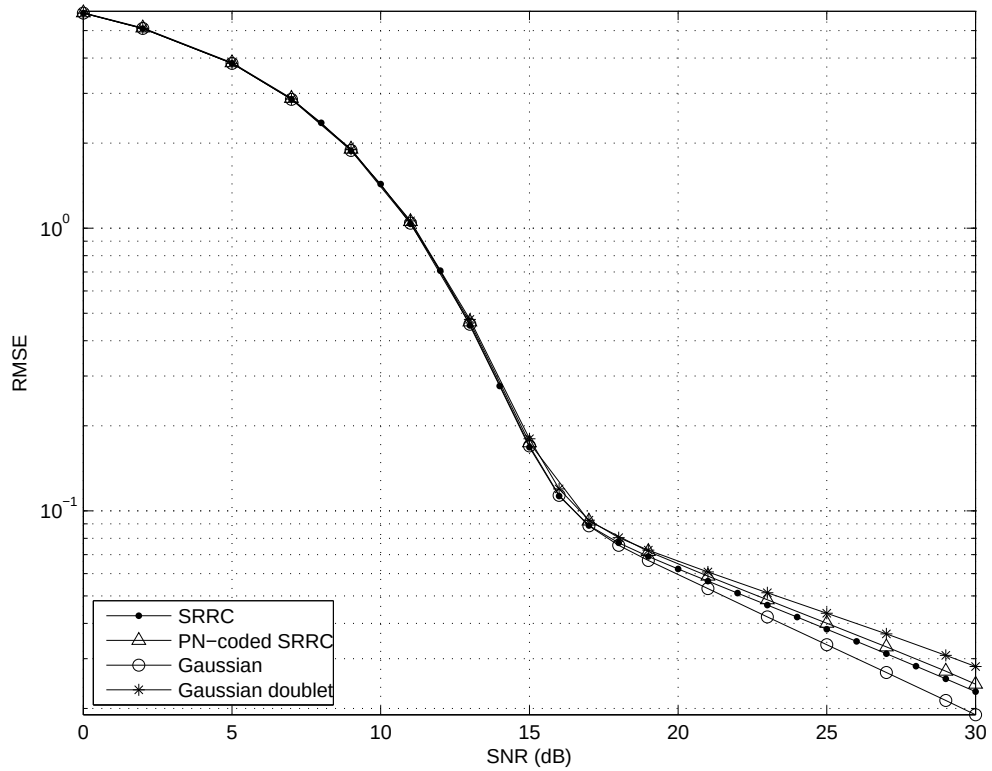

Figure 3.5: Ziv-Zakai bounds on time delay, comparing several different signals, all with identical root-mean squared bandwidth. The threshold and low SNR behaviors are identical, while the high SNR performance depends on the detailed structure of the signal autocorrelation.

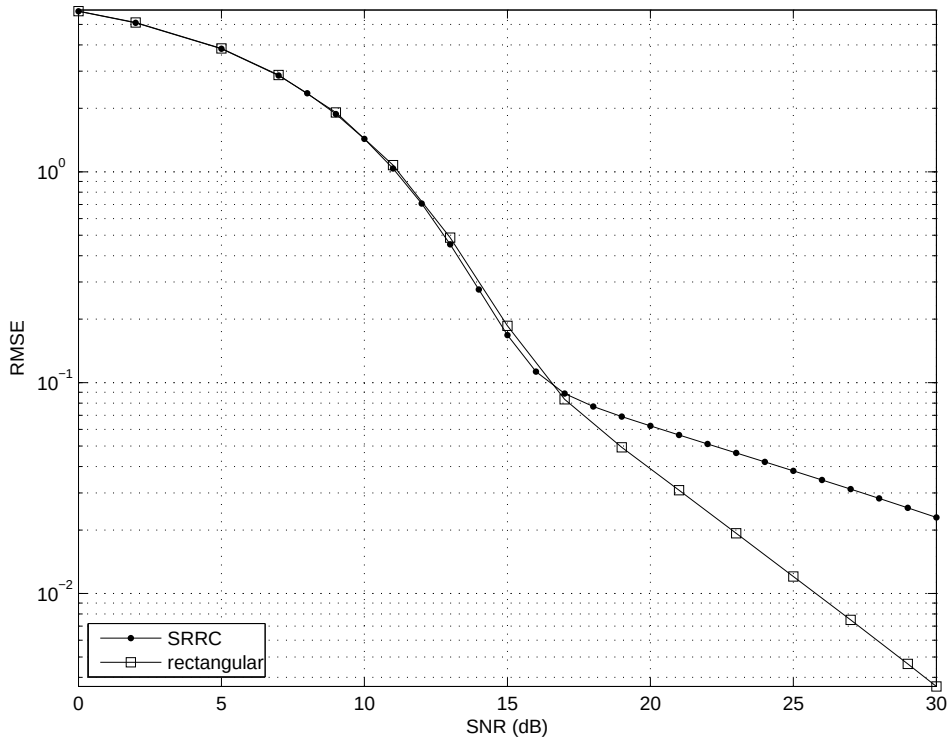

Figure 3.6: Ziv-Zakai bounds on time delay, comparing SRRC and ideal rectangular signals, assuming the main lobe bandwidth of the rectangular signal is same as the SRRC bandwidth of 0.5. The ideal rectangular pulse yields significantly better TDE performance at high SNR due to its broad spectral occupancy compared to the SRRC pulse.

As a final example, Figure 3.6 compares a rectangular pulse of duration $T_p = 2$ with the bandlimited SRRC. For comparison, the SRRC bandwidth is set to the width of the rectangular pulse spectrum main lobe, which is $1/T_p$. While these two signals have nominally the same bandwidth, the rectangular pulse yields a TDE RMSE slope of -1 (consistent with [38]) versus $-\frac{1}{2}$ for the SRRC. This illustrates the difficulty in selecting a universal definition of bandwidth, without accounting for the rate of spectral decay. The rectangular pulse has much broader spectral shape, and leads to significantly better TDE performance, although the ideal rectangular pulse is not bandlimited and can only be approximated in practice.

3.4 Ziv-Zakai Bounds for Frequency Hopping Waveform

In this section the ZZB for pulsed signal in Section 3.3 is extended to the case of frequency hopping transmission in random frequency-selective fading channels [91]. The wideband frequency hopping waveforms are readily employed for both communications and TDE. Similarly, the receiver does not know the channel realization to assist in estimating the time delay, but does know the channel statistics. The development procedure is similar as that in Section 3.3, while the waveform overlaps at the receiver are incorporated into the signal model and then in the ZZB development. In addition to tight mean-square error prediction for the MAP estimator performance, the bounds also accurately predict the TDE frequency diversity gain from multi-frequency transmission in fading channels. The special case of independent flat-fading is discussed, including both Rician and Rayleigh fading, and closed-form expressions enable easy study of the effects of SNR, frequency diversity, and channel statistics on TDE.

3.4.1 Models for Frequency Hopping Transmission

Frequency-hopping waveforms are formed by basic pulses $p(t)$ modulated by known symbols. Here, $p(t)$ is assumed to be a SRRC pulse with unit energy, symmetrically truncated to the symbol duration T_s, though the results are general. During an N-hop frequency-hopping cycle, the pulse during the ith ($i = 1, \cdots, N$) hop and kth symbol period is denoted as $p_{i,k}(t) = p(t - (i-1)MT_s - kT_s)$, where each hop has M symbols with hop dwell time MT_s. The the ith hop waveform is represented as

$$\begin{aligned} s_i(t) &= \sum_{k=-K_1}^{K_2} a_{i,k} p_{i,k}(t) \\ &= \sum_{k=-K_1}^{K_2} a_{i,k} p(t - (i-1)MT_s - kT_s), \quad t \in [(i-1)MT_s,\ iMT_s] \end{aligned} \tag{3.104}$$

in which $M = K_1 + K_2 + 1$. The symbols $a_{i,k}$ can be taken from a constellation such as PSK or QAM, and they are assumed known to the receiver.

The transmitted ith hop signal $s_i(t)$ propagates through a convolutive random channel modeled as a tapped delay line with fixed spacing T_t and fading gains $\alpha_{i,l}$, given by [46], [92]

$$g_i(t) = \sum_{l=1}^{L} \alpha_{i,l}\delta(t - (l-1)T_t). \tag{3.105}$$

Let the L gains be in the $L \times 1$ vector $\boldsymbol{\alpha}_i$, modeled as a complex Gaussian random vector with distribution $\mathcal{CN}(\boldsymbol{\mu}_{\alpha i}, \mathbf{V}_i)$, where $\boldsymbol{\mu}_{\alpha i}$ is the mean vector and $\mathbf{V}_i$ is the covariance matrix. Further, stacking $\boldsymbol{\alpha}_i$ over N hops into vector $\boldsymbol{\alpha}$ gives a $LN \times 1$ complex Gaussian vector with mean $\boldsymbol{\mu}_\alpha$ and variance $\mathbf{V}$. The ith row and jth column block $\mathbf{V}_{ij}$ of $\mathbf{V}$ represents the covariance between the ith and jth hops. This complex-valued channel model encompasses a variety of scenarios, including correlated FIR taps and sub-channels of different hops.

Denote the propagation delay as t_0. For simplicity, the channel delay spread is assumed less than each hop dwell time. Extension to a much longer channel case is straightforward. Thus, due to any overlap in the time domain, there arises only inter-hop interference from the previous hop signal. The received signal for the ith hop spanning the time interval $[(i-1)MT_s,\ iMT_s]$ is given by

$$\begin{aligned} y_i(t) &= \sum_{l=1}^{L} \alpha_{i,l} s_i(t - (l-1)T_t - t_0) + \alpha_{i-1,l} s_{i-1}(t - (l-1)T_t - t_0) + n_i(t) \\ &= \boldsymbol{\alpha}_i^T \mathbf{s}_i(t - t_0) + \boldsymbol{\alpha}_{i-1}^T \mathbf{s}_{i-1}(t - t_0) + n_i(t), \quad t \in [(i-1)MT_s,\ iMT_s], \end{aligned} \tag{3.106}$$

where

$$\mathbf{s}_i(t - t_0) = [s_i(t - t_0), s_i(t - T_t - t_0), \cdots, s_i(t - (L-1)T_t - t_0)]^T, \tag{3.107}$$

$n_i(t)$ is complex AWGN with spectral density N_0. Also define $\boldsymbol{\alpha}_0 \triangleq \mathbf{0}$, $\mathbf{s}_0(t - t_0) \triangleq \mathbf{0}$

for the model to cover $y_1(t)$ in a unified form. The second term in (3.106) denotes the inter-hop interference from the $(i-1)$th hop to the ith hop because of the multipath propagation. The SNR of the ith hop is defined by $\text{SNR}_i = tr(\boldsymbol{\mu}_{\alpha i}\boldsymbol{\mu}_{\alpha i}^H + \mathbf{V}_i)/N_0$, where tr is the trace operator. As in the last section, the uniform prior distribution is assumed for the propagation delay t_0 on $[0, T]$, and the ZZB on the estimation of t_0 is derived next.

3.4.2 Development

The development of the ZZB for frequency hopping waveforms is a similar procedure as that for pulsed signal in Subsection 3.3.1. The LLR for the hypothesis test is considered to evaluate (3.6), and $P_e(\Delta)$ is found by the MGF approach as in Subsection 3.4.3.

3.4.2.1 Received Signal Distribution

From equation (3.106), the received signal for the ith hop can be written as

$$y_i(t) = \boldsymbol{\alpha}_i^T \mathbf{s}_{m,i} + \boldsymbol{\alpha}_{i-1}^T \mathbf{s}_{m,i-1} + n_i(t), \quad t \in [(i-1)MT_s,\ iMT_s] \tag{3.108}$$

where $\mathbf{s}_{m,i} = \mathbf{s}_i(t - m\Delta)$ and m takes the value 0 or 1 corresponding to hypotheses H_0 or H_1, respectively. Note that, in the context of bound development, the delay t_0 has been replaced by $m\Delta$. Collecting $y_i(t)$ and $n_i(t)$ in vectors generates,

$$\mathbf{y}(t) = [y_1(t), \cdots, y_N(t)]^T, \quad \mathbf{n}(t) = [n_1(t), \cdots, n_N(t)]^T, \quad t \in [0,\ NMT_s].$$

From (3.108) and the noise independence, the distribution of $\mathbf{y}(t)$ conditioned on the channel gain and time delay $m\Delta$ is given by [82]

$$\begin{aligned} p(\mathbf{y}(t)|\boldsymbol{\alpha}, m\Delta) &= \mathcal{K} \exp \sum_{i=1}^{N} \Big[-\frac{1}{N_0} \int_{(i-1)MT_s}^{iMT_s} \left\| y_i(t) - \boldsymbol{\alpha}_i^T \mathbf{s}_{m,i} - \boldsymbol{\alpha}_{i-1}^T \mathbf{s}_{m,i-1} \right\|^2 dt \Big] \\ &= \mathcal{K} \exp \sum_{i=1}^{N} \Big\{ -\frac{1}{N_0} \int_{(i-1)MT_s}^{iMT_s} \Big[\boldsymbol{\alpha}_i^H \mathbf{s}_i^* \mathbf{s}_i^T \boldsymbol{\alpha}_i + \boldsymbol{\alpha}_{i-1}^H \mathbf{s}_{i-1}^* \mathbf{s}_{i-1}^T \boldsymbol{\alpha}_{i-1} \\ &\qquad + \boldsymbol{\alpha}_i^H \mathbf{s}_i^* \mathbf{s}_{i-1}^T \boldsymbol{\alpha}_{i-1} + \boldsymbol{\alpha}_{i-1}^H \mathbf{s}_{i-1}^* \mathbf{s}_i^T \boldsymbol{\alpha}_i - 2\mathrm{Re}\{(\mathbf{s}_{m,i}^* y_i(t))^H \boldsymbol{\alpha}_i\} \\ &\qquad - 2\mathrm{Re}\{(\mathbf{s}_{m,i-1}^* y_i(t))^H \boldsymbol{\alpha}_{i-1}\} + \|y_i(t)\|^2 \Big] dt \Big\} \\ &= \mathcal{K} \exp \left[-\frac{1}{N_0} \left(\boldsymbol{\alpha}^H \mathbf{S}_{00} \boldsymbol{\alpha} - 2\mathrm{Re}\left\{ \mathbf{r}_m^H \boldsymbol{\alpha} \right\} + I_y \right) \right], \end{aligned} \tag{3.109}$$

where $\mathcal{K}$ absorbs all the terms independent of $\boldsymbol{\alpha}_i$ and $m\Delta$, and other quantities are defined as follows

$$\mathbf{S}_{m_1 m_2} \triangleq \begin{bmatrix} \mathbf{S}_{m_1 m_2,1,1} & \mathbf{S}_{m_1 m_2,1,2} & 0 & \cdots & \cdots & 0 \\ \mathbf{S}_{m_1 m_2,2,1} & \mathbf{S}_{m_1 m_2,2,2} & \mathbf{S}_{m_1 m_2,2,3} & \ddots & & \vdots \\ 0 & \ddots & \ddots & \ddots & \ddots & \vdots \\ \vdots & \ddots & \ddots & \ddots & \ddots & 0 \\ \vdots & & \ddots & \ddots & \ddots & \mathbf{S}_{m_1 m_2,N-1,N} \\ 0 & \cdots & \cdots & 0 & \mathbf{S}_{m_1 m_2,N,N-1} & \mathbf{S}_{m_1 m_2,N,N} \end{bmatrix},$$

$$\begin{aligned} &\mathbf{S}_{m_1 m_2,i} = \mathbf{S}_{m_1 m_2,i,i} \triangleq \int_{(i-1)MT_s}^{(i+1)MT_s} \mathbf{s}_{m_1,i}^* \mathbf{s}_{m_2,i}^T dt, \\ &\mathbf{S}_{m_1 m_2,i,i-1} \triangleq \int_{(i-1)MT_s}^{iMT_s} \mathbf{s}_{m_1,i}^* \mathbf{s}_{m_2,i-1}^T dt, \quad \mathbf{S}_{m_1 m_2,i-1,i} \triangleq \int_{(i-1)MT_s}^{iMT_s} \mathbf{s}_{m_1,i-1}^* \mathbf{s}_{m_2,i}^T dt, \\ &\mathbf{r}_m = [\mathbf{r}_{m,1}^T, \cdots, \mathbf{r}_{m,N}^T]^T, \quad \mathbf{r}_{m,i} \triangleq \int_{(i-1)MT_s}^{iMT_s} \mathbf{s}_{m,i}^* y_i(t) dt + \int_{iMT_s}^{(i+1)MT_s} \mathbf{s}_{m,i}^* y_{i+1}(t) dt, \end{aligned} \tag{3.110}$$

$$I_y = \sum_{i=1}^{N} I_{yi}, \quad I_{yi} \triangleq \int_{(i-1)MT_s}^{iMT_s} \|y_i(t)\|^2 dt,$$

with $m, m_1, m_2 \in \{0, 1\}$, and $y_{N+1}(t) \triangleq 0$ is defined for the expression of $\mathbf{r}_{m,i}$ to cover $i = N$ as well. Note that if each sub-channel is flat fading and signals from different

hops do not overlap, the expression of $\mathbf{S}_{m1,m2}$ will be block diagonal, and $\mathbf{r}_{m,i}$ only has the first term. This case will be discussed in detail in Section 3.4.4.

The exponent of (3.109) has a quadratic form in the complex Gaussian random vector $\boldsymbol{\alpha}$, which is averaged over the channel $\boldsymbol{\alpha}$ using (B.14) from the Appendix with $s = 1$, yielding

$$p(\mathbf{y}(t)|m\Delta) = E_{\boldsymbol{\alpha}}[p(\mathbf{y}(t)|\boldsymbol{\alpha}, m\Delta)] = \mathcal{K}|\mathbf{X}|^{-1} \exp\left\{\mathbf{r}_m^H \mathbf{W} \mathbf{r}_m + 2\mathrm{Re}\{\mathbf{h}^H \mathbf{r}_m\} + c\right\}, \tag{3.111}$$

where

$$\begin{aligned}
\mathbf{X} &= \mathbf{I} + \frac{1}{N_0}\mathbf{V}^{\frac{1}{2}}\mathbf{S}_{00}\mathbf{V}^{\frac{1}{2}}, \quad \mathbf{W} = \frac{1}{N_0^2}\mathbf{V}^{\frac{1}{2}}\mathbf{X}^{-1}\mathbf{V}^{\frac{1}{2}}, \\
\mathbf{h} &= \frac{1}{N_0}\left(\mathbf{I} - \frac{1}{N_0}\mathbf{V}^{\frac{1}{2}}\mathbf{X}^{-1}\mathbf{V}^{\frac{1}{2}}\mathbf{S}_{00}\right)\boldsymbol{\mu}_\alpha = \mathbf{H}\boldsymbol{\mu}_\alpha, \\
c &= \boldsymbol{\mu}_\alpha^H \left(\frac{1}{N_0^2}\mathbf{S}_{00}\mathbf{V}^{\frac{1}{2}}\mathbf{X}^{-1}\mathbf{V}^{\frac{1}{2}}\mathbf{S}_{00} - \frac{1}{N_0}\mathbf{S}_{00}\right)\boldsymbol{\mu}_\alpha - \frac{I_y}{N_0}.
\end{aligned}$$

3.4.2.2 Log-likelihood Ratio Test

From (3.111), the LLR for the test of hypothesis $H_m,\ m = 0, 1$ is

$$\begin{aligned}
\mathcal{L} \overset{\Delta}{=} \ln \frac{p(\mathbf{y}(t)|0)}{p(\mathbf{y}(t)|\Delta)} &= \mathbf{r}_0^H \mathbf{W} \mathbf{r}_0 - \mathbf{r}_1^H \mathbf{W} \mathbf{r}_1 + 2\mathrm{Re}\{\mathbf{h}^H \mathbf{r}_0 - \mathbf{h}^H \mathbf{r}_1\} \\
&= \mathbf{r}^H \boldsymbol{\Psi} \mathbf{r} + 2\mathrm{Re}\{\mathbf{g}^H \mathbf{r}\} \qquad (3.112) \\
&\underset{H_1}{\overset{H_0}{\gtrless}} 0,
\end{aligned}$$

where

$$\mathbf{r} = \begin{bmatrix} \mathbf{r}_0 \\ \mathbf{r}_1 \end{bmatrix}, \quad \boldsymbol{\Psi} = \begin{bmatrix} \mathbf{W} & \mathbf{0} \\ \mathbf{0} & -\mathbf{W} \end{bmatrix}, \quad \mathbf{g} = \begin{bmatrix} \mathbf{h} \\ -\mathbf{h} \end{bmatrix} = \mathbf{G}\boldsymbol{\mu}_\alpha. \tag{3.113}$$

An error occurs if $\mathcal{L} < 0 | m = 0$, or if $\mathcal{L} > 0 | m = 1$. Letting $\mathcal{L}_m \overset{\Delta}{=} \mathcal{L}|H_m$, and $\widetilde{\mathbf{r}}_m \overset{\Delta}{=} \mathbf{r}|H_m$, (3.112) becomes

$$\mathcal{L}_m = \widetilde{\mathbf{r}}_m^H \boldsymbol{\Psi} \widetilde{\mathbf{r}}_m + 2\mathrm{Re}\{\mathbf{g}^H \widetilde{\mathbf{r}}_m\}, \tag{3.114}$$

and the hypothesis test minimum error probability is

$$P_e(\Delta) = \frac{1}{2}\Pr\{\mathcal{L}_0 < 0\} + \frac{1}{2}\Pr\{\mathcal{L}_1 > 0\}. \tag{3.115}$$

Our goal now is to evaluate the probabilities in (3.115), yielding $P_e(\Delta)$ for use in the ZZB equation (3.6). Next the distribution of $\widetilde{\mathbf{r}}_m$ is derived, and then used to find the distribution of $\mathcal{L}_m$.

3.4.2.3 The Distribution of $\widetilde{\mathbf{r}}_m$

Using (3.110) and (3.108) conditioned on H_0, then $\mathbf{r}_{m,i}$ $(m = 0, 1)$ can be expressed as

$$\begin{aligned}\mathbf{r}_{m,i}|H_0 &= \int_{(i-1)MT_s}^{iMT_s} \mathbf{s}_{m,i}^* y_i(t) + \int_{iMT_s}^{(i+1)MT_s} \mathbf{s}_{m,i}^* y_{i+1}(t) \\ &= \mathbf{S}_{m0,i,i}\boldsymbol{\alpha}_i + \mathbf{S}_{m0,i,i-1}\boldsymbol{\alpha}_{i-1} + \mathbf{S}_{m0,i,i+1}\boldsymbol{\alpha}_{i+1} + \mathbf{z}_{m,i},\end{aligned} \tag{3.116}$$

where $\mathbf{z}_{m,i} \triangleq \int_{(i-1)MT_s}^{(i+1)MT_s} \mathbf{s}_{m,i}^*[n_i(t) + n_{i+1}(t)]dt$. Stacking all N vectors $\mathbf{z}_{m,i}$ into a big vector $\mathbf{z}_m$, and similarly for $\mathbf{r}_{m,i}|H_0$, one can obtain $\mathbf{r}_m|H_0 = \mathbf{S}_{m0}\boldsymbol{\alpha} + \mathbf{z}_m$. Further stacking $\mathbf{r}_0|H_0$ and $\mathbf{r}_1|H_0$ as in (3.112) obtains

$$\widetilde{\mathbf{r}}_0 = \mathbf{r}|H_0 = \mathbf{R}_0\boldsymbol{\alpha} + \mathbf{z}, \quad \mathbf{R}_0 = \begin{bmatrix} \mathbf{S}_{00} \\ \\ \mathbf{S}_{10} \end{bmatrix}, \quad \mathbf{z} = \begin{bmatrix} \mathbf{z}_0 \\ \\ \mathbf{z}_1 \end{bmatrix}. \tag{3.117}$$

Similarly, conditioned on H_1, it follows that

$$\widetilde{\mathbf{r}}_1 = \mathbf{r}|H_1 = \mathbf{R}_1\boldsymbol{\alpha} + \mathbf{z}, \quad \mathbf{R}_1 = \begin{bmatrix} \mathbf{S}_{01} \\ \\ \mathbf{S}_{00} \end{bmatrix}. \tag{3.118}$$

Therefore, under either hypothesis the data vector $\widetilde{\mathbf{r}}_0$ or $\widetilde{\mathbf{r}}_1$ is a linear combination of Gaussian vectors $\boldsymbol{\alpha}$ and $\mathbf{z}$, so that $\widetilde{\mathbf{r}}_m$ follows a Gaussian distribution $\widetilde{\mathbf{r}}_m \sim \mathcal{N}(\boldsymbol{\mu}_m, \boldsymbol{\Sigma}_m)$, where the mean and covariance are

$$\boldsymbol{\mu}_m = \mathbf{R}_m\boldsymbol{\mu}_\alpha, \quad \boldsymbol{\Sigma}_m = \left(\mathbf{R}_m\mathbf{V}\mathbf{R}_m^H + \boldsymbol{\Gamma}\right),$$

with

$$\mathbf{\Gamma} = E\{\mathbf{z}\mathbf{z}^H\} = N_0 \begin{bmatrix} \mathbf{S}_{00} & \mathbf{S}_{01} \\ \mathbf{S}_{10} & \mathbf{S}_{00} \end{bmatrix} = N_0 \begin{bmatrix} \mathbf{R}_0 & \mathbf{R}_1 \end{bmatrix}.$$

With the pdf of $\widetilde{\mathbf{r}}_m$, each of the two probabilities $\Pr\{\mathcal{L}_0 < 0\}$ and $\Pr\{\mathcal{L}_1 > 0\}$ in (3.115) can be expressed as a $2LN$-dimensional integral as in [86]. However, it is computationally difficult to directly evaluate those integrals. In the next sub-section the MGF approach is employed to find the distribution of $\mathcal{L}_m$ that results in a computationally attractive 2-dimensional integral.

3.4.3 MGF Approach for FH Waveform

The LLR $\mathcal{L}_m$ in (3.114) is a quadratic form of the Gaussian vector $\widetilde{\mathbf{r}}_m$. To find the probability distribution of $\mathcal{L}_m$, the author first obtains its MGF (or characteristic function) and then apply the Fourier transform implemented efficiently using an FFT. Then, the distribution of $\mathcal{L}_m$ is used to evaluate the error probabilities in (3.115) via 1-dimensional integration, and the resulting $P_e(\Delta)$ is used to find the ZZB in (3.6).

By the definitions in (3.113), $\mathbf{g}^T\mathbf{\Psi}^{-1}\mathbf{g} = 0$. Using this, rewrite $\mathcal{L}_m$ in (3.114) as follows,

$$\mathcal{L}_m = \widetilde{\mathbf{x}}_m^H \mathbf{\Psi} \widetilde{\mathbf{x}}_m, \tag{3.119}$$

where $\widetilde{\mathbf{x}}_m = \widetilde{\mathbf{r}}_m + \mathbf{\Psi}^{-1}\mathbf{g}$. Note that $\widetilde{\mathbf{x}}_m$ is Gaussian distributed with variance $\mathbf{\Sigma}_m$ and mean

$$\boldsymbol{\mu}_{xm} = \boldsymbol{\mu}_m + \mathbf{\Psi}^{-1}\mathbf{g} = (\mathbf{R}_m + \mathbf{\Psi}^{-1}\mathbf{G})\boldsymbol{\mu}_\alpha.$$

Introduce a zero-mean Gaussian random vector $\mathbf{u}_m$, obtained from $\widetilde{\mathbf{x}}_m$ by the transformation

$$\widetilde{\mathbf{x}}_m = \mathbf{\Sigma}_m^{\frac{1}{2}} \mathbf{P}_m \mathbf{u}_m + \boldsymbol{\mu}_{xm} = \mathbf{\Sigma}_m^{\frac{1}{2}} \mathbf{P}_m (\mathbf{u}_m + \mathbf{b}_m),$$

so that the variance of $\mathbf{u}_m$ is the identity matrix $\mathbf{I}$, and the vector $\mathbf{b}_m$ is a linear transformation of channel mean $\boldsymbol{\mu}_\alpha$ given by

$$\mathbf{b}_m = \mathbf{P}_m^H \boldsymbol{\Sigma}_m^{-\frac{1}{2}} \boldsymbol{\mu}_{xm} = \mathbf{P}_m^H \boldsymbol{\Sigma}_m^{-\frac{1}{2}} (\mathbf{R}_m + \boldsymbol{\Psi}^{-1}\mathbf{G}) \boldsymbol{\mu}_\alpha. \tag{3.120}$$

In this transformation, $\mathbf{P}_m$ is a unitary matrix in the eigendecomposition of the Hermitian matrix given by

$$\boldsymbol{\Sigma}_m^{\frac{1}{2}} \boldsymbol{\Psi} \boldsymbol{\Sigma}_m^{\frac{1}{2}} = \mathbf{P}_m \text{diag}\{\lambda_1, \cdots, \lambda_{2LN}\} \mathbf{P}_m^H = \mathbf{P}_m \boldsymbol{\Lambda} \mathbf{P}_m^H.$$

From this, the elements u_{mk} of $\mathbf{u}_m$ are independent Gaussian random variables, each with zero mean and unit variance. It follows that (3.119) can be written as

$$\mathcal{L}_m = (\mathbf{u}_m + \mathbf{b}_m)^H \boldsymbol{\Lambda} (\mathbf{u}_m + \mathbf{b}_m) = \sum_{k=1}^{2LN} \lambda_k |u_{mk} + b_{mk}|^2, \tag{3.121}$$

where b_{mk} is the k-th element of $\mathbf{b}_m$. The MGF is obtained from (3.121) by applying eq. (B.15) from the Appendix yielding

$$\Theta_m(s) = \prod_{k=1}^{2LN} (1 - s\lambda_k)^{-1} \exp\left\{ \frac{s\lambda_k |b_{mk}|^2}{(1 - s\lambda_k)} \right\}. \tag{3.122}$$

In (3.122), each of the $2LN$ product factors stems from the MGF of a scaled noncentral Chi-square random variable with one degree of freedom [87]. This observation is consistent with (3.121), a weighted sum of independent noncentral Chi-square random variables, where each summation term corresponds to a factor in (3.122).

3.4.4 The Independent Flat Fading Case

Now let us discuss the ZZB when the channels are flat fading, corresponding to narrowband frequency-hopping. With $L = 1$, the channel gain α_i of the ith hop follows $\mathcal{N} \sim (\mu_{\alpha i}, V_i)$, which is Rician or Rayleigh flat fading. Then the dimension of the total channel covariance matrix $\mathbf{V}$ reduces to $N \times N$, in which V_{ij} is determined by V_i, V_j

and the channel correlation coefficient between the two hops. Also the channel mean vector reduces to $\boldsymbol{\mu}_\alpha = [\mu_{\alpha 1}, \cdots, \mu_{\alpha N}]^T$.

The flat fading channel has no memory and so there will be no overlap between hops in the time domain. So the inter-hop interference terms disappear in the signal and distribution expressions. The received signal in (3.108) becomes

$$y_i(t) = \alpha_i s_{m,i} + n_i(t), \quad t \in [(i-1)MT_s,\ iMT_s] \tag{3.123}$$

and the quantities in (3.109) reduce to

$$\mathbf{S}_{m1m2} = \text{diag}\{S_{m1m2,1,1}, \cdots, S_{m1m2,N,N}\}, \quad r_{m,i} = \int_{(i-1)MT_s}^{iMT_s} s^*_{m,i} y_i(t) dt. \tag{3.124}$$

Moreover, the channel α_i over each hop is assumed independent and identical distributed (i.i.d), and then the signal correlation $S_{m1m2,i}$ is the same for each hop. By this assumption, $\mathbf{V}$ becomes diagonal. The joint distribution of the received signal over independent flat fading channels becomes

$$p(\mathbf{y}(t)|m\Delta) = \prod_{i=1}^{N} p(y_i(t)|m\Delta) \propto \prod_{i=1}^{N} \exp\left\{W_i r_{m,i}^2 + 2\text{Re}\{h_i^* r_{m,i}\}\right\}, \tag{3.125}$$

where

$$W_i = \frac{V_i}{N_0(N_0 + V_i S_{00,i})}, \quad h_i = \frac{\mu_i}{N_0 + V_i S_{00,i}}, \quad S_{00,i} \triangleq S_{00,i,i}.$$

In this case, the LLR is

$$\mathcal{L} = \mathbf{r}^H \boldsymbol{\Psi} \mathbf{r} + 2\text{Re}\{\mathbf{g}^H \mathbf{r}\} = \sum_{i=1}^{N} W_i (r_{0,i}^2 - r_{1,i}^2) + 2\text{Re}\{h_i^* (r_{0,i} - r_{1,i})\}. \tag{3.126}$$

This is the sum of the LLRs corresponding to each sub-channel. Accumulation helps to improve the decision performance in fading and noise, a benefit of frequency hopping diversity.

Conditioned on hypothesis H_m, the statistics of $\widetilde{\mathbf{r}}_{m,i} \triangleq [r_{0,i}|H_m \; r_{1,i}|H_m]^T$ are

$$H_0: \quad \boldsymbol{\mu}_{0,i} = \begin{bmatrix} S_{00,i}\mu_{\alpha i} \\ S_{10,i}\mu_{\alpha i} \end{bmatrix}, \quad \boldsymbol{\Sigma}_{0,i} = \begin{bmatrix} S_{00,i}^2 V_i + N_0 S_{00,i} & S_{00,i}S_{10,i}^* V_i + N_0 S_{10,i}^* \\ S_{00,i}S_{10,i} V_i + N_0 S_{10,i} & |S_{10,i}|^2 V_i + N_0 S_{00,i} \end{bmatrix}, \tag{3.127}$$

$$H_1: \quad \boldsymbol{\mu}_{1,i} = \begin{bmatrix} S_{10,i}^*\mu_{\alpha i} \\ S_{00,i}\mu_{\alpha i} \end{bmatrix}, \quad \boldsymbol{\Sigma}_{1,i} = \begin{bmatrix} |S_{10,i}|^2 V_i + N_0 S_{00,i} & S_{00,i}S_{10,i}^* V_i + N_0 S_{10,i}^* \\ S_{00,i}S_{10,i} V_i + N_0 S_{10,i} & S_{00,i}^2 V_i + N_0 S_{00,i} \end{bmatrix}. \tag{3.128}$$

Next, the Rician (line-of-sight) and Rayleigh (non-line-of-sight) cases are considered respectively.

3.4.4.1 Rician Fading Case

Under the i.i.d condition, W_i and h_i are the same for each i, and $\widetilde{\mathbf{r}}_{m,i}$ is also i.i.d. Then with $W_i > 0$, the error probability $P_e(\Delta)$ becomes

$$P_e(\Delta) = \Pr\{\mathcal{L}_0 < 0\} = \Pr\left\{\sum_{i=1}^{N}\left[\left|r_{0,i}|H_0 + \frac{h_i}{W_i}\right|^2 - \left|r_{1,i}|H_0 + \frac{h_i}{W_i}\right|^2\right] < 0\right\}. \tag{3.129}$$

Denote the Gaussian variables within the brackets as $A = r_{0,i}|H_0 + \frac{h_i}{W_i}$ and $B = r_{1,i}|H_0 + \frac{h_i}{W_i}$, where $r_{0,i}|H_0$ and $r_{1,i}|H_0$ are elements of $\widetilde{\mathbf{r}}_{0,i}$. For these two variables, mean μ_A, μ_B, variance Σ_A, Σ_B and covariance Σ_{AB} can be found from (3.127) as

$$[\mu_A, \mu_B]^T = \boldsymbol{\mu}_{i,0} + \frac{h_i}{W_i}[1,1]^T, \quad \boldsymbol{\Sigma}_{i,0} = \begin{bmatrix} \Sigma_A & \Sigma_{AB} \\ \Sigma_{AB}^* & \Sigma_B \end{bmatrix}.$$

Thus from the results in [82, pp. 619-624] (eq. (9A.11)) or [84, pp. 943-948] (eq. (B-21)), a closed form for $P_e(\Delta)$ can be obtained

$$P_e(\Delta) = Q_1(a,b) - \left[1 - \frac{\sum_{i=0}^{N-1}\binom{2N-1}{i}\eta^i}{(1+\eta)^{2N-1}}\right]\exp\left(-\frac{a^2+b^2}{2}\right)I_0(ab) + \frac{1}{(1+\eta)^{2N-1}}$$
$$\times\left\{\sum_{i=2}^{N}\binom{2N-1}{N-i}\left\{\eta^{N-i}[Q_i(a,b) - Q_1(a,b)] - \eta^{N-1+i}[Q_i(b,a) - Q_1(b,a)]\right\}\right\}, \tag{3.130}$$

in which $Q_i(a,b)$ is the ith order Marcum Q-function [93, 94], and

$$a = \left[\frac{2v_1^2 v_2(\xi_1 v_2 - \xi_2)}{(v_1+v_2)^2}\right]^{1/2}, \quad b = \left[\frac{2v_1^2 v_2(\xi_1 v_1 + \xi_2)}{(v_1+v_2)^2}\right]^{1/2},$$

$$\eta = v_2/v_1, \quad v_{\frac{1}{2}} = \sqrt{w^2 + \frac{1}{\Sigma_A\Sigma_B - |\Sigma_{AB}|^2}} \mp w, \quad w = \frac{\Sigma_A - \Sigma_B}{2(\Sigma_A\Sigma_B - |\Sigma_{AB}|^2)},$$

$$\xi_1 = N(|\mu_A|^2\Sigma_B + |\mu_B|^2\Sigma_A - \mu_A^*\mu_B\Sigma_{AB} - \mu_A\mu_B^*\Sigma_{AB}^*), \quad \xi_2 = N(|\mu_A|^2 + |\mu_B|^2).$$

3.4.4.2 Rayleigh Fading Case

For the Rayleigh fading case as studied in [43], $\mu_i = 0$ and so $h_i = 0$. The LLR becomes $\mathcal{L} = \sum_{i=1}^{N}(|r_{0,i}|^2 - |r_{1,i}|^2)$, and the test reduces to the comparison of the signal power $|r_{0,i}|^2$ with $|r_{1,i}|^2$. The error probability expression (3.129) matches eq. (113) in [43], and $\boldsymbol{\mu}_{i,0} = [0,0]^T$ and $\boldsymbol{\Sigma}_{i,0}$ in (3.127) matches distribution parameters of eq. (115) in [43]. Therefore the same closed form expression for error probability $P_e(\Delta)$ as in eqs. (116) and (117) of [43] follows,

$$P_e(\Delta) = \sum_{i=0}^{N-1}\binom{2N-1}{i}\left(\frac{1+\nu(\Delta)}{2}\right)^i\left(\frac{1-\nu(\Delta)}{2}\right)^{2N-1-i}, \tag{3.131}$$

with

$$\nu(\Delta) = \left[1 + \frac{4(1+\mathrm{SNR}_i \cdot S_{00,i})}{(S_{00,i}\cdot \mathrm{SNR}_i)^2 \cdot [1 - |S_{10,i}/S_{00,i}|^2]}\right]^{-1/2}.$$

Each summation term in (3.131) is a binomial distribution $f(i; 2N-1, \frac{1+\nu(\Delta)}{2})$. When the number of hops N is large, it can be approximated by a Gaussian distribution for simplified evaluation [95]. Moreover, $\nu(\Delta)$ is close to 1 in the high SNR region and then P_e is dominated by the last several summation terms with large i. Selecting the last U summation terms, P_e can be approximated as

$$\begin{aligned} P_e(\Delta) &\approx \sum_{i=N-U}^{N-1}\binom{2N-1}{i}\left(\frac{1+\nu(\Delta)}{2}\right)^i\left(\frac{1-\nu(\Delta)}{2}\right)^{2N-1-i} \\ &\approx \sum_{i=N-U}^{N-1}\frac{\exp\left\{-\frac{[i-(2N-1)(1+\nu(\Delta))/2]^2}{(2N-1)(1-\nu^2(\Delta))/2}\right\}}{\sqrt{2\pi(2N-1)(1-\nu^2(\Delta))/4}}. \end{aligned} \tag{3.132}$$

For large N, it suffices to choose a small U. This approximate expression shows the effect of frequency hopping diversity (in terms of N) on P_e, and therefore on the ZZB. The next subsection will show numerically how the ZZB decreases with increasing N.

3.4.5 Numerical Examples

As before, the RMSE of the TDE is adopted as the performance metric, and use both the MGF approach in Section 3.4.3 and the closed-form expressions in Sections 3.4.4.1 and 3.4.4.2 to evaluate the ZZB. Unless otherwise specified, $p(t)$ is a normalized SRRC pulse with roll-off factor $\beta = 0$ and mean-square bandwidth $B = 1/12$. The SRRC pulse is used due to its common use in communications systems, and its good spectral occupancy properties. Actually a rectangular pulse can produce better TDE results, but at the cost of more spectral occupancy (see the results in Section 3.3.7). The SRRC pulse is symmetrically truncated to duration $T_s = 12$, i.e., 12 times beyond the first zero-crossing point. The channel has tap spacing $T_t = 1$ and $L = 5$ taps. Note that all the time variables are normalized to T_t. The time delay has a uniform prior over $[0, 30]$; i.e., $T = 30$. The transmission duration is NMT_s, which is a cycle of N hops, where the number of transmitted symbols per hop is set to $M = 80/N$. As the transmitted pulse has unit energy, and the number of symbols in one cycle is fixed to $MN = 80$, the total transmitted energy for one-shot TDE is fixed and independent of N. The hops are equally spaced, and the center frequency separation of neighboring hops is set to $\Delta f = 1$. Then, the ith and jth hops are separated by $|i - j|\Delta f$.

The channel fading distribution of $\boldsymbol{\alpha}_i$ and SNR_i are the same for each hop. To obtain the covariance between the pth and qth channel taps ($p, q = 1, \cdots, LN$), both the tap variance and the correlation coefficients are needed. The mean $\boldsymbol{\mu}_{\alpha i}$ and the variance $\mathbf{V}_i$ for all the channel taps in the ith hop are generated using the exponential

power decay profile given in [46], with the mean of the first tap obtained from a Rician-K factor, and all other taps with zero mean. The frequency-hopping channel correlation coefficient between the pth and qth channel taps from the ith and jth hops, respectively, is expressed as $\rho_{p,q} = \rho^t_{p,q}(1+\sqrt{-1}\sigma 2\pi|i-j|\Delta f)/(1+(\sigma 2\pi|i-j|\Delta f)^2)$, which is developed in [96] following the classical Jakes model [92, pp. 46-51]. The temporal correlation $\rho^t_{p,q}$ depends on the time separation between the pth and qth taps. In the following numerical examples $\rho^t = 0.8$ is adopted for the first two neighboring taps, and $\sigma = 1$ is the root-mean-square value of the delay spread.

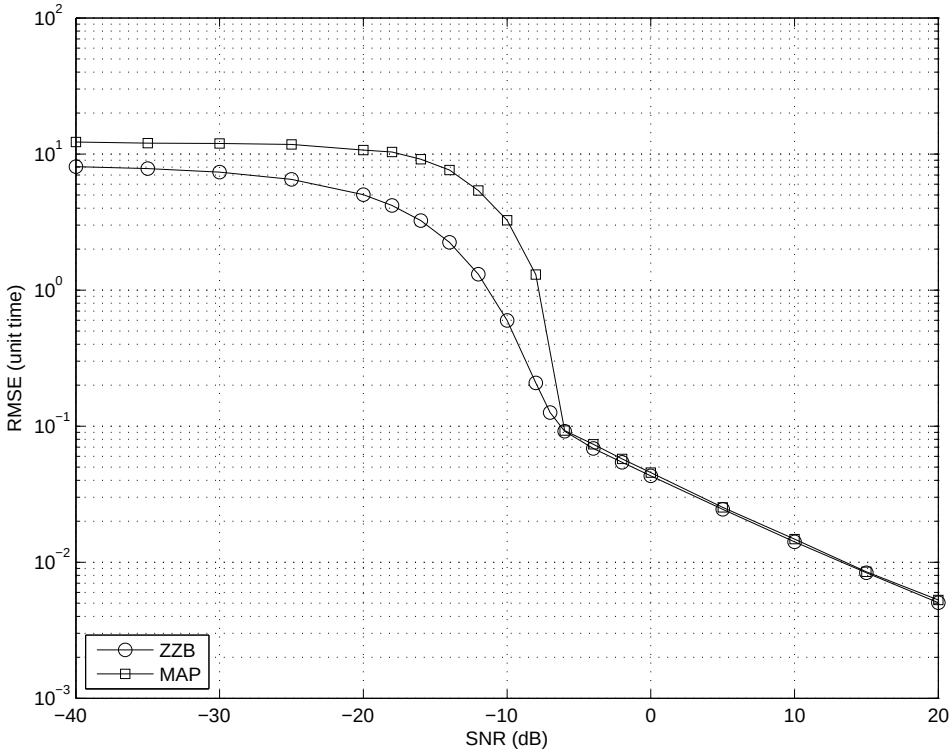

Figure 3.7: Time delay estimation results, comparing the ZZB and the corresponding MAP estimation performance. $N = 4$ hops, $M = 20$ symbols, and an FIR random channel, with first tap Rician-$K = 20$dB, and later taps Rayleigh distributed.

Figure 3.7 plots the ZZB for a frequency-hopping waveform with $N = 4$ hops in comparison with the performance of the optimum MAP estimator. The MAP estimator

is implemented by using (3.111) as follows (see also eq. (78) in [86])

$$\widehat{t}_{0,\mathrm{MAP}} = \arg\max_{t_0} \left\{ \frac{1}{T} \exp\left(\mathbf{r}_{t_0}^H \mathbf{W} \mathbf{r}_{t_0} + 2\mathrm{Re}\{\mathbf{h}^H \mathbf{r}_{t_0}\} \right) \right\}, \tag{3.133}$$

where $1/T$ is the prior on delay t_0, and $\mathbf{r}_{t_0}$ is defined by replacing $m\Delta$ with t_0 in $\mathbf{r}_m$. The channel Rician-K factor is set to $K = 20$dB. The ZZB predicts typical behavior for TDE. At low SNR, the ZZB converges to $T/\sqrt{12}$, similar to other cases [46, 86]. High SNR threshold occurs at about -6 dB, below which TDE performance rapidly degrades. Above the high SNR threshold, the ZZB decreases linearly with increasing SNR, with a slope of about -0.5, similar to bandwidth limited pulse cases studied by Ziv and Zakai [38, 39]. Moreover, the ZZBs track the MAP estimator threshold behavior and the MAP RMSE converges to the ZZB at high SNR as expected. At low SNR, the MAP RMSE converges to $T/\sqrt{6}$, higher than the ZZB's convergence level. The gap has been quantitatively analyzed in [86], and occurs due to approximations in the derivation of the original ZZB inequality by Ziv and Zakai.

The closed-form expressions of the ZZB in (3.130) and (3.131) for independent flat fading channels have much lower numerical complexity than the MGF approach, and are useful for quickly testing parameter effects on the ZZB. Figure 3.8 compares the ZZBs at various number of hops, $N = 1, 2, 4, 8$, and 16, under the independent flat Rayleigh fading channel discussed in Section 3.4.4.2. The ZZB without the Gaussian approximation in (3.131), and with the Gaussian approximation in (3.132), are plotted with $U = 3$ for $N > 2$, and $U = N$ when $N \leq 2$. As can be seen, larger N leads to lower RMSE level and the high SNR threshold occurs at lower SNR, about 25dB, 14dB, 5dB, and 0dB for $N = 2$, 4, 8 and 16, respectively. Recalling that the total transmitted energy is fixed and independent of N, the RMSE reduction arises solely from the frequency-hopping diversity available via hopping through different channel

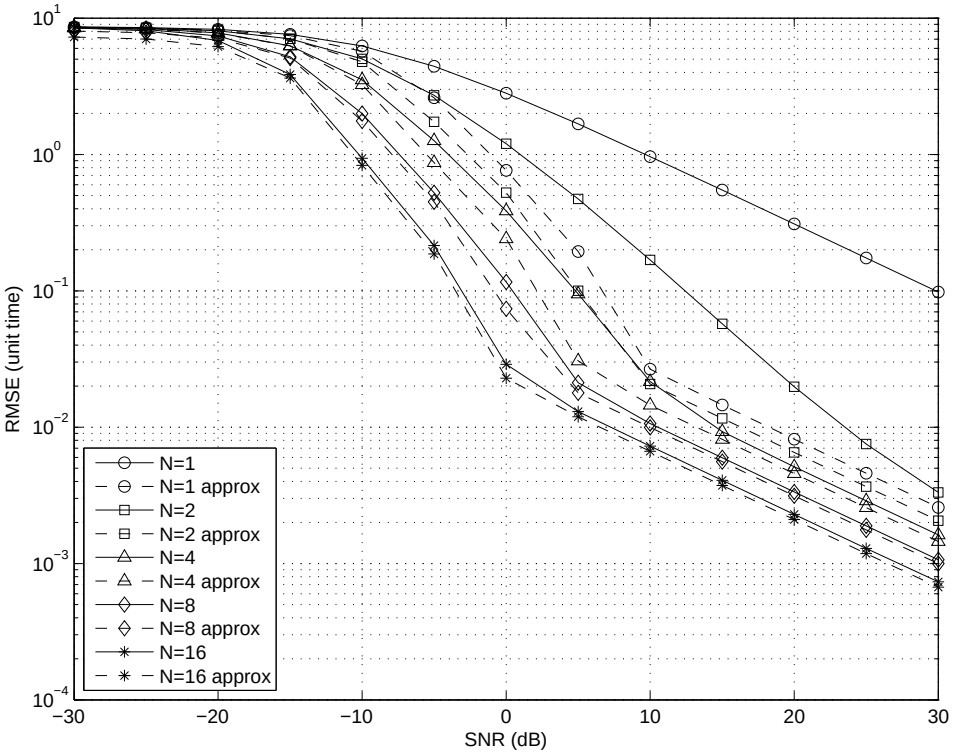

Figure 3.8: ZZBs with independent flat Rayleigh channels show the frequency hopping diversity gain, with curves parameterized by the number of hops $N = 1, 2, 4, 8$ and 16.

realizations. This comparison clearly exemplifies the frequency diversity effect on TDE. The diversity gain from increasing N over 2 to 16 achieves a maximum of about 18dB at RMSE of 2×10^{-2}, with a constant gain of about 12dB in the high SNR regime.

In Figure 3.9, (3.130) is used to evaluate the effect of Rician-K factor on the ZZB under independent flat Rician fading. The FH transmission has $N = 4$ hops and K varies from -20dB to 20dB. The ZZBs exhibit the most difference in the moderate SNR region over -10dB to 5dB, and the maximum difference is about 11dB at RMSE 10^{-1}. In this region, the ambiguities in signal correlation dominate the TDE error, which occur due to fading. In the high SNR region, the effects of varying K are minimized and the bounds for different K coincide.

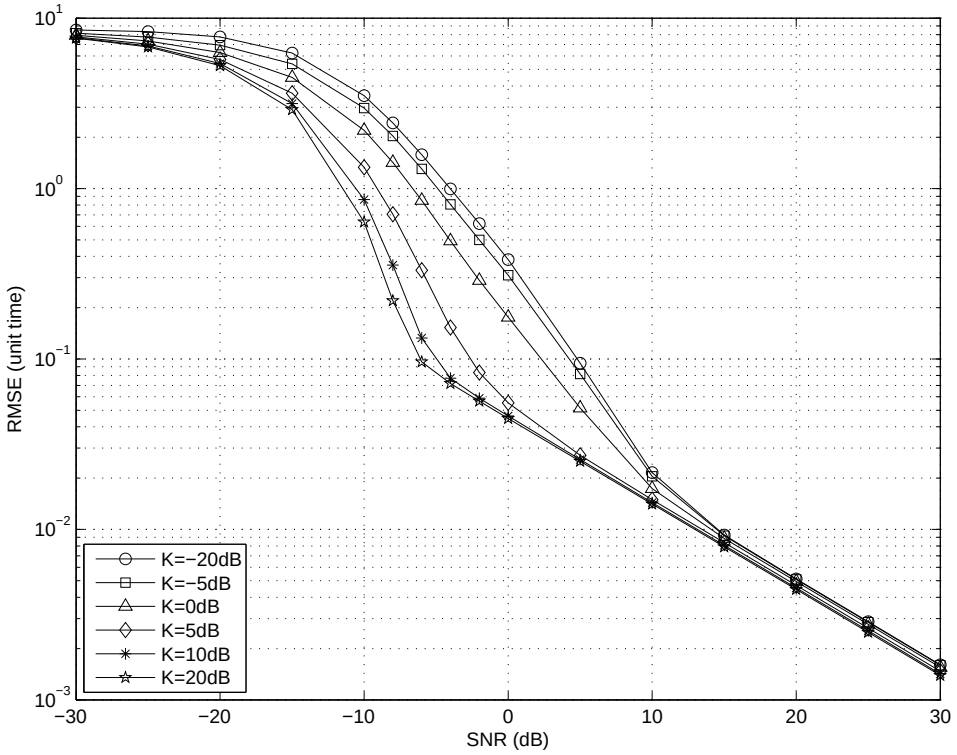

Figure 3.9: ZZBs for varying Rician-K factor, with independent flat fading channels. The stronger Rician channel yields significant TDE performance gain in the mid-SNR range.

3.5 Summary

This chapter discusses the theoretical performance limits of time delay estimation in multipath channels. Ziv-Zakai bounds on Bayesian estimation of time delay are developed for the known pulsed signal or frequency hopping waveforms propagating through unknown random multipath channels, with a uniform prior on the delay. The multipath channel model includes important special cases, such as Rayleigh/Rician flat fading channels, wideband multipath channels, and known channels. With appropriate power delay profiles, the channel model can be readily adapted to the strong LOS channel, or multipath channel with weak LOS path, or even NLOS channel. In each of the assumed channels, the bounds assume channel statistics known to receivers but without knowledge of the channel realizations.

The ZZBs provide good performance prediction for MAP time delay estimation, tracking the low, medium, and high SNR regimes. The associated Cramér-Rao bound is shown tight only at high SNR, whereas the ZZBs predict threshold behavior and TDE breakdown as the SNR decreases. When compared to the average ZZB that assumes knowledge of the channel realization, the ZZBs developed by the author provides more realistic and tighter performance limits, revealing the performance penalty due to lack of channel knowledge. The non-convergence to the prior uniform distribution when the SNR goes to zero is well known for the ZZB, and this was accounted for by studying the ZZB approximations at low SNR. Moreover, the ZZB for frequency hopping waveforms shows the benefit of frequency diversity for TDE in frequency-selective fading channels. The special case of independent flat-fading is discussed, including both Rician and Rayleigh fading, and closed-form expressions enable easy study of the effects of SNR, frequency diversity, and channel statistics on TDE.

Chapter 4

Performance of ToA Localization

4.1 Introduction

By the discussion in previous chapters, it is known that range estimates or time delay estimation may have a positive bias in multipath environments, where a line-of-sight path may be weak or essentially nonexistent. In Chapter 3 the performance limits of time delay estimates are throughly developed. In range-based localization systems, the errors in range measurements will essentially be converted to the position estimation error by different localization schemes. In this chapter the author analyzes the performance of localization in multipath channel, based on multiple erroneous range estimates from reference points.

There are different cases in unknown location estimation in multipath channel, dependent on the assumption on the bias in range estimation: (a) bias is known; (b) bias is an unknown nuisance deterministic parameter embedded in measurement error; (c) bias is an unknown nuisance deterministic parameter jointly estimated with the source location; and (d) bias is random following certain distribution. These cases lead to different estimators and corresponding localization performance. Case (a) becomes an

easy one after subtracting the bias from each measurement to obtain an unbiased measurement. In related recent works, [47] studied Case (c) assuming the deterministic bias is identical for all sensors , and [48] developed a localization bound in an ultra-wideband environment, where the bias is assumed uniformly distributed and the statistics were obtained experimentally in an indoor scenario.

In this chapter, the author focuses on Case (b) and Case (d), deriving the bias and mean-square error of the widely adopted weighted least-square and maximum-likelihood location estimators, as a function of deterministic or random measurement bias with different distributions, receiver noise and other parameters. The error expressions are developed via perturbation analysis, providing a means to study achievable localization performance, as a function of the measurement bias and variance, as well as the reference array geometry and number of reference transceivers (beacons). Other nuisance parameters such as clock bias are omitted and assumed perfect in the analysis.

4.2 Models for Biased Range Measurement

Consider a range-based localization problem employing K beacon nodes at known locations $\mathbf{p}_i = [x_i, y_i]^T, i = 1, \cdots, K$. The range from the signal source at $\mathbf{p}_s = [x_s \ y_s]^T$ to the ith beacon at $\mathbf{p}_i$ is

$$d_i = \sqrt{(x_s - x_i)^2 + (y_s - y_i)^2}. \tag{4.1}$$

Denote the angle between the source and the ith beacon with respect to the horizontal as θ_i, then

$$\cos\theta_i = \frac{x_s - x_i}{d_i}, \quad \sin\theta_i = \frac{y_s - y_i}{d_i}. \tag{4.2}$$

By measuring the first signal arriving at the i beacon receiver from the source, the range measurement at the ith beacon is modeled as

$$\begin{aligned} r_i &= d_i + v_i \\ &= d_i + b_i + n_i, \end{aligned} \tag{4.3}$$

in which $v_i = b_i + n_i$ is the total ranging error, composed of a non-negative bias $b_i \geq 0$ with mean μ_{b_i} and standard deviation σ_{b_i}, and the white Gaussian noise n_i with zero mean, standard deviation σ_{n_i}.

The estimation of $\mathbf{p}_s = (x_s, y_s)$ is based on the measurements of $\mathbf{r} = [r_1, \cdots, r_K]$, in a noisy fading channel. The bias is assumed either unknown deterministic, or random with known distributions in multipath fading channels where LOS path is weak or non-existent. The most widely adopted models for the random time delay bias include exponential, Maxwell, uniform, and Bernoulli distributions [71, pp. 340-341]. Since time delay mainly depends on the propagation environment, all bias b_i are assumed independent.

4.2.1 Exponential Distribution

The bias follows an exponential distribution $\mathcal{E}(1/\sigma_{b_i}, b_i^0)$ if its pdf is

$$h_i(b_i) = \frac{1}{\sigma_{b_i}} \exp\left[-\frac{1}{\sigma_{b_i}}(b_i - b_i^0)\right], \quad b_i \geq b_i^0, \tag{4.4}$$

where b_i^0 is the known location parameter, σ_{b_i} is the mean and standard deviation of the variable $b_i - b_i^0$.

4.2.2 Maxwell Distribution

The Maxwell distribution has the following form

$$h_i(b_i) = \begin{cases} \frac{\sqrt{2/\pi}(3-8/\pi)^{3/2}}{\sigma_{bi}^3} b_i^2 \exp\left[-\frac{(3-8/\pi)b_i^2}{2\sigma_{bi}^2}\right], & b_i \geq 0 \\ 0, & b_i < 0 \end{cases}, \tag{4.5}$$

with a distribution parameter σ_{b_i}.

4.2.3 Uniform Distribution

The bias b_i follows a uniform distribution in $[\beta_s, \beta_m]$ if its pdf takes the following form.

$$h_i(b_i) = \begin{cases} \frac{1}{\beta_m - \beta_s} = \frac{1}{2\sqrt{3}\sigma_{bi}}, & \beta_s \leq b_i \leq \beta_m \\ 0, & \text{others} \end{cases}. \tag{4.6}$$

In the above, it is assumed $\beta_s \geq 0$.

4.2.4 Bernoulli Distribution

The Bernoulli distribution is given by

$$h_i(b_i) = \begin{cases} \frac{1}{2}, & b_i = 0 \\ \frac{1}{2}, & b_i = 2\sigma_{bi} \\ 0, & \text{others} \end{cases}. \tag{4.7}$$

The above models have their respective merits and deficiencies in different application scenarios. The bias distribution parameter could vary in a particular scenario even if the distribution type might be invariant. In extreme cases, it may be zero for a subset of references. For the random bias case, the analysis in the following sections mainly focuses on the exponential model and then detail the corresponding discussions. Only brief discussions are provided on other models.

4.3 Convolved Distributions of Range Measurements

The location estimation depends on the distribution of the range measurement r_i at the ith reference point, that in turn depends on the total measurement error v_i. With random bias assumption and sensor measurement model (4.3), the distribution $f_i(v_i)$ of v_i is the convolution the pdf $h_i(b_i)$ of the bias b_i and $g_i(n_i)$ of the noise n_i, given by

$$f_i(v_i) = \int_{-\infty}^{\infty} h_i(x) g_i(v_i - x) dx. \tag{4.8}$$

Denote the pdf of the Gaussian noise n_i as

$$g_i(n_i) = \frac{1}{\sqrt{2\pi}\sigma_{n_i}} e^{-\frac{n_i^2}{2\sigma_{n_i}^2}}. \tag{4.9}$$

The standard deviation of bias σ_{b_i} is normalized for each specific distribution model, while its mean μ_{b_i} is different. Since all b_i and n_i are independent, the joint pdf of all r_i is simply the product of individuals that will be shown later in the next section. In the following, $f_i(v_i)$ or $f_i(r_i)$ are developed for each possible bias model respectively. In addition, the first-order partial derivative of $f_i(r_i)$ with respect to d_i is found for the CRB derivation in the next section.

4.3.1 Exponential Bias Model

Assume the bias b_i at the ith beacon follows an exponential distribution $\mathcal{E}(1/\sigma_{b_i}, b_i^0)$ by (4.4). By (4.8), the pdf of v_i is

$$\begin{aligned} f_i(v_i) &= \int_{b_i^0}^{\infty} h_i(x) g_i(v_i - x) dx \\ &= \frac{1}{\sqrt{2\pi}\sigma_{n_i}\sigma_{b_i}} \int_{b_i^0}^{\infty} \exp\left[-\frac{1}{\sigma_{b_i}}(x - b_i^0)\right] \exp\left[-\frac{(v_i - x)^2}{2\sigma_{n_i}^2}\right] dx. \end{aligned} \tag{4.10}$$

After some manipulations, it can be simplified as

$$f_i(v_i) = \frac{1}{\sqrt{2\pi}\sigma_{n_i}\sigma_{b_i}} \exp\left(\frac{b_i^0 - v_i}{\sigma_{b_i}} + \frac{\sigma_{n_i}^2}{2\sigma_{b_i}^2}\right) \int_{b_i^0}^{\infty} \exp\left[-\frac{(x - v_i + \sigma_{n_i}^2/\sigma_{b_i})^2}{2\sigma_{n_i}^2}\right] dx$$
$$= \frac{1}{\sigma_{b_i}} \exp\left(\frac{b_i^0 - v_i}{\sigma_{b_i}} + \frac{\sigma_{n_i}^2}{2\sigma_{b_i}^2}\right) Q\left(\frac{b_i^0 - v_i + \sigma_{n_i}^2/\sigma_{b_i}}{\sigma_{n_i}}\right). \tag{4.11}$$

Note that at $v_i = b_i^0$, it takes a value of

$$f_i(b_i^0) = \frac{1}{\sigma_{b_i}} e^{\frac{\sigma_{n_i}^2}{2\sigma_{b_i}^2}} Q\left(\frac{\sigma_{n_i}}{\sigma_{b_i}}\right). \tag{4.12}$$

The pdf of r_i is the same as $f_i(v_i)$ in eq.(4.10) except the variable v_i is replace by $r_i - d_i$, expressed as

$$f_i(r_i) = \frac{1}{\sigma_{b_i}} \exp\left(\frac{b_i^0 - r_i + d_i}{\sigma_{b_i}} + \frac{\sigma_{n_i}^2}{2\sigma_{b_i}^2}\right) Q\left(\frac{b_i^0 - r_i + d_i + \sigma_{n_i}^2/\sigma_{b_i}}{\sigma_{n_i}}\right). \tag{4.13}$$

The derivative on (4.13) with respect to d_i is

$$\frac{\partial f_i(r_i)}{\partial d_i} = \frac{1}{\sigma_{b_i}} \left[f_i(r_i) - g_i(r_i - d_i - b_i^0)\right], \tag{4.14}$$

where $g_i(r_i - d_i - b_i^0)$ is the Gaussian noise pdf in (4.9).

4.3.2 Maxwell Bias Model

The bias distribution follows (4.5). The distribution of v_i is

$$f_{v_i}(v_i) = \int_0^{\infty} f_{b_i}(x) f_{n_i}(v_i - x) dx$$
$$= \frac{(3 - 8/\pi)^{3/2}}{\pi\sigma_{bi}^3\sigma_n} \int_0^{\infty} x^2 \exp\left[-\frac{(3 - 8/\pi)x^2}{2\sigma_{bi}^2} - \frac{(v_i - x)^2}{2\sigma_n^2}\right] dx, \tag{4.15}$$

which does not have a closed-form expression. Note that the standard deviation σ_{bi} is normalized to be the same as the exponential distribution, and the mean $\mu_{bi} = \frac{2\sqrt{2}}{\sqrt{3\pi - 8}}\sigma_{bi}$. The pdf of r_i, $f_i(r_i)$, is found by variable substitution, and its derivative is

$$\frac{\partial f_i(r_i)}{\partial d_i} = \frac{(3 - 8/\pi)^{3/2}}{\pi\sigma_{bi}^3\sigma_n^3} \int_0^{\infty} x^2 (r_i - d_i - x) \exp\left[-\frac{(3 - 8/\pi)x^2}{2\sigma_{bi}^2} - \frac{(r_i - d_i - x)^2}{2\sigma_n^2}\right] dx. \tag{4.16}$$

The derivative does not have closed-form either and can only be evaluated numerically.

4.3.3 Uniform Bias Model

The bias b_i follows a uniform distribution (4.6). The distribution of v_i is

$$\begin{aligned} f_{v_i}(v_i) &= \int_{\beta_s}^{\beta_m} f_{b_i}(x) f_{n_i}(v_i - x) dx \\ &= \frac{1}{\beta_m - \beta_s} \int_{\beta_s}^{\beta_m} \frac{1}{\sqrt{2\pi}\sigma_n} \exp\left[-\frac{(v_i - x)^2}{2\sigma_n^2}\right] dx \\ &= \frac{1}{\beta_m - \beta_s} \left[Q\left(\frac{v_i - \beta_m}{\sigma_n}\right) - Q\left(\frac{v_i - \beta_s}{\sigma_n}\right)\right]. \end{aligned} \tag{4.17}$$

Similarly, the distribution is normalized to have standard deviation σ_{bi} and mean $\mu_{bi} = \frac{\beta_s + \beta_m}{2}$. which is a special case of the piece-wise uniform model in [48]. By variable substitution, $f_{r_i}(r_i)$ can be obtained and its derivative is

$$\frac{\partial f_i(r_i)}{\partial d_i} = \frac{1}{\sqrt{2\pi}\sigma_n(\beta_m - \beta_s)} \left[e^{-(r_i - d_i - \beta_m)^2/2\sigma_n^2} - e^{-(r_i - d_i - \beta_s)^2/2\sigma_n^2}\right]. \tag{4.18}$$

4.3.4 Bernoulli Bias Model

Using the Bernoulli distribution (4.7) for the bias, the distribution of v_i is

$$\begin{aligned} f_{v_i}(v_i) &= f_{b_i}(x) f_{n_i}(v_i - x)|_{x=0} + f_{b_i}(x) f_{n_i}(v_i - x)|_{x=2\sigma_{bi}} \\ &= \frac{1}{2\sqrt{2\pi}\sigma_n} \left\{\exp\left(-\frac{v_i^2}{2\sigma_n^2}\right) + \exp\left[-\frac{(v_i - 2\sigma_{bi})^2}{2\sigma_n^2}\right]\right\} \\ &= \frac{1}{2}\left[g_i(v_i) + g_i(v_i - 2\sigma_{bi})\right]. \end{aligned} \tag{4.19}$$

The bias standard deviation is also normalized to σ_{bi} and bias mean is $\mu_{bi} = \sigma_{bi}$. The derivative of $f_{r_i}(r_i)$ is

$$\frac{\partial f_i(r_i)}{\partial d_i} = \frac{1}{2\sqrt{2\pi}\sigma_n^3} \left\{(r_i - d_i) \exp\left[-\frac{(r_i - d_i)^2}{2\sigma_n^2}\right] + (r_i - d_i - 2\sigma_{bi}) \exp\left[-\frac{(r_i - d_i - 2\sigma_{bi})^2}{2\sigma_n^2}\right]\right\}. \tag{4.20}$$

4.4 Cramér-Rao Bound on ToA Localization with Biased TDE

Based on the bias models for TDE and the distributions of range measurements developed in the previous sections, the ToA localization Cramér-Rao Bounds can be obtained. With the independent measurements corresponding to all the reference points, the joint distribution of the range measurement vector $\mathbf{r} = [r_1, r_2, \cdots, r_K]$ is

$$f(\mathbf{r}; \mathbf{p}_s) = \prod_{i=1}^{K} f_i(r_i; \mathbf{p}_s), \tag{4.21}$$

in which $f_i(r_i; \mathbf{p}_s) \triangleq f_i(r_i)$ is the unknown-location-dependent pdf of the range measurement at the ith reference point. The pdf expressions for all the possible bias models can be found in the previous section. The Fisher information matrix (FIM) is given by [48]

$$\begin{aligned}
\mathbf{J} &= \mathbb{E}_{\mathbf{r}} \left\{ \left[\nabla_{\mathbf{p}_s} \ln(f(\mathbf{r}; \mathbf{p_s})) \right] \left[\nabla_{\mathbf{p}_s} \ln(f(\mathbf{r}; \mathbf{p_s})) \right]^T \right\} \\
&= \mathbb{E}_{\mathbf{r}} \left\{ \sum_{i=1}^{K} \frac{1}{f_i(r_i; \mathbf{p}_s)^2} \begin{bmatrix} \left(\frac{\partial f_i(r_i; \mathbf{p}_s)}{\partial x_s} \right)^2 & \frac{\partial f_i(r_i; \mathbf{p}_s)}{\partial x_s} \frac{\partial f_i(r_i; \mathbf{p}_s)}{\partial y_s} \\ \frac{\partial f_i(r_i; \mathbf{p}_s)}{\partial y_s} \frac{\partial f_i(r_i; \mathbf{p}_s)}{\partial x_s} & \left(\frac{\partial f_i(r_i; \mathbf{p}_s)}{\partial y_s} \right)^2 \end{bmatrix} \right\} \\
&= \sum_{i=1}^{K} \rho(\nu_i) \begin{bmatrix} \cos^2 \theta_i & \cos \theta_i \sin \theta_i \\ \sin \theta_i \cos \theta_i & \sin^2 \theta_i \end{bmatrix},
\end{aligned} \tag{4.22}$$

where

$$\nu_i = v_i - \mu_{b_i} = r_i - d_i - \mu_{b_i}, \quad \rho(\nu_i) = \int_{-\infty}^{\infty} \frac{1}{f_i(r_i; \mathbf{p}_s)} \left(\frac{\partial f_i(r_i; \mathbf{p}_s)}{\partial d_i} \right)^2 d\nu_i. \tag{4.23}$$

The CRB is expressed as

$$\mathbb{E}_{\mathbf{r}} \left\{ (\mathbf{p}_s - \widehat{\mathbf{p}}_s)(\mathbf{p}_s - \widehat{\mathbf{p}}_s)^T \right\} \geq \mathbf{J}^{-1}. \tag{4.24}$$

The lower bound for the RMSE of the location estimation can also be expressed by FIM as

$$\text{RMSE} \triangleq \sqrt{\mathbb{E}_{\mathbf{r}}\left\{(x_s - \widehat{x}_s)^2 + (y_s - \widehat{y}_s)^2\right\}} \geq \sqrt{tr\{\mathbf{J}^{-1}\}}, \tag{4.25}$$

where tr denotes the trace of a square matrix.

In (4.22) and (4.23), the pdf $f_i(r_i; \mathbf{p}_s)$ of the measurement r_i has the same expression as $f_{v_i}(v_i)$ in the previous section. Computing $\rho(\nu_i)$ with (4.23) by taking the differentials on $f_i(r_i; \mathbf{p}_s)$ and substituting $\rho(\nu_i)$ into (4.22), one can find the FIM and the CRBs. Because the expression (4.23) of $\rho(\nu_i)$ is an integration and the integrand incorporates the squared derivative, $\rho(\nu_i)$ generally does not have a closed-form expression, and it can only be evaluated numerically in most cases.

4.5 Weighted Least-Square Location Estimator

In the absence of bias distribution, the best location estimator based on biased measurements is a WLS estimator. This section presents this estimator, and analyze its estimation performance from a perturbation viewpoint (assuming error is small). A special case of uniform circular array is examined. This configuration leads to some interesting observations. Finally performance optimization utilizing analytical results is discussed.

4.5.1 WLS Estimator

The WLS estimation of the source location is given by

$$\min_{(x_s, y_s)} \sum_{i=1}^{K} (r_i - d_i)^2 w_i, \tag{4.26}$$

where w_i is a weight that can be chosen as desired, for example, letting $w_i = \sigma_{ni}^{-2}$. The solution to the optimization problem (4.26) can be obtained by differentiating with

respect to both x_s and y_s and equating with zero, satisfying the two equations [97]

$$\sum_{i=1}^{K} w_i(r_i - d_i)\cos\theta_i = 0, \tag{4.27}$$

$$\sum_{i=1}^{K} w_i(r_i - d_i)\sin\theta_i = 0. \tag{4.28}$$

These equations are highly nonlinear due to (4.1) and (4.2), and x_s and y_s can only be solved numerically.

4.5.2 First-Order Error Analysis on WLS Estimation

To study the estimation error from the estimator (4.26), a perturbation analysis is carried out around the optimal solution $\widehat{\mathbf{p}}_{\mathrm{s}} = [\widehat{x}_s, \widehat{y}_s]^T$, e.g., see [66]. Let $\delta r_i = v_i$ denote a small measurement error that includes the measurement bias and noise. The error δr_i causes an estimation error δx_s, δy_s, and associated error δd_i in d_i, with x_i and y_i known. Reference position errors are omitted here but can be incorporated easily.

Note that the perturbed quantities still satisfy (4.27) and (4.28). Under the small error assumption, perturbation analysis is equivalent to differentiation, i.e., replacing the total differential operator by the error operator δ at the true solution point. In order to relate δx_s and δy_s to δr_i, first re-express δd_i here. According to (4.1) and (4.2), and applying the total differential theorem, the first-order error terms are related by

$$\delta d_i \approx \cos\theta_i \delta x_s + \sin\theta_i \delta y_s. \tag{4.29}$$

Next, δx_s and δy_s are related to δr_i from equations (4.27) and (4.28), yielding two equations for δx_s and δy_s. Term-by-term differentiation on (4.27) and (4.28) yields

$$\sum_{i=1}^{K} w_i[(\delta r_i - \delta d_i)\cos\theta_i + (r_i - d_i)\delta(\cos\theta_i)] = 0, \tag{4.30}$$

$$\sum_{i=1}^{K} w_i[(\delta r_i - \delta d_i)\sin\theta_i + (r_i - d_i)\delta(\sin\theta_i)] = 0. \tag{4.31}$$

In our error analysis, r_i represents the measurement in the absence of error n_i, and δr_i represents the error v_i. Replacing r_i by d_i and δr_i by v_i, the above becomes

$$\sum_{i=1}^{K} w_i(v_i - \delta d_i)\cos\theta_i = 0, \tag{4.32}$$

$$\sum_{i=1}^{K} w_i(v_i - \delta d_i)\sin\theta_i = 0. \tag{4.33}$$

Substituting (4.29) into (4.32) and (4.33) and combining corresponding terms, one can obtain a compact matrix equation for location estimation error vector $\delta\mathbf{p}$ to satisfy as

$$\mathbf{C}\delta\mathbf{p} \approx \mathbf{D}\mathbf{v}, \tag{4.34}$$

where

$$\mathbf{C} = \begin{bmatrix} c_{11} & c_{12} \\ \\ c_{21} & c_{22} \end{bmatrix}, \quad \delta\mathbf{p} = \begin{bmatrix} \delta x_s \\ \\ \delta y_s \end{bmatrix}, \quad \mathbf{D} = \begin{bmatrix} \mathbf{d}_1^T \\ \\ \mathbf{d}_2^T \end{bmatrix}, \quad \mathbf{v} = \begin{bmatrix} v_1 & \cdots & v_K \end{bmatrix}^T, \tag{4.35}$$

with

$$c_{11} = \sum_{i=1}^{K} w_i \cos^2\theta_i, \quad c_{12} = \sum_{i=1}^{K} w_i \cos\theta_i \sin\theta_i, \quad c_{22} = \sum_{i=1}^{K} w_i \sin^2\theta_i,$$

$$\mathbf{d}_1 = [w_1\cos\theta_1, \cdots, w_K\cos\theta_K]^T, \quad \mathbf{d}_2 = [w_1\sin\theta_1, \cdots, w_K\sin\theta_K]^T. \tag{4.36}$$

So the first order estimation error vector for source location is

$$\delta\mathbf{p} \approx \mathbf{C}^{-1}\mathbf{D}\mathbf{v} = \mathbf{G}\mathbf{v}, \tag{4.37}$$

where $\mathbf{G} = \mathbf{C}^{-1}\mathbf{D}$.

Eq. (4.37) is the desired relation of location perturbation error $\delta\mathbf{p}$ with measurement noise and system parameters. The MSE of the estimator is

$$\bar{\epsilon}^2_{\text{WLS}} = \mathbb{E}\{|\delta\mathbf{p}|^2\} \approx tr\{\mathbf{G}\mathbf{\Phi}_v\mathbf{G}^T\}, \tag{4.38}$$

where $\mathbf{\Phi}_v$ is the correlation matrix of $\mathbf{v}$. Stacking the range bias from different sensor measurements into $\mathbf{b} = [b_1, \cdots, b_K]^T$, then $\mathbf{\Phi}_v$ is related to bias and noise variance by

$$\mathbf{\Phi}_v = \mathbb{E}\{\mathbf{v}\mathbf{v}^T\} = \mathbf{R}_b + \text{diag}\{\sigma^2_{n1}, \cdots, \sigma^2_{nK}\}, \tag{4.39}$$

in which $\mathbf{R}_b$ is the correlation matrix of $\mathbf{b}$, and $\mathbf{R}_b = \mathbf{b}\mathbf{b}^T$ for deterministic bias. The resulting bias in the location estimate is given by

$$\beta_{\text{WLS}} = \mathbb{E}\{\delta\mathbf{p}\} \approx \mathbf{G}\mathbf{b} = \mathbf{C}^{-1}\mathbf{D}\mathbf{b}. \tag{4.40}$$

Thus the WLS estimator will be biased in general if $\mathbf{b} \neq \mathbf{0}$. However, it is possible to make the estimation bias to be zero while $\mathbf{b} \neq \mathbf{0}$ for some special cases, for example, when $\mathbf{G}\mathbf{b} = \mathbf{0}$. Next, these expressions are applied for studying a localization example with a uniform circular sensor array.

4.5.3 An Example of Circularly Uniform Array

Consider an example where the sensors are uniformly and circularly placed around the source, so that $\theta_i = 2\pi(i-1)/K$. This includes special cases of linear, triangular and square sensor configurations, corresponding to $K = 2, 3, 4$, respectively. For simplicity, assume a common measurement bias so that all elements in $\mathbf{b}$ are equal, i.e., $\mathbf{b} = b\mathbf{1}$ for $b \neq 0$. Let $w_i = w = \sigma_n^{-2}$ for all sensors. Under these assumptions, $\theta_i = 2\pi(i-1)/K$ and the elements in $\mathbf{C}$ and the vector $\mathbf{D}\mathbf{b}$ in (4.40) can be rewritten as

$$c_{11} = w\sum_{i=1}^{K}\cos^2\frac{2\pi(i-1)}{K} = \frac{1}{2}w\left(K + \sum_{i=1}^{K}\cos\frac{4\pi(i-1)}{K}\right), \tag{4.41}$$

$$c_{22} = w\sum_{i=1}^{K}\sin^2\frac{2\pi(i-1)}{K} = \frac{1}{2}w\left(K - \sum_{i=1}^{K}\cos\frac{4\pi(i-1)}{K}\right), \tag{4.42}$$

$$c_{12} = c_{21} = w\sum_{i=1}^{K}\sin\frac{2\pi(i-1)}{K}\cos\frac{2\pi(i-1)}{K} = \frac{1}{2}w\sum_{i=1}^{K}\sin\frac{4\pi(i-1)}{K}, \tag{4.43}$$

$$\mathbf{D}\mathbf{b} = wb\left[\sum_{i=1}^{K}\cos\frac{2\pi(i-1)}{K},\ \sum_{i=1}^{K}\sin\frac{2\pi(i-1)}{K}\right]^T. \tag{4.44}$$

Based on the Euler's identities

$$\cos x = \frac{1}{2}(e^{jx} + e^{-jx}), \quad \sin x = \frac{1}{2j}(e^{jx} - e^{-jx}), \tag{4.45}$$

where $j = \sqrt{-1}$, and the following result for a geometric series

$$\begin{aligned}\sum_{k=1}^{K} e^{j(k-1)x} &= \frac{e^{jKx}-1}{e^{jx}-1} = \frac{e^{jKx/2}(e^{jKx/2}-e^{-jKx/2})}{e^{jx/2}(e^{jx/2}-e^{-jx/2})} \\ &= \frac{\sin\frac{Kx}{2}}{\sin\frac{x}{2}} e^{j\frac{K-1}{2}x}, \end{aligned} \tag{4.46}$$

the following equations are obtained

$$\sum_{k=1}^{K} \cos(k-1)x = \frac{\sin\frac{Kx}{2}\cos\frac{K-1}{2}x}{\sin\frac{x}{2}}, \tag{4.47}$$

$$\sum_{k=1}^{K} \sin(k-1)x = \frac{\sin\frac{Kx}{2}\sin\frac{K-1}{2}x}{\sin\frac{x}{2}}. \tag{4.48}$$

Substituting these results into (4.41), (4.42), (4.43) and (4.44) yields

$$c_{11} = c_{22} = \frac{1}{2}wK, \quad c_{12} = c_{21} = 0, \quad \mathbf{Db} = \mathbf{0}. \tag{4.49}$$

So $\mathbf{C} = \frac{wK}{2}\mathbf{I}$. Applying these results to (4.40) generates $\mathbb{E}\{\delta\mathbf{p}\} = \mathbf{0}$. Therefore, for this special geometry and with common measurement bias, the WLS estimation has no bias (up to the first order error). This is intuitively pleasing, and indicates that spatially diverse sensor placement can reduce estimation bias.

The MSE (4.38) can also be simplified for this special case. With $\mathbf{Db} = \mathbf{0}$ and $\text{diag}\{\sigma_1^2, \cdots, \sigma_K^2\} = \sigma^2\mathbf{I}$, it can be easily verified that $\mathbf{DD}^T = w\mathbf{C}$. Then (4.38) becomes

$$\bar{\epsilon}^2_{\text{WLS}} \approx \sigma_n^2 tr\{\mathbf{C}^{-1}\mathbf{DD}^T\mathbf{C}^{-1}\} = \frac{4\sigma_n^2}{K}. \tag{4.50}$$

The expression is consistent with the CRB of eq. (28) developed in [47] for the case of a common bias for all sensors. It is interesting that without any knowledge of the measurement bias, for this example, the WLS MSE approaches the CRB at high SNRs (i.e., under the small error assumption).

4.5.4 Geolocation Performance Optimization

The analytical results on the location estimation bias and MSE relate WLS performance to measurement bias, noise variance, sensor locations, and WLS weights. Here the optimization rely on analytical results to adjust the weights and sensor locations in order to minimize the localization error.

From (4.40), a general condition for WLS to produce an unbiased location estimates is $\mathbf{Gb} = \mathbf{0}$. It requires vector $\mathbf{b}$ to be in the null subspace of matrix $\mathbf{G}$. This can be achieved with $\mathbf{Db} = \mathbf{0}$, i.e., when

$$\sum_{i=1}^{K} w_i b_i \cos\theta_i = 0, \quad \sum_{i=1}^{K} w_i b_i \sin\theta_i = 0. \tag{4.51}$$

This sufficient condition suggests a possible method for sensor placement and weight selection that results in a small location estimation bias.

To gain some insight into bias reduction, let $b_i = b$ and $w_i = w$. The squared norm of $\mathbf{Db}$ can now be expressed as

$$\begin{aligned} |\mathbf{Db}|^2 &= b^2 w^2 \left[\left(\sum_{i=1}^{K} \cos\theta_i \right)^2 + \left(\sum_{i=1}^{K} \sin\theta_i \right)^2 \right] \\ &= b^2 w^2 \left[K + \sum_{i_1 \neq i_2 = 1}^{K} \cos(\theta_{i_1} - \theta_{i_2}) \right]. \end{aligned} \tag{4.52}$$

This quantity depends on the measurement bias b, and all possible sensor placement angle differences. Consider an extreme sensor configuration where all the sensors are located in a cluster at angle zero with respect to the source; then $|\mathbf{Db}|^2$ reaches its maximum value of $K^2 b^2 w^2$ since all θ_i are equal. This worst case leads to a large estimation bias and consequently an increased MSE. Now suppose half of the even number of sensors are located at angle zero, and the other half at angle 180 degrees. Then, $|\mathbf{Db}|^2$ reaches its minimum value of zero, and WLS is unbiased. This is also similar to the circular array case discussed in Section 4.5.3. For arbitrary sensor configurations,

$|\mathbf{Db}|^2$ takes a value between zero and its maximum. For example, if half the sensors are at angle zero and half at 90 degrees, then $|\mathbf{Db}|^2$ takes the medium value $K^2b^2w^2/2$. These examples indicate that sensor location angle diversity helps to reduce the impact of measurement bias.

The WLS weight can be employed to reduce the localization error. Intuitively, according to (4.51), the weight for a particular sensor should be chosen to be smaller when the measurement bias is larger, although tuning the weight in this way requires additional information about the bias. It is also of interest to consider the bias-variance tradeoff. The MSE, given by (4.38), can also be minimized with respect to sensor locations and weights. In Section 4.7 some numerical results will be presented on the impact of bias and sensor placement.

4.6 ML Estimation with Random Biased Range Measurement

In the case of range measurement with random bias, v_i in the measurement model (4.3) becomes a sum of two random variables: random bias b_i and Gaussian noise n_i. The optimum estimator for $\mathbf{p}_s$ based on the maximum-likelihood criterion depends on the distribution of v_i which is a convolution of the pdfs of the two random variables, developed in Section 4.3. In this section, the author first finds the generic equations for the optimal estimator to satisfy. Since these equations are non-linear, no closed-form solution exists. However, applying the perturbation technique can obtain location estimation errors from those equations. Afterward, with those general results, the following subsection focuses on the widely adopted exponential bias distribution model and obtain the estimation error results. An equivalence of this model is established with the

deterministic bias case under the limit of the bias standard deviation $\sigma_{b_i} \to 0$. The last subsection also shows the respective ML estimator for uniform distribution.

Since all b_i and n_i are independent, the joint pdf of all r_i is simply the product of individuals. The ML estimator can be formulated based on the log-likelihood function

$$\begin{aligned}\widehat{\mathbf{p}_s} &= \max_{(x_s,y_s)} \mathcal{L} = \max_{(x_s,y_s)} \ln f(\mathbf{r};\mathbf{p}_s) \\ &= \max_{(x_s,y_s)} \ln \prod_{i=1}^{K} f_i(r_i - d_i) = \max_{(x_s,y_s)} \sum_{i=1}^{K} \ln f_i(r_i - d_i). \end{aligned} \tag{4.53}$$

Setting the partial derivatives of $\mathcal{L}$ with respective to x_s and y_s equal to zero, two equations for optimal location estimates follow

$$\sum_{i=1}^{K} \frac{f_i'(r_i - d_i)}{f_i(r_i - d_i)} \cos\theta_i = 0, \tag{4.54}$$

$$\sum_{i=1}^{K} \frac{f_i'(r_i - d_i)}{f_i(r_i - d_i)} \sin\theta_i = 0, \tag{4.55}$$

where $f_i'(r_i - d_i)$ is the derivative with respect to d_i, which can be found from the derivative of $f_i(v_i)$ with respect to v_i since $f_i'(r_i - d_i) = -f_i'(v_i)$. Substituting $f_i'(v_i)$ or $f_i'(r_i - d_i)$ of a specific bias model into (4.54) and (4.55) can find the solutions to x_s and y_s.

Localization errors are analyzed for the ML estimator using the similar perturbation analysis procedure as in Section 4.5 for the WLS estimator. Expanding (4.54) and (4.55) around $r_i = d_i + b_i^0$ will yield two equations, which build the connection of δx_s and δy_s with the perturbation in the range measurement $\delta r_i = v_i - b_i^0 = b_i - b_i^0 + n_i$ in the first order. Writing those equations in a matrix form, the localization error vector $\delta\mathbf{p}$ can be solved. Then the bias and MSE are found easily.

4.6.1 Exponential Distribution Case

This subsection follows the general analysis procedure described above and focuses on the exponential bias distribution model. In addition, several limiting cases are analyzed based on the analytical results.

4.6.1.1 ML Estimator

Based on (4.54) and (4.55), to obtain the ML estimator the derivative of $f_i(v_i)$ in (4.11) with respect to v_i is needed. As is known, differentiation under the integral sign for function

$$F(x) = \int_{a(x)}^{b(x)} f(x,t)dt$$

follows a general formula

$$\frac{dF(x)}{dx} = f(x,b(x))\frac{db(x)}{dx} - f(x,a(x))\frac{da(x)}{dx} + \int_{a(x)}^{b(x)} \frac{\partial}{\partial x} f(x,t)dt. \tag{4.56}$$

Thus by the definition of Q-function [98] it shows that

$$\frac{d}{dv_i} Q\left(\frac{b_i^0 - v_i + \sigma_{n_i}^2/\sigma_{b_i}}{\sigma_{n_i}}\right) = \frac{1}{\sqrt{2\pi}\sigma_{n_i}} \exp\left[-\frac{(b_i^0 - v_i + \sigma_{n_i}^2/\sigma_{b_i})^2}{2\sigma_{n_i}^2}\right]. \tag{4.57}$$

Applying (4.57) to (4.11) produces

$$\begin{aligned} f_i'(v_i) &= -\frac{1}{\sigma_{b_i}} f_i(v_i) + \frac{1}{\sigma_{b_i}} \exp\left(\frac{b_i^0 - v_i}{\sigma_{b_i}} + \frac{\sigma_{n_i}^2}{2\sigma_{b_i}^2}\right) \frac{1}{\sqrt{2\pi}\sigma_{n_i}} \exp\left[-\frac{(b_i^0 - v_i + \sigma_{n_i}^2/\sigma_{b_i})^2}{2\sigma_{n_i}^2}\right] \\ &= -\frac{1}{\sigma_{b_i}} f_i(v_i) + \frac{1}{\sigma_{b_i}\sqrt{2\pi}\sigma_{n_i}} \exp\left[-\frac{(v_i - b_i^0)^2}{2\sigma_{n_i}^2}\right] \\ &= \frac{1}{\sigma_{b_i}}[g_i(v_i - b_i^0) - f_i(v_i)]. \end{aligned} \tag{4.58}$$

Using (4.58) in (4.54) and (4.55), the constraint equations of the ML estimator become

$$\sum_{i=1}^{K} \frac{1}{\sigma_{b_i}} \left[\frac{g_i(r_i - d_i - b_i^0)}{f_i(r_i - d_i)} - 1\right] \cos\theta_i = 0, \tag{4.59}$$

$$\sum_{i=1}^{K} \frac{1}{\sigma_{b_i}} \left[\frac{g_i(r_i - d_i - b_i^0)}{f_i(r_i - d_i)} - 1\right] \sin\theta_i = 0. \tag{4.60}$$

Substituting (4.9) and (4.11), and noticing (4.1) and (4.2), the above become nonlinear equations for x_s and y_s. They can be solved numerically as functions of measurements.

Instead of pursuing optimal solutions, the author investigates how estimation errors are affected by the measurement error in the neighborhood of optimal solutions, in particular by measurement bias. That is, the range measurement $r_i = d_i + b_i^0$ is perturbed with error $b_i - b_i^0 + n_i$. It causes a small estimation error in source location (at high SNR).

4.6.1.2 Error Analysis on Location Estimation

The perturbed estimates still satisfy (4.59) and (4.60), which are expanded around $r_i = d_i + b_i^0$ to obtain two equations for δx_s and δy_s with the perturbation in the range measurement $\delta r_i = v_i - b_i^0 = b_i - b_i^0 + n_i$ as input. For notational simplicity, the following development focuses on the i-th term in the summation and also temporarily suppress multiplicative constant $1/\sigma_{b_i}$. Later on both the summation and this constant will be put back. Applying differential theorem to the left hand side of (4.59) and (4.60) obtains

$$\delta\left[\frac{g_i(r_i - d_i - b_i^0)}{f_i(r_i - d_i)}\right]\cos\theta_i + \left[\frac{g_i(r_i - d_i - b_i^0)}{f_i(r_i - d_i)} - 1\right]\delta(\cos\theta_i), \tag{4.61}$$

$$\delta\left[\frac{g_i(r_i - d_i - b_i^0)}{f_i(r_i - d_i)}\right]\sin\theta_i + \left[\frac{g_i(r_i - d_i - b_i^0)}{f_i(r_i - d_i)} - 1\right]\delta(\sin\theta_i). \tag{4.62}$$

Since

$$\delta g_i(r_i - d_i - b_i^0) \approx g_i'(r_i - d_i - b_i^0)(\delta r_i - \delta d_i),$$

$$\delta f_i(r_i - d_i) \approx f_i'(r_i - d_i)(\delta r_i - \delta d_i),$$

and $r_i = d_i + b_i^0$, the first error term in (4.61) and (4.62) is

$$\delta\left[\frac{g_i(r_i - d_i - b_i^0)}{f_i(r_i - d_i)}\right] \approx \frac{g_i'(0)f_i(b_i^0) - g_i(0)f_i'(b_i^0)}{f_i^2(b_i^0)}(\delta r_i - \delta d_i). \tag{4.63}$$

According to (4.9), $g_i'(0) = 0$. Also together with (4.9) and (4.58), it follows that

$$f_i'(b_i^0) = \frac{1}{\sigma_{b_i}}[g_i(0) - f_i(b_i^0)], \quad g_i(0) = \frac{1}{\sqrt{2\pi}\sigma_{n_i}}, \tag{4.64}$$

where $f_i(b_i^0)$ is given by (4.12). Substituting (4.64) and (4.29) into (4.63) yields

$$\delta\left[\frac{g_i(r_i - d_i - b_i^0)}{f_i(r_i - d_i)}\right] \approx \frac{g_i(0)f_i'(b_i^0)}{f_i^2(b_i^0)}(\cos\theta_i\delta x_s + \sin\theta_i\delta y_s - \delta r_i). \tag{4.65}$$

The second error terms in (4.61) and (4.62) are

$$\delta(\cos\theta_i) \approx \frac{\sin\theta_i}{d_i}(\sin\theta_i\delta x_s - \cos\theta_i\delta y_s), \tag{4.66}$$

$$\delta(\sin\theta_i) \approx -\frac{\cos\theta_i}{d_i}(\sin\theta_i\delta x_s - \cos\theta_i\delta y_s). \tag{4.67}$$

Substituting (4.64), (4.65), (4.66) and (4.67) into (4.61) and (4.62), and adding back summation and the multiplicative constant $1/\sigma_{b_i}$, the constraint equations are found as

$$u_{11}\delta x_s + u_{12}\delta y_s \approx \mathbf{t}_1^T\delta\mathbf{r}, \tag{4.68}$$

$$u_{21}\delta x_s + u_{22}\delta y_s \approx \mathbf{t}_2^T\delta\mathbf{r}, \tag{4.69}$$

with

$$u_{11} = \sum_{i=1}^{K}\frac{[g_i(0) - f_i(b_i^0)]}{\sigma_{b_i}d_i f_i^2(b_i^0)}[d_i g_i(0)\cos^2\theta_i/\sigma_{b_i} + f_i(b_i^0)\sin^2\theta_i], \tag{4.70}$$

$$u_{12} = u_{21} = \sum_{i=1}^{K}\frac{[g_i(0) - f_i(b_i^0)]\cos\theta_i\sin\theta_i}{\sigma_{b_i}d_i f_i^2(b_i^0)}[d_i g_i(0)/\sigma_{b_i} - f_i(b_i^0)], \tag{4.71}$$

$$u_{22} = \sum_{i=1}^{K}\frac{[g_i(0) - f_i(b_i^0)]}{\sigma_{b_i}d_i f_i^2(b_i^0)}[d_i g_i(0)\sin^2\theta_i/\sigma_{b_i} + f_i(b_i^0)\cos^2\theta_i], \tag{4.72}$$

$$\mathbf{t}_1 = [t_{1,1}, \cdots, t_{1,K}]^T, \quad \mathbf{t}_2 = [t_{2,1}, \cdots, t_{2,K}]^T, \tag{4.73}$$

$$t_{1,i} = \frac{g_i(0)[g_i(0) - f_i(b_i^0)]\cos\theta_i}{\sigma_{b_i}^2 f_i^2(b_i^0)}, \quad t_{2,i} = \frac{g_i(0)[g_i(0) - f_i(b_i^0)]\sin\theta_i}{\sigma_{b_i}^2 f_i^2(b_i^0)}. \tag{4.74}$$

These two equations can be compactly written in a matrix form

$$\mathbf{U}\delta\mathbf{p} \approx \mathbf{T}\delta\mathbf{r}. \tag{4.75}$$

So, by (4.75), the first order estimation error vector for source location in this case is

$$\delta\mathbf{p} \approx \mathbf{U}^{-1}\mathbf{T}\delta\mathbf{r}. \tag{4.76}$$

The bias and MSE of this estimator can be studied. Since

$$\mathbb{E}\{\delta r_i\} = \sigma_{b_i}, \quad \mathbb{E}\{(\delta r_i)^2\} = 2\sigma_{b_i}^2 + \sigma_{n_i}^2$$

and the mean and correlation of the vector $\delta\mathbf{r}$ is

$$\boldsymbol{\mu}_b = \mathbb{E}\{\delta\mathbf{r}\} = [\sigma_{b_1}, \cdots, \sigma_{b_K}]^T, \tag{4.77}$$

$$\boldsymbol{\Psi} = \mathbb{E}\{\delta\mathbf{r}\delta\mathbf{r}^T\} = \boldsymbol{\mu}_b\boldsymbol{\mu}_b^T + \mathrm{diag}\{(\sigma_{b_1}^2 + \sigma_{n_1}^2), \cdots, (\sigma_{b_K}^2 + \sigma_{n_K}^2)\}, \tag{4.78}$$

then the bias and MSE of the location estimate are

$$\beta_{\mathrm{ML}} = \mathbb{E}\{\delta\mathbf{p}\} \approx \mathbf{U}^{-1}\mathbf{T}\boldsymbol{\mu}_b, \tag{4.79}$$

$$\epsilon_{\mathrm{ML}}^2 = \mathbb{E}\{\delta\mathbf{p}^T\delta\mathbf{p}\} \approx tr\{\mathbf{U}^{-1}\mathbf{T}\boldsymbol{\Psi}\mathbf{T}^T\mathbf{U}^{-1}\}. \tag{4.80}$$

These statistics are functions of sensor locations, bias distribution parameters, noise variance, and number of sensors.

4.6.1.3 Discussion on a limiting case $\forall\sigma_{b_i} \to 0$

The assumption of $\forall\sigma_{b_i} \to 0$ means both the mean and the standard deviation of the exponentially distributed bias diminish. So the randomness of the bias tends to fade out and the bias b_i reverts back to the deterministic known value b_i^0. In this case, the exponential distribution function reduces to a delta function and $f_i(v_i)$ takes a form as a Gaussian distribution. In fact, the pdf expression of v_i can also be obtained from (4.11) by taking the limit as

$$\lim_{\sigma_{b_i}\to 0} f_i(v_i) = \lim_{\sigma_{b_i}\to 0} \frac{Q\left(\frac{b_i^0 - v_i + \sigma_{n_i}^2/\sigma_{b_i}}{\sigma_{n_i}}\right)}{\sigma_{b_i}\exp\left(\frac{v_i - b_i^0}{\sigma_{b_i}} - \frac{\sigma_{n_i}^2}{2\sigma_{b_i}^2}\right)}. \tag{4.81}$$

Considering $Q(\infty) = 0$, the L'Hopital's rule can be applied to simplify. By the definition of Q-function

$$\frac{d}{d\sigma_{b_i}} Q\left(\frac{b_i^0 - v_i + \sigma_{n_i}^2/\sigma_{b_i}}{\sigma_{n_i}}\right) = \frac{\sigma_{n_i}}{\sqrt{2\pi}\sigma_{b_i}^2} \exp\left[-\frac{(b_i^0 - v_i + \sigma_{n_i}^2/\sigma_{b_i})^2}{2\sigma_{n_i}^2}\right]. \tag{4.82}$$

Applying L'Hopital's rule and (4.82), (4.81) becomes

$$\begin{aligned}
\lim_{\sigma_{b_i}\to 0} f_i(v_i) &= \lim_{\sigma_{b_i}\to 0} \frac{\frac{\sigma_{n_i}}{\sqrt{2\pi}\sigma_{b_i}^2} \exp\left[-\frac{(b_i^0 - v_i + \sigma_{n_i}^2/\sigma_{b_i})^2}{2\sigma_{n_i}^2}\right]}{\left(\sigma_{b_i} - \frac{v_i - b_i^0}{\sigma_{b_i}} + \frac{\sigma_{n_i}^2}{\sigma_{b_i}^2}\right) \exp\left(\frac{v_i - b_i^0}{\sigma_{b_i}} - \frac{\sigma_{n_i}^2}{2\sigma_{b_i}^2}\right)} \\
&= \frac{1}{\sqrt{2\pi}\sigma_{n_i}} \exp\left[-\frac{(v_i - b_i^0)^2}{2\sigma_{n_i}^2}\right] \\
&= g_i(v_i - b_i^0).
\end{aligned} \tag{4.83}$$

This means that in the limiting case, $f_i(v_i)$ is a Gaussian variable with mean b_i^0 and variance $\sigma_{n_i}^2$.

Additionally one should expect the error analysis result for the ML estimation in this limiting case to be the same as the WLS result (4.37) with $w_i = \frac{1}{\sigma_i^2}$. Taking derivative on (4.83) generates

$$\lim_{\sigma_{b_i}\to 0} f_i'(v_i) = -\frac{v - b_i^0}{\sigma_{n_i}^2} g_i(v - b_i^0) = -\frac{v - b_i^0}{\sigma_{n_i}^2} \lim_{\sigma_{b_i}\to 0} f_i(v_i). \tag{4.84}$$

Substituting (4.84) into (4.54) and (4.55), the ML estimates satisfy

$$\sum_{i=1}^{K} \frac{1}{\sigma_{n_i}^2}[(r_i - b_i^0) - d_i]\cos\theta_i = 0, \tag{4.85}$$

$$\sum_{i=1}^{K} \frac{1}{\sigma_{n_i}^2}[(r_i - b_i^0) - d_i]\sin\theta_i = 0, \tag{4.86}$$

which have the same form as the WLS equations (4.27) and (4.28) with $w_i = \frac{1}{\sigma_i^2}$ except that the deterministic known bias b_i^0 is deducted from the measurement r_i. In error analysis, since $\delta(r_i - b_i^0) = \delta(r_i)$ and replacing $r_i - b_i^0$ with d_i, the same expression as (4.37) will be obtained. Therefore, the performance of the ML estimation for this limiting case and the WLS estimation for the deterministic bias case are equivalent.

In fact, it is straightforward to directly prove that the error analysis results for the two cases are equivalent. It suffices to show

$$\lim_{\forall\sigma_{b_i}\to 0}\mathbf{U}=\mathbf{C},\quad \lim_{\forall\sigma_{b_i}\to 0}\mathbf{T}=\mathbf{D}. \tag{4.87}$$

Notice that elements of matrices $\mathbf{U}$ and $\mathbf{T}$ depend on $f_i(b_i^0)$ given by (4.12). So expansion of Q-function for large x is necessary, which is given by [46]

$$Q(x)=\frac{e^{-\frac{x^2}{2}}}{x\sqrt{2\pi}}\sum_{k=0}^{\infty}\frac{(-1)^k(2k)!}{k!(\sqrt{2}x)^{2k}}\qquad \text{for large } x. \tag{4.88}$$

So (4.12) becomes

$$f_i(b_i^0)=\frac{1}{\sqrt{2\pi}\sigma_{n_i}}\sum_{k=0}^{\infty}\frac{(-1)^k(2k)!\sigma_{b_i}^{2k}}{k!(\sqrt{2}\sigma_{n_i})^{2k}}, \tag{4.89}$$

from which

$$\lim_{\sigma_{b_i}\to 0}f_i(b_i^0)=\frac{1}{\sqrt{2\pi}\sigma_{n_i}}=g_i(0), \tag{4.90}$$

which matches the result in (4.83). Continuing leads to

$$\lim_{\sigma_{b_i}\to 0}\frac{g_i(0)-f_i(b_i^0)}{\sigma_{b_i}^2}=\frac{1}{\sqrt{2\pi}\sigma_{n_i}^3}=\frac{g_i(0)}{\sigma_{n_i}^2}. \tag{4.91}$$

With these results, the limiting results for elements of $\mathbf{U}$ will be obtained. Discard the second term in (4.70) since it is negligible as compared to the first term with a factor $1/\sigma_{b_i}$. Applying (4.91) and (4.90) successively to that equation yields

$$\lim_{\sigma_{b_i}\to 0}u_{11}=\lim_{\sigma_{b_i}\to 0}\sum_{i=1}^{K}\frac{\cos^2\theta_i g_i(0)[g_i(0)-f_i(b_i^0)]}{\sigma_{b_i}^2 f_i^2(b_i^0)}=\lim_{\sigma_{b_i}\to 0}\sum_{i=1}^{K}\frac{\cos^2\theta_i g_i^2(0)}{\sigma_{n_i}^2 f_i^2(b_i^0)}=\sum_{i=1}^{K}\frac{\cos^2\theta_i}{\sigma_{n_i}^2}, \tag{4.92}$$

which is the same as c_{11} in (4.36) if $w_i=1/\sigma_{n_i}^2$. Similarly one can establish convergence of the other elements of $\mathbf{U}$ to those of $\mathbf{C}$, and $\mathbf{T}$ to $\mathbf{D}$. Therefore, (4.87) follows, and the two cases are equivalent. In fact, the above equivalence proof partially validates the derivations in Section 4.6.1.2.

4.6.1.4 Other limiting cases

A few other limiting cases are also interesting:

1. $\forall \sigma_{b_i} \to \infty$

   As $\forall \sigma_{b_i} \to \infty$, the mean of measurement bias goes to infinity. Therefore bias has a very long tail. Those quantities in matrices $\mathbf{U}$ and $\mathbf{T}$ can be simplified. First,

$$\lim_{\sigma_{b_i} \to \infty} f_i(b_i^0) = \frac{1}{2\sigma_{b_i}}, \tag{4.93}$$

   according to (4.12) since $Q(0) = 1/2$. Then

$$\begin{aligned}
\lim_{\forall \sigma_{b_i} \to \infty} u_{11} &= \sum_{i=1}^{K} \frac{2g_i(0)}{d_i}[2\cos\theta_i^2 d_i g_i(0) + \sin\theta_i^2], \\
\lim_{\forall \sigma_{b_i} \to \infty} u_{12} &= \lim_{\forall \sigma_{b_i} \to \infty} u_{21} = \sum_{i=1}^{K} \frac{2\cos\theta_i \sin\theta_i g_i(0)}{d_i}[2d_i g_i(0) - 1], \\
\lim_{\forall \sigma_{b_i} \to \infty} u_{22} &= \sum_{i=1}^{K} \frac{2g_i(0)}{d_i}[2\sin\theta_i^2 d_i g_i(0) + \cos\theta_i^2], \\
\lim_{\forall \sigma_{b_i} \to \infty} t_{1,i} &= 4\cos\theta_i g_i^2(0), \\
\lim_{\forall \sigma_{b_i} \to \infty} t_{2,i} &= 4\sin\theta_i g_i^2(0).
\end{aligned} \tag{4.94}$$

   Once elements of matrices are obtained, limiting matrices $\mathbf{U}_\infty = \lim_{\forall \sigma_{b_i} \to \infty} \mathbf{U}$ and $\mathbf{T}_\infty = \lim_{\forall \sigma_{b_i} \to \infty} \mathbf{T}$ follow. Then the MSE (4.80) has a limiting result

$$\lim_{\forall \sigma_{b_i} \to \infty} \mathrm{MSE}_{\mathrm{ML}} \approx tr\{\mathbf{U}_\infty^{-1} \mathbf{T}_\infty \mathbf{\Psi}_\infty \mathbf{T}_\infty^T \mathbf{U}_\infty^{-1}\}, \tag{4.95}$$

   where

$$\mathbf{\Psi}_\infty = \boldsymbol{\mu}_b \boldsymbol{\mu}_b^T + \mathrm{diag}\{\sigma_{b_1}^2, \cdots, \sigma_{b_K}^2\}. \tag{4.96}$$

   The MSE increases with increased σ_{b_i}, which is the mean and standard deviation of the measurement bias. Thus the effect of measurement bias is pronounced for large σ_{b_i}.

2. $\forall \sigma_{n_i} \to \infty$ No particular insight can be made except that the noise is a dominant error factor. It is similar to a typical noise-corrupted measurement case.

3. $\forall \sigma_{n_i} \to 0$ This limiting case corresponds to diminishing Gaussian noise while only random bias is dominant in the measurement error. According to (4.11), and due to $v_i \geq b_i^0$ and $Q(-\infty) = 1$, v_i has an exponential distribution $\mathcal{E}(1/\sigma_{b_i}, b_i^0)$

$$f_i(v_i) = \frac{1}{\sigma_{b_i}} \exp\left[-\frac{1}{\sigma_{b_i}}(v_i - b_i^0)\right], \quad v_i \geq b_i^0, \tag{4.97}$$

the same as the distribution of b_i. It is not surprising since the noise effect diminishes and $v_i = b_i$. Then the ML estimator needs to satisfy (4.53), reduced to

$$\max_{(x_s, y_s)} \mathcal{L} = \sum_{i=1}^{K} \left[-\ln \sigma_{b_i} - \frac{1}{\sigma_{b_i}}(r_i - d_i - b_i^0)\right]. \tag{4.98}$$

Its partial derivatives with respective to x_s and y_s become

$$\frac{\partial \mathcal{L}}{\partial x_s} = \sum_{i=1}^{K} \frac{\cos\theta_i}{\sigma_{b_i}}, \quad \frac{\partial \mathcal{L}}{\partial y_s} = \sum_{i=1}^{K} \frac{\sin\theta_i}{\sigma_{b_i}}.$$

The derivatives are independent of d_i and (x_s, y_s), and thus there is no solution for arbitrary (x_s, y_s) by setting them to zeros. In fact, the objective function $\mathcal{L}$ does not have a maximum. It increases unbounded with increasing magnitudes of unknown variables x_s and y_s that can be observed in eq.(4.98).

4.6.2 Uniform Distribution Case

The bias model assuming uniform distribution has also been measured in experiment and of research interest in the literature [48]. To obtain the ML estimator for this model, the derivative of $f_{v_i}(v_i)$ is found as

$$f'_{v_i}(v_i) = -\frac{1}{\beta_m - \beta_s}\left[e^{-\frac{(v_i-\beta_m)^2}{2\sigma_n^2}} - e^{-\frac{(v_i-\beta_s)^2}{2\sigma_n^2}}\right].$$

Substituting $f_{v_i}(v_i)$ and $f'_{v_i}(v_i)$ into (4.54) and (4.55), the ML estimation constraint equations are found as

$$\frac{1}{\sqrt{2\pi}\sigma_n}\sum_{i=1}^{K}\frac{e^{-\frac{(r_i-d_i-\beta_m)^2}{2\sigma_n^2}}-e^{-\frac{(r_i-d_i-\beta_s)^2}{2\sigma_n^2}}}{Q\left(\frac{r_i-d_i-\beta_m}{\sigma_n}\right)-Q\left(\frac{r_i-d_i-\beta_s}{\sigma_n}\right)}\cos\theta_i=0, \tag{4.99}$$

$$\frac{1}{\sqrt{2\pi}\sigma_n}\sum_{i=1}^{K}\frac{e^{-\frac{(r_i-d_i-\beta_m)^2}{2\sigma_n^2}}-e^{-\frac{(r_i-d_i-\beta_s)^2}{2\sigma_n^2}}}{Q\left(\frac{r_i-d_i-\beta_m}{\sigma_n}\right)-Q\left(\frac{r_i-d_i-\beta_s}{\sigma_n}\right)}\sin\theta_i=0. \tag{4.100}$$

The error analysis can follow the same procedure as in Subsection eq.(4.6.1.2), while the analytical results would not provide more insight than the exponential case. So in the following section the numerical study on the estimation error will still focus on the exponential distribution model.

4.7 Numerical Examples

This section presents numerical results of the error analysis for both WLS and ML location estimation, and compare them with simulation performance as well as CRB. The random bias with exponential distribution is assumed for all the testing cases. The RMSE and estimation bias are adopted as localization performance metrics as [66]

$$\text{RMSE}=\sqrt{\mathbb{E}\{(\delta x_s)^2\}+\mathbb{E}\{(\delta y_s)^2\}},$$

$$\text{Bias}=\sqrt{(\mathbb{E}\{\delta x_s\})^2+(\mathbb{E}\{\delta y_s\})^2}.$$

As the estimation RMSE and bias are affected by the statistics of measurement bias $\boldsymbol{\mu}_b$ and $\boldsymbol{\sigma}_b$ and Gaussian noise $\boldsymbol{\sigma}_n$, the reference array geometry and estimation methods together, the effects of all these parameters are examined on estimator performance in the following. All simulation results are based on 50000 independent realizations, and the expectations in RMSE and bias are replaced with sample averages.

Consider a fixed reference array with $K=10$ reference transceivers either uniformly or non-uniformly placed on a circle with normalized radius of one distance unit (DU),

centered at the unknown source location. The exponential distributed bias and Gaussian noise at each sensor are assumed i.i.d. with $\sigma_{b_i} = \sigma_b$ and $\sigma_{n_i} = \sigma_n$ unless explicitly stated. Note that the errors are expressed relative to the source range of 1 DU. Thus, for example, $\sigma_n = 0.1$ corresponds to Gaussian noise with a standard deviation of 10% of the true range (a large range error). For the simulations, the expectations in the RMSE and bias are replaced with sample averages. The WLS weights are set to $w_i = w = 1/\sigma^2$ in all experiments.

Figure 4.1 depicts the impact of deterministic bias in range measurements on the RMSE and bias of WLS estimator, with both uniform and non-uniform beacon array. For the non-uniform configurations, the beacon location angles are randomly generated once in $[0, 2\pi)$ and fixed for the duration of the experiment. Here Gaussian noise level is fixed to $\sigma = 0.1$. The RMSE error floor is due to the fixed non-zero value of σ_{n_i}. It can be observed that the RMSE with a uniform array is almost insensitive to the measurement bias and the corresponding estimation bias is zero. However, the RMSE for the non-uniform array increases linearly with, and is at a similar level to, the measurement bias. Similarly, estimation bias increases quickly with the measurement bias.

Figure 4.2 plots the RMSE of both WLS and ML estimation in 3D with contours, which provide intuitive view on how the RMSE varies with the increasing exponential bias and Gaussian noise standard deviations. The circular array has 10 uniformly placed beacons. The analytical results are compared with the simulated RMSE for both WLS and ML location estimation.

Figure 4.3 and Figure 4.4 are the corresponding 2D plots of Fig. 4.2. Figure 4.3 shows the impact of increasing bias on location estimate RMSE and bias, with a fixed Gaussian noise level of $\sigma_n = 0.05$. It can be observed that the RMSEs of both WLS and MLE with a uniform array are insensitive to the measurement bias and the corresponding

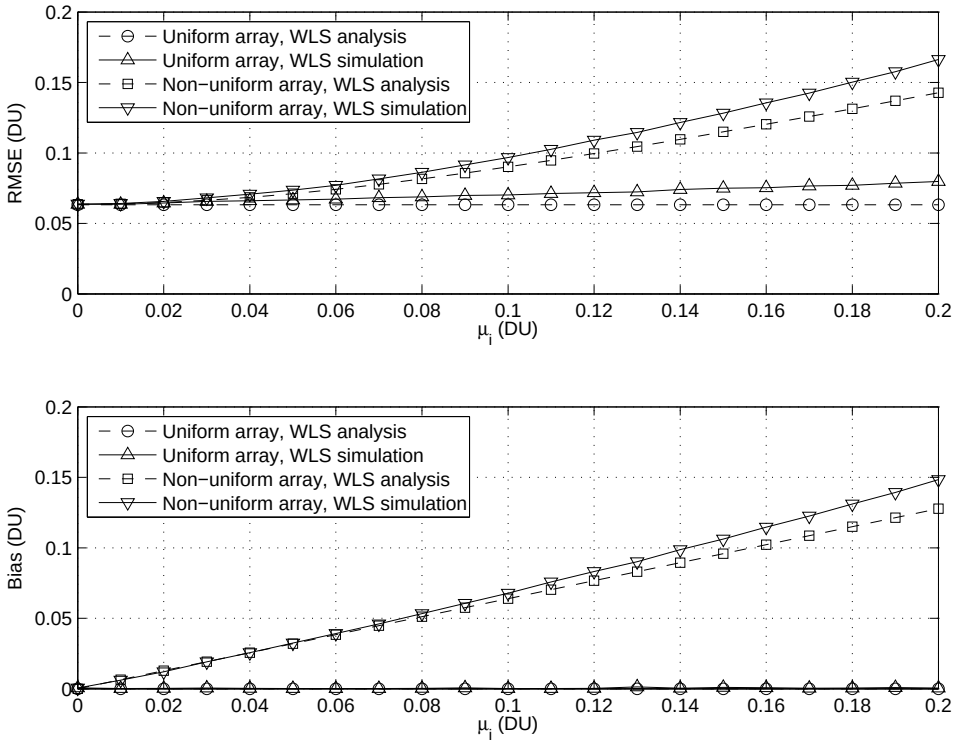

Figure 4.1: Localization performance of WLS estimation based on range measurement of deterministic bias with uniform circular array of 10 sensors. RMSE and bias of WLS estimation vary with the deterministic bias μ_i. The standard deviation of additive noise $\sigma_{n_i} = 0.1$.

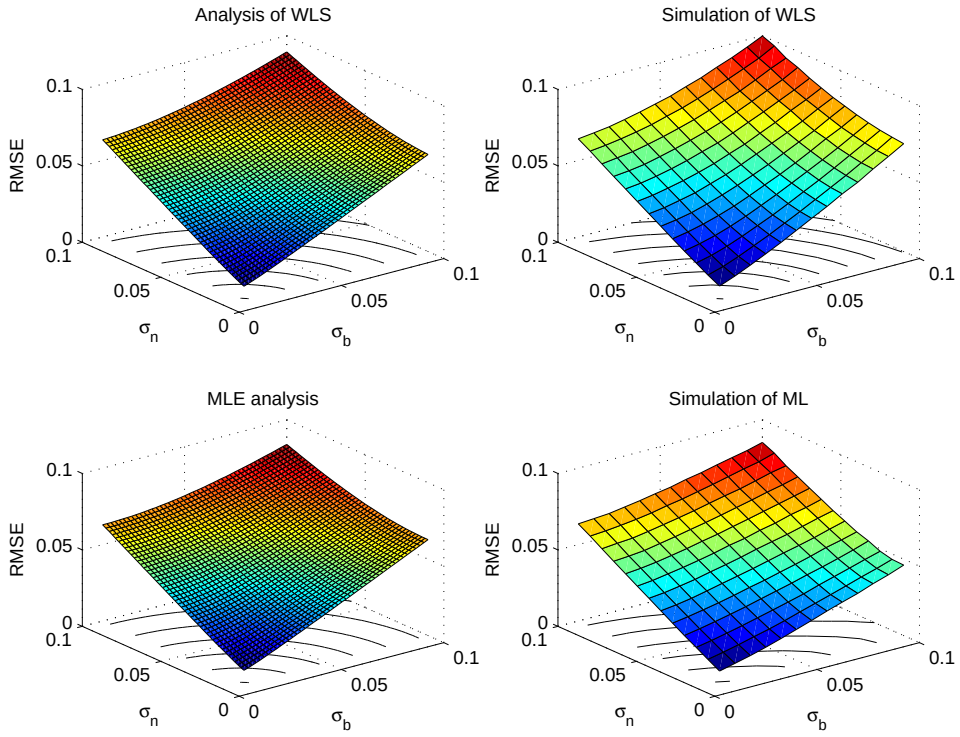

Figure 4.2: Localization by biased range measurement with uniform circular array of 10 sensors. 3D and contour plots of WLS and ML location estimation RMSE. Bias follows exponential distribution.

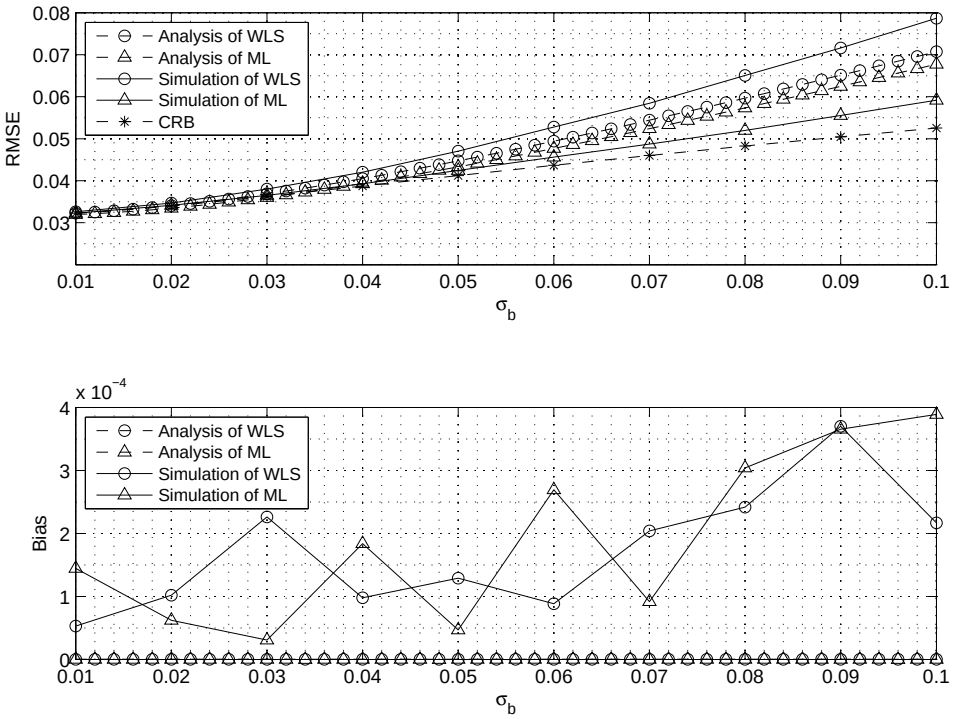

Figure 4.3: Localization by biased range measurement with uniform circular array of 10 sensors. RMSE and bias of WLS and ML estimation vary with the exponential bias standard deviation σ_b. The analysis and simulation results are plotted in comparison with CRB.

estimation bias is almost zero. The analytical results overlap with the simulation when σ_b is close to zero, showing the first-order error analysis provides good prediction over small-error region. As expected, the theory-simulation gap increases when the fixed σ_b increases from $\sigma_b = 0.01$ to $\sigma_b = 0.1$. The simulated ML estimation has a lower RMSE than WLS. Moreover, the RMSE results asymptotically converge to the CRB.

Figure 4.4 depicts the estimation RMSE and bias against Gaussian noise standard deviation σ_n for uniform circular reference placement. For all the reference points, the unknown bias is fixed at $\sigma_b = 0.05$. As σ_n increases over 0.05 (lower SNR), Gaussian noise has a larger effect on the location estimation when σ_b is relatively smaller, and the bias effect tends to be overridden by the noise effect. In that region both the WLS and ML estimation bias are averaged to a negligible level by the additive noise. The RMSE

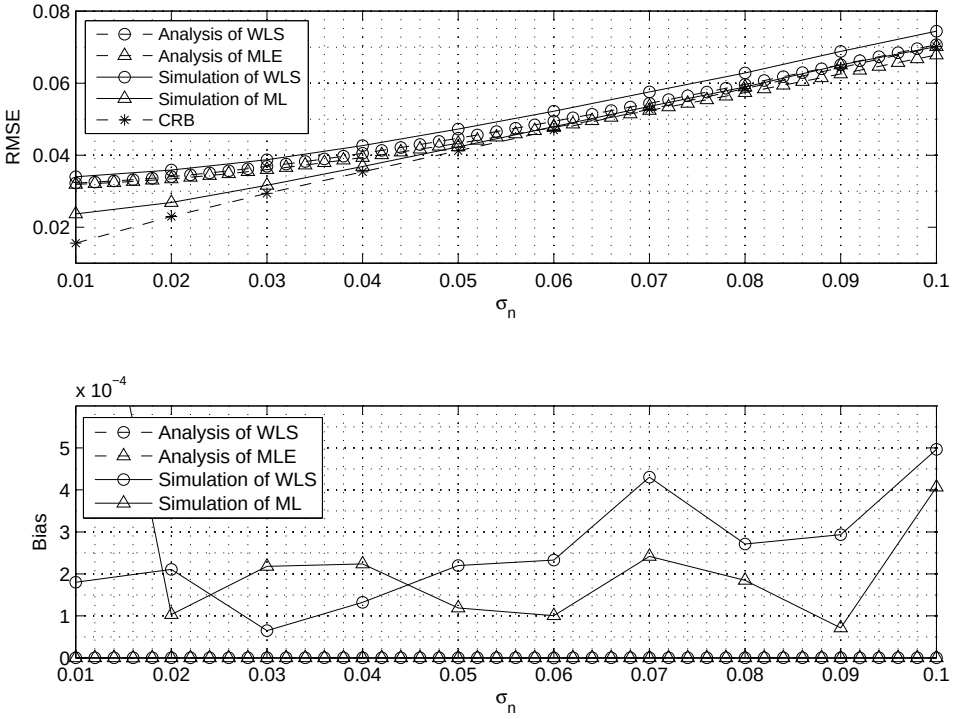

Figure 4.4: Localization by biased range measurement with uniform circular array of 10 sensors. RMSE and bias of WLS and ML estimation vary with the Gaussian noise standard deviation σ_n. The anlysis and simulation results are plotted in comparison with CRB.

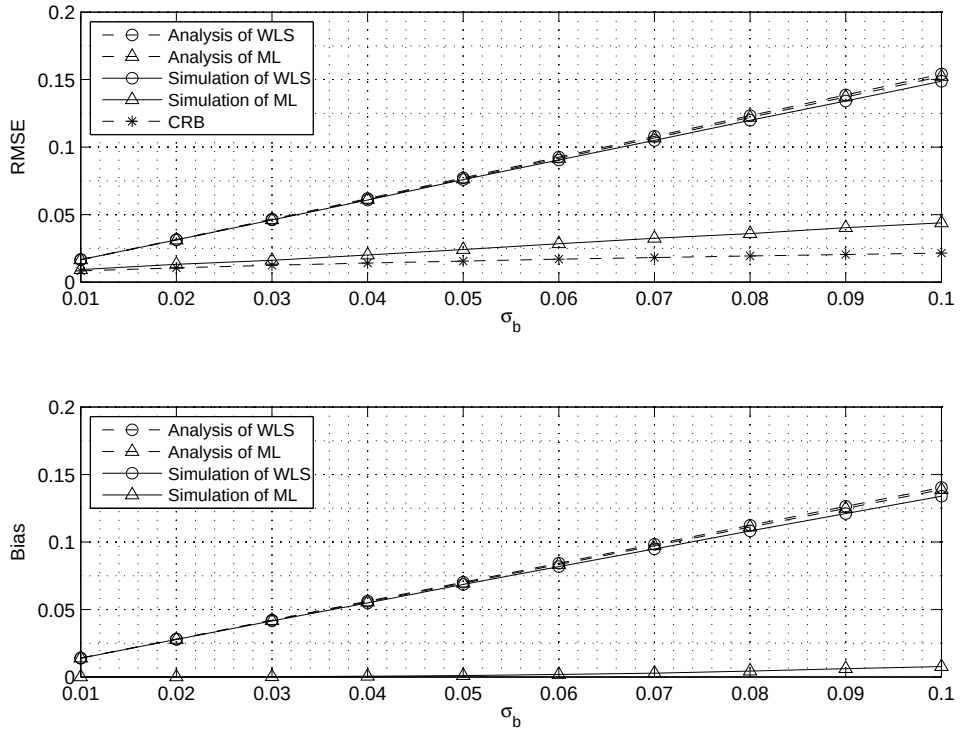

Figure 4.5: A case of non-uniform circular array with two groups of 5 sensors placed at 0 and 90 degrees, respectively. RMSE and bias of WLS and ML estimations are plotted versus the exponential bias standard deviation σ_b in comparison with CRB.

increases slowly for small σ_n and then linearly after σ_n exceeds 0.05. However, when σ_n is small, the measurement bias $\sigma_b = 0.05$ causes a floor for each of the estimators, and the RMSE curve of MLE deviate from the CRB.

Figure 4.5 tests a case of fixed non-uniform reference placement. The $K = 10$ beacon sensors of a circular array are split into two groups. The first group of 5 sensors is placed around 0 degree as $(0, \pm 5, \pm 10)$ degrees, and the second group of 5 sensors is around 90 degree as $(80, 85, 90, 95, 100)$ degrees. It can be observed that the RMSE of WLS estimation for this non-uniform array increases linearly with, and is at a similar level to, the measurement bias. Similarly, estimation bias of WLS increases quickly with the measurement bias and contributes the most part of RMSE. In comparison, the RMSE and bias of ML estimation have much smaller increasing rates with σ_b than

WLS, and the RMSE is close to CRB. The ML estimation has an obvious suppression effect on the estimation bias for this non-uniform array configuration.

Figure 4.6 studies the effect of non-i.i.d. random measurement bias at different reference beacons. Here, $K = 10$ beacons are uniformly circularly spaced in order to avoid the geometry introduced estimation bias. The beacons are divided into five groups with 2 beacons in each. Each group has a common measurement bias standard deviation, with groups from 1 to 5 keeping a constant ratio of $1 : 2 : 4 : 2 : 0.5$ between each other, starting from the beacon at 0 degree and proceeding counter-clockwise. All range measurements have the same noise standard deviation $\sigma_n = 0.01$. Then in Fig. 4.6a, the estimation RMSE and bias are plotted versus the measurement bias standard deviation σ_b of the first group. It can be seen that the bias and RMSE of WLS increase at an approximate rate of twice the measurement bias σ_b. The ML estimation exploits the distribution information of the random measurement bias and greatly mitigates the estimation bias and RMSE. The increasing rates of ML RMSE and bias are only $1/2$ and $1/8$ of σ_b, and the RMSE has a very small gap with CRB. The scatter plots in Fig. 4.6b and Fig. 4.6c show that the resulting WLS location estimates cluster in the fourth quadrant, which is predominantly opposite to beacon group 3 whose measurements bias have the largest standard deviation. On the other hand, the ML estimates cluster in the second quadrant as the ML compensates the measurement bias by exploiting the known error distributions.

To gain more intuitive insight into the beacon geometry effect on the estimation bias, Figure 4.7 illustrates scatter plots of WLS and ML estimation from 300 random realizations on measurement bias and noise, respectively. The uniform circular array is compared with three configurations of non-uniform circular array, with $K = 10$ beacons again confined to the circle with unity radius. In the three non-uniform cases, the bea-

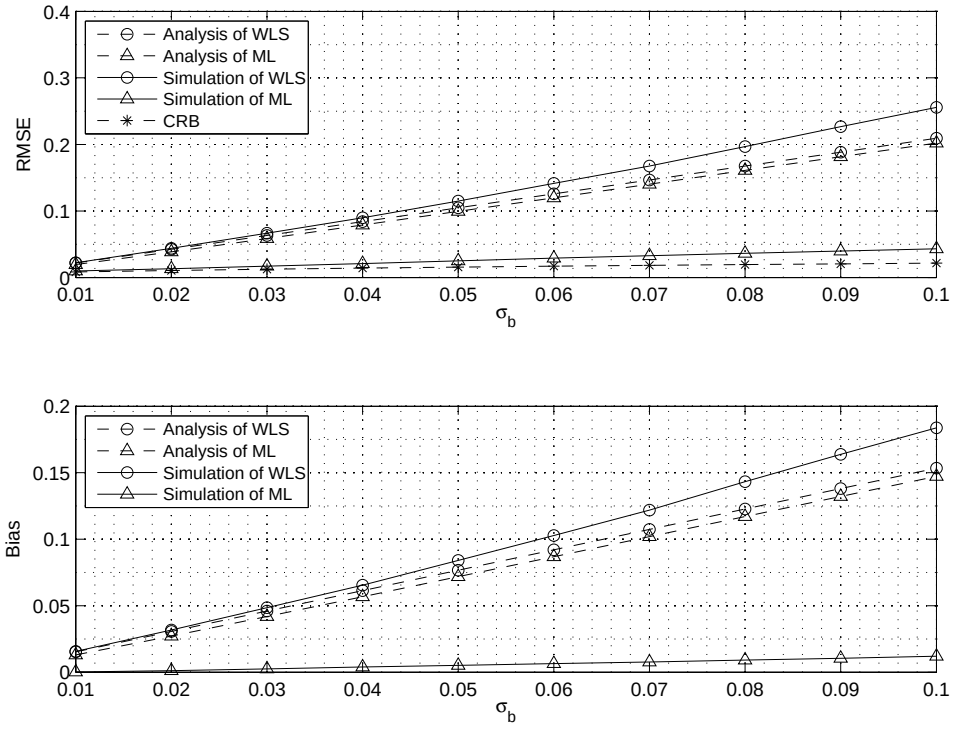

(a) RMSE and bias plots.

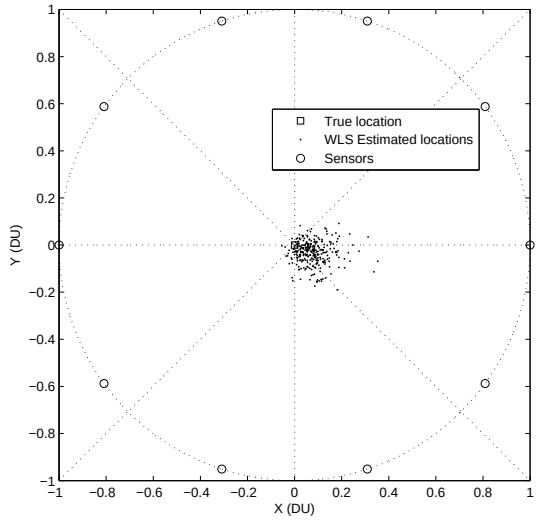

(b) Scatter plot with WLS estimation.

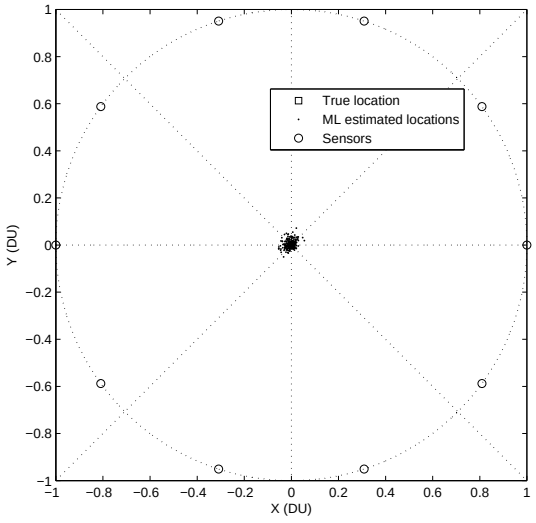

(c) Scatter plot with ML estimation.

Figure 4.6: The case of non-identically distributed measurement bias. The standard deviation σ_b of the exponential bias at five sensor groups (2 beacons per group) keep the constant ratio of 1:2:4:2:0.5, starting from the sensor at 0 degree. Estimation RMSE and bias are plotted versus σ_b of the first group of beacons.

cons are split into two groups of five beacons per group. In configuration 1, both groups are placed around 0 degrees as $(\pm 1, \pm 5, \pm 10, \pm 15, \pm 20)$ degrees. Configuration 2 centers groups around 0 and 90 degrees, given by $(-10, -5, 0, 5, 10, 80, 85, 90, 95, 100)$ degrees. Configuration 3 centers around 0 and 180 degrees, at $(-10, -5, 0, 5, 10, 170, 175, 180, 185, 190)$ degrees. The measurement error distribution is identical at all beacons and the standard deviations are set to $\sigma_b = 0.2$ and $\sigma_n = 0.05$.

The scatter figures clearly show that the estimated locations are significantly affected by the geometry of beacon groups. The uniform array suppresses estimation bias and both WLS and ML estimation are unbiased. The ML estimation has smaller variance. With non-uniform configuration 1 and 2, the WLS estimated locations depart from the true source location along the direction from beacon groups to the true source location (pushed by beacons), and the ML estimated locations approach the true location along the same direction. For example, with configuration 2, WLS estimated points are located in the third quadrant while the center of the ML estimated points are in the first quadrant. The extent of departure depends on measurement bias. Configuration 3 is different as its horizontal symmetric placement helps to mitigate the estimation bias along x-axis, and the ML estimation bias along y-axis is spread.

The corresponding RMSE and bias plots to the scatter figures are shown in Figure 4.8. As expected, the uniform array shows better performance than non-uniform configurations, and configuration 3 has the best estimation among three non-uniform cases due to its special x-axis symmetric geometry. For small measurement bias, the array geometry does not create much difference on RMSE, but that difference increases with increased measurement bias.

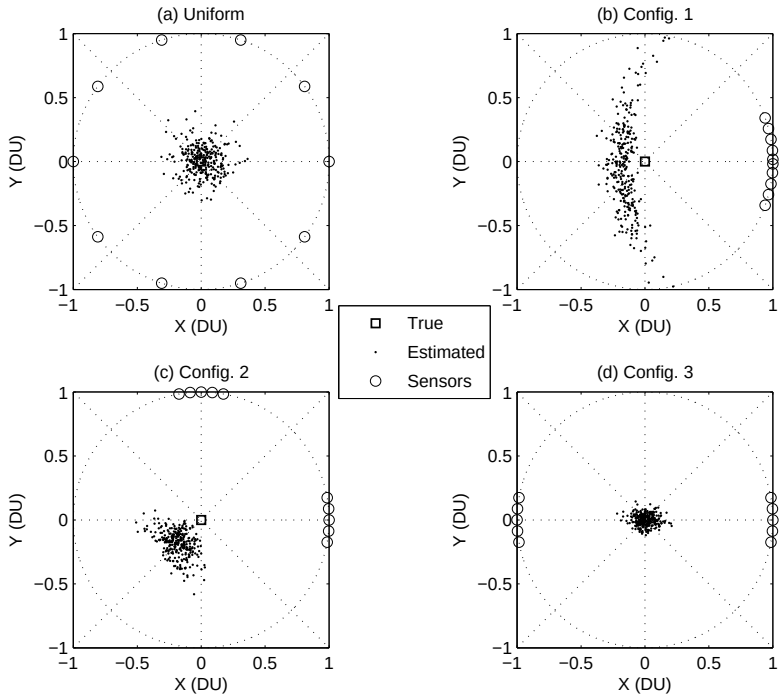

(a) Scatter plot with WLS estimation.

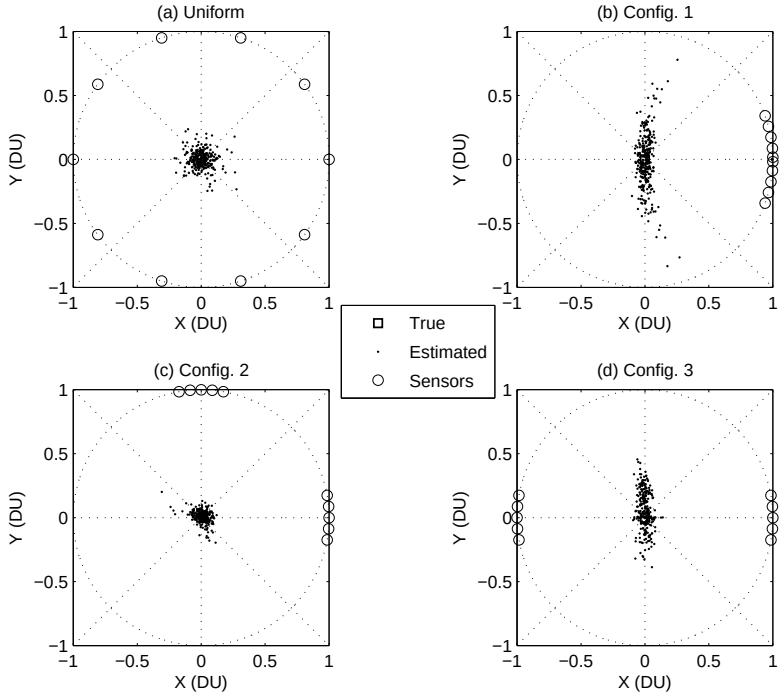

(b) Scatter plot with ML estimation.

Figure 4.7: Scatter plots with uniform and three non-uniform circulary arrays. $\sigma_b = 0.2$, $\sigma_n = 0.05$.

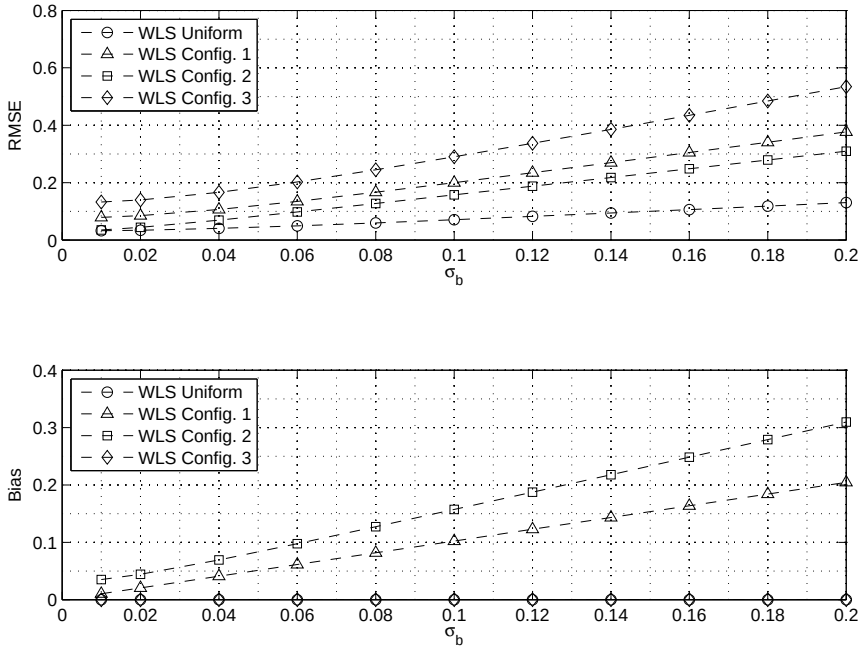

(a) RMSE and bias of WLS estimation.

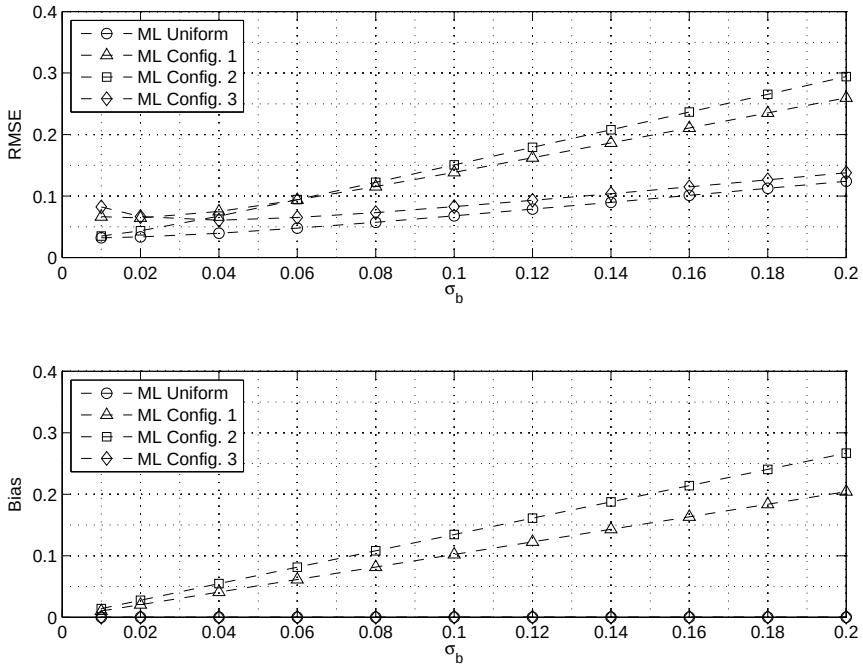

(b) RMSE and bias of ML estimation.

Figure 4.8: Estimation RMSE and bias are plotted versus σ_b for uniform and three non-uniform circular arrays.

4.8 Summary

The performance of source location estimation is severely deteriorated in a multipath fading propagation environment due to weak LOS or NLOS signal paths. This chapter models the range measurement error by both additive Gaussian noise and possibly positive bias, either deterministic or random. The random measurement bias follows widely adopted distribution models for time delay over multipath channels, and the analysis mainly focuses on the exponential distribution. The analytical estimation bias and MSE for the WLS and ML estimators are derived to assess the localization performance, showing that in general the estimator produces biased estimates, and the MSE and bias performance is determined by the statistics of measurement bias and noise, the beacon sensor geometry as well as the estimator type. The analysis and numerical evaluations show that the ML estimation has a better performance than WLS in terms of both MSE and bias in typical cases, and is closer to the CRBs.

Chapter 5

Conclusions

This thesis explored the performance of time delay estimation and transceiver localization in wireless multipath channels. In the multipath environment, range measurements suffer from the errors due to weak LOS and rich NLOS signal paths. The research focused on range-based localization schemes, especially ToA trilateration and TDoA multilateration, and analyzed the algorithm performance of TDoA and ToA localization as well as the performance limits of time delay estimation. Instead of proposing algorithms for LOS identification and NLOS mitigation, the thesis was devoted to develop theoretical performance lower bounds of TDE that are used to guide algorithm design as benchmark and help to provide insight into the behavior of time delay estimation.

Ziv-Zakai bounds on Bayesian estimation of time delay were developed for known pulsed signal propagating through an unknown random multipath channel following Rayleigh/Rician distribution, with a uniform prior on the delay. The bound does not assume knowledge of the channel at the receiver, providing a tighter bound than the average ZZB that assumes channel realizations known to receivers. Differences between the two bounds are pronounced at moderate and high SNRs. In comparison the ECRB,

conditioned on the channel, is reasonably tight at high SNR, but does not capture the threshold TDE behavior and is not tight below the high SNR threshold. The special cases of independent fading channel, flat fading channel and known channel were discussed. Furthermore, the ZZB was extended to cover frequency hopping waveforms, showing the particular benefit of frequency diversity for TDE in frequency-selective fading channels. The development incorporated both correlation among FIR channel taps as well as frequency-hopping sub-channels. The closed-form expressions of ZZB for frequency hopping waveforms in independent flat-fading channels, including both Rician and Rayleigh fading, enable easy study of the effects of SNR, frequency diversity, and channel statistics on TDE.

Comparisons with the RMSE performance of MAP estimation indicate that the ZZB is tight for a large range of SNRs, and thresholds can be found that separate low, medium, and high SNR regimes. Lack of precise convergence to the prior as the SNR goes to zero is accounted for by studying the ZZB approximations at low SNR. In addition, an GML/MMSE time delay estimator was evaluated that does not exploit the channel statistics, and the GML/MMSE estimator was shown considerably poorer than the MAP estimator that does account for the random channel.

The ranging errors due to multipath propagation finally lead to location estimation inaccuracy, and the performance of localization is deteriorated by the noisy and biased range measurements in multipath fading environment. The last part of the thesis modeled the range measurement error by the sum of additive Gaussian noise and possibly positive bias. The random measurement bias followed widely adopted distribution models for time delay over multipath channels. The analytical estimation bias and MSE for the WLS and ML estimators were focused on the exponential distribution, showing that in general the estimator produces biased estimates, and the MSE and bias performance

is determined by the statistics of measurement bias and noise, the beacon array geometry as well as the estimator type. Numerical evaluations showed that the ML estimation has a better performance than WLS in terms of both MSE and bias in typical cases, and is closer to the CRBs.

Appendix A

CRB for TDoA Multilateration

The derivation of the Cramér-Rao bound for TDoA multilateration is presented in this section, cited from [63].

Define $\mathbf{z}_p^0$ and $\mathbf{z}_p$ are the true and estimated transmitter locations, respectively. A vector of TDoA $\mathbf{d}$ is known to be asymptotically Gaussian with covariance matrix given by $\mathbf{Q}$. The conditional probability density function of $\mathbf{d}$ is

$$p(\mathbf{d}|\mathbf{z}_p) = \frac{1}{(2\pi)^{(M-1)/2}|\mathbf{Q}|^{1/2}}\exp\{-\frac{1}{2}(\mathbf{d} - \frac{1}{v_c}\mathbf{r})^T\mathbf{Q}^{-1}(\mathbf{d} - \frac{1}{v_c}\mathbf{r})\}, \tag{A.1}$$

where $\mathbf{r} = [r_{2,1}, r_{3,1}, \ldots, r_{M,1}]^T$ is a function of $\mathbf{z}_p$. The transmitter position can be expressed as a nonlinear function of $\mathbf{d}$, i.e., $x = f_1(\mathbf{d})$ and $y = f_2(\mathbf{d})$. Using Talor-series expansion of x and y around the true TDoA vector, it can be verified that both the bias and variance of transimitter position are proportional to the TDoA covariance matrix $\mathbf{Q}$. If variations in TDoA's are small so that the bias square is insignificant compared with the variance, the CRLB of $\mathbf{z}_p$ is given by

$$\Phi^0 = \{E[(\frac{\partial}{\partial \mathbf{z}_p}\ln p(\mathbf{d}|\mathbf{z}_p))(\frac{\partial}{\partial \mathbf{z}_p}\ln p(\mathbf{d}|\mathbf{z}_p))^T]|_{\mathbf{z}_p=\mathbf{z}_p^0}\}^{-1} \tag{A.2}$$

The partial derivative of $\ln p(\mathbf{d}|\mathbf{z}_p)$ with respect to $\mathbf{z}_p$ is

$$\frac{\partial}{\partial \mathbf{z}_P} \ln p(\mathbf{d}|\mathbf{z}_p) = -\frac{1}{v_c} \frac{\partial \mathbf{r}^T}{\partial \mathbf{z}_p} \mathbf{Q}^{-1} (\mathbf{d} - \frac{\mathbf{r}}{v_c}). \tag{A.3}$$

Hence

$$\Phi^0 = v_c^2 (\frac{\partial \mathbf{r}^T}{\partial \mathbf{z}_p} \mathbf{Q}^{-1} \frac{\partial \mathbf{r}}{\partial \mathbf{z}_p})^{-1}|_{\mathbf{z}_p = \mathbf{z}_p^0} \tag{A.4}$$

where $\frac{\partial \mathbf{r}^T}{\partial \mathbf{z}_p}$ is from the definition of $\mathbf{r}$ to be $\mathbf{G}_t$ given by

$$\mathbf{G}_t = \begin{bmatrix} (x_1 - x)/r_1 - (x_2 - x)/r_2 & (y_1 - y)/r_1 - (y_2 - y)/r_2 \\ (x_1 - x)/r_1 - (x_3 - x)/r_3 & (y_1 - y)/r_1 - (y_3 - y)/r_3 \\ \vdots & \vdots \\ (x_1 - x)/r_1 - (x_M - x)/r_M & (y_1 - y)/r_1 - (y_M - y)/r_M \end{bmatrix}. \tag{A.5}$$

Appendix B

MGF of Quadratic Function of a Gaussian Random Vector

B.1 Case of a Real Gaussian Random Vector

Assume $\mathbf{r}$ is a real Gaussian vector with distribution $\mathbf{r} \sim \mathcal{N}(\boldsymbol{\mu}, \mathbf{C})$, where $\mathbf{C} > 0$. For constant $\boldsymbol{\Psi}$, $\mathbf{g}$ and d, the MGF of $Q = \mathbf{r}^T\boldsymbol{\Psi}\mathbf{r} + \mathbf{g}^T\mathbf{r} + d$ is defined as

$$\Theta(s) = E\{\exp(sQ)\} = E\{\exp\left[s(\mathbf{r}^T\boldsymbol{\Psi}\mathbf{r} + \mathbf{g}^T\mathbf{r} + d)\right]\}. \tag{B.1}$$

According to Theorem (3.2a.1) in [87], if $\boldsymbol{\Psi}$ is a real symmetric matrix, then the MGF is

$$\begin{aligned}\Theta(s) &= |\mathbf{I} - 2s\boldsymbol{\Psi}\mathbf{C}|^{-\frac{1}{2}}\exp\{-\frac{1}{2}(\boldsymbol{\mu}^T\mathbf{C}^{-1}\boldsymbol{\mu} - 2sd) \\ &\quad +\frac{1}{2}(\boldsymbol{\mu} + s\mathbf{C}\mathbf{g})^T(\mathbf{I} - 2s\boldsymbol{\Psi}\mathbf{C})^{-1}\mathbf{C}^{-1}(\boldsymbol{\mu} + s\mathbf{C}\mathbf{g})\} \qquad \text{(B.2)} \\ &= |\mathbf{I} - 2s\mathbf{C}^{\frac{1}{2}}\boldsymbol{\Psi}\mathbf{C}^{\frac{1}{2}}|^{-\frac{1}{2}}\exp\{s(d + \boldsymbol{\mu}^T\boldsymbol{\Psi}\boldsymbol{\mu} + \mathbf{g}^T\boldsymbol{\mu}) \\ &\quad +(s^2/2)(\mathbf{C}^{\frac{1}{2}}\mathbf{g} + 2\mathbf{C}^{\frac{1}{2}}\boldsymbol{\Psi}\boldsymbol{\mu})^T(\mathbf{I} - 2s\mathbf{C}^{\frac{1}{2}}\boldsymbol{\Psi}\mathbf{C}^{\frac{1}{2}})^{-1}(\mathbf{C}^{\frac{1}{2}}\mathbf{g} + 2\mathbf{C}^{\frac{1}{2}}\boldsymbol{\Psi}\boldsymbol{\mu})\}. \qquad \text{(B.3)}\end{aligned}$$

Both equivalent forms (B.2) and (B.3) can be useful. Equation (B.2) does not require the square root $\mathbf{C}^{\frac{1}{2}}$, but the matrix $(\mathbf{I} - 2s\mathbf{\Psi C})$ is asymmetric, whereas (B.3) does require $\mathbf{C}^{\frac{1}{2}}$, but the symmetry of $(\mathbf{I}-2s\mathbf{C}^{\frac{1}{2}}\mathbf{\Psi C}^{\frac{1}{2}})$ can lead to efficient calculation of the inverse and determinant.

A form without $\mathbf{C}^{\frac{1}{2}}$ can also be obtained. Noting that $|\mathbf{I}-2s\mathbf{C}^{\frac{1}{2}}\mathbf{\Psi C}^{\frac{1}{2}}| = |\mathbf{I}-2s\mathbf{C\Psi}|$, and

$$\mathbf{C}^{\frac{1}{2}}(\mathbf{I} - 2s\mathbf{C}^{\frac{1}{2}}\mathbf{\Psi C}^{\frac{1}{2}})^{-1}\mathbf{C}^{\frac{1}{2}} = (\mathbf{C}^{-\frac{1}{2}} - 2s\mathbf{C}^{\frac{1}{2}}\mathbf{\Psi})^{-1}\mathbf{C}^{\frac{1}{2}} = (\mathbf{I} - 2s\mathbf{C\Psi})^{-1}\mathbf{C},$$

then (B.3) can be expressed as

$$\Theta(s) = |\mathbf{I}-2s\mathbf{C\Psi}|^{-\frac{1}{2}}\exp\{s(d+\boldsymbol{\mu}^T\mathbf{\Psi}\boldsymbol{\mu}+\mathbf{g}^T\boldsymbol{\mu})+(s^2/2)(\mathbf{g}+2\mathbf{\Psi}\boldsymbol{\mu})^T(\mathbf{I}-2s\mathbf{C\Psi})^{-1}\mathbf{C}(\mathbf{g}+2\mathbf{\Psi}\boldsymbol{\mu}). \tag{B.4}$$

If $\mathbf{g} = \mathbf{0}$ and $d = 0$, then Q degrades to $Q = \mathbf{r}^T\mathbf{\Psi r}$. In this case, $\Theta(s)$ of Q is given by

$$\Theta(s) = |\mathbf{I} - 2s\mathbf{C}^{\frac{1}{2}}\mathbf{\Psi C}^{\frac{1}{2}}|^{-\frac{1}{2}}\exp\{s\boldsymbol{\mu}^T\mathbf{C}^{-\frac{1}{2}}(\mathbf{C}^{\frac{1}{2}}\mathbf{\Psi C}^{\frac{1}{2}})(\mathbf{I} - 2s\mathbf{C}^{\frac{1}{2}}\mathbf{\Psi C}^{\frac{1}{2}})^{-1}\mathbf{C}^{-\frac{1}{2}}\boldsymbol{\mu})\} \tag{B.5}$$

according to the last equality of $M_Q(t)$ on p. 40 in [87].

When $\mathbf{\Psi}$ is asymmetric, since $\mathbf{r}^T\mathbf{\Psi r} = \mathbf{r}^T\mathbf{\Psi}^T\mathbf{r}$, one can obtain an equivalent expression for Q as $Q = \frac{1}{2}\mathbf{r}^T(\mathbf{\Psi} + \mathbf{\Psi}^T)\mathbf{r} + \mathbf{g}^T\mathbf{r} + d$. Therefore, the above results are also applicable after replacing $\mathbf{\Psi}$ by $\frac{1}{2}(\mathbf{\Psi} + \mathbf{\Psi}^T)$.

B.1.1 Taylor Expansion of the Inverse and Determinant of a Matrix

Let square matrix $\mathbf{B}$ have a second order expansion for small α given by $\mathbf{B} = \mathbf{A} + \alpha\mathbf{X} + \alpha^2\mathbf{Y}$, where $\mathbf{A}$ is non-singular. Expansion of $\mathbf{B}^{-1}$ in a power series of α requires derivatives of $\mathbf{B}^{-1}$ with respect to α. Since $\mathbf{BB}^{-1} = \mathbf{I}$, it follows that

$$\mathbf{B}\frac{d\mathbf{B}^{-1}}{d\alpha} + \frac{d\mathbf{B}}{d\alpha}\mathbf{B}^{-1} = \mathbf{0},$$

that leads to

$$\frac{d\mathbf{B}^{-1}}{d\alpha} = -\mathbf{B}^{-1}\frac{d\mathbf{B}}{d\alpha}\mathbf{B}^{-1}. \tag{B.6}$$

$$\begin{aligned}\frac{d^2\mathbf{B}^{-1}}{d\alpha^2} &= -\frac{d\mathbf{B}^{-1}}{d\alpha}\frac{d\mathbf{B}}{d\alpha}\mathbf{B}^{-1} - \mathbf{B}^{-1}\frac{d^2\mathbf{B}}{d\alpha^2}\mathbf{B}^{-1} - \mathbf{B}^{-1}\frac{d\mathbf{B}}{d\alpha}\frac{d\mathbf{B}^{-1}}{d\alpha} \\ &= 2\mathbf{B}^{-1}\frac{d\mathbf{B}}{d\alpha}\mathbf{B}^{-1}\frac{d\mathbf{B}}{d\alpha}\mathbf{B}^{-1} - \mathbf{B}^{-1}\frac{d^2\mathbf{B}}{d\alpha^2}\mathbf{B}^{-1} \\ &= 2\mathbf{B}^{-1}\mathbf{X}\mathbf{B}^{-1}\mathbf{X}\mathbf{B}^{-1} - 2\mathbf{B}^{-1}\mathbf{Y}\mathbf{B}^{-1}. \end{aligned} \tag{B.7}$$

Therefore $\mathbf{B}^{-1}$ has a Taylor expansion given by

$$\begin{aligned}\mathbf{B}^{-1} &= \mathbf{B}^{-1}|_{\alpha=0} + \alpha\frac{d\mathbf{B}^{-1}}{d\alpha}|_{\alpha=0} + \frac{1}{2}\alpha^2\frac{d^2\mathbf{B}^{-1}}{d\alpha^2}|_{\alpha=0} + \mathbf{O}(\alpha^3) \\ &= \mathbf{A}^{-1} - \alpha\mathbf{A}^{-1}\mathbf{X}\mathbf{A}^{-1} + \alpha^2[\mathbf{A}^{-1}(\mathbf{X}\mathbf{A}^{-1})^2 - \mathbf{A}^{-1}\mathbf{Y}\mathbf{A}^{-1}] + \mathbf{O}(\alpha^3). \end{aligned} \tag{B.8}$$

The expansion of the determinant $|\mathbf{B}|$ requires associated derivatives as well. From (A.390) in Appendix A of [99]

$$\frac{d|\mathbf{B}|}{d\alpha} = |\mathbf{B}|\frac{d\ln|\mathbf{B}|}{d\alpha} = |\mathbf{B}|tr(\mathbf{B}^{-1}\frac{d\mathbf{B}}{d\alpha}),$$

so that

$$\begin{aligned}\frac{d^2|\mathbf{B}|}{d\alpha^2} &= \frac{d|\mathbf{B}|}{d\alpha}tr(\mathbf{B}^{-1}\frac{d\mathbf{B}}{d\alpha}) + |\mathbf{B}|tr(\frac{d\mathbf{B}^{-1}}{d\alpha}\frac{d\mathbf{B}}{d\alpha} + \mathbf{B}^{-1}\frac{d^2\mathbf{B}}{d\alpha^2}) \\ &= |\mathbf{B}|tr^2(\mathbf{B}^{-1}\frac{d\mathbf{B}}{d\alpha}) + |\mathbf{B}|tr(-(\mathbf{B}^{-1}\frac{d\mathbf{B}}{d\alpha})^2 + \mathbf{B}^{-1}\frac{d^2\mathbf{B}}{d\alpha^2}). \end{aligned} \tag{B.9}$$

Therefore, $|\mathbf{B}|$ has the following expansion

$$\begin{aligned}|\mathbf{B}| &= |\mathbf{B}|_{\alpha=0} + \alpha\frac{d|\mathbf{B}|}{d\alpha}|_{\alpha=0} + \frac{1}{2}\alpha^2\frac{d^2|\mathbf{B}|}{d\alpha^2}|_{\alpha=0} + O(\alpha^3) \\ &= |\mathbf{A}| + \alpha|\mathbf{A}|tr(\mathbf{A}^{-1}\mathbf{X}) + \frac{\alpha^2}{2}|\mathbf{A}|\left\{tr^2[\mathbf{A}^{-1}\mathbf{X}] + tr[2\mathbf{A}^{-1}\mathbf{Y} - (\mathbf{A}\mathbf{X})^2]\right\} + O(\alpha^3) \end{aligned} \tag{B.10}$$

If $\mathbf{A} = \mathbf{I}$, then

$$(\mathbf{I} + \alpha\mathbf{X} + \alpha^2\mathbf{Y})^{-1} = \mathbf{I} - \alpha\mathbf{X} + \alpha^2[\mathbf{X}^2 - \mathbf{Y}] + \mathbf{O}(\alpha^3). \tag{B.11}$$

$$|\mathbf{I} + \alpha\mathbf{X} + \alpha^2\mathbf{Y}| = 1 + \alpha tr(\mathbf{X}) + \frac{\alpha^2}{2}\left\{tr^2(\mathbf{X}) + tr(2\mathbf{Y} - \mathbf{X}^2)\right\} + O(\alpha^3). \tag{B.12}$$

The above also readily leads to

$$|\mathbf{I}+\alpha\mathbf{X}+\alpha^2\mathbf{Y}|^{-\frac{1}{2}} = 1-\frac{\alpha}{2}tr(\mathbf{X})+\frac{\alpha^2}{4}\left[\frac{1}{2}tr^2(\mathbf{X})-tr(2\mathbf{Y}-\mathbf{X}^2)\right]+O(\alpha^3). \quad \text{(B.13)}$$

B.2 Case of a Complex Gaussian Random Vector

Assume $\mathbf{r}$ is a complex Gaussian vector with distribution $p(\mathbf{r})$ denoted by $\mathbf{r} \sim \mathcal{N}(\boldsymbol{\mu}, \boldsymbol{\Sigma})$. For Hermitian symmetric matrix $\boldsymbol{\Psi}$, complex vector $\mathbf{g}$ and real scalar d, the MGF of $Q = \mathbf{r}^H\boldsymbol{\Psi}\mathbf{r} + 2\text{Re}\{\mathbf{g}^H\mathbf{r}\} + d$ is defined as $\Theta(s) = E\{\exp(sQ)\}$. Using the same integration technique as shown in [100] for the quadratic form $\mathbf{r}^H\boldsymbol{\Psi}\mathbf{r}$, and after a similar manipulation as Theorem 3.2a.1 in [87], a symmetric form of the MGF is given by

$$\begin{aligned}\Theta(s) =&|\mathbf{I}-s\boldsymbol{\Sigma}^{\frac{1}{2}}\boldsymbol{\Psi}\boldsymbol{\Sigma}^{\frac{1}{2}}|^{-1}\exp\Big\{s(\boldsymbol{\mu}^H\boldsymbol{\Psi}\boldsymbol{\mu}+\text{Re}\{\mathbf{g}^H\boldsymbol{\mu}\}+d)\\ &+s^2(\boldsymbol{\Sigma}^{\frac{1}{2}}\mathbf{g}+\boldsymbol{\Sigma}^{\frac{1}{2}}\boldsymbol{\Psi}\boldsymbol{\mu})^H(\mathbf{I}-s\boldsymbol{\Sigma}^{\frac{1}{2}}\boldsymbol{\Psi}\boldsymbol{\Sigma}^{\frac{1}{2}})^{-1}(\boldsymbol{\Sigma}^{\frac{1}{2}}\mathbf{g}+\boldsymbol{\Sigma}^{\frac{1}{2}}\boldsymbol{\Psi}\boldsymbol{\mu})\Big\}. \quad \text{(B.14)}\end{aligned}$$

If $\mathbf{g}=0$ and $d=0$, then Q shrinks to $Q=\mathbf{r}^H\boldsymbol{\Psi}\mathbf{r}$. Then, $\Theta(s)$ can be found as

$$\Theta(s) = |\mathbf{I}-s\boldsymbol{\Sigma}^{\frac{1}{2}}\boldsymbol{\Psi}\boldsymbol{\Sigma}^{\frac{1}{2}}|^{-1}\exp\Big\{s\boldsymbol{\mu}^H\boldsymbol{\Sigma}^{-\frac{1}{2}}(\boldsymbol{\Sigma}^{\frac{1}{2}}\boldsymbol{\Psi}\boldsymbol{\Sigma}^{\frac{1}{2}})(\mathbf{I}-s\boldsymbol{\Sigma}^{\frac{1}{2}}\boldsymbol{\Psi}\boldsymbol{\Sigma}^{\frac{1}{2}})^{-1}\boldsymbol{\Sigma}^{-\frac{1}{2}}\boldsymbol{\mu}\Big\}. \quad \text{(B.15)}$$

Appendix C

Pulse Signals and Their Autocorrelation and Bandwidth Expressions

The numerical examples of ZZBs in this thesis adopt mean-square bandwidth (MSB) defined by [101]

$$B^2 = \int_{-\infty}^{\infty} \frac{|\dot{p}(t)|^2}{R(0)(2\pi)^2} dt = \int_{-\infty}^{\infty} \frac{f^2 |P(f)|^2}{\beta(0)} df, \tag{C.1}$$

where $p(t)$ and $P(f)$ are, respectively, the time and frequency-domain expressions of the signal, and $\beta(t)$ is the autocorrelation. B is also known as the root-mean-squared equivalent bandwidth (RMSB).

C.1 Square-Root Raised Cosine (SRRC) Pulse

The spectrum of a square-root raised cosine (SRRC) pulse is given by [84]

$$P_{\mathrm{SRRC}}(f)=\begin{cases}\sqrt{T_p/2}, & 0\leqslant|f|\leqslant\frac{1-\widetilde{\beta}}{T_p}\\ \sqrt{\frac{T_p}{4}\left\{1+\cos\left[\frac{\pi T_p}{2\widetilde{\beta}}\left(|f|-\frac{1-\widetilde{\beta}}{T_p}\right)\right]\right\}}, & \frac{1-\widetilde{\beta}}{T_p}\leqslant|f|\leqslant\frac{1+\widetilde{\beta}}{T_p}\\ 0, & |f|>\frac{1+\widetilde{\beta}}{T_p}\end{cases}, \tag{C.2}$$

where $T_p/2$ is the first zero-crossing time, and $\widetilde{\beta}$ is the roll-off factor. The time-domain expression is

$$p_{\mathrm{SRRC}}(t)=\begin{cases}\frac{\sin\left[\pi(1-\widetilde{\beta})\frac{2t}{T_p}\right]+\frac{8\widetilde{\beta}t}{T_p}\cos\left[2\pi(1+\widetilde{\beta})\frac{t}{T_p}\right]}{\frac{2\pi t}{T_p}\left[1-\left(\frac{8\widetilde{\beta}t}{T_p}\right)^2\right]}, & t\neq 0,\quad t\neq\pm\frac{T_p}{8\widetilde{\beta}},\\ 1-\widetilde{\beta}+\frac{4\widetilde{\beta}}{\pi}, & t=0,\\ \frac{\widetilde{\beta}}{\sqrt{2}}\left[(1+\frac{2}{\pi})\sin(\frac{\pi}{4\widetilde{\beta}})+(1-\frac{2}{\pi})\cos(\frac{\pi}{4\widetilde{\beta}})\right], & t=\pm\frac{T_p}{8\widetilde{\beta}}\end{cases} \tag{C.3}$$

The autocorrelation and squared MSB of the SRRC pulse are

$$\beta_{\mathrm{SRRC}}(\tau)=\mathrm{sinc}\left(\frac{2\tau}{T_p}\right)\frac{\cos(2\pi\widetilde{\beta}\tau/T_p)}{1-(4\widetilde{\beta}\tau/T_p)^2},\quad B^2_{\mathrm{SRRC}}=\frac{1}{3T_p^2}\left[1+\widetilde{\beta}^2\left(3-\frac{24}{\pi^2}\right)\right]. \tag{C.4}$$

where $\mathrm{sinc}(x)\triangleq\frac{\sin(\pi x)}{\pi x}$.

C.2 Gaussian Pulse

The Gaussian pulse, its spectrum and autocorrelation are [102, pp.28-31]

$$p_{\mathrm{G}}(t)=\pm c\frac{1}{\sqrt{2\pi\sigma^2}}e^{-\frac{t^2}{2\sigma^2}}=\pm c\frac{\sqrt{2}}{\widetilde{\alpha}}e^{-\frac{2\pi t^2}{\widetilde{\alpha}^2}},\quad P_{\mathrm{G}}(f)=ce^{-\frac{\pi}{2}\widetilde{\alpha}^2f^2},\quad \beta_{\mathrm{G}}(\tau)=\frac{c^2}{\widetilde{\alpha}}e^{-\frac{\pi}{\widetilde{\alpha}^2}\tau^2}. \tag{C.5}$$

where $\widetilde{\alpha}\triangleq 4\pi\sigma^2$. Set $c^2=\widetilde{\alpha}$ for normalizing the autocorrelation, which makes $\beta_{\mathrm{G}}(0)=1$ and does not affect the bandwidth. The squared MSB of the Gaussian pulse is obtained by the second-order moment of the Gaussian distribution as

$$B^2_{\mathrm{G}}=\int_{-\infty}^{\infty}f^2\left|P_{\mathrm{G}}(f)\right|^2df=\frac{1}{2\pi\widetilde{\alpha}^2}. \tag{C.6}$$

C.3 Gaussian Doublet Pulse

The Gaussian doublet pulse (the second derivative of the Gaussian pulse) is a common pulse in UWB systems, given by [102, pp.28-31]

$$p_{\mathrm{G2}}(t) = \frac{d^2 p_{\mathrm{G}}(t)}{dt^2} = cK(1 - \frac{4\pi}{\widetilde{\alpha}^2}t^2)e^{-\frac{2\pi}{\widetilde{\alpha}^2}t^2}, \tag{C.7}$$

where $K = -\frac{\sqrt{32}\pi}{\widetilde{\alpha}^3} = -\frac{1}{\sqrt{2\pi}\sigma^3}$ is a coefficient inherited from the above Gaussian pulse. Its autocorrelation is

$$\beta_{\mathrm{G2}}(\tau) = \frac{d^4\beta_{\mathrm{G}}(\tau)}{d\tau^4} = c^2K^2\left(\frac{\pi^2}{2\widetilde{\alpha}^3}\tau^4 - \frac{3\pi}{2\widetilde{\alpha}}\tau^2 + \frac{3\widetilde{\alpha}}{8}\right)e^{-\frac{\pi}{\widetilde{\alpha}^2}\tau^2}. \tag{C.8}$$

To normalize set $c^2K^2 = \frac{8}{3\widetilde{\alpha}}$. The spectrum of the pulse and its squared MSB are given by

$$P_{\mathrm{G2}}(f) = c(j2\pi f)^2 e^{-\frac{\pi}{2}\widetilde{\alpha}^2 f^2}, \qquad B_{\mathrm{G2}}^2 = \int_{-\infty}^{\infty} f^2 \left|P_{\mathrm{G2}}(f)\right|^2 df = \frac{5}{2\pi\widetilde{\alpha}^2}. \tag{C.9}$$

C.3.1 Square-Root Raised Cosine Pulse Modulated by a PN Code

The SRRC pulse modulated by a pseudorandom noise (PN) code generates a pulse train. Suppose the code has N chips with a duration of T_c for each chip. The SRRC pulse with the first zero-crossing point $T_p/2$ is cut at $\pm\frac{T_c}{2} \geqslant 3T_p$. The length of pseudo-random m-sequences is set to 15, corresponding to the generating polynomial $g(x) = x^4 + x^3 + 1$. The discrete periodic autocorrelation of binary (± 1) m-sequence is [103]

$$\theta(k) = \frac{1}{N}\sum_{n=0}^{N-1} c_n c_{n+k} = \begin{cases} 1, & k = \widetilde{L}N \\ -\frac{1}{N}, & k \neq \widetilde{L}N \end{cases} \tag{C.10}$$

where $\widetilde{L}$ is an integer. The pulse train and autocorrelation are given by

$$p_{\mathrm{PN}}(t) = \sum_{i=0}^{N-1} c_i p_{\mathrm{SRRC}}(t - iT_c), \tag{C.11}$$

$$\beta_{\mathrm{PN}}(\tau) = \int_{-\infty}^{\infty} p_{\mathrm{PN}}(t) p_{\mathrm{PN}}(t+\tau) dt = \sum_{i=0}^{N-1} \sum_{j=0}^{N-1} c_i c_j \int_{-\infty}^{\infty} p_{\mathrm{SRRC}}(t-iT_c) p_{\mathrm{SRRC}}(t-jT_c+\tau) dt. \tag{C.12}$$

The delay τ can be expressed as $\tau = kT_c + \tau_\epsilon$, where $0 \leq \tau_\epsilon < T_c$, and then the SRRC pulses overlap only for $j = k + m$ and $j = k + m + 1$. So the autocorrelation of the PN pulse train becomes [103]

$$\beta_{\mathrm{PN}}(\tau) = \beta_{\mathrm{PN}}(k, \tau_\epsilon) = \theta(k) \cdot \beta_{\mathrm{SRRC}}(\tau_\epsilon) + \theta(k+1) \cdot \beta_{\mathrm{SRRC}}(T_c - \tau_\epsilon). \tag{C.13}$$

Appendix D

Acronyms

AoA	Angle of Arrival
AWGN	Additive White Gaussian Noise
BCRB	Bayesian Cramér-Rao Bound
Conn	transceiver Connectivity
CRB	Cramér-Rao Bound
DSSS	Direct-Sequence Spread Spectrum
ECRB	Expectation of conditional Cramér-Rao Bound
FFT	Fast Fourier Transform
GML	Generalized Maximum Likelihood
LBS	Location Based Services
LLR	Log-Likelihood Ratio
LR	Likelihood Ratio
LOS	Line Of Sight
LS	Least Square
MAP	Maximum A Posteriori
MGF	Moment Generating Function
ML	Maximum Likelihood
MMSE	Minimum Mean Square Error
MSB	Mean-Square Bandwidth
MSE	Mean Square Error
NLOS	Non-Line Of Sight
pdf	probability density function
PDP	Power Delay Profile
PN	Pseudo Noise
PPM	Pulse-Position Modulation
RMSE	Root Mean Square Error
RSS	Received Signal Strength
SNR	Signal-to-Noise Ratio
SRRC	Square-Root Raised Cosine

TDE	Time Delay Estimation
TDoA	Time Difference of Arrival
ToA	Time of Arrival
UWB	Ultra-WideBand
WLS	Weighted Least Square
ZZB	Ziv-Zakai Bound

Bibliography

[1] J. Caffery, Jr. and G. L. Stuber. Subscriber location in CDMA cellular networks. *IEEE Trans*, 47(2):406–416, May 1998.

[2] N. Patwari, J. Ash, S. Kyperountas, R. M. Moses, A. O. Hero, III, and N. S. Correal. Locating the nodes: Cooperative localization in wireless sensor networks. *IEEE Signal Processing Magazine*, 22(4):54–69, July 2005.

[3] J. A. Farrell and M. Bath. *The Global Positioning System & Inertial Navigation*. McGraw-Hill Professional, 1998.

[4] S. Pandey and P. Agrawal. A survey on localization techniques for wireless networks. *J. Chinese Institute of Engineers*, 29(7):1125–1148, 2006.

[5] S. Swales, J. Maloney, and J. Stevenson. Locating mobile phones and the US wireless E-911 mandate. In *IEE Colloquium on Novel Methods of Location and Tracking of Cellular Mobiles and Their System Applications*, pages 2/1 – 2/6, London, UK, May 1999.

[6] S. Larder. EOTD based location service implementation. In *Mobile Location Workshop (MLW'01)*, 2001.

[7] M. Moeglein and N. Krasner. An introduction to SnapTrack server-aided GPS technology. In *Institute of Navigation GPS Meeting Proceedings*, pages 333–342, Sept. 1998.

[8] N. B. Priyantha. *The cricket indoor location system*. PhD thesis, Massachussette Institute of Technology, 2005.

[9] P. Krishnan, A. S. Krishnakumar, W. H. Ju, C. Mallows, and S. Ganu. A system for LEASE: System for location estimation assisted by stationary emitters for indoor RF wireless networks. In *Proceedings of IEEE INFOCOM*, volume 2, pages 1001–1011, 2004.

[10] M. Youssef and A. Agrawala. The Horus WLAN location determination system. In *Proc. of the 3rd Int'l Conf. on Mobile Systems, Applications, and Services*, pages 205–218, 2005.

[11] D. Niculescu and B. Nath. Ad hoc positioning system (APS). In *Proc. IEEE Global Communications (GLOBECOM)*, 2001.

[12] L. Lazos and R. Poovendran. SeRLoc: Secure range-independent localization for wireless sensor networks. In *Proc. of the 2004 ACM Workshop on Wireless Security (WiSe'04)*, pages 21–30, 2004.

[13] S. Čapkun, M. Hamdi, and J.-P. Hubaux. GPS-free positioning in mobile ad-hoc networks. *Cluster Computing*, 5(2):157–167, April 2002.

[14] A. Savvides, C.-C. Han, and M. Srivastava. Dynamic fine-grained localization in ad-hoc networks of sensors. In *Proc. ACM Int'l. Conf. Mobile Computing and Networking (MOBICOM)*, pages 166–179, Rome, Italy, 2001.

[15] T. He, C. Huang, B. M. Blum, J. A. Stankovic, and T. F. Abdelzaher. Range-free localization schemes in large scale sensor networks. In *Proc. of the Annual Int'l. Conf. on Mobile Computing and Networking (MOBICOM'03)*, pages 81–95, 2003.

[16] N. Patwari. *Location estimation in sensor networks*. PhD thesis, University of Michigan, 2005.

[17] C. Savarese, J. M. Rabaey, and J. Beutel. Location in distributed ad-hoc wireless sensor networks. In *Proc. IEEE Int. Conf. Acoustics, Speech, Signal Process.*, pages 2037–2040, May 2001.

[18] H. Lee. A novel procedure for assessing theaccuracy of hyperbolic multilateration systems. *IEEE Trans. on Aerospace and Electronic Systems*, AES-11(1):2–15, Jan. 1975.

[19] W. H. Foy. Position-location solutions by taylor-series estimation. *IEEE Trans. on Aerospace and Electronic Systems*, 12:183–198, Mar. 1976.

[20] G. C. Carter. Time delay estimation for passive sonar signal processing. *IEEE Trans. Acoust., Speech, Signal Process.*, ASSP-29:463–470, June 1981.

[21] D. J. Torrieri. Statistical theory of passive location systems. *IEEE Trans. on Aerospace and Electronic Systems*, AES-20(2):183–198, Mar. 1984.

[22] K. K. Chintalapudi, A. Dhariwal, R. Govindan, and G. Sukhatme. Ad hoc localization using ranging and sectoring. In *Proc. IEEE INFOCOM*, volume 4, pages 2662–2672, 2004.

[23] C. Siva Ram Murthy and B. S. Manoj. *Ad hoc wireless networks: Architectures and protocols*. Prentice Hall, 2004.

[24] David Tse and Pramod Viswanath. *Fundamentals of wireless communication*. Cambridge University Press, 2005.

[25] B. B. Peterson, C. Kmiecik, R. Hartnett, P. M. Thompson, J. Mendoza, and H. Nguyen. Spread spectrum indoor geolocation. *Journal of the Institute of Navigation*, 45(2):97–102, Summer 1998.

[26] J. Y. Lee and R. A. Scholtz. Ranging in a dense multipath environment using an UWB radio link. *IEEE J. Sel. Areas Commun.*, 20(9):1677–1683, Dec. 2002.

[27] J. Borrás, P. Hatrack, and N. B. Mandayam. Decision theoretic framework for NLOS identification. In *IEEE Vehicular Tech. Conf. (VTC'98)*, volume 2, pages 1583–1587, May 1998.

[28] M. P. Wylie and J. Holtzman. The non-line of sight problem in mobile location estimation. In *5th IEEE Int. Conf. on Universal Personal Commun.*, volume 2, pages 827–831, Cambridge, MA, USA, 1996.

[29] P.-C. Chen. A non-line-of-sight error mitigation algorithm in location estimation. In *IEEE Wireless Comm. and Network. Conf.*, pages 316–320, Sept. 1999.

[30] S. Al-Jazzar, J. Caffery, Jr., and H. R. You. Scattering-model-based methods for TOA location in NLOS environments. *IEEE Trans. on Vehicular Technology*, 56(2):583–593, Mar. 2007.

[31] J. Riba and A. Urruela. A non-line-of-sight mitigation technique based on ML-detection. In *Proc. of IEEE Intl. Conf. on Acoustics, Speech, and Signal Proc. (ICASSP'04)*, volume 2, pages 153–156, 2004.

[32] B. Denis and N. Daniele. NLOS ranging error mitigation in a distributed positioning algorithm for indoor UWB ad-hoc networks. In *International Workshop on Wireless Ad-Hoc Networks (IWWAN'04)*, pages 356–360, 2004.

[33] J. F. Liao and B. S. Chen. Robust mobile location estimator with NLOS mitigation using interacting multiple model algorithm. *IEEE Trans. on Wireless Comm.*, 5(11):3002–3006, Nov. 2006.

[34] W. Wang, J. Y. Xiong, and Z. L. Zhu. A new NLOS error mitigation algorithm in location estimation. *IEEE Trans. on Vehicular Technology*, 54(6):2048–2053, Nov. 2005.

[35] B. M. Sadler and R. J. Kozick. A survey of time delay estimation performance bounds. In *Proc. Fourth IEEE Workshop on Sensor Array and Multichannel Signal Processing*, pages 282–288, July 2006.

[36] S. F. Yau and Y. Bresler. A compact Cramér-Rao bound expression for parametric estimation of superimposed signals. *IEEE Trans. Signal Process.*, 40(5):1226–1230, May 1992.

[37] H. Saarnisaari. ML time delay estimation in a multipath channel. In *Proc. IEEE 4th Intl. Symp. on Spread Spectrum Tech. and Appl.*, pages 1007–1011, Sept. 1996.

[38] J. Ziv and M. Zakai. Some lower bounds on signal parameter estimation. *IEEE Trans. Inf. Theory*, IT-15(3):386–391, May 1969.

[39] D. Chazan, M. Zakai, and J. Ziv. Improved lower bounds on signal parameter estimation. *IEEE Trans. Inf. Theory*, 21(1):90–93, Jan. 1975.

[40] H. L. van Trees and K. L. Bell. *Bayesian Bounds for Parameter Estimation and Nonlinear Filtering/Tracking*. IEEE Press, 2007.

[41] R. J. Kozick and B. M. Sadler. Frequency hopping waveform diversity for time delay estimation. In *Proc. 2006 Intl. Waveform Diversity and Design Conference*, Jan. 2006.

[42] R. J. Kozick and B. M. Sadler. Bounds and algorithms for time delay estimation on parallel, flat fading channels. In *Proc. IEEE Int. Conf. Acoust., Speech, Signal Process.*, pages 2413–2416, Apr. 2008.

[43] R. J. Kozick and B. M. Sadler. Communication channel estimation and waveform design: time delay estimation on parallel, flat fading channels. Technical Report TCN 05244, U. S. Army Research Office Technical Report, Jan. 2007.

[44] B. M. Sadler, L. Huang, and Z. Xu. Ziv-zakai time delay estimation bound for ultra-wideband signals. In *Proc. of IEEE Intl. Conf. on Acoustics, Speech, and Signal Proc.*, Honolulu, Hawaii, Apr. 15-20 2007.

[45] E. Weinstein and A. J. Weiss. A general class of lower bounds in parameter estimation. *IEEE Trans. Inf. Theory*, 34:338–342, Mar. 1988.

[46] Z. Xu and B. M. Sadler. Time delay estimation bounds in convolutive random channels. *IEEE J. Sel. Topics Signal Process.*, 1(3):418–430, Oct. 2007.

[47] A. J. Weiss and J. S. Picard. Network localization with biased range measurements. *IEEE Trans. Wireless Commun.*, 7(1):298–304, January 2008.

[48] D. B. Jourdan, D. Dardari, and M. Z. Win. Position error bound for UWB localization in dense cluttered environments. *IEEE Trans. Aerosp. Electron. Syst.*, 44(2):613–628, April 2008.

[49] T. S. Rappaport. *Wireless Communications: Principles And Practice*. Prentice Hall, 2nd edition, 2002.

[50] H. Hashemi. The indoor radio propagation channel. *Proceedings of the IEEE*, 81(7):943–968, July 1993.

[51] G. Durgin, T. S. Pappaport, and H. Xu. Measurements and models for radio path loss and penetration loss in and around homes and trees at 5.85 GHz. *IEEE Journal on Sel. Areas in Commun.*, 46(11):1484–1496, Nov. 1998.

[52] E. G. Larsson. Cramér-rao bound analysis of distributed positioning in sensor networks. *IEEE Signal Processing Letters*, 11(3):334–337, March 2004.

[53] A. Catovic and Z. Sahinoglu. The Cramér-Rao bounds of hybrid TOA/RSS and TDOA/RSS location estimation schemes. Technical Report TR-2003-143, Mitsubishi Electric Research Lab, Jan. 2004. Online: http://www.merl.com/reports/docs/TR2003-143.pdf.

[54] N. Patwari, A. O. Hero, III, M. Perkins, N. Correal, and R. J. O'Dea. Relative location estimation in wireless sensor networks. *IEEE Trans. Signal Process.*, 51(8):2137–2148, Aug. 2003.

[55] N. S. Correal, S. Kyperountas, Q. Shi, and M. Welborn. An UWB relative location system. In *IEEE Conf. on Ultra Wideband Systems and Technologies*, pages 394–397, Nov. 2003.

[56] S. Bancroft. An algebraic solution of the GPS equations. *IEEE Transactions on Aerospace and Electronic Systems*, AES-21(7):56–59, 1985.

[57] B. T. Fang. Trilateration and extension of global positioning system navigation. *Journal of Guidance, Control, and Dynamics*, 9(6):715–717, 1986.

[58] J. Leva. An alternative closed form solution to the GPS pseudorange equations. In *Proceedings of the Institute of Navigation (ION) National Technical Meeting*, Anahiem, CA, Jan. 1995.

[59] A. Gray. *Modern Differential Geometry of Curves and Surfaces*. CRC Press, 1993.

[60] B. Friedlander. A passive localization algorithm and its accuracy analysis. *IEEE J. Ocean. Eng.*, OE-12:234–245, Jan. 1987.

[61] H. C. Schau and A. Z. Robinson. Passive source localization employing intersecting spherical surfaces from time-of-arrival differences. *IEEE Trans. Acoust., Speech, Signal Process.*, ASSP-35:1223–1225, Aug. 1987.

[62] J. O. Smith and J. S. Abel. Closed-form least-squares source location estimation from range-difference measurements. *IEEE Trans*, ASSP-35:1661–1669, Dec. 1987.

[63] Y. T. Chan and K. C. Ho. A simple and efficient estimator for hyperbolic location. *IEEE Trans. on Signal Processing*, 42(8):1905–1915, Aug. 1994.

[64] W. R. Hahn. Optimum signal processing for passive sonar range and bearing estimation. *Journal of the Acoustical Society of America*, 58:201–207, July 1975.

[65] J. S. Abel and J. O. Smith. Source range and depth estimation from multipath range difference measurements. *IEEE Trans. Acoust., Speech, Signal Process.*, 37:1157–1165, Aug. 1989.

[66] N. Liu, Z. Xu, and B. M. Sadler. Low-complexity hyperbolic source localization with a linear sensor array. *IEEE Signal Process. Lett.*, 15:865–868, 2008.

[67] M. I. Silventoinen and T. Rantalainen. Mobile station emergency locating in GSM. In *IEEE Intl. Conf. on Personal Wireless Communications*, Feb. 1996.

[68] J. L. Caffery and G. L. Stuber. Radio location in urban CDMA microcells. In *Proc. of the Personal, Indoor and Mobile Radio Commun. (PIMRC'95)*, volume 2, pages 858–862, 1995.

[69] K. Pahlavan, P. Krishnamurthy, and A. Beneat. Wideband radio propagation modeling for indoor geolocation applications. *IEEE Communications Magazine*, 36:60–65, 1998.

[70] J. N. Ash and R. L. Moses. Outlier compensation in sensor network self-localization via the EM algorithm. In *IEEE Int. Conf. Acoust., Speech, Signal Process. (ICASSP'05)*, March 2005.

[71] W. C. Y. Lee. *Mobile Communications Engineering: Theory and Applications*. McGraw-Hill, 2nd edition, 1998.

[72] M. Z. Win and R. A. Scholtz. Energy capture versus correlator resources in ultra-wide bandwidth indoor wireless communications channels. In *IEEE Proc. Milcom (MILCOM'97)*, volume 3, pages 1277–1281, Nov. 1997.

[73] J. Schroeder, S. Galler, K. Kyamakya, and K. Jobmann. NLOS detection algorithms for ultra-wideband localization. In *4th Workshop on Positioning, Navigation and Communication (WPNC'07)*, pages 159–166, Hannover, Germany, 2007.

[74] J. S. Al-Jazzar and J. Caffery. New algorithm for NLOS identification. In *IST Mobile and Wireless Commun. Summit*, Dresden, Germany, 2005.

[75] I. Oppermann, M. Hamalainen, and J. Iinatti. *UWB: Theory and Applications*. UK Wiley, 2004.

[76] A. Lakhzouri, E. S. Lohan, R. Hamila, and M. Renfors. Extended kalman filter channel estimation for line-of-sight detection in WCDMA mobile positioning. *EURASIP Journal on Applied Signal Processing*, 13:1268–1278, 2003.

[77] S. Venkatraman, J. Caffery, Jr., and H. R. You. Location using LOS range estimation in NLOS environment. In *IEEE 55th Vehicular Technology Conference (VTC'02)*, volume 2, pages 856–860, Spring 2002.

[78] J. Yung-Hoon, L. Joon-Yong, H. Dong-Heon, and K. Shin-Hoo. Accuracy enhancement for UWB indoor positioning using ray tracing. In *Position, Location and Navigation Symposium (PLANS)*, pages 565–568, San Diego, CA, USA, 2006.

[79] D. E. Gustafson, J. M. Elwell, and J. A. Soltz. Innovative indoor geolocation using RF multipath diversity. In *Position, Location, and Navigation Symposium (PLANS)*, pages 904–912, San Diego, CA, USA, 2006.

[80] M. Tuchler and A. Huber. An improved algorithm for UWB-based positioning in a multi-path environment. In *Int'l Zurich Seminar on Commun.*, Zurich, Switzerland, 2006.

[81] R. Casas, A. Marco, J. J. Guerrero, and J. Falco. Robust estimator for non-line-of-sight error mitigation in indoor localization. *EURASIP Journal on Applied Signal Processing*, 2006:Article ID 43429, 8 pages, 2006.

[82] M. K. Simon and M.-S. Alouini. *Digital Communication over Fading Channels: A Unified Approach to Performance Analysis*. John Wiley & Sons, New Jersey, 2nd edition, 2005.

[83] H. L. van Trees. *Detection, Estimation, and Modulation Theory: Part I - Detection, Estimation, and Linear Modulation Theory*. John Wiley & Sons, 2001.

[84] J. G. Proakis. *Digital Communications*. McGraw-Hill, 4th edition, 2000.

[85] U. G. Schuster and H. Bolcskei. Ultra-wideband channel modeling on the basis of information-theoretic criteria. *IEEE Trans. Wireless Commun.*, 6(7):2464–2475, July 2007.

[86] B. M. Sadler, N. Liu, and Z. Xu. Ziv-zakai bounds on time delay estimation in unknown convolutive random channels. *IEEE Trans. Signal Process.*, 58(5):2729–2745, May 2010.

[87] A. M. Mathai and S. B. Provost. *Quadratic Forms in Random Variables: Theory and Applications*. Marcel Dekker, 1992.

[88] S. M. Kay. *Fundamentals of Statistical Processing, Volume I: Estimation Theory*. Prentice Hall, 1993.

[89] M. Z. Win and R. A. Scholtz. Characterization of ultra-wide bandwidth wireless indoor channels: A communication-theoretic view. *IEEE J. Sel. Areas Commun.*, 20:1613–1627, Dec. 2002.

[90] E. Weinstein and A. Weiss. Fundamental limitations in passive time delay estimation - part II: Wide-band systems. *IEEE Trans. Acoust., Speech, Signal Process.*, 32:1064–1078, Oct. 1984.

[91] N. Liu, Z. Xu, and B. M. Sadler. Ziv-Zakai time delay estimation bounds for frequency-hopping waveforms under frequency-selective fading. *IEEE Trans. Signal Process.*, 2010. In press.

[92] William C. Jakes, Jr., editor. *Microwave mobile communications*. John Wiley & Sons, 1974.

[93] B. Niu, O. Simeone, O. Somekh, and A. M. Haimovich. On the sum-rate of broadcast channels with outdated 1-bit feedback. In *Proc. Asilomar Conference on Signals, Systems and Computers*, pages 201–205, Pacific Grove, CA, 2006.

[94] B. Niu, O. Simeone, O. Somekh, and A. M. Haimovich. Ergodic and outage sum-rate of fading broadcast channels with 1-bit feedback. *IEEE Trans. on Vehicular Technology*, 59(3):1282 – 1293, Mar. 2010.

[95] A. Papoulis and S. U. Pillai. *Probability, Random Variables and Stochastic Processes*. McGraw-Hill, 4th edition, 2002.

[96] M. Pätzold, F. Laue, and U. Killat. A frequency hopping rayleigh fading channel simulator with given correlation properties. In *Proc. IEEE Int. Workshop on Intelligent Signal Processing and Communication Systems (ISPACS'97)*, Kuala Lumpur, Malaysia, Nov. 1997.

[97] B. M. Sadler, N. Liu, Z. Xu, and R. Kozick. Range-based geolocation in fading environments. In *46th Annual Allerton Conf. Commun., Control, Comput.*, pages 15–20, Urbana-Champaign, IL, Sept. 2008.

[98] B. Niu, M. C. Beluri, Z. Lin, P. Chitrapu, and A. Reznik. Relay assisted cooperative OSTBC transmission with SNR imbalance and channel estimation error. In *IEEE 69th Vehicular Tech. Conf.*, pages 1–5, Barcelona, Spain, April 2009.

[99] H. L. van Trees. *Detection, Estimation, and Modulation Theory: Part IV - Optimum Array Processing*. John Wiley & Sons, 2002.

[100] G. L. Turin. The characteristic function of Hermitian quadratic forms in complex normal variables. *Biometrika*, 47(1/2):199–201, June 1960.

[101] A. H. Nuttall. Minimum rms bandwidth of M time-limited signals with specified code or correlation matrix. *IEEE Trans. Inf. Theory*, IT-14:699–707, Sept. 1968.

[102] M. Ghavami, L. Michael, and R. Kohno. *Ultra Wideband Signals and Systems in Communication Engineering*. John Wiley & Sons, 2nd edition, 2007.

[103] R. L. Peterson, R. E. Ziemer, and D. E. Borth. *Introduction to Spread Spectrum Communications*. Prentice Hall, 1995.